Tesis Doctoral

Epigenetic Footprint of Gene-Environment Interactions: From High-Throughput Screening to Causality

Marta Alaiz Noya

Director de Tesis: Dr. Ángel Luis Barco Guerrero

Co-directora de Tesis: Dra. Beatriz del Blanco Pablos

Programa de Doctorado en Neurociencias

Universidad Miguel Hernández de Elche

Instituto de Neurociencias UMH-CSIC

- 2024 -

La presente Tesis Doctoral, titulada "Epigenetic footprint of gene-environment interactions: from high-throughput screening to causality" se presenta bajo la modalidad de tesis convencional con el siguiente indicio de calidad:

Sant Joan d'Alacant, 17 de Abril 2024

El Dr. D. Ángel Luis Barco Guerrero, director, y la Dra. Dña. Beatriz del Blanco Pablos, codirectora de la tesis doctoral titulada ""Epigenetic footprint of gene-environment interactions: from high-throughput screening to causality"

INFORMAN:

Que Dña. Marta Alaiz Noya ha realizado bajo nuestra supervisión el trabajo titulado

"Epigenetic footprint of gene-environment interactions: from high-throughput screening to causality"

conforme a los términos y condiciones definidos en su Plan de Investigación y de acuerdo al Código de Buenas Prácticas de la Universidad Miguel Hernández de Elche, cumpliendo los objetivos previstos de forma satisfactoria para su defensa pública como tesis doctoral.

Lo que firmamos para los efectos oportunos, en San Juan de Alicante a 17 de Abril de 2024

Director de la tesis

Dr. D. Ángel Luis Barco Guerrero

Codirectora de la tesis

Dra. Dña. Beatriz del Blanco Pablos

Sant Joan d'Alacant, 17 de Abril 2024

Dña. María Cruz Morenilla Palao, Coordinadora del programa de Doctorado en Neurociencias del Instituto de Neurociencias de Alicante, centro mixto de la Universidad Miguel Hernández (UMH) y de la Agencia Estatal Consejo Superior de Investigaciones Científicas (CSIC),

INFORMA:

Que Dña. Marta Alaiz Noya ha realizado bajo la supervisión de nuestro Programa de Doctorado el trabajo titulado

"Epigenetic footprint of gene-environment interactions: from high-throughput screening to causality"

conforme a los términos y condiciones definidos en su Plan de Investigación y de acuerdo al Código de Buenas Prácticas de la Universidad Miguel Hernández de Elche, cumpliendo los objetivos previstos de forma satisfactoria para su defensa pública como tesis doctoral.

Lo que firmo para los efectos oportunos, en San Juan de Alicante, a 17 de Abril de 2024

Y para que conste, a los efectos oportunos, firmo el presente certificado.

Dra. María Cruz Morenilla Palao

Coordinadora del Programa de Doctorado en Neurociencias

E-mail : cruz@umh.es
www.in.umh.es

Tel: +34 965 919229
Fax: +34 965 919549

Av Ramón y Cajal s/n
CAMPUS DE SANT JOAN
03550 SANT JOAN D'ALACANT– ESPAÑA

La presente tesis doctoral, titulada

"Epigenetic footprint of gene-environment interactions: from high-throughput screening to causality"

A mis abuelos

AGRADECIMIENTOS

Aún no me creo del todo que esté escribiendo, por fin, estas líneas. El camino, o más bien, montaña rusa, no ha sido fácil, pero he tenido la gran suerte de contar a mi lado con multitud de personas increíbles a las que tengo mucho que agradecer.

Empezaré por las personas que forman el eje vertebral de Barco Lab…

Ángel, gracias por darme la oportunidad de formar parte de tu laboratorio y por compartir conmigo tantos conocimientos. Eres el principal responsable de que haya podido cumplir el sueño de dedicarme a la investigación.

Bea, ¡qué de paciencia has tenido conmigo! Siempre dispuesta a ayudar y a sacar un hueco a pesar de la multitud de cosas que llevas para adelante. ¡Es admirable la capacidad que tienes! Gracias por dedicarme tu tiempo y enseñarme tantísimas cosas.

Román, gracias por ayudarme tantas veces, por compartir tus conocimientos sobre ratoncitos y por las charlas en el lab. Me alegro muchísimo de haber visto la tremenda transformación que has hecho en estos años, no solo cuidándote más por fuera, sino también abriéndote con nosotros y dejándonos que conozcamos lo buena persona que eres.

Siguiendo por implicación directa en estos años de tesis, quiero continuar con mis Barquitos. Habéis sido mi familia alicantina, y eso no se puede agradecer en unas pocas líneas. Aunque el formato oficial de la tesis no me deje poneros, quiero que sepáis que para mí sois co-autores de pleno derecho de esta tesis, porque sin vosotros no hubiera sido posible.

Sergio, gracias por los paseos por la playa, los helados y las charlas, tanto científicas como motivadoras. Gracias por perdonar todas mis miradas bordes, por tenerme tanta paciencia y aprender a entender cuando era mejor tomar el café sin mucha conversación.

Isa, mi primer polluelito, gracias por tu amabilidad infinita y por estar siempre disponible para lo que haga falta. Gracias por tu energía y vitalidad contagiosas, y por todos esos abrazos en los momentos que más los necesitaba. Espero que estos años no hayan sido más que el comienzo de muchos más viajes juntas.

Miguel, tengo tantas cosas que agradecerte que no sé ni por dónde empezar… Gracias por estar siempre disponible, por ayudarme tantísimo con la tesis y por la review. Esta tesis no podría ser defendida sin tu generosidad infinita, así que ¡MIL GRACIAS! Eres un auténtico crack, solo te falta creértelo un poco. Estoy segura de que vas a llegar muy lejos, solo espero tener una camita para poder visitarte (ya sabes que Isa y yo cabemos en cualquier lado).

Juan Paraíso, es admirable la capacidad que tienes para llevarte a todo el mundo de calle y saber sacar sonrisas independientemente de lo que haya pasado. Gracias por las tardes de reflexiones en el lab, por saber animarme, por los ruidos de pipetas rotas y por los mimitos. ¡Ah! Y gracias por EL susto… (esto es extensible para ti también, Miguel).

Mirjam, gracias por tu alegría contagiosa, tus palabras bonitas y por ser tan buena compañera. Por favor, no cambies nunca porque eres maravillosa y, sobre todo, ¡una REINA! Gracias por elegir Alicante y unirte al lab, porque te has convertido en un elemento indispensable.

Maca, nadie me ha vuelto a mirar de la forma que tú lo hacías… Gracias por ser inspiración y ejemplo, por ayudarme tantísimo y por tu disponibilidad absoluta. Sé que llegarás allá donde te propongas, porque no conozco a nadie más preparado y capaz que tú.

Rafa, ¡qué grande eres! No creo que tengas suerte con las becas, simplemente eres muy especial y todos los comités evaluadores lo saben. Gracias por enseñarme tanto en tan poco tiempo, por las bromas, por ser tan generoso con todos y tener siempre tiempo para mis dudas.

Carina, gracias por todas las veces que me has ayudado, que han sido muchas y siempre con una sonrisa. Gracias por las charlas sobre la vida y el millón de preguntas. ¡Eres una mamá gatuna estupenda!

Fede, gracias por tu paciencia y por ayudarme en esta etapa final. Estoy segura de que sabrás conducir al proyecto a muy buen puerto.

Patri, mi segundo polluelito. Gracias por ser tan independiente y adaptarte a mi falta de tiempo de los últimos meses. No pierdas nunca la constancia que tienes, porque es admirable.

Pero ellos no han sido los únicos que han hecho mi vida más bonita y alegre durante estos años en Alicante…

Aysha, gracias por ser fuente de luz y contagiarla allá donde vas. Por favor, no pierdas nunca la fantasía y la alegría que tanto te caracterizan porque son maravillosas.

Ángel Márquez, gracias por la infinidad de charlas y consejos. Tu compromiso y dedicación son impresionantes, estoy segura de que triunfarás allá donde decidas ir.

Alejandro, gracias por los ratos de desconexión en la montaña, las charlas y por contagiarnos de tu espíritu aventurero.

Ángel Sierra, gracias por integrarte tan bien y rápido, por vivir la vida con tanta filosofía y por cuidar de Juan. Estoy segura de que conseguirás contagiarle tu amor por los peludos, ya sean gatos o perros.

Juan Medrano, gracias por preocuparte de que tuviera un sitio y un ordenador nada más entrar el primer día en el lab, me hiciste sentir muy arropada. Pero, sobre todo, gracias por todo lo que vino después: por hacerme sentir parte del grupo, por hacer que desarrollara un sexto sentido anti-sustos-de-Juan, por ayudarme tanto con los ratoncitos y por el millón de consejos y enseñanzas sobre la vida.

Ana, gracias por ser como una hermana mayor, siempre pendiente de que estuviera bien y dándome consejos que valían millones. Gracias por ser tan buen ejemplo a seguir.

Mayte, Marian, gracias por los ratitos que compartimos en ese rinconcito del lab y por los planes al principio del todo.

Marta Arumi, mi Marta A., y Fran, gracias por las charlas, los ánimos, los abrazos y vuestra ayuda.

Miembros oficiales de las escaleras del INA y compis de doctorado. No os nombro a todos por miedo a dejarme algún nombre, pero sé que sabéis quiénes sois. Gracias por hacer más amenas las horas de la comida, por formar una piña tan bonita, por los muchos consejos sobre la vida científica y el apoyo continuo.

Compis del máster, y en especial, Jeiny. Gracias por dar forma a los inicios, por formar parte del camino y seguir ahí en el final. Gracias por tantos momentos, por las confidencias y por las reflexiones.

Trini, gracias por ser el alma del instituto. Antonio y Pep, gracias por el millón de horas de sorting, por estar pendientes de los experimentos de todos y resolver todas las dudas. María José y Maite, muchas gracias por vuestra ayuda y múltiples gestiones a lo largo de estos años. Cruz y Elvira, gracias por vuestra dedicación al programa de doctorado y por vuestra infinita paciencia resolviendo mil y una dudas y haciendo el proceso mucho más sencillo.

Ahora me gustaría acercarme a casa, y agradecer a todas las personas que eran familia antes de que la aventura tesis comenzara…

Biomédicos, gracias por seguir ahí a pesar de la distancia, el COVID y los años que han pasado ya desde que la Sopeña, las conchas que pinchan y "¡ay, qué dolor!", las fotos pre-exámenes y las tardes de biblioteca nos unieran por primera vez. Inma, gracias por ser la líder durante tanto tiempo. Esteban, gracias por adaptarte a todo y mantener al grupo unido. Inés, gracias por las charlas, los ánimos y por seguir siendo mi exonucleasa. Fati P., gracias por ayudarme a ver las cosas desde otra perspectiva en un momento en el que tanto lo necesitaba. Fati R., gracias por empezar a quererte y a confiar más en ti. Por fin has salido del capullo, pequeña mariposa. No abandones esta nueva versión alegre, extrovertida y que se apunta a un bombardeo, porque te queda muy bien. Pequeña Eli, gracias por no decir nunca que no a nada y estar dispuesta a jugar hasta al Time's Up. Vane, gracias por la convivencia, las visitas y las risas.

Niñas, hace mucho que os ganasteis el estar entre las personas más importantes de mi vida. Gracias por cuidarme, por la infinidad de videollamadas, por los viajes, los reencuentros, por las risas y también por los llantos. Gracias por conocerme mejor que yo misma y apoyarme en absolutamente todo, sin condiciones. Marina, gracias por hablar sin parar, por vivir tan intensamente y por contagiarnos a todos la pasión que sientes por lo que haces. Andrea, gracias por saber escuchar, por tener siempre un buen consejo que dar y por incluir a todos en todo. Hace mucho que dijimos para siempre, ya no tenéis escapatoria.

Papi, mami, ¡GRACIAS! No podría haber llegado a ningún lado sin vuestro apoyo y vuestra confianza en mí. Gracias por escucharme TODOS los días, por frenarme cuando me caliento demasiado y animarme cuando me achanto. Gracias por los consejos, por venir a verme, por las comiditas y por todos los planes juntos. Me siento muy afortunada de teneros como padres porque sois increíbles. Gracias por ser mis referentes, por vuestro amor incondicional y por ser los mejores padres que se pueden tener.

Jorgito, pequeño enano, ¡qué rápido estás creciendo y qué lejos vas a llegar! Sigue así, apostando fuerte, porque vales millones. Gracias por contagiar la pasión con la que vives la ciencia, por las llamadas de vez en cuando pero de gran duración, por tus orejitas y por ser el mejor tito de Leo.

Manolito, gracias por compartir con nosotros tus conocimientos sobre el mundo científico y por estar siempre ahí para lo que necesitemos. Gracias por tu generosidad absoluta tito.

Cristina, Antonio, Ale, Álvaro, Pili, María, Valentina… gracias por ser una bonita familia con la que contar y a la que acudir cada vez que lo necesito.

Isabel, Manolo y Chatán, gracias por hacerme sentir parte de la familia desde el principio, por escuchar con atención y mimo cada batalla relacionada con la tesis y cuidar de Alex todas las veces que yo no he podido.

Leo, pequeño gamberro adorable. ¡Cuántos días te has colocado entre el portátil y yo reclamando cosquillas! Gracias por tu amor incondicional, por la cara bobalicona y la alegría de "*¿Vamos a la calle?*". No sabía que una frase tan simple podía generar tantos sentimientos bonitos.

Pufo, gracias por absolutamente todo. Gracias por no dejarme abandonar, por abrirme los ojos antes las excusas y por cuidarme tanto. Gracias por aguantar la distancia, por las cenas sorpresa en los días más grises, por escucharme siempre y por encontrar la solución a cualquier problema, hasta los científicos. Tienes un corazón que no te cabe en el pecho, una generosidad desbordante y una personalidad tan especial, que haces que la vida sea mucho más bonita y divertida a tu lado. Gracias, gracias y mil veces gracias.

Y por último, pero no por ello menos importante, me gustaría terminar haciendo algo que no hago muy a menudo, y es dándome las gracias. Por sobrevivir a la montaña rusa de la tesis, por coger el toro por los cuernos y por saber apoyarme en los demás cuando no podía sola. Sigue aprendiendo a escuchar lo que necesitas y a priorizarte por encima del "debo". Estoy muy orgullosa de ti.

INDEX

ABBREVIATIONS

A

AAV – Adeno-associated virus

AGO – Argonaute

AP1 – Activator protein 1

Arc – Activity regulated cytoskeleton-associated protein

ATAC-seq – Assay for transposase-accessible chromatin sequencing

B

Bdnf – Brain-derived neurotrophic factor

bp – Base pairs

C

5C – Chromosome conformation capture carbon copy

caC – Carboxylation

CaMKIIα – Calcium/calmodulin-dependent protein kinase II alpha

Cas – CRISPR-associated proteins

CDR – Complementarity-determining regions

CFC – Contextual fear conditioning

CH – Heavy chain's constant domain

ChEC-seq – Chromatin endogenous cleavage sequencing

ChIA-PET – Chromatin interaction analysis by paired-end tag sequencing

ChIP – Chromatin immunoprecipitation

CL – Light chain's constant domain

CMD – Chromatin modifying domain

CREB – cAMP response element binding protein

CRISPR – Clustered regularly interspaced short palindromic repeats

crRNA – CRISPR-derived RNA

CUT&RUN – Cleavage under targets & release using nuclease

CUT&TAG – Cleavage under targets & tagging

D

DAPI – 4,6-diamidino-2-phenylindole

DARs – Differentially accessible regions

DBD – DNA binding domain

dCas9 – Nuclease-dead Cas9

DEGs – Differentially expressed genes

DMEM – Dulbecco's modified Eagle's medium

Dox – Doxycycline

Dox-OFF – Doxycycline removal

E

EE – Environmental enrichment

EI – Environmental impoverishment

F

FACS – Fluorescence-activated cell sorting

FANS – Fluorescence-activated nuclear sorting

fC – Formylation

FISH – Fluorescence in situ hybridization

FITC-A – Fluorescein isothiocyanate-A

FP – Fluorescent protein

FR – Framework regions

G

Gfap – Glial fibrillary acidic protein

GFP – Green fluorescent protein

gRNA – Guide RNA

GSEA – Gene set enrichment analysis

GWAS – Genome-wide association studies

H

4-OHT – Hydroxy-tamoxifen

H1 – Histone protein 1

H3K4me1 – Histone 3 lysine 4 monomethylation

H3K4me2 – Histone 3 lysine 4 dimethylation

H3K4me3 – Histone 3 lysine 4 trimethylation

H3K9me3 – Histone 3 lysine 9 trimethylation

H3K27me3 – Histone 3 lysine 27 trimethylation

H3K36me3 - Histone 3 lysine 36 trimethylation

HCAb – Heavy-chain only antibodies

HEK293T – Human embryonic kidney cells with a mutant version of the SV40 large T antigen

Hi-C – High-throughput chromosome conformation capture

hmC – Hydroxymethylation

HSV – Herpes simplex virus

I

IEGs – Immediate early genes

IgG – Immunoglobulin G

IHC – Immunohistochemistry

iNCS – Heat inactivated newborn calf serum

K

K – Lysine

KA – Kainic acid

KAT – Lysine acetyltransferase

Kbp – Kilobase pairs

KRAB – Krüppel-associated box

L

lncRNAs – Long non-coding RNAs

LV – Lentivirus

M

m6A – N6-methyladenosine

mC – Methyl cytosine

MeCP2 – Methyl-CpG binding protein 2

Min – Minute

miRNAs – MicroRNAs

MWM – Morris water maze

N

N2a – *Mus musculus* brain neuroblastoma cell line

NAR – New antigen receptors

Nb – Nanobody

ncRNAs – Non-coding RNAs

NEB – Nuclei extraction buffer

NES – Normalized enrichment score

NGS – Next-generation sequencing

NIB – Nuclei incubation buffer

NLS – Nuclear localization sequence

NOR – Novel object recognition

nt - Nucleotide

nuRNA – Nuclear RNA

nuRNA-seq – Nuclear RNA sequencing

O

OF – Open field test

ORA – Over-representation analysis

P

PAM – Protospacer adjacent motif

PCA – Principal component analysis

pcHi-C – Promoter capture Hi-C

pEF1α – Promoter of elongation factor 1 alpha

PET – Positron emission tomography

PFA – Paraformaldehyde

piRNAs – PIWI-interacting RNAs

pre-crRNA – Precursor CRISPR RNA

PT – Probe trial

PTMs – Post-translational modifications

R

Ribo-seq – Ribosomal RNA immunoprecipitation sequencing

RISC – RNA-induced silencing complex

RNA-seq – RNA sequencing

RPM – Reads per million

RRBS – Reduced representation bisulphite sequencing

rRNAs – Ribosomal RNAs

S

SC – Standard cages

Sec – Second

siRNAs – Small interfering RNAs

snoRNAs – Small nucleolar RNAs

snRNAs – Small nuclear RNAs

SPECT – Single photon emission computed tomography

Syn1 – Synapsin 1

T

TADs – Topologically associated domains

TALE – Transcription activator-like effector

TET – Ten-eleven translocation proteins

TF – Transcription factor

THS-seq – Transposase hypersensitive site sequencing

TMX – Tamoxifen

TOBIAS – Transcription factor occupancy prediction by investigation of atac-seq signal

tracrRNA – Trans-activating crRNA

TRAP2 – Targeted recombination in active populations reporter strain

tRNAs – Transfer RNAs

tTA – Tetracycline transactivator

U

UTR – Untranslated región

V

VH – Heavy chain's variable domain

VHH – HCAb's variable domain

vhh – vhhGFP4 nanobody

VL – Light chain's variable domain

V-NAR – Variable domain of NAR

W

WebGestalt – WEB-based gene set analysis toolkit

WGBS – Whole genome bisulphite sequencing

Z

ZFPs – Zinc finger proteins

ABSTRACT

Both genetic and environmental factors influence the development of cognitive abilities. For instance, the housing conditions of laboratory animals exert a significant impact on their behaviour and cognitive development, especially during early life. While environmental enrichment (EE) is linked to cognitive enhancement, environmental impoverishment (EI) is associated with chronic stress and cognitive impairment. In this study, we investigated enduring changes in hippocampal function associated with early exposure to EE and EI. Furthermore, we employed various sequencing techniques to analyse the transcriptomic and epigenetic changes underlying the neuroadaptation to environmental conditions in the main types of excitatory neurons in the hippocampus. Our experiments revealed the differential impact of environmental conditions on the chromatin of these cells, supporting the hypothesis that modulation of cognitive performance by environmental factors is linked to changes in the epigenome. Additionally, to deepen our understanding of the necessity and/or sufficiency of epigenetic mechanisms in neuronal adaptation to environmental conditions, we have developed an innovative epigenome editing system combining CRISPR (Clustered Regularly Interspaced Short Palindromic Repeats) technology with nanobodies, taking their ability to bind with high affinity to the recognized epitope. Specifically, the nuclease-deficient dCas9 protein is fused with a nanobody specifically recognizing GFP (Green Fluorescent Protein), and GFP is linked to the catalytic domain of various effector proteins, generating a two smaller-module epi-editing system that does not exceed the packaging capacity of neurotropic vectors. Results combining our tool with synthetic and epigenetic effectors underscore the potential of this new modular toolbox for precise *in vitro* neuronal epigenome editing, and open new avenues for the development of innovative therapies to tackle diseases associated with epigenome dysregulation.

RESUMEN

Tanto los factores genéticos como los ambientales influyen en el desarrollo de las capacidades cognitivas. Así, las condiciones de estabulación de los animales de laboratorio ejercen un impacto significativo en su desarrollo y comportamiento, especialmente en etapas tempranas. Mientras que el enriquecimiento ambiental (EE, del inglés *Environmental Enrichment*) se relaciona con mejoras cognitivas, el empobrecimiento ambiental (EI, del inglés *Environmental Impoverishment*) se asocia con estrés crónico y deterioro cognitivo. En este estudio, hemos investigado los cambios duraderos en la función del hipocampo asociados a la exposición temprana a EE y EI. Además, hemos utilizado diversas técnicas de secuenciación para analizar los cambios transcriptómicos y epigenéticos subyacentes a la neuroadaptación a las condiciones ambientales en los principales tipos de neuronas excitatorias del hipocampo. Nuestros experimentos revelan el impacto diferencial de las condiciones ambientales en la cromatina de estas células, respaldando la hipótesis de que los factores ambientales modulan el rendimiento cognitivo a través de cambios en el epigenoma. Además, para profundizar en nuestra comprensión de la necesidad y/o suficiencia de los mecanismos epigenéticos en la adaptación neuronal a las condiciones ambientales, hemos desarrollado un innovador sistema de edición del epigenoma que combina la tecnología CRISPR (del inglés *Clustered Regularly Interspaced Short Palindromic Repeats*) con la capacidad de los nanocuerpos de unirse con alta afinidad al epítopo reconocido. Específicamente, la proteína nucleasa deficiente dCas9 se ha fusionado con un nanocuerpo que reconoce específicamente a GFP (del inglés *Green Fluorescent Protein*), y GFP se ha unido al dominio catalítico de distintas proteínas efectoras, generando un sistema de edición del epigenoma formado por dos módulos más pequeños que no exceden la capacidad de empaquetamiento de los vectores neurotrópicos. Los resultados combinando nuestra herramienta con efectores sintéticos y epigenéticos destacan el potencial de esta nueva caja de herramientas modular para la edición precisa del epigenoma neuronal *in vitro*, y abren nuevas vías para el desarrollo de terapias innovadoras que permitan abordar enfermedades asociadas a la desregulación del epigenoma.

1. INTRODUCTION

1.1 Modulation of cognitive abilities by gene-environment interactions

Parents have always been fascinated by the rapid growth and development that occurs in the early years of their children's lives. Each milestone, from the first steps to the first words, is a significant personal achievement and a cause for celebration within the family. As the months turn into years, awkward movements transform into agile runs, spontaneous smiles evolve into friendships, and single words develop into complex conversations.

To achieve all these milestones, numerous events take place during this early stage that are crucial for brain and cognitive development. These events include the formation of glial cells (Roessmann & Gambetti, 1986), the maturation and birth of neurons in specific brain areas (Bergmann et al., 2012; Boldrini et al., 2018; Kempermann et al., 2015), and the establishment of connections between neurons (Huttenlocher & Dabholkar, 1997). The infant brain exhibits twice the number of synapses compared to the adult brain. This richness gradually decreased through synaptic pruning, a process that intensifies from youth to adolescence (Huttenlocher, 1979; Huttenlocher & Dabholkar, 1997). Additionally, myelination occurs, enhancing axonal conduction and neuronal communication (Gibson et al., 2014).

All these structural and functional events contribute to brain development during early stages (Casey et al., 2000), when the brain's volume increases from 36% of an adult brain's total volume at birth to around 70% within the first year (Dekaban & Sadowsky, 1978; Knickmeyer et al., 2008). These changes are fundamental for the proper development of cognitive abilities (Gilmore et al., 2018; Paterson et al., 2006), which are modulated by the continuous interaction between the genes and the environment.

The term "gene" refers to the information encoded in the DNA sequence needed to specify physical and biological traits, while the term "environment" includes both local signals and external stimuli. The question of what of these two factors

determine the development of cognitive abilities has provoked the longstanding "nature vs. nurture" debate. Some pioneers on human development, such as Arnold Gesell (Gesell, 1925; Wilkes & Gesell, 1930), believed that development was primarily influenced by genes, while others, like John B. Watson (Watson, 1928), argued that the environment played a dominant role.

Over the years, numerous studies have addressed this question by quantifying the heritability of cognitive capacities, a statistical parameter that measures the extent to which genetic differences account for the variation observed in a specific trait (Sauce & Matzel, 2018). Longitudinal family studies focusing on twins and siblings show an increased heritability of cognitive abilities with development, ranging from 20-40% in childhood to around 60% in adolescence, and rising to 80% in late adulthood (Bartels et al., 2002; Briley & Tucker-Drob, 2013; Haworth et al., 2010; Panizzon et al., 2014; Pedersen et al., 1992; Plomin & Deary, 2015). However, the cumulative effect of the identified DNA variants in Genome-Wide Association Studies (GWAS, Uffelmann et al., 2021) accounts for fewer than 5% of the disparities between individuals (Manolio et al., 2009). This suggests that the increase in heritability of cognitive abilities throughout life cannot be attributed solely to genetic effects; the environment may also play a role.

The current model emphasizes the inseparability and complementarity of genes and environment elements rather than their distinction, underscoring that their dynamic and continuous interaction is crucial for the proper development of cognitive abilities (Sauce & Matzel, 2018). Based on this model, the increase in heritability over the lifespan could be attributed to the idea that an individual's cognitive capacity shapes their attraction to specific cognitive environments. As a result, people with varying cognitive capacities would pursue distinct cognitive tasks, whereas those sharing similar cognitive capacities would be inclined towards comparable challenges. As we age, the genetic disparities that initially contribute to cognitive distinctions become more pronounced by the accumulation of cognitive demands introduced by various environments (Lykken et al., 1993; McGue et al., 1993), leading to an overall increase in heritability estimates. Thus, despite the high heritability of cognitive abilities, numerous studies also suggest that their variation is significantly influenced by environmental factors, indicating their high malleability (Sauce & Matzel, 2018).

1.2 From genomic plasticity to synaptic plasticity: the role of epigenetics

To ensure that cognitive abilities are both heritable and malleable at the same time, neurons must exhibit a high level of plasticity. This enables them to adapt precisely to the constantly shifting demands in the short and long term, while ensuring optimal cellular functioning.

Plasticity refers to the ability to rapidly detect and respond to dynamic changes in the environment (Hebb, 1949; Konorski, 1948; Woldemichael et al., 2014). When an external stimulus arrives, the first manifestation is genomic plasticity, triggering the swift activation of numerous immediate early genes (IEGs), including regulatory molecules like transcription factors and protein phosphatases, as well as synaptic effector molecules such as the activity regulated cytoskeleton (*Arc*) gene (Bramham et al., 2008) and the brain-derived neurotrophic factor (*Bdnf*) (Cohen-Cory et al., 2010; Lu et al., 2008). These molecules play a vital role in the development of new axons, dendritic branching, the formation of fresh synapses, and the adjustment of the strength of existing connections in response to experiences (Caroni et al., 2012; Dudai, 2012; Redondo & Morris, 2011). In essence, they instigate cellular changes that underlie a second form of plasticity, specifically at the synaptic level.

For these changes to persist in the long term, a mechanism is required to ensure their maintenance for years or even decades, even after RNA and proteins have degraded due to their shorter half-life (Robertson, 1992). Epigenetic mechanisms, involving chemical and physical modifications of the DNA molecule that functionally regulate genome activity without altering its sequence (Waddington, 2012), have been proposed as a potential substrate for translating environmental stimuli into lasting physiological and behavioural changes. Epigenetics explains how the genetic information contained in DNA, which is typically considered static, can dynamically respond to environmental factors, inducing stable changes in an organism without altering the genetic code itself. The main mechanisms of epigenetic regulation (**Figure 1**), including the spatial organization of chromatin, post-translational modifications of histones, DNA methylation, and non-coding RNAs, are described below.
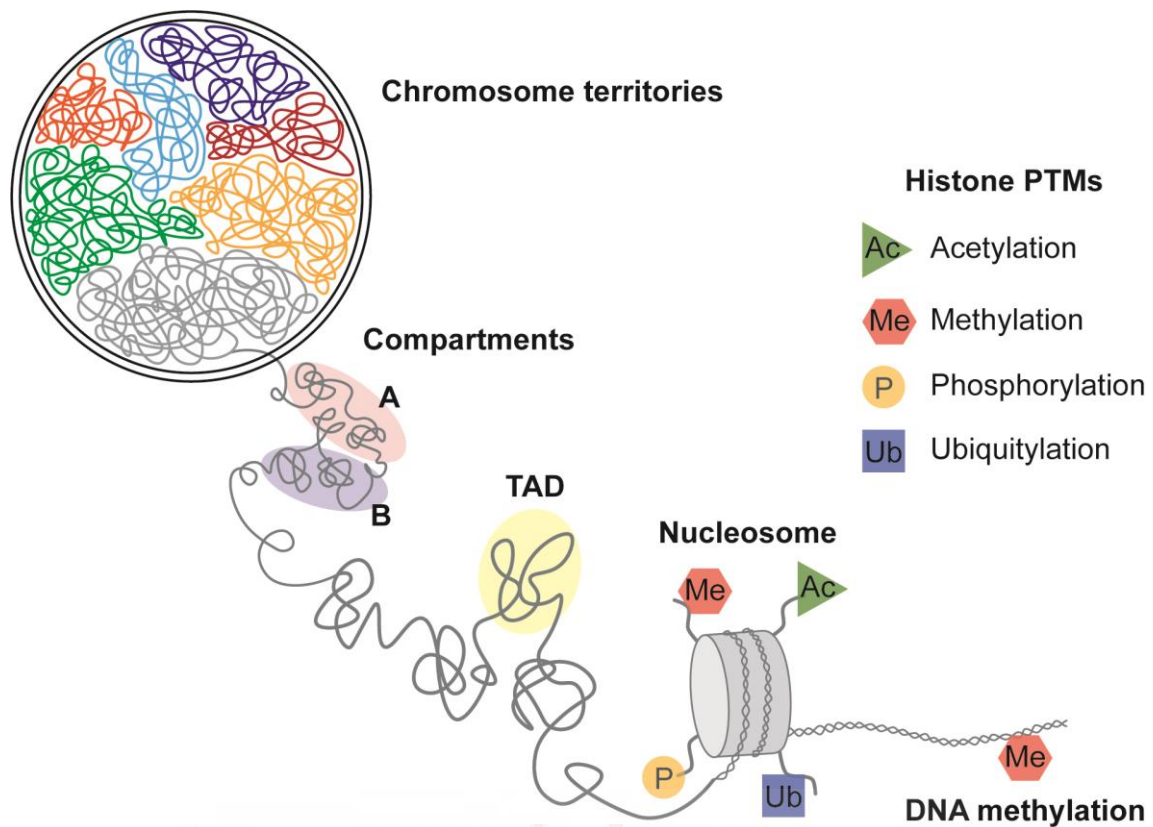
Figure 1. Schematic representation of the hierarchical organization observed in the eukaryotic genome. Within the nucleus, chromosomes tend to occupy specific regions, giving rise to chromosome territories (depicted in different colours). Intrachromosomal regions divide into A (active) and B (repressed) compartments, resulting in selective interactions among chromatin regions sharing similar epigenetic characteristics. Chromatin folds into topologically associated domains (TADs), characterized by internal preferential interactions. The finest level of chromatin folding occurs when the DNA molecule associates with histone proteins to form nucleosomes. Modifications of DNA and histone tails (histone post-translational modifications, PTMs), such as acetylation, methylation, phosphorylation and ubiquitylation (depicted as various coloured shapes), regulate genome architecture. (Adapted from Szabo et al., 2019; Li et al., 2022).

1.2.1 Spatial organization of chromatin

To accommodate the more than 5 billion base pairs (bp) constituting the mouse diploid genome within the nuclei, which have a diameter of about 6 μm, eukaryotic cells utilize chromatin. Chromatin is a complex formed by DNA and proteins that allows for the flexible packaging of the genome (Fujita et al., 2022). The nucleosome serves as the fundamental unit of chromatin, consisting of two subunits, each containing four core histone proteins: H2A, H2B, H3, and H4. Surrounding each nucleosome is ~ 146 base pairs of DNA, and they are

40

interconnected through DNA sequences of 20-90 base pairs. These internucleosomal DNA sequences are stabilized by the histone protein 1 (H1), which acts as a linker histone.

Chromatin is organized into hierarchical three-dimensional structures that are essential for regulating gene transcription. At the first level of three-dimensional organization, chromosomes territories are found, which are nuclear regions preferentially occupied by specific chromosomes (Kempfer & Pombo, 2019). The arrangement of chromosomes within these territories has been extensively visualized using chromosomal painting (Lichter et al., 1988; Pinkel et al., 1988) and later confirmed through Hi-C (Lieberman-Aiden et al., 2009), a technique that comprehensively detects chromatin interactions throughout the genome.

Going one level deeper, Hi-C studies combined with imaging studies (Su et al., 2020; Wang et al., 2016) have revealed that chromosomes organize into defined subcompartments, with one associated with active transcription (termed the A compartment) and another linked to repression (known as the B compartment). Compartment A comprises euchromatic regions marked by their abundance of genes, active transcription, and sensitivity to DNase I. In contrast, compartment B encompasses heterochromatic sequences, exhibiting a lower gene count and transcriptional inactivity.

At a smaller scale, advanced techniques, such as high-resolution Hi-C and 5C (chromosome conformation capture carbon copy, a large-scale technique for mapping of cis- and trans- interaction networks of genomic elements (Dostie et al., 2006)) have identified small domains known as topologically associated domains (TADs). TADs are characterized by having many interactions among loci within their boundaries, while interactions between loci in contiguous domains are restricted (Dixon et al., 2012; Nora et al., 2012). Active TADs aggregate to form compartment A, while a collection of inactive TADs constitutes compartment B. This arrangement allows transcription factories to form in compartments A, where groups of active genes interact with focal points rich in elements of the transcriptional machinery (Osborne et al., 2004), facilitating gene expression. Conversely, compartment B reflects the aggregation of inactive chromatin at the nuclear envelope, nucleoli, and other subnuclear regions.

Within each TAD, smaller chromatin loops are present, which bring together genome regions that are separated by tens or hundreds of kilobases *in cis*, enabling interactions between genes and their regulatory regions and influencing precise transcriptional regulation (Kleinjan & Van Heyningen, 2005).

1.2.2 Histones post-translational modifications

Post-translational modifications (PTMs) of histones are essential for chromatin remodelling, a process that governs the regulation of gene expression. These PTMs involve chemical modifications such as acetylation, methylation, phosphorylation, and ubiquitination, among others, occurring on the tails and globular domains of histone proteins. Enzymes of the epigenetic machinery, known as writers, erasers, and readers, introduce, remove, and recognize these epigenetic marks, respectively. Together, these modifications control the interaction between DNA and nucleosomes, influencing the access of the epigenetic machinery and transcription factors to the underlying DNA sequence. Consequently, each gene carries a specific code of histone marks, which can lead to gene activation or repression based on the nature of the modification (Huang et al., 2014; Shahid et al., 2023).

For instance, the acetylation of histones at lysine residues leads to the neutralization of their positive charge, thereby reducing their affinity for the DNA, which carries negative charges (Ip et al., 1988). This relaxation of chromatin structure causes nucleosomes to shift (Reinke & Hörz, 2003; Zhao et al., 2005), promoting the binding of transcription factors and increasing gene expression (Roth et al., 2001). Additionally, phosphorylation of histones at threonine, serine, or tyrosine residues leads to increased DNA accessibility by introducing a negative charge that promotes separation of DNA from histone proteins, also facilitating nucleosome mobility (North et al., 2011).

On the other hand, arginine and lysine residues can undergo methylation, leading to distinct transcriptional outcomes. The methylation of arginine residues has been associated with gene expression, while lysine methylation exhibits a dual role in gene regulation, either promoting expression or repression. This duality hinges on the precise deposition site and the number of methyl groups (mono-, di-, or trimethylation) that are added (Greer & Shi, 2012). For example, H3K4

monomethylation (H3K4me1), dimethylation (H3K4me2) and trimethylation (H3K4me3) are activation marks found at different genomic elements. Typically, H3K4me1 marks transcriptional enhancers (Heintzman et al., 2007), while H3K4me2 and H3K4me3 are present at gene promoters and within gene bodies of active or poised genes (Santos-Rosa et al., 2002). Similarly, H3K36 trimethylation (H3K36me3) functions as an activation signal and is commonly found within the gene bodies of active regions (Zaghi et al., 2020). Alternatively, trimethylation at lysine 9 and 27 on histone H3 (H3K9me3 and H3K27me3, respectively) are repressive marks that contribute to reduce gene expression through the establishment of heterochromatic regions (Zhang et al., 2015). The versatility of methylation outcomes arises because this modification neither affects the charge of histone residues nor influences histone-DNA interactions, in contrast to the effects of acetylation and phosphorylation.

In addition to PTMs, nucleosomes can undergo modifications through the exchange of core histones with histone variants like CENP-A, H3.3, and H2A.Z, among others (Becker & Workman, 2013). These variants exhibit variations in both function and structure, which can influence the functioning of the genomic region where they are localized.

1.2.3 DNA methylation

DNA methylation entails the modification of cytosine bases by the addition of a methyl group (mC), typically at cytosines followed by guanines, which are referred to as CpG sites (Lister et al., 2009; Ziller et al., 2013). Traditionally, a negative correlation has been observed between the levels of mCpG in a gene's promoter and its expression levels (Deaton & Bird, 2011). This repression is mediated either by direct blocking of the binding site of transcription factors due to the presence of the methyl group or by the engagement of binding proteins, like methyl-CpG binding protein 2 (MeCP2), which interacts with histone-modifying enzymes to induce heterochromatin formation (Fan & Hutnick, 2005). However, technological advances that allow measurement of mCpG levels and gene expression across the entire genome have revealed a more subtle relationship between mCpG and gene expression, which fluctuates based on the genomic location of the mCpG marks (Lam et al., 2012; Lea et al., 2018).

Moreover, cytosine methylation is not limited to CpG sites; it can also occur in regions where the cytosine is followed by a non-guanine base, such as adenine, cytosine, or thymine (Ramsahoye et al., 2000; Schultz et al., 2015). This non-CpG methylation is found in numerous tissues and cell types, being particularly abundant in neurons. Notably, during postnatal development, neurons show comparatively elevated mCpA levels (He & Ecker, 2015). This specific methylation pattern is associated with the accurate control of gene expression, essential for optimal brain development and function (Stroud et al., 2017).

Additionally, DNA methylation can undergo further modifications via oxidation by ten-eleven translocation (TET) proteins, leading to hydroxymethylation (hmC), formylation (fC), and carboxylation (caC) of DNA. These modifications ultimately result in active DNA demethylation (Shen et al., 2013). HmC is predominantly found at the 5' end of genes and correlates with gene transcription (Mellén et al., 2012; Song et al., 2011). Interestingly, the brain exhibits particularly high levels of hmC, suggesting its essential role in neuronal functions (Khare et al., 2012; Kriaucionis & Heintz, 2009). fC has also been detected as a stable DNA modification in mammalian genomes (Song et al., 2021), although its biological function in the brain remains uncertain.

1.2.4 Non-coding RNAs

High-throughput transcriptomic analyses have shown that as many as 90% of eukaryotic genomes undergo transcription (Feingold et al., 2004). However, less than 2% of these transcripts are translated into proteins, with the majority being transcribed as non-coding RNAs (ncRNAs). ncRNAs can be categorized into structural and functional ncRNAs.

Structural ncRNAs are constitutively expressed and play an essential role in maintaining cellular viability (Zhang et al., 2019). Ribosomal RNAs (rRNAs) form the core of the ribosomal machinery, crucial for protein synthesis (Henras et al., 2015). Transfer RNAs (tRNAs), ranging from 72 to 95 nucleotides (nt) in length, are responsible for decoding codons and delivering the correct amino acids during protein synthesis (Odonoghue et al., 2018). Small nuclear RNAs (snRNAs), approximately 150 nt long, are involved in the splicing of pre-mRNA, ensuring proper mRNA maturation (Valadkhan, 2005; Will & Lührmann, 2011).

Meanwhile, small nucleolar RNAs (snoRNAs), with a length of 60-300 nt, are responsible for directing specific modifications of rRNAs, tRNAs and mRNAs at precise sites (Huang et al., 2022; Kiss, 2002; Maxwell & Fournier, 1995). Interestingly, some of these structural ncRNAs also possess regulatory functions, particularly those derived from tRNA cleavage, contributing to a diverse range of cellular processes (Fu et al., 2009; Lee et al., 2009).

Conversely, functional ncRNAs play critical roles in various cellular functions, including chromatin remodelling, gene expression regulation, DNA repair, and defence against foreign genetic material (Francia, 2015; Holoch & Moazed, 2015). MicroRNAs (miRNAs) are single-stranded, short (~ 22 nt in size) RNAs (Kim et al., 2016) derived from transcripts that form specific hairpin structures. The proteins DROSHA and DICER process these hairpins into mature miRNAs, enabling them to interact with argonaute proteins (AGO) and form the RNA-induced silencing complex (RISC) (Davis-Dusenbery & Hata, 2010). RISC mediates post-transcriptional gene silencing by either degrading target mRNAs or inhibiting their translation into proteins (Beveridge et al., 2014). Small interfering RNAs (siRNAs) are linear double stranded RNAs processed by DICER into 20-24 nt siRNAs, which are then incorporated into RISC. These siRNAs are responsible for direct transcriptional silencing of specific gene sequences, leading to the accumulation of epigenetic marks characteristic of heterochromatin (Carthew & Sontheimer, 2009; Grewal, 2010). PIWI-interacting RNAs (piRNAs), 24-31 nt in size, interact with Piwi proteins of the argonaute family (Siomi & Siomi, 2009). They exhibit complementarity to transposable and repetitive regions (Aravin et al., 2003) and play a crucial role in suppressing transposon activity (Brennecke et al., 2007; Gunawardane et al., 2007) by interacting with specific target DNA regions and Piwi proteins. Finally, long non-coding RNAs (lncRNAs) form a broad family of RNAs exceeding 200 nt in length (Zuo et al., 2016). These lncRNAs have diverse functions, including regulation of transcription, modulation of alternative splicing, and influencing the activity of miRNAs (Li et al., 2019).

Additionally, RNA nucleotides can undergo modifications through the addition of chemical groups (Boccaletto et al., 2018), influencing their structure, stability, and localization within specific subcellular compartments. There are over 160 known mRNA modifications, with N6-methyladenosine (m6A) being the most extensively

studied and abundant modification (Fu et al., 2014), with evidence linking it to behavioural phenotypes.

1.3   Unveiling epigenetic mechanisms in targeted brain cell populations

Epigenetic mechanisms play a crucial role throughout brain development and plasticity. Within the complex composition of brain tissue, myriad cell types intermingle, each with distinct gene expression signatures, intricate connectivity, and specialized behavioural roles (McKenzie et al., 2018). The dissection of bulk tissues, such as the hippocampus, affords the opportunity to elucidate the epigenetic mechanisms that support swift detection and response to ever-changing environmental cues in specific brain regions. However, to achieve a finer granularity of understanding, genetic strategies, coupled with advanced cell isolation techniques, facilitate the elucidation of transcriptional and chromatin dynamics occurring within discrete cell subpopulations (**Figure 2A**).

These genetic strategies can be based on cell-type-selective promoters, such as the calcium/calmodulin-dependent protein kinase II alpha (*CaMKIIα*) promoter, tailored to excitatory forebrain neurons (Mayford et al., 1996) or the microglia marker *Iba1* (Shapiro et al., 2009), among many others. Alternatively, the promoter of activity-regulated genes, like *Arc* (Link et al., 1995; Lyford et al., 1995) and *Fos* (Schilling et al., 1991), can be used for the temporal detection of actively responsive cells. By fusing these promoters with reporter genes, such as the green fluorescent protein (GFP), cells are labelled and can be isolated via fluorescence-activated cell sorting (FACS) (McKinnon, 2018).

A recent development consisted on fusing these fluorescent reporters with a protein of the nuclear envelope, such as SUN1, enabling the labelling of specific nuclei with a fluorescent tag instead of labelling entire cells (Mo et al., 2015). This genetic strategy can be combined with fluorescence-activated nuclear sorting (FANS), a technique that offers some benefits over traditional cell sorting by mitigating the inherent variability introduced by tissue disruption, which might stochastically retain cytoplasmic fractions, axons, and dendritic components.

Additionally, nuclei exhibit greater resistance to tissue dissociation than cells, thereby safeguarding the induction of genes associated with neuronal plasticity from being obscured by the stress response. Moreover, nuclear RNA (nuRNA) offers finer temporal resolution than mRNA, providing a better strategy for studying processes characterized by dynamic transcriptional cascades (Fernandez-Albert et al., 2019; Stroud et al., 2020).

Following their isolation, the sorted cells or nuclei can be employed across a spectrum of next-generation sequencing (NGS) applications, spanning from methodologies investigating the three-dimensional chromatin configuration and its accessibility to the creation of transcriptomic and epigenetic profiles (**Figure 2B**). Specifically:

- For the evaluation of the three-dimensional chromatin architecture, methodologies like Hi-C (Belton et al., 2012) or chromatin interaction analysis by paired-end tag sequencing (ChIA-PET) (Li et al., 2014) come into play, which enable the identification of the complete spectrum of chromosomal interactions within a cellular population. Moreover, the promoter capture Hi-C method (pcHi-C) (Schoenfelder et al., 2018) enhances promoter regions in Hi-C datasets, thereby enabling studies of higher resolution concerning interactions between regulatory domains and promoters.

- For the examination of chromatin accessibility, methodologies like the assay for transposase-accessible chromatin using high-throughput sequencing (ATAC-seq) (Buenrostro et al., 2013) or transposase hypersensitive site sequencing (THS-seq) (Sos et al., 2016) are utilized. Both methods rely on the action of the bacterial transposase Tn5, which integrates DNA fragments into nucleosome-free genomic regions, enabling the differentiation between accessible and inaccessible chromatin.

- For the investigation of interactions between proteins and DNA or to detect epigenetic histone marks, various techniques are utilized, including chromatin immunoprecipitation (ChIP)-seq (Park, 2009), chromatin endogenous cleavage coupled with high-throughput sequencing (ChEC-seq) (Zentner et al., 2015), cleavage under targets & release using nuclease (CUT&RUN) (Skene & Henikoff, 2017), and cleavage under targets & tagging (CUT&Tag) (Kaya-Okur et al., 2019). All these methodologies are based on the specific

binding of an antibody to the target protein or epigenetic mark, facilitating its selective isolation and comprehensive genomic analysis. Variations among these techniques primarily stem from the prerequisites of cellular fixation and/or the quantity of initial material required, with CUT&RUN and CUT&Tag demanding a smaller amount of material.

- Transcriptome analyses are carried out through cellular RNA sequencing (RNA-seq) when isolating cells (Wang et al., 2009), or nuclear RNA sequencing (nuRNA-seq) when isolating nuclei (Dhaliwal & Mitchell, 2016). Additionally, we can investigate actively translating RNA using Ribo-Seq (Ingolia et al., 2009), which offers insights into the proteins being actively translated within a cell.

- For studying DNA methylation several methods can be used, including reduced representation bisulphite sequencing (RRBS) (Meissner et al., 2005) and whole genome bisulphite sequencing (WGBS) (Lister et al., 2009). Both techniques utilize bisulphite treatment to convert unmethylated cytosines into uracils, distinguishing them from methylated cytosines. The differences between them lies in RRBS's incorporation of a restriction enzyme to enhance sequencing in CpG-rich regions, while WGBS omits the use of enzymes, allowing for a less biased analysis of the entire genome. However, WGBS requires a greater depth of sequencing reads to detect all variations (Beck et al., 2022).
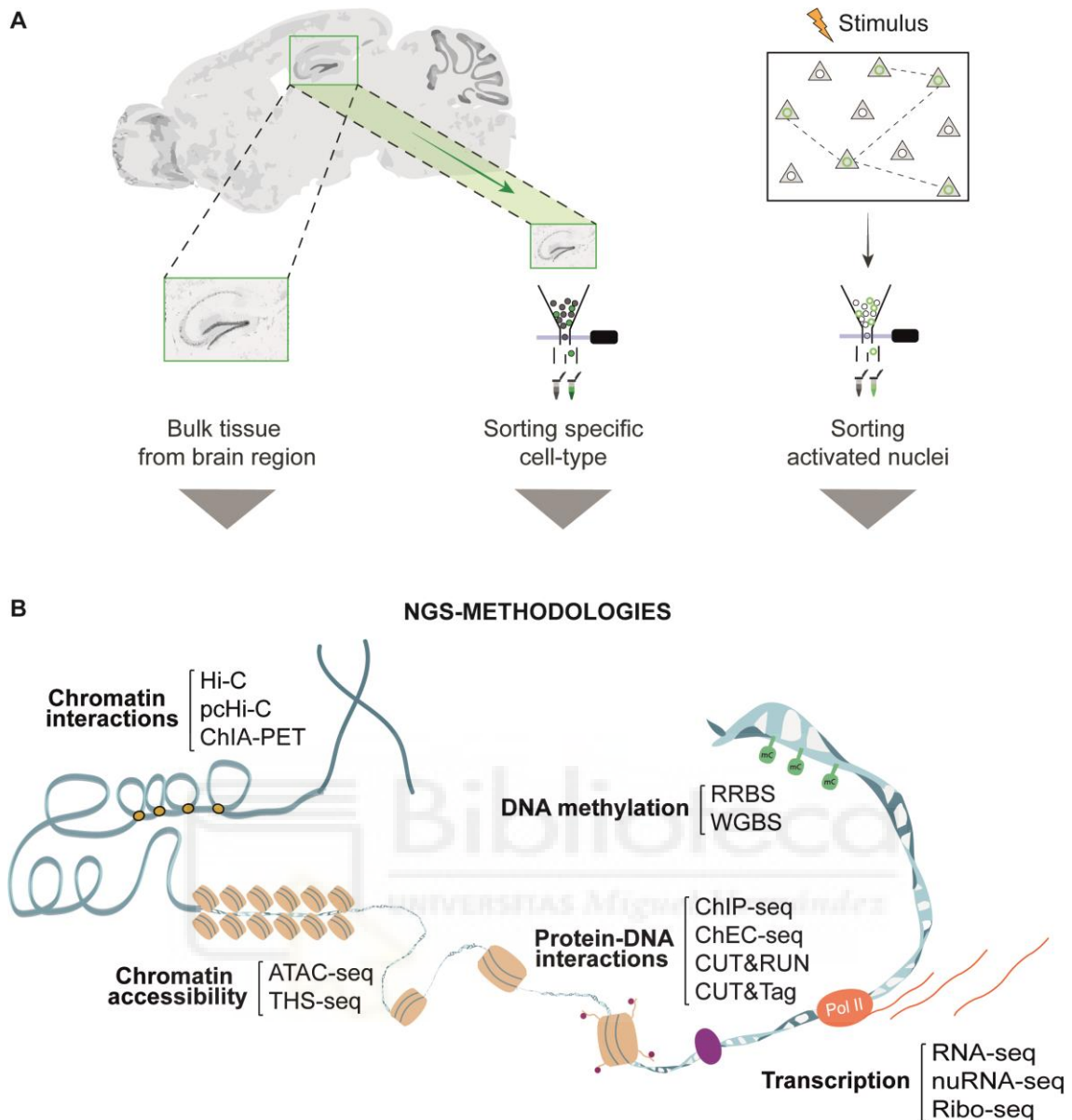
Figure 2. Techniques to unravel the epigenetic mechanisms that support swift detection and response to ever-changing environmental cues. **A**. Transcriptome and epigenetic changes involved in gene-environment interactions can be studied by analysing bulk tissue or specific cell subpopulations. As examples, the left diagram shows a zoomed-in view of the hippocampus that represents analysis from specific bulk brain regions. The middle diagram illustrates the use of cell-type-specific promoters combined with GFP labelling and isolation by FACS. The right diagram depicts activity-dependent promoters that enable Sun1-GFP expression in the cells activated upon stimulation, whose nuclei are then isolated by FANS. Neurons are represented by grey triangles. Activated neurons are connected by dashed lines and their green nuclei represents the expression of Sun1-GFP. **B**. NGS-methodologies for transcriptome and epigenome analysis are represented in the diagram, classified based on their applications for studying chromatin interactions, chromatin accessibility, protein-DNA interactions, transcription or DNA methylation. Hi-C: high-throughput chromosome conformation capture; pcHi-C: promoter

capture Hi-C; ChIA-PET: chromatin interaction analysis by paired-end tag sequencing; ATAC-seq: assay for transposase accessible chromatin with high-throughput sequencing; THS-seq: transposome hypersensitive site sequencing; ChIP-seq: chromatin immunoprecipitation; ChEC-seq: chromatin endogenous cleavage with high-throughput sequencing; CUT&RUN: cleavage under targets and release using nuclease; CUT&Tag: cleavage under targets and tagmentation; RNA-seq: RNA sequencing; nuRNA-seq: nuclear RNA-seq; Ribo-seq: ribosomal RNA immunoprecipitation sequencing; RRBS: reduced representation bisulphite sequencing; WGBS: whole-genome bisulphite sequencing (Adapted from Fuentes-Ramos, Alaiz-Noya and Barco, 2021).

1.4 Environmental paradigms for studying gene-environment interactions

Alongside the array of genetic strategies and NGS methodologies that allow us to address longstanding questions about the role of epigenetic mechanisms in gene-environment interactions, there arises a concurrent need for standardizing experimental paradigms that facilitate the controlled manipulation of environmental conditions while treating the genetic component as a constant. To fulfil this requirement, various laboratory-based environmental paradigms have emerged over the years, where genetically identical inbred rodents are used to maintain genetic constancy (Kempermann, 2019).

After Donald O. Hebb's early discovery that domestic rats performed better in problem-solving tests than rats raised in laboratory cages (Hebb, 1947), numerous studies have embraced the concept of an Environmental Enrichment (EE) paradigm to explore the impact of exposure to a stimulating setting on cognitive development. Mark R. Rosenzweig defined the EE paradigm as "a combination of inanimate and social stimuli" (Rosenzweig & Bennett, 1996). While the basic setup involves housing groups of rodents in larger-than-standard cages, often equipped with toys, wheels, hiding tubes and nesting materials, the precise configurations in each study can exhibit substantial variability. On occasion, the cage dimensions remain standard, yet a higher number of animals are accommodated to foster social interaction. Alternatively, solely toys are used as enrichment within standard cages. Moreover, the duration of exposure to

enrichment is occasionally manipulated, ranging from brief daily intervals to representing a long-term living condition.

It is important to recognize that the various components of the EE paradigm – physical activity, social interaction, and cognitive stimulation through exploration (Kempermann, 2019) – are interconnected and should be considered collectively, including their interactions. For instance, while physical activity by itself produces some effects that initially may seem quite similar to those of the EE paradigm (Van Praag et al., 1999), a detailed examination unveils the disparities in these seemingly analogous effects, particularly in terms of learning and memory (Garthe et al., 2016).

Numerous studies have described anatomical and cellular changes associated with EE (Diamond et al., 1964, 1972; Krech et al., 1960, 1962; Rosenzweig et al., 1962) and have demonstrated that laboratory mice subjected to EE exhibit enduring enhancement in cognitive abilities, along with morphological, molecular and electrophysiological changes within the hippocampus and other brain areas implicated in the establishment of memories. Specifically, the changes entail increased adult neurogenesis within the dentate gyrus, heightened synaptogenesis and neuronal complexity across distinct hippocampal subfields, and modifications in the inherent excitability and synaptic responses of hippocampal neurons (Ohline & Abraham, 2019; van Praag et al., 2000). Additionally, the EE condition ameliorates chronic disease phenotypes, enhances recovery from acute conditions both autonomously and as an adjunctive intervention (Nithianantharajah & Hannan, 2006), and sustains efficacy throughout life into advanced age (Diamond et al., 1985; Kempermann et al., 2002).

Interestingly, opposing outcomes in terms of modulating cognitive capacities, adult neurogenesis in the dentate gyrus, and structural changes in pyramidal neurons emerge following Environmental Impoverishment (EI) (Gregory & Szumlinski, 2008; Ibi et al., 2008; Melendez et al., 2004). In this paradigm, mice are housed in individual small cages without toys or nesting material. Consequently, this condition induces social and stimulus deprivation, with minimal interaction during scheduled bedding changes before the beginning of the experimental protocol. Widely employed, the EI paradigm explores the impact

of early-life stress and aids in understanding the pathogenesis of certain neurological and psychiatric disorders, including depression, anxiety, and diseases characterized by social deficits such as autism (Ago et al., 2007; Amiri et al., 2015; Koike et al., 2009; Okada et al., 2015).

Epigenetic chromatin changes have been proposed as a potential substrate for the enduring changes in behaviour and neuronal and circuit activity associated with both EE and EI. Supporting this perspective, previous investigations have demonstrated how specific chromatin modifications, including lysine (K) residue acetylation in histone tails and DNA methylation, are influenced by environmental conditions. Particularly, the acetylation of histone tails emerges as a pivotal player in mediating the benefits linked to EE (Fischer et al., 2007), and the lysine acetyltransferase (KAT) CBP has been identified as a significant mediator of EE-induced benefits (Lopez-Atalaya et al., 2011). Recent studies have also uncovered numerous enduring DNA methylation changes in neuronal plasticity genes within the hippocampus of mice subjected to early EE (Zocher et al., 2020), and have unveiled differences in DNA methylation between the dorsal and ventral hippocampus following EE exposure (Zhang et al., 2018). Moreover, early exposure to EE resulted in heightened chromatin accessibility and enhanced CTCF binding within postnatal cortical tissue (Espeso-Gil et al., 2021). Conversely, several commonly employed paradigms in laboratory animals to induce chronic stress have been documented to modify epigenetic marks, such as histone 3 phosphoacetylation and DNA methylation (Stankiewicz et al., 2013). It has been demonstrated that chromatin changes, spanning from epigenetic modifications to transposon mobilization, shift in response to environmental adversities in rodents (del Blanco & Barco, 2018; Kundakovic & Champagne, 2015; Roth et al., 2009; Weaver et al., 2004), primates (Provençal et al., 2012), and human subjects (McGowan et al., 2009). These changes have been identified within the hypothalamic-pituitary-adrenal axis, heavily involved in stress response, as well as in structures like the hippocampus, which are functionally compromised by EI.

It is important to note that in rodents, extended postnatal maternal separation leads to elevated levels of glucocorticoid hormones (Stanton & Levine, 1988), heightened stress responses, and impaired cognitive function (Andersen et al.,

1999; Lehmann et al., 1999). To mitigate the potential influence of these effects on our study conditions, mice in this thesis project are placed in distinct environmental conditions after weaning, when they are naturally separated from their mother. As a result, our focus is not investigating the negative outcomes arising from maternal separation on offspring cognitive development, but rather on understanding how the environment shapes cognitive abilities development during post-weaning stages.

1.5   Assessing cognitive capacities through memory engram formation

Up to this point, we have outlined how cognitive abilities are determined by the ongoing interplay between the genes and the environment, postulating that epigenetics could serve as the underlying substrate of this interaction. Cognitive abilities encompass a diverse array of skills, including attention, decision-making, reasoning, problem-solving, abstract thinking, and memory (Gottfredson, 1997).

Memory can be defined as the capacity to preserve and recover information (Zlotnik & Vansintjan, 2019). In psychology, memory is often divided in three phases, including encoding, storage and retrieval of information (Squire, 2009) (**Figure 3**). During memory encoding, the arrival of novel information triggers physical and/or chemical changes in a discrete set of cells which become allocated to that memory, designated as engram cells (Han et al., 2009; Josselyn & Frankland, 2018; Liu et al., 2012; Roy et al., 2016). During the subsequent storage phase, engram cells experience molecular consolidation, resulting in the enduring storage of memory across diverse levels of brain organization, spanning from the hippocampal area to the cortex (Kitamura et al., 2017; Tonegawa et al., 2018; Vetere et al., 2011). Lastly, the third phase involves memory retrieval, entailing the reactivation of engram cells upon encountering certain aspects of the previous experience, facilitating the recall of previously stored information (Reijmers et al., 2007). This thesis project will focus on exploring memory and engram cells as a correlate of how exposure to varying environmental conditions shapes cognitive abilities and the associated epigenetic changes.
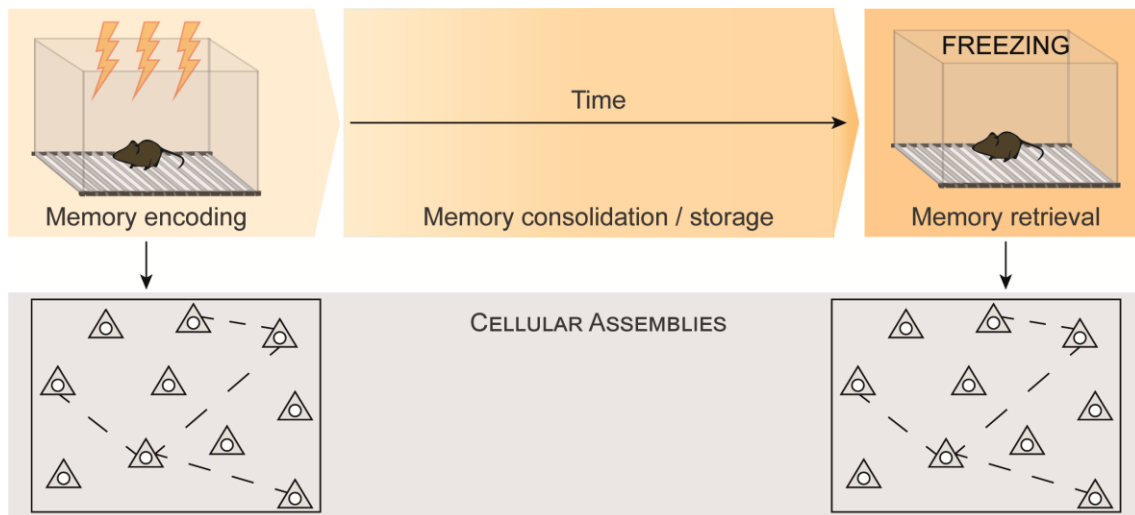
Figure 3. Memory phases. During memory encoding, a subset of cells (depicted by grey triangles) becomes activated in response to a stimulus (like an electric shock in a fear conditioning paradigm as illustrated in the upper-left scheme) and is allocated to that specific experience, forming the engram cells (cells connected by dashed lines). Over time, these cells undergo stabilization during the memory consolidation or storage phase, which can span from hours to days. Finally, memory retrieval occurs when engram cells are reactivated upon the presentation of elements from the initial experience. Obtained from (Fuentes-Ramos, Alaiz-Noya and Barco, 2021).

To explore engram cells and gain insights into the precise molecular changes that underlie the processes of encoding, consolidation, and long-term maintenance of memory, various genetic tools have emerged through decades of research (**Figure 4**). Initial strategies relied on techniques like fluorescence in situ hybridization (FISH) and immunohistochemistry (IHC) to identify mRNA and resulting proteins produced by the activation of IEGs like *Fos* and *Arc*. However, IEGs expression is inherently short-lived, imposing limitations on the assessment of later memory phases, such as consolidation or retrieval of stored information.

The development of genetic approaches enables the delayed or lasting tagging of active cells, facilitating longitudinal examination and exploration of molecular processes associated with memory storage and consolidation (Choi et al., 2020). The first approach relies on using IEG promoters to direct the expression of a fluorescent protein (FP), such as Venus or GFP, in active cells. The primary constrain of this strategy is that neuronal labelling is transient (lasting less than 24 hours) and depends on the activation dynamics of the IEG promoter (DeNardo & Luo, 2017).

The second approach also employs IEG promoters, but this time to direct the expression of an effector protein that subsequently regulates the expression of a secondary component situated within a distinct genomic region or introduced via a viral vector. This establishes a versatile binary framework with an extended temporal window, significantly enhancing the labelling of engram cells. As effector proteins, we can differentiate between the tetracycline transactivator (tTA) system, tightly regulated through the administration of doxycycline (dox), and the bacterial recombinase CreER^{T2} system, whose expression is controlled by tamoxifen administration (Allen et al., 2017; Guenthner et al., 2013; Reijmers et al., 2007). The main limitation of the tTA system is the slow clearance of doxycycline from the animal's body, resulting in a delayed marking of active cells after dox removal from the diet, whereas hydroxy-tamoxifen (4-OHT) administration allows for the immediate translocation of CreER^{T2} to the nucleus, improving temporal resolution.
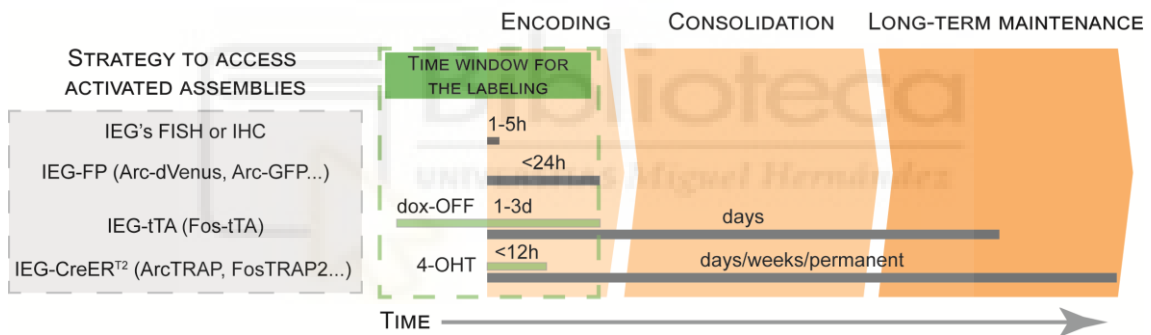
Figure 4. **Main strategies for labelling activated cells across memory phases**. The duration of labelling can vary from a few hours to a permanent state, depending on the strategy employed to access activated assemblies. While labelling based on FISH or IHC exhibits limited duration, approaches involving binary systems (such as IEG-tTA and IEG-CreER^{T2}) allow for more extended labelling (duration indicated by the grey bars). The intervals required for marking active cells with doxycycline (dox) and hydroxy-tamoxifen (4-OHT) are illustrated by the green bars – note that doxycycline removal (dox-OFF) from the organism is gradual and does not produce the prompt labelling of active cells. The consideration of these temporal intervals is essential to achieve precise labelling of engram cells based on the specific memory phase under investigation (orange boxes). Obtained from (Fuentes-Ramos, Alaiz-Noya and Barco, 2021).

Collectively, these cellular tagging techniques have enabled the recognition and exploration of cell assemblies responsive to experiences across various brain regions, including the amygdala, hippocampus, and cortex (DeNardo et al., 2019; Nonaka et al., 2014; Ramirez et al., 2013). This has opened avenues to delve

into their morphological characteristics, excitability, connectivity, and synaptic plasticity (Choi et al., 2018; Erwin et al., 2020; Josselyn & Tonegawa, 2020; Nonaka et al., 2014; Redondo et al., 2014; Roy et al., 2022; Ryan et al., 2015). Nevertheless, we remain unaware of whether specific changes occur in the formation of engrams after exposure to distinct environmental conditions and what specific epigenetic modifications are associated with these changes.

1.6 Editing the epigenome: From experience-driven epi-editing to "at-will" epi-editing

To fully grasp how epigenetic modifications lead to changes in gene expression that enable us to respond and adapt to a dynamic environment, we need tools that allow us to assess whether these alterations are necessary and/or sufficient to trigger transcriptional and functional modifications within the cellular ensemble.

While traditional approaches, based on inhibitor drugs for epigenetic enzymes and genetic strategies, have established connections between epigenetic modifications and alterations in gene expression, these analyses face constraints in elucidating the precise cause-and-effect relationship between the two (Hamilton et al., 2018). Experience-driven epigenetic mark deposition on a specific target gene using these approaches is studied in a genome-wide scale; hence, it is challenging to distinguish specific effects from pleiotropic consequences.

The development of epigenome editing tools, capable of introducing specific chromatin modifications at a desired target locus (described in detail in the following sections), offers a means to differentiate between the simple existence, or appearance, of epigenetic marks and the direct impact of these modifications on gene function and animal behaviour (Hamilton et al., 2018). For example, mimicking experience-triggered changes in engram cells or by erasing particular epigenetic marks linked to memory encoding or consolidation (**Figure 5**).
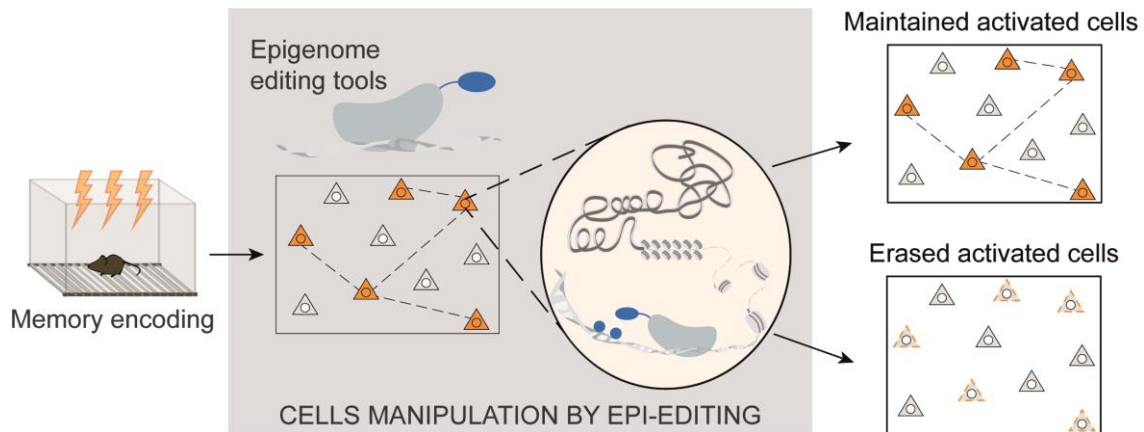
Figure 5. Evaluation of experience-driven epigenetic mark deposition on specific target genes by epi-editing tools. The epigenetic alterations taking place in cells activated by environmental stimuli or fear-inducing experiences (represented by yellow triangles), for example, could be precisely manipulated by epigenome editing tools. This approach would facilitate the exploration of which epigenetic marks contribute to the sustained maintenance of these activated cells over the long term (yellow solid neurons in the upper-right diagram), and even enable the erasing of specific epigenetic marks associated with this activation (yellow dashed neurons in the bottom-right diagram). Modified from (Fuentes-Ramos, Alaiz-Noya and Barco, 2021).

1.6.1 Initial genome and epigenome editing tools

The first epi-editing tools developed were based on Zinc Finger Proteins (ZFPs). These proteins belong to a large superfamily of eukaryotic transcription factors that present a Cys2-His2 zinc finger domain (Beerli & Barbas, 2002). This domain consists of 30 amino acids with the ability to interact with a precise DNA sequence made up of three nucleotides (and an additional one in the adjacent triplet). To increase binding specificity, individual finger motifs with established and verified sequence specificity can be combined to create arrays of ZFPs capable of recognizing 2, 3, 4 or even more DNA triplets (Sander et al., 2011). However, each of the selected ZFP might affect the binding affinity of the adjacent ZFP, which complicate the production of an efficient ZFP for epigenome editing.

The next type of epi-editing tool developed were transcription activator-like effector (TALE) proteins. TALEs are DNA-binding proteins derived from plant pathogenic bacteria and modified for genome and epigenome editing applications (Bashtrykov & Jeltsch, 2017). Their DNA-binding domain comprise a series of highly conserved tandem repeats of 33-35 amino acids sequences (termed monomers) (Yim et al., 2020), which interact with a single nucleotide within the

major groove of the DNA. TALEs offer greater customization compared to ZFPs due to their ability to bind to a single nucleotide, as they can also be organized in arrays of repeats to recognize a precise DNA target sequence (Boch et al., 2009; Jankele & Svoboda, 2014). However, their binding properties can differ based on the total monomer count, the specific identity of adjacent monomers and their arrangement within the TALE array.

Therefore, both ZFs and TALEs rely on the assembly of modules that enable specific protein-DNA interactions for target site recognition. This structure makes their construction time-consuming and technically challenging due to fixed DNA sequence binding requirements, laborious protein engineering for different genomic sequences and repetitive composition and size (Gilbert et al., 2013; Yim et al., 2020).

1.6.2 CRISPR: a ground-breaking genome editing tool

The discovery of Clustered Regularly Interspaced Short Palindromic Repeats (CRISPR) and CRISPR-associated (Cas) proteins has been one of the most impactful events for genome and epigenome editing, producing a dramatically accelerated progress in the field.

CRISPR-Cas system is an RNA-mediated immune adaptive defence system against invasive viruses and plasmids specific to bacteria and archaea (Ishino et al., 1987; Mojica et al., 2005). It uses an RNA molecule to form base pairs with foreign DNA target sequences and cleaves them by inducing double-stranded breaks within the DNA.

CRISPR-Cas systems have been classified into three types (I, II and III) based on their molecular mechanism to achieve nucleic acid identification and cutting. While types I and III need diverse proteins to function (Brouns et al., 2008), the type II system uses a singular endonuclease protein (Cas9), and a dual RNA molecule to guide DNA cleavage (Barrangou et al., 2007; Deltcheva et al., 2011; Garneau et al., 2010), making it the most widely used.

In type II CRISPR-Cas systems, adaptive immunity occurs in three stages (**Figure 6**). Initially, during the adaptation phase, small fragments of foreign nucleic acids (called spacers) are interspaced with identical repeats within the

CRISPR locus (Wiedenheft et al., 2012). The subsequent stage – termed biogenesis – involves transcribing the entire repeat-spacer element into precursor CRISPR RNA (pre-crRNA). The repeat sequences within the pre-crRNA are recognized by the small non-coding trans-activating crRNA (tracrRNA) through base pair complementary, which initiates a maturation process catalysed by the double-stranded RNA-specific ribonuclease RNase III and Cas9. This maturation results in the generation of individual CRISPR-derived RNAs (crRNAs), each comprising a repeat segment and a spacer portion that targets invading sequences (Deltcheva et al., 2011). Finally, in the interference phase, the RNA duplex formed by tracRNA and crRNA (tracrRNA:crRNA) identifies foreign nucleic acids (called protospacers), recognizing them through complementary sites within the crRNA spacer sequence (Brouns et al., 2008).

The invading nucleic acids are cleaved by Cas9 at specific positions determined by the complementary base pairs between the crRNA and the targeted protospacer DNA, in addition to a compact motif (called the protospacer adjacent motif or PAM), which is positioned adjacent to the complementary segment within the target DNA (Jinek et al., 2012). This PAM sequence is only preserved in the foreign genome, distinguishing self from foreign DNA (Mojica et al., 2009; Sapranauskas et al., 2011). PAM motifs consist of a small number of nucleotides, and their stringency varies among different types of CRISPR-Cas systems. For instance, the widely used Cas9 protein from *Staphylococcus pyogenes* requires a consensus NGG PAM sequence (Jinek et al., 2012), wherein "N" denotates any nucleotide.
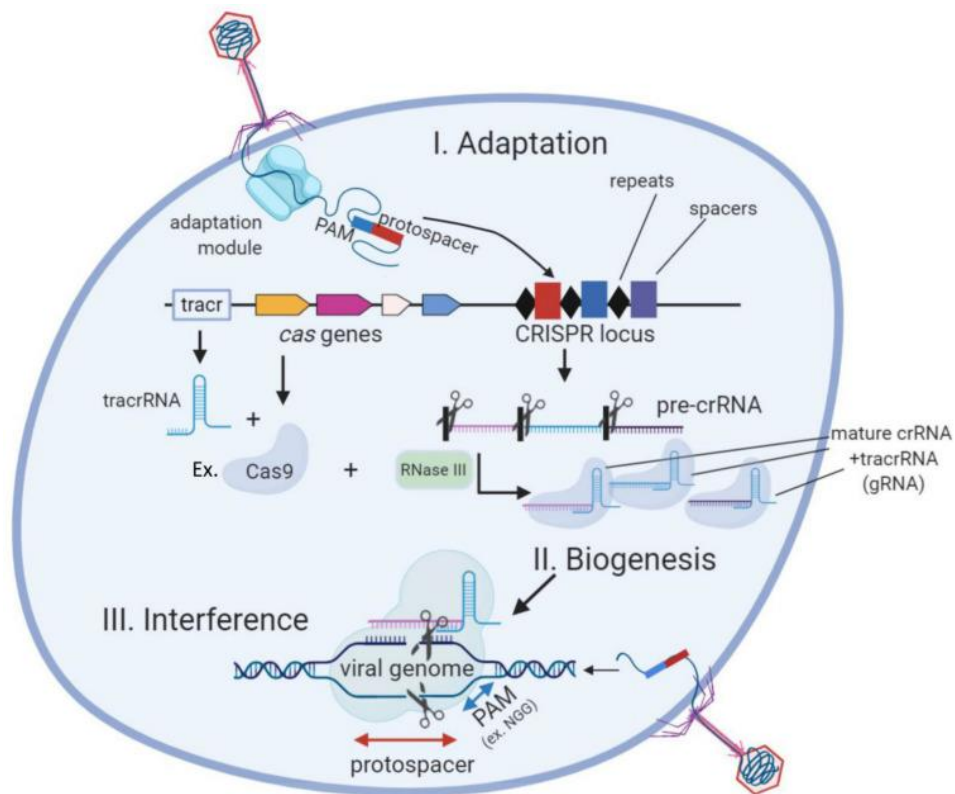
Figure 6. Stages of the immune adaptive CRISPR-Cas type II defence system. The adaptation phase begins with the infection of the DNA from an invasive phage into a bacterial cell, which is cut into small fragments (called spacers) and interspaced with identical repeats within the CRISPR locus. During the biogenesis phase, the CRISPR locus is transcribed into precursor CRISPR RNA (pre-crRNA). A complex involving tracrRNAs, Cas9 and RNase III processes this pre-crRNA, leading to the formation of mature crRNAs. Finally, in the interference phase, mature crRNAs pair with individual tracrRNAs and recognize foreign nucleic acids (called protospacers) through complementary sites within the crRNA spacer sequence and the presence of a PAM sequence, allowing Cas9 to induce precise double-strand breaks within the foreign DNA. Obtained from (Arroyo-Olarte et al., 2021).

1.7   Adaptation of the CRISPR system as an epi-editing tool

The field of biology experienced a transformative phase when the dual crRNA:tracrRNA was reconfigured as a single chimeric RNA molecule (termed guide RNA, gRNA) that retained two main characteristics: a target recognition sequence formed by 20 nucleotides and located at the 5' end of the gRNA, and a hairpin RNA structure located at the 3' end of the gRNA that interacts with Cas9 (Jinek et al., 2012). This finding allowed the creation of a simple two-component

system – the Cas9 protein and the gRNA – that can target any DNA sequence of interest by changing the 20-nucleotide target recognition sequence of the gRNA.

Moreover, early work showed that inactivating the two endonuclease domains of Cas9 – the HNH domain that cleaves the target DNA strand and the RuvC domain that cuts the non-target DNA strand – by point mutations (dCas9; Asp10 → Ala, His840 → Ala) resulted in a nuclease-dead Cas9 (dCas9) that retained DNA binding capacity without inducing cleavage (Jinek et al., 2013; Qi et al., 2013). The catalytically inactive dCas9 protein has emerged as a modular RNA-guided platform, enabling the targeted recruitment of different effectors to DNA with exceptional precision. This dCas9 protein serves as a DNA binding domain (DBD) and can be fused with distinct chromatin modifying domains (CMD), forming the chimeric protein dCas9-CMD. This allows for the interrogation of various facets of transcriptional regulation, epigenetic modifications, or even 3D genome architecture, depending on the specific CMD linked to dCas9 (Nakamura et al., 2021). In addition, employing dCas9-based molecules to regulate gene expression provides a diverse range of "gene switches", which serve as a versatile toolkit for investigating the causal associations between genes and their function, unravelling the functionalities of regulatory elements within the genome and delineating the roles of non-coding genes (Xu & Qi, 2019). In essence, the dCas9 system can be the foundation of a comprehensive toolbox for dissecting gene functionality and orchestrating modifications in cellular behaviours.

These advancements have profound implications across various fields, spanning from biotechnology to biomedicine, as epigenetic manipulations are no longer a constraining factor in experiments. The simplicity, efficiency, and versatility of this single RNA-single protein CRISPR system makes, in principle, possible the precise and efficient targeting, editing and regulation of genomic sites across a broad range of cells and organisms. However, there are still important challenges that should be faced for efficient epigenome editing in neuroscience (Hamilton et al., 2018), including the spatial and temporal control of CRISPR system expression in the wide variety of cell types present in the brain, and the selection of the best method for transgene delivery.

1.7.1 Cellular diversity and temporal control

Within the brain, there exist numerous intertwined cell types, each possessing distinct genetic expression signatures, connectivity patterns, and contributions to behaviour. However, many applications may require that epigenome editing only occurs in certain cell types. As a result, the development of methods for cell-type specific CRISPR system expression is necessary. One approach involves coupling Cre recombinase expression with recombination-dependent expression of CRISPR elements (Yim et al., 2020). Alternatively, promoters like the human synapsin 1 gene (*Syn1*) promoter for neurons (Kügler et al., 2003), or the glial fibrillary acidic protein (*Gfap*) promoter for astrocytes (Sofroniew & Vinters, 2010), have been utilized to direct transgene expression to the desired cell populations. However, the specificity of promoters for specific cellular subtypes is often limited, driving the expression of the construct of interest to a broader spectrum of cells than intended and, thereby, limiting the effective targeting of specific brain cell subtypes. Recent research suggests that enhancers might offer superior cell-type specificity; however, only a limited number have been currently empirically verified (Blankvoort et al., 2020).

Furthermore, achieving precise temporal control over epigenetic editing is essential for revealing the underlying causal significance of experience-dependent gene regulation. While light- or chemical-inducible epigenome-editing systems have been utilized to enhance temporal control over genetic manipulations, applying these techniques within the brain presents notable technical complexities (Day, 2019).

1.7.2 Delivering into postmitotic cells

Delivering dCas9 derivatives into the cells can be achieved by different approaches. Although it is feasible to transduce the elements of this tool to cells in culture through traditional transfection techniques and biolistical particle delivery (also known as "gene gun") (Xu & Heller, 2019), these approaches have not found widespread use for brain delivery *in vivo*.

Viral vectors expressing the gene-of-interest are the leading platform for *in vivo* delivery of genetic constructs in the brain (Policarpi et al., 2021). Such vectors include those based on (i) herpes simplex virus (HSV), characterized by large

packaging capacity (~14 kb), but short half-life (~ 7 days) and frequent neurotoxicity (WA et al., 2000); (ii) lentivirus (LV), that presents long-term expression and a relatively large packaging capacity (~ 8.5 kb), although it exhibits low infection rates *in vivo* and its safety profile remains variable due to genomic integration and high immunogenicity; and (iii) adeno-associated virus (AAV), which is distinguished by its long-term expression and low immunogenicity, yet it exhibits restricted payload capacity (~ 4.5 kb) (Nelson & Gersbach, 2016). Currently, AAV is the most commonly utilized viral vector for *in vivo* delivery due to its favourable safety profile – being non-pathogenic to humans, eliciting minimal immune reactions, and rarely resulting in undesired genome integration occurrences (Lau & Suh, 2018) –, as well as its very efficient viral delivery, transduction capabilities, and ability to achieve long-term and consistent transgene expression within specific tissues (Colella et al., 2017; Mingozzi & High, 2011).

The primary limitation of the AAVs for editing the neuronal epigenome lies in their restricted payload capacity, which is insufficient to incorporate a plasmid vector expressing both a dCas9 fused with an effector domain and a gRNA. Combining substantial effector domains with dCas9 is frequently necessary to achieve potent *in vivo* epigenome editing. Additionally, realizing synergistic outcomes demands the involvement of numerous dCas9 fusion proteins along with concurrent expression of multiple gRNAs. These various limitations collectively hinder the widespread adoption of AAVs for neuro-epi-editing delivery in adult organisms (Lau & Suh, 2018).

The discovery of compact Cas9 systems that fits AAV packaging limitations could potentially enable the use of these tools in strategies for editing the neuronal epigenome. Remarkably, Cas12f and Cas12j are a source of natural compact Cas effectors (Nguyen et al., 2022). Additionally, the adapted Cas12f system (termed CasMINI), exhibits a size that is 62% smaller than the widely used *S. pyogenes* Cas9 (Xu et al., 2021). However, these small variants usually exhibit limited performance in mammalian systems, necessitating the use of larger gRNAs to establish a suitably stable complex with the dCas9 protein capable of interacting with the DNA (Chang & Qi, 2023). Moreover, effector domains are also

large in size, hence the fusion proteins of those effectors with smaller Cas variants may still confront packaging issues in AAV vectors (Lau & Suh, 2018).

As an alternative approach, the split-intein system has been utilized for *in vivo* editing, where Cas9 was split into two parts, generating an N-terminal lobe (Cas9N) and a C-terminal lobe (Cas9C) using its disordered linker (V713-D718). Through this protein trans-splicing approach, full-length Cas9 is seamlessly reconstituted, maintaining its structure and function when both lobes are co-expressed (Chew et al., 2016). This strategy has also been used for *in vivo* gene repression using AAVs that express a split-KRAB-dCas9 system (Moreno et al., 2018) – KRAB (Krüppel-associated box) is a domain that recruits different epigenetic and chromatin modifiers to induce heterochromatin formation (Ying et al., 2015). Moreover, photoactivatable split dCas9-CMD tools have been develop to induce gene activation in human cell lines (Nihongaki et al., 2017), as well as to either activate or knock-down target genes in organoids for the spatiotemporal control of gene expression patterns (Legnini et al., 2023).

Lastly, efforts have been made to develop Cre-inducible mice expressing dCas9-effectors to overcome viral packaging constraints (Gemberling et al., 2021; Li et al., 2020; Zhou et al., 2018), as well as some rat transgenic lines that express Cre-dependent CRISPR gRNA constructs for achieving cell type specificity (Bäck et al., 2019b). A notable drawback of these approaches is their dependency on specific transgenic model systems, requiring resource-intensive crossbreeding with Cre lines and time-consuming management of animal colonies (Carullo et al., 2021).

Therefore, there is an ongoing need for alternative strategies to manipulate the neuronal epigenome *in vivo* efficiently and precisely, ensuring accurate experimental outcomes and advancing our understanding of complex neurological processes, such as plasticity.

1.8   Nanobody-based technologies

Conventional antibodies are structurally complex, large heterotetrameric proteins consisting of two light chains and two heavy chains, collectively referred to as

immunoglobulins (Janeway et al., 2001). While five distinct classes of immunoglobulins exist – A, D, E, G and M –, we will focus on immunoglobulin G (IgG) to describe conventional antibodies characteristics in humans and other mammals. IgG has a total molecular mass of 150 kDa. Each of its light chains is formed by a constant domain (CL) and a variable domain (VL) located at the tip of the Y-shaped molecule. In contrast, each of the heavy chains has three constant domains (CH1 to CH3) plus the variable domain (VH) (**Figure 7A**). Thus, the antigen binding site, also known as the paratope, is formed by the combination of the paired VL and VH domains (Könning et al., 2017).

In 1993, Professor Raymond Hamers-Casterman and colleagues discovered antibodies originating from dromedary camels infected with *Trypanosoma evansi* (Hamers-Casterman et al., 1993). These antibodies, prevalent among the *Camelidae* family and known as heavy-chain only antibodies (HCAb), lack light chains and CH1 domains, essential for light chain coupling, resulting in a decreased molecular mass of 90 kDa (**Figure 7B**). Consequently, they feature just a pair of heavy chains, each carrying a variable antigen binding domain, named VHH (Muyldermans, 2013).

The VHH fragment of an HCAb, termed "nanobody" by the Belgian company Ablynx®, derives its name from its diminutive dimensions, characterized by a width of 2.5 nm, a length of 4 nm, and a molecular weight of just 15 kDa (Bao et al., 2021; Revets et al., 2005; Wolfson, 2006). Nanobodies (Nbs), similar to VH domains of conventional antibodies, encompass three hypervariable complementarity-determining regions (CDR) and four conserved framework regions (FR), which determine antigen specificity (**Figure 7C**), but contrary to conventional antibodies, these are encode by a single polypeptide chain.

Regarding the CDR domains, they congregate at Nbs' N-terminal to fashion the antigen binding site (Jin et al., 2023; Wagner & Rothbauer, 2021). While Nbs require only three CDRs to form the paratope, conventional antibodies pair the VH domain with the VL domain, necessitating six CDRs in total for the full recognition of antigens (Sun et al., 2021). Although Nbs are thought to have a limited antigen-binding range owing to the lack of the VL domain, this restriction is overcome by an expanded CDR1 that amplifies the size of the paratope, resulting in a broader spectrum of loop structures that deviate from the typical

configurations seen in other VH domains (Decanniere et al., 2000; Nguyen et al., 2000). Furthermore, while the three CDR domains of both VH and VL conventional antibodies have been demonstrated to uniformly contribute to antigen binding, Nbs deviate from this pattern; the CDR3 domain of Nbs is elongated and exhibits a heightened propensity to interact with the antigen, serving as the primary element influencing paratope affinity (De Genst et al., 2006; Mitchell & Colwell, 2018; Muyldermans et al., 1994; Vu et al., 1997). Moreover, CDR3 increased dimensions result in a convex paratope surface, differing from the typical flat or concave paratopes observed in VH-VL antibody domains (Muyldermans et al., 2009). This leads the paratopes of Nbs to selectively target concealed epitopes or cavities that remain inaccessible for conventional antibody paratopes, including enzyme active sites and receptor-binding pockets (Bao et al., 2021).

Regarding FR domains, one notable structural feature of Nbs is the specific arrangement of hydrophilic amino acid residues within FR2, which contrasts with the hydrophobic amino acid residues found in the FR2 of the VH domain of conventional antibodies due to its interaction with the VL domain, essential for its functionality. This disparity explains their capability to exist independently as soluble monomers.
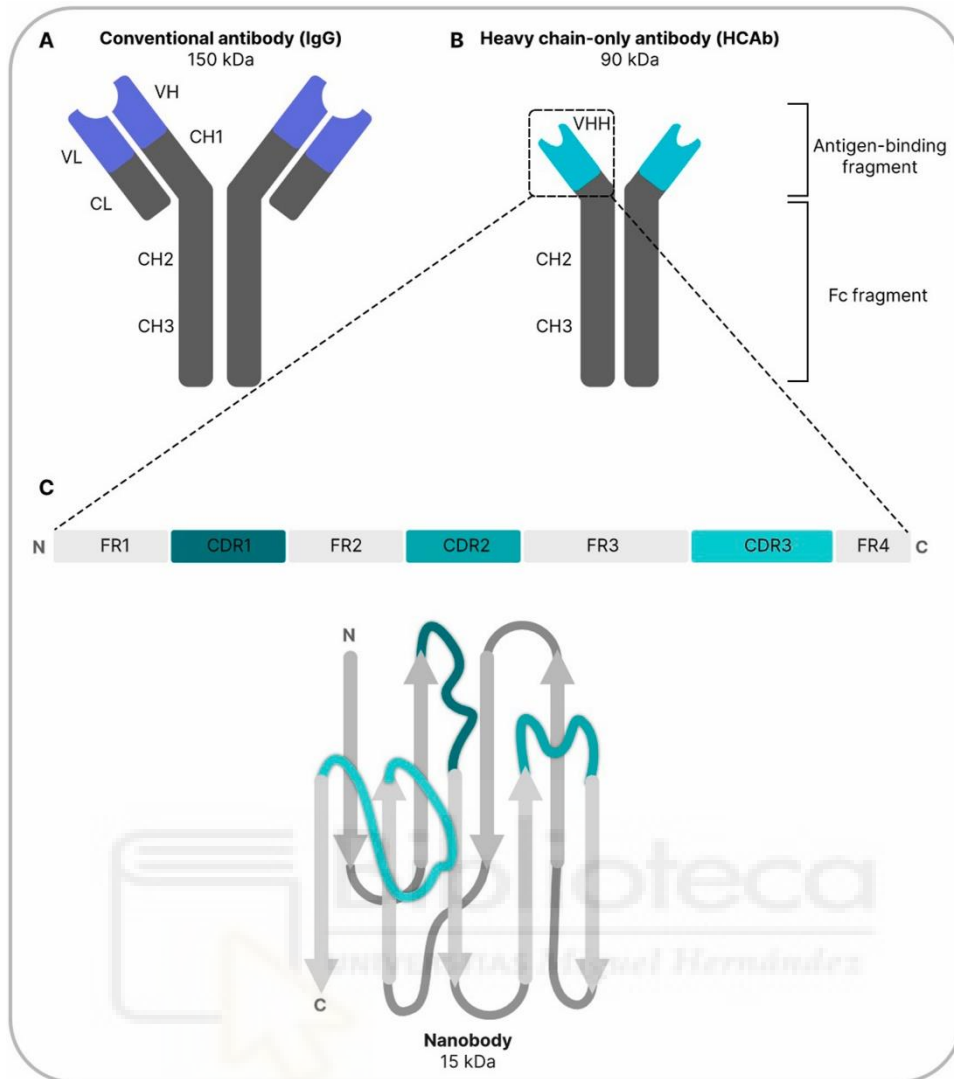
Figure 7. Comparison scheme illustrating the paratopes of IgGs (conventional antibodies), HCAbs (heavy chain-only antibodies) and Nbs (nanobodies). A. IgGs' paratope (depicted in cyan) is constituted by the paired variable domains (VL and VH) from the two identical light and heavy chains comprising IgGs. **B**. HCAbs' paratope (depicted in turquoise) is exclusively formed by the VHH fragment, as HCAbs lack the light chain and the CH1 domain. **C**. The VHH fragment, also referred to as nanobody (Nb), comprises four framework regions (FR1–4) and three hypervariable domains (CDR1-3) that fold into two beta-sheets, with the CDRs forming the paratope located at the N-terminal of the Nb. Obtained from (Wagner & Rothbauer, 2021).

In addition to camelids, certain shark species also possess HCAbs, known as immunoglobulin new antigen receptors (NAR), which recognize antigens using a sole variable domain termed the variable domain of NAR (V-NAR). The VHHs and V-NARs share numerous characteristics, including the tendency to selectively bind to cavities or grooves on the antigen's surface (Flajnik et al., 2011). However, their structural architecture differs slightly and V-NARs exhibit

higher level of sequence divergence from the variable domains of mammalian immunoglobulins, such as VHH or human VH (Muyldermans, 2021). They are also used less frequently due to the increased challenges associated with the handling of such animals (Flajnik & Kasahara, 2009; Streltsov et al., 2005).

1.8.1 Nanobodies applications

Nbs find extensive utilization in both research and clinical context due to their exceptional target specificity and compact size.

On the one hand, Nbs fusion with radioisotopes holds great potential for diagnostic purposes such as single photon emission computed tomography (SPECT) or positron emission tomography (PET), due to their high specificity, good tissue penetration, and rapid elimination from the bloodstream, which significantly reduces the signal-to-noise ratio compared with conventional IgGs (Huang et al., 2008; Keyaerts et al., 2016; Movahedi et al., 2012). Nbs have also found applications in visualizing and tracking alterations in the dynamics of tumour cells when they are treated with different agents (Traenkle et al., 2015). In addition, new Nbs are continuously being developed to interfere with the function of proteins associated with diseases such as cancer, or to prevent viral or bacterial infections by blocking the interaction of the target protein with other proteins, preventing its stabilization, blocking its active conformation, or preventing the activation of an agonist (Böldicke, 2017).

On the other hand, in research, Nbs fused to a fluorescent protein, called chromobodies, can be used to visualize nano-sized cytoskeleton components by super-resolution microscopy (Ries et al., 2012; Virant et al., 2018) or to study the dynamics of proteins of interest over time by imaging in living cells (Boersma et al., 2019; Burgess et al., 2012). Fusing Nbs with fluorophores instead of the proteins of interest has the main advantage that the native protein state is not affected. Hence, their expression level, activity, or localization within the cell remains unaltered. Moreover, to understand signalling cascades and cross-talk between proteins, Nbs are fused with sensors of cellular activities, e.g., sensors of Ca^{2+} level, pH, or ATP/ADP balance (Prole & Taylor, 2019). Nbs have also been engineered to sense conformational changes of proteins and to observe rapid changes in receptor states once they are activated or their ligand binds within live

cells. In a different application, Nbs have been fused with Tn5 bacterial transposase, allowing for the simultaneous mapping of up to three epigenetic marks at the single-cell resolution level, shedding light on the collaborative functioning of distinct epigenetic layers in the precise regulation of gene expression (Bartosovic & Castelo-Branco, 2022). Nbs have also found utility in loss-of-function experiments through knockout or knockdown of the target protein. In the former approach, a Nb that recognize the protein of interest is fused to an element of the intracellular degradation machinery (Caussinus et al., 2011), leading to its targeted degradation. In the latter approach, the Nb can induce mislocalization of the protein of interest by binding to a specific cellular compartment (Jayanthi et al., 2021), or it can recruit an epigenetic repressor domain to the gene of interest to decrease its expression without modifying its DNA sequence (Van et al., 2021).

Additionally, Nbs can be readily generated and produced in distinct expression systems, including yeast cells and E. coli (Kim et al., 2023), and the genetic fusion of the Nb coding sequence with other gene is highly efficient, providing the designed construct upon expression.

All these advantageous properties of Nbs – particularly their compact size and remarkable target specificity – have been harnessed in this thesis to develop an epigenome editing system, termed split dCas9-CMD toolbox (fully described in the *Results* section 2), that stays within the packaging capacity limitations of neurotropic vectors.

1.9 *Bdnf* as a target gene to explore experience and "at-will" changes in the epigenome

Brain-derived neurotrophic factor (*Bdnf*) is the most abundant neurotrophin in the mammalian brain (Huang & Reichardt, 2001) and plays significant roles in cell differentiation, neuronal survival, synaptogenesis, and different activity-dependent synaptic plasticity forms, such as long-term potentiation (LTP) and memory (Black, 1999; H. Park & Poo, 2013).

The rodent *Bdnf* gene spans approximately 50 kilobase pairs (kbp) and comprises eight 5' non-coding exons and a single 3' coding exon (Aid et al., 2007; Cunha et al., 2010). There is a unique promoter in each of these non-coding exons which governs the expression of specific *Bdnf* transcript variants. This arrangement allows for the precise regulation of *Bdnf* expression in response to neuronal activity and tissue-specific demands during both development and adulthood (Esvald et al., 2023; Liu et al., 2006; Nair et al., 2007; Sathanoori et al., 2004; West et al., 2014). As a result, depending on factors such as the developmental stage, brain region, and neuronal activity, specific *Bdnf* transcripts are produced containing the upstream spliced non-coding exon along with the common coding exon. Furthermore, within the *Bdnf* coding exon, several polyadenylation sites can be found, leading to the production of *Bdnf* transcripts featuring either a short (approximately 1.6 kbp) or a long (around 4.2 kbp) 3' untranslated region (UTR) (Fukuchi & Tsuda, 2010; Timmusk et al., 1993). The length of the 3' UTR influences the secondary structure of the resulting mRNA, which impacts mRNA stability by altering the accessibility of miRNA target sites. Consequently, *Bdnf* transcripts with short 3' UTRs are more stable than transcripts with long 3' UTRs (Castren et al., 1998; Varendi et al., 2014; Will et al., 2013). Moreover, different *Bdnf* 3' UTRs lead to distinct localization patterns of *Bdnf* transcripts within cellular compartments. The majority of *Bdnf* transcripts possess short 3' UTRs and are primarily located in the cell soma (Will et al., 2013), whereas transcripts with long 3' UTRs are found in dendrites, where they promote the maturation of dendritic spines (An et al., 2008).

This intricate arrangement, in combination with its important role for neuronal plasticity, allows us to assess the functionality and effectiveness of the split dCas9-CMD toolbox using *Bdnf* as a target gene (**Figure 8**). Specifically, promoters I and IV of the *Bdnf* gene have been selected as target regions, as they produce two *Bdnf* transcript variants that respond to neuronal stimulation, are regulated by the epigenetic machinery and are involved in the regulation of LTP and memory formation (Bredy et al., 2007; Lubin et al., 2008; Panja & Bramham, 2014).
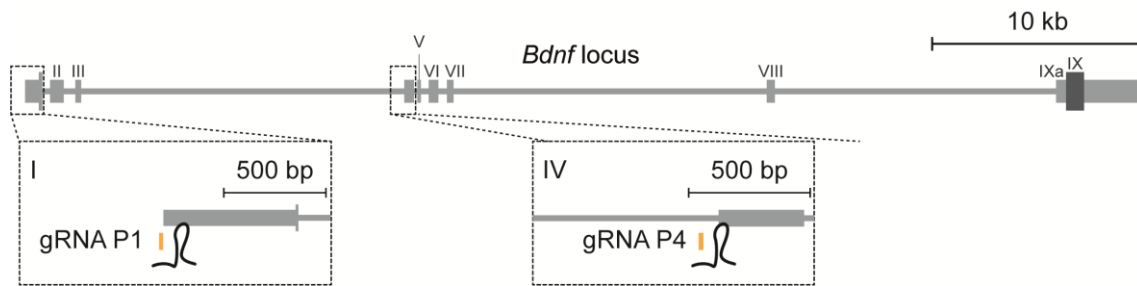
Figure 8. *Bdnf* locus structure and specific gRNAs to *Bdnf* promoters I and IV. *Bdnf* exons are represented by rectangles (non-coding exons in grey and coding sequence in exon IX in darker grey). Roman numerals above each rectangle indicate exon numbers. Grey line represents introns. The specific binding sites for the gRNAs used in this thesis project are represented in orange in the enlarged view of exons I and IV. The gRNA specific for promoter I is named gRNA P1 and the gRNA specific for promoter IV is called gRNA P4.

Furthermore, there is evidence supporting the experience-dependent regulation of neurotrophins production. Particularly, during early developmental stages, experiences such as maternal separation led to a reduction in *Bdnf* levels within the hippocampus (Bai et al., 2012). Similarly, early exposure to abusive maternal care results in increased *Bdnf* methylation levels in the prefrontal cortex and reduced expression (Roth et al., 2009). However, changes in *Bdnf* levels within the hippocampus were not exclusive to offspring subjected to abusive mothers but also in offspring exposed to nurturing mothers. This suggests that variations in *Bdnf* levels are influenced not only by caregiving experiences but also by factors like exposure to novel caregivers, adaptation to new environments, and the separation of offspring from their original home and maternal attachment (Roth et al., 2009).

Positive experiences also modulate *Bdnf* levels in the brain. For example, exposing 3-week-old mice to an enriched environment leads to an increase in *Bdnf* within the arcuate nucleus of the hypothalamus after 2 weeks of exposure, and this elevation persists throughout time in this condition (Cao et al., 2010). Moreover, there is an upregulation in H3K4me3 and a downregulation in H3K9me3 and H3K27me3 at *Bdnf* promoters (Kuzumaki et al., 2011).

In adulthood, it has been shown that *Bdnf* levels rise in various brain regions, such as the cerebral cortex, the basal forebrain, and the posterior brain, when adult animals are housed in an enriched environment for a year, compared to animals exposed to an impoverished environment during the same period (Ickes

et al., 2000). Similarly, *Bdnf* levels increase in the hippocampus of adult mice subjected to 8 weeks of environmental enrichment (Rossi et al., 2006). However, *Bdnf* levels remain unaffected when adult rats were exposed to different environmental stressors for 3 weeks (Bai et al., 2012).

In summary, these findings suggest that neurotrophins play a pivotal role as intermediary factors in brain plasticity (Branchi et al., 2004), contributing to the intricate interplay between the genes and the environment explored in the first *Results* section of this thesis. Moreover, the unique features of the *Bdnf* gene makes this locus particularly suitable for testing the efficacy and specificity of the epi-editing split dCas9-CMD toolbox, addressed in the second *Results* section of this thesis.

2. AIM OF THE PROJECT

While epigenetic mechanisms have been proposed as the substrate for gene-environment interactions, a comprehensive model that explains this interplay within the context of neural circuit adaptation to environmental cues and their impact on the formation of memory engrams remains elusive. Moreover, to elucidate the significance of epigenetic modifications in pivotal transcriptional programs during plasticity and enduring alterations in behavioural outcomes, it is necessary to develop epigenome editing tools for the precise manipulation of the neuronal epigenome to rigorously investigate the causality behind these modifications. According to these needs, this thesis is structured into two sections, each with its own set of specific objectives.

Section 1: Transcriptional and epigenetic bases of modulation of cognitive abilities by rearing conditions

I.   To assess the persistence of changes induced by early exposure to different environmental conditions on cognitive performance in adulthood.

II.   To analyse engram formation following early exposure to different environmental conditions.

III.   To examine changes in transcriptional and chromatin accessibility patterns promoted by exposure to different environmental conditions in early stages.

Section 2: Development of a toolbox for precise neuronal epigenome editing

IV.   To test an innovative and versatile toolbox for neuronal epigenome editing based on CRISPR-dCas9 and nanobody technologies in neural cell lines.

V.   To evaluate the efficacy of the toolbox through gain and loss of function experiments in primary neuronal cultures.

VI.   To adapt the toolbox for *in vivo* epigenome editing experiments.

3. MATERIALS AND METHODS

3.1 Mice

Mice were kept in a controlled environment with a constant temperature (23 ºC) and humidity (40-60 %), on 12 h light/dark cycles, with food and water *ad libitum*. They were maintained in a sterile room located within the Animal House at the Instituto de Neurociencias (CSIC-UMH). All animal experiments were performed in agreement with Spanish and European regulations and received approval from the Institutional Animal Care and Use Committee.

The pCamKIIα-CreER[T2] mouse strain (Erdmann et al., 2007) and the TRAP2 (pFos-CreER[T2]) mouse strain (Allen et al., 2017; DeNardo et al., 2019) were bred with the pCAG-[STOP]-Sun1-GFP mouse strain (Mo et al., 2015) to label the nuclei of forebrain principal neurons or activated neurons, respectively, using the nuclear envelope protein Sun1 fused with the reporter GFP. The recombinant protein CreER[T2] is dependent on tamoxifen administration. Hence, to remove the STOP cassette and enable Sun1-GFP expression, pCamKIIα-CreERT2xpCAG-[STOP]-Sun1-GFP mice received 5 doses of tamoxifen orally every other day, whereas TRAP2xpCAG-[STOP]-Sun1-GFP mice were given 4-hydroxytamoxifen via intraperitoneal injection. All these mouse strains were maintained on a C57BL/6J genetic background. The primers used for genotyping are listed in **Table 1**.

Mouse strain	Primer 1	Primer 2	Primer 3
pCamKIIα-CreER[T2]	GGTTCTCCGTTTGCACTCAGGA	CTGCATGCACGGGACAGCTCT	GCTTGCAGGTACAGGAGGTAGT
pCAG-[STOP]-Sun1-GFP	GCACTTGCTCTCCCAAAGTC	CATAGTCTAACTCGCGACACTG	GTTATGTAACGCGGAACTCC
pFos-CreER[T2]	GTCCGGTTCCTTCTATGCAG	GAACCTTCGAGGGAAGACG	CCTTGCAAAAGTATTACATCACG

Table 1. Primer pairs used in this study for genotyping.

3.2   Behavioural testing

All behavioural tests were performed with female mice to reduce the frequent fighting among male mice housed in an enriched environment (n = 10-15 C57BL/6J wild type mice per environmental condition – unless otherwise specified). Mice were handled for several days prior to the start of the battery of behavioural tests. Before performing each of the behavioural tests, a period of habituation to the behavioural room of about 30 minutes (min) was carried out, where the animals remained in their cages inside the room.

3.2.1   Open field

The Open field test (OF) was conducted in 48 x 48 x 30 cm white acrylic glass boxes, where mice were allowed to freely move for 20-30 min. Mice behaviour was monitored by the video tracking system SMART (Panlab S.L. Barcelona, Spain). The arena was divided into centre, middle and periphery, and the time spent in each area, the total distance travelled, and the average speed were estimated.

3.2.2   Y-maze

Mice were allowed to freely explore a Y-shaped maze constructed from transparent Plexiglas for the assessment of their working memory. An error was recorded each time a mouse revisited the same arm more than once.

3.2.3   Morris water maze

To assess spatial memory, we conducted the Morris water maze test (MWM) within a circular tank with a diameter of 170 cm, which was filled with non-toxic white paint. Mice behaviour was monitored using the video tracking system SMART (Panlab S.L. Barcelona, Spain). During the initial three days of the test, referred to as visible phase (V1-V3), a 10 cm diameter platform with a black flag was provided, and mice were trained to locate it in order to exit the water. From days four to seven, known as the hidden phase (H1-H4), the platform was submerged beneath the water surface in the centre of the target quadrant and external cues were placed on the walls of the room. Subsequently, during days eight to twelve, referred to as the reversal phase (R1-R5), the platform was

relocated to a new position, requiring the animals to learn its new location for their exit from the water. Each day, every mouse underwent four trials, with inter-trial intervals lasting from 30 to 60 min. The trials continued until the mouse reached the platform or for a maximum of 2 min. If the mice did not find the platform after 2 min, they were gently guided to it. Mice were returned to their cages only after remaining on the platform for at least 10 seconds (sec). Memory retention probe trials (PT) of 1-min duration were conducted at the beginning of session R1 and on the day following R5 to assess mice's memory from previous sessions. During these probe trials, the platform was removed from the water, and the number of entries made by the mice into each quadrant of the pool were recorded.

3.2.4 Novel object recognition

The novel object recognition (NOR) test was performed in 48 x 48 x 30 cm white acrylic glass boxes to which mice were habituated for 15 min one day before the training session. The next day, mice were exposed to a 3 min (EE vs SC) or a 15 min (EI vs SC) training session, when two identical objects were located inside the boxes. 24 h later, mice underwent a 10-min test session, when one of the identical objects was substituted by a new different one. The discrimination index was calculated by the formula: (TN – TF) / (TN + TF), where T = time of exploration, N = new object, F = familiar object.

3.2.5 Contextual fear conditioning

For the standard contextual fear conditioning (CFC) protocol, mice were introduced into a fear conditioning chamber (Panlab S.L., Barcelona, Spain), which was equipped with an electrified grid. On the conditioning session, mice were allowed to explore the fear conditioning chamber for 2 min. Afterwards, they received a single 0.4 mA, 2 sec footshock and mice remained in the box for 1 additional minute. The time animals remained still (freezing) was registered through a piezoelectric sensor located at the bottom of the fear box. To assess contextual memory, 24 h after the conditioning session mice were returned to the same box for 3 min, and their freezing behaviour was measured.

For the stronger CFC protocol, mice were trained for 30 min in a 40 x 40 cm arena with objects and an electrified grid and received footshocks (0.5 mA, 2 sec) every

77

5 min. After 6 days, mice were re-exposed to the same context to evaluate long-term memory and sacrificed 75 min after recall to evaluate engram formation. This protocol was used with TRAP2-Sun1-GFP mice (n = 4-6 per environmental condition).

3.2.6 Context discrimination and fear extinction

A different cohort of C57BL/6J mice were used (n = 4-9 per environmental condition). Mice were trained for 30 min in a 40 x 40 cm arena with objects and an electrified grid, termed Context A, and received footshocks (0.5 mA, 2 sec) every 5 min. After 6 days, mice were first re-exposed to Context A to evaluate long-term memory and after to a completely different context, termed Context B, to assess context discrimination ability. Extinction learning was evaluated by exposing the mice to Context A consecutively for 1 week.

3.3 CA1 and DG dissection

Manual dissection of CA1 and DG has been previously described (Hagihara et al., 2009). Briefly, mice were euthanized via cervical dislocation and their brains were removed from the skull. The brain was bisected along the longitudinal fissure of the cerebrum and the olfactory bulbs and cerebellum were removed. Positioning the cerebral hemisphere upwards allowed for the removal of the diencephalon (thalamus and hypothalamus) under a dissection microscope, thereby exposing the medial side of the hippocampus. Hippocampus boundaries were separated from the entorhinal cortex and, subsequently, CA3, CA1 and DG were brought into view. CA3 was initially removed, leaving the remaining DG and CA1 regions to be carefully separated along the septo-temporal axis of the hippocampus. The primers used for evaluating the accuracy of the dissections are listed in **Table 2**.

Target	Forward	Reverse
Dsp	GCTGAAGAACACTCTAGCCCA	ACTGCTGTTTCCTCTGAGACA
Tdo2	TTTATGGGCACTCTGCTT	GGCTCTGTTTACACCAGTTTGAG
Nov	GTCACCAACAGGAATCGCCAGT	TACCTTGTCTGTTACTTCCTC

Table 2. Primer sequences used for CA1 and DG dissection evaluation.

3.4   Fluorescence-activated nuclei sorting (FANS)

All steps were performed at 4 ºC unless indicated otherwise. Mice were euthanized via cervical dislocation and the CA1 and DG hippocampal layers were dissected from the brain and processed independently. The cell membrane was disrupted, and the nuclei extracted by mechanical homogenization using a 2 ml Dounce homogenizer (Sigma-Aldrich) containing 500 µl of Nuclei Extraction Buffer (NEB: Sucrose 250 mM, KCl 25 mM, $MgCl_2$ 5 mM, HEPES-KOH 20 mM (pH 7.8), IGEPAL CA-630 0.5 %, Spermine 0.2 mM, Spermidine 0.5 mM, and 1x proteinase inhibitors (cOmplete EDTA-free, Roche)). A pool of 3 mice were mix (CA1 and DG independently), having a total volume of 1.5 ml NEB containing the nuclei for each hippocampal layer. Samples were filtered in a 35 µm mesh capped tube and incubated with 0.01 mM DAPI (4,6-diamidino-2-phenylindole; Invitrogen) for 10 min in darkness in a rotator. Nuclei isolation was accomplished by the preparation of a gradient of different densities in which nuclei stay in the interphase. Nuclei were diluted in Optiprep density gradient medium (1114542, Proteogenix) to a final concentration of 22 %. For the density gradient, 44 % Optiprep was added to a centrifuge tube followed by 22 % Optiprep containing the nuclei. Additional 22 % Optiprep was added until the tube was filled. After 23 min of centrifugation at 7500 x rpm, the phase containing the nuclei was collected in a new tube containing Nuclei Incubation Buffer (NIB: sucrose 340 mM, KCl 25 mM, $MgCl_2$ 5 mM, HEPES-KOH 20 mM (pH 7.8), Spermine 0.2 mM, Spermidine 0.5 mM, 1x proteinase inhibitors, Newborn calf serum 5 %). Sorting of Sun1-GFP+ nuclei was performed in a flow-cytometer FACS Aria III (BD Bioscience) in collaboration with the technical personnel of the Omics facility in Instituto de Neurociencias. Every day, a pool of 3 mice was processed to obtain one sample of CA1 nuclei and one sample of DG nuclei. These samples were then utilized for both ATAC-seq, where 75,000 nuclei underwent tagmentation, DNA purification, and were stored at -20 ºC, and nuRNA-seq, where the remaining nuclei were mixed with TRI-reagent and stored at -80 ºC.

3.5   Perfusion

Mice were anesthetized using a combination of ketamine 100 mg/kg and xylazine 20 mg/kg. Once they lost any kind of reflex, mice were perfused with PBS to wash out the blood by injection into the left ventricle until the liver was turning from dark red to light brown colour. Then, 4 % paraformaldehyde (PFA, Merck) was injected until the animals were completely stiff (around 200 ml). Brains were carefully removed from the skull and immersed in 4 % PFA for an overnight incubation. Brains were sectioned into 50 μm slides using a vibratome.

3.6   Cell lines

Mus musculus brain neuroblastoma cell line (N2a) was used for split dCas9-CMD toolbox evaluation. N2a cells were maintained in Dulbecco's modified Eagle's medium (DMEM) high glucose and pyruvate, with heat-inactivated foetal bovine serum 10% (Thermo Scientific), L-glutamine 2 % (Thermo Scientific) and penicillin/streptomycin 1 % (Thermo Scientific) at 37 ºC and 5 % CO_2. Mycoplasma test was negative.

Human embryonic kidney cells that express a mutant version of the SV40 large T antigen (HEK293T) were used for virus production. HEK-293T cells were maintained in Dulbecco's modified Eagle's medium (DMEM) with heat-inactivated foetal bovine serum 10 %, L-glutamine 1 % and penicillin/streptomycin 1 % at 37 ºC and 5 % CO_2. Mycoplasma test was negative.

3.7   Primary hippocampal neuronal cultures

Primary neuronal cultures from Swiss albino mice were prepared as previously described (Benito et al., 2011). Briefly, pregnant female mice were euthanized through cervical dislocation, and embryos of either sex were taken out for hippocampi dissection. Roughly 24-28 hippocampi, pooled from 12-14 embryos, were combined in a 15 ml tube for each culture. Dissected hippocampi were digested with trypsin 2.5 % (Thermo Scientific) and homogenised by pipetting.

Cell numbers were determined using a Neubauer chamber, and cells were cultured in 24-well plates that have been pre-coated with poly-D-lysine (Merck), with a density of 130,000 cells per well. For immunostaining experiments, 12 mm glass coverslips (VWR), also coated with poly-D-lysine, were added to the wells. Cultures were maintained at 37 °C with 0.5 % CO_2, and after an incubation period of 2–3 h, the plating medium (DMEM supplemented with FBS 10 %, glucose 0.45 % (Merck), glutamine 2 mM, and penicillin/streptomycin 2 mM) was replaced with maintenance medium (Neurobasal medium supplemented with B27 (Thermo Scientific), glutamine 2 mM, and penicillin/streptomycin 2 mM).

In experiments requiring the induction of neuronal activity, D-AP5 100 µM (Tocris) and TTX 1 µM (Tocris) were added one day prior to the administration of KCl buffer (KCl 170 mM, $CaCl_2$ 2 mM, $MgCl_2$ 1 mM, HEPES 10 mM pH 7.4) to induce synchronous neuronal activation.

3.8   Lentivirus production and concentration

The production of lentiviral particles was conducted following established procedures, as previously described (Benito et al., 2011; Gascón et al., 2008). Briefly, HEK293T cells were plated at a density ranging from 8 to 10^7 cells in 15 cm dishes and incubated overnight. Transfection was accomplished using the calcium phosphate method, with a mixture consisting of either 20 or 40 µg of transgene-bearing plasmid (20 µg of gRNA plasmids, 40 µg of dCas9-vhhGFP4 plasmid or 40 µg of GFP-CMD plasmids), 15 µg of pCMV–∂8.9 plasmid containing the gag and pol viral genes, and an equal quantity (20 or 40 µg) of the pCAG–VSV-G plasmid encoding the vesicular stomatitis virus G protein (VSV-G) for pseudotyping. To mitigate potential cell toxicity, media was replaced 4–6 h post-transfection.

72 h after transfection, media containing viral particles was centrifuged at 3,000 rpm for 4 min and then filtered to yield a clear solution containing the viral particles. This solution was poured into ultra-clear centrifuge tubes and placed in the tube holders of the SW32 Ti rotor. The tubes were ultracentrifuged at 25,000 rpm for 90 min at 4 °C to pellet viral particles.

As an alternative to ultracentrifugation, 3 volumes of filtered supernatant were combined with 1 volume of Lenti-X (Takara, 631231) and gently inverted. Mixture was incubated overnight and centrifuged at 1,500 x g for 45 min at 4 ºC to pellet viral particles.

The viral stocks were quantified using RT-qPCR – viral titter was ~ 10^7 particles/ml – and were promptly used for infections. The primer used for quantifications is listed in **Table 3**.

Target	Forward	Reverse
RRE	GTTCTTGGGAGCAGCAGGA	CCTCAATAGCCCTCAGCAAA

Table 3. Primer sequence used for viral titration.

3.9   Infection and sorting of N2a cells

N2a cells were plated on 24-well plates and infected with a mixture of lentiviral vectors expressing the different constituents of the split dCas9-CMD toolbox in a 2:2:1 proportion (dCas9-vhhGFP4 : GFP-CMD : gRNA). Media was changed 24 h after infection to mitigate cell toxicity.

Sorting of infected N2a cells was performed in a flow-cytometer FACS Aria III (BD Bioscience) in collaboration with the technical personnel of the Omics facility in Instituto de Neurociencias. FITC-A channel detects the expression of the GFP-CMD component and PE-Texas Red-A channel detects mCherry signal expressed by the gRNA plasmid. When cells were infected with constructs that did not contain any fluorescent cassette (such as the DBD module dCas9-vhhGFP4), they were collected based on the absence of fluorescence.

3.10 Infection of primary mouse hippocampal neuronal cultures

Hippocampal neurons at DIV0 in culture were infected with a mixture of lentiviral vectors expressing the different constituents of the split dCas9-CMD toolbox in a 2:2:1 proportion (dCas9-vhhGFP4 : GFP-CMD : gRNA). Media was changed 24 h after infection to mitigate cell toxicity.

3.11 Immunostaining

3.11.1 Brain sections

Antigen retrieval was performed prior to immunostaining when needed. For antigen retrieval, brain sections were incubated in 10 mM sodium citrate buffer 0,05 % tween 20 (pH 6.0) for 30 min at 80 ºC and allowed to reach room temperature.

Brain sections were permeabilized in PBS 0.3 % triton x-100 (PBS-T) and incubated in blocking solution (4 % heat inactivated newborn calf serum (iNCS) in PBS-T) for 2 h at room temperature in agitation. The primary antibody (see **Table 4**) diluted in PBS-T with 4 % iNCS was added at the appropriate concentration and incubated overnight at 4 ºC in agitation. Sections were washed with PBS and incubated with the secondary antibody diluted in PBS-T with 4 % iNCS for 90 min in darkness and agitation, at room temperature. Same washes as after primary antibody were repeated. Next, brain slices were incubated with 1 nM DAPI in PBS for 14 min at room temperature to counterstain the DNA and washed 3 times for 5 min in PBS-T. Sections were mounted in tissue slides with Fluoromount aqueous mounting medium (Merck) and sealed with nail polish to avoid air-drying.

Image acquisition was conducted in Vertical Confocal Microscope Leica SPEII and analysis and quantification of GFP$^+$, Fos$^+$ and GFP$^+$/Fos$^+$ cells were carried out manually using Fiji/ImageJ software.

3.11.2 N2a cells and primary hippocampal neurons

N2a cells or primary hippocampal neurons were fixed with PFA 4 % for 12 min, washed with 1x PBS and permeabilized with PBS-T before blocking with 3 % iNCS in PBS-T for 30 min at room temperature in agitation. The primary antibody (see **Table 4**) diluted in PBS-T with 2 % iNCS was added at the appropriate concentration and incubated overnight at 4 ºC in agitation. Cells were washed with PBS and incubated with the secondary antibody diluted in PBS-T with 2 % iNCS for 90 min in darkness and agitation, at room temperature. Same washes as after primary antibody were repeated. Next, cells were incubated with 1 nM DAPI in PBS for 1 min at room temperature to counterstain the DNA and washed

3 times for 5 min in PBS-T. Glass coverslips were mounted in slides with antifade reagent in glycerol/PBS (Invitrogen) and sealed with nail polish to avoid air-drying.

Photos were taken using a Confocal Olympus Fluoview FV1200 microscope and images were processed with ImageJ/Fiji.

	Antibody	Animal of origin	Reference	Type of samples	Concentration
Immunostaining (primary ab)	GFP	Chicken polyclonal	Aves (GFP-1020)	Bran sections	1:1000
				N2a and primary cultures	1:500
	c-Fos	Rabbit monoclonal	Thermo scientific (T.142.5)	Bran sections	1:500
	Cas9	Mouse monoclonal	Abcam (ab191468)	N2a and primary cultures	1:500
	Flag M2	Mouse monoclonal	Sigma (F1804)	Primary cultures	1:500
Immunostaining (secondary ab)	Anti-chicken 488	Goat	Invitrogen (a-Chicken IgG (H+L) Alexa 488)	Brain sections, N2a and primary cultures	1:400
	Anti-rabbit 594	Goat	Invitrogen (a-Rabbit IgG (H+L) Alexa 594)	Brain sections	1:400
	Anti-mouse 647	Goat	Invitrogen (a-Mouse IgG (H+L) Alexa 647 F(ab')2 fragm.)	N2a and primary cultures	1:400
ChIP-qPCR	GFP	Rabbit polyclonal	Molecular Probes (A-11122)	N2a	3:2000
	H3K27ac	Rabbit polyclonal	Abcam (ab4729)	N2a	3:2000

Table 4. Antibodies used in the study.

3.12 Chromatin immunoprecipitation assay (ChIP)

N2a cells were fixed in 1.1 % formaldehyde (Thermo Scientific) for 10 min at room temperature, and fixation was blocked with 0.125 M glycine (Merck) for 5 min. N2a plates were washed twice with cold HBSS and cells were scraped and

resuspended in 400 µl of RIPA lysis buffer (containing NP40 1%, SDS 0.1 %, sodium deoxycholate 0.5 %). Cells were sonicated in a Branson Sonifier (Emerson) for 8 cycles of 15 sec, with an inter-sample interval of about 15 min. Samples were centrifuged for 15 min at 17,000 x g at 4 ºC and the supernatants were divided: half of the supernatant was stored at -80 ºC and the rest was diluted in 1.8 ml of ChIP dilution buffer (containing SDS 0.01 %, Triton X-100 1.1 %, EDTA 1.2 mM, Tris-HCl 16.7 mM, NaCl 167 mM; pH 8.1). 5 % of the sample was saved as Input and the rest incubated overnight at 4 ºC with the antibody (see **Table 4**, ChIP-qPCR section). The following day, protein G Dynabeads (Thermo Scientific) were washed in ChIP dilution buffer and incubated with the samples in a rotator, at 4 ºC, for 3 h. Samples were rinsed with several washes, 5 min each, as follows: 2x in RIPA-150 buffer (containing Tris-HCl 50 mM, NaCl 150 mM, EDTA 1 mM, SDS 0.1 %, Triton X-100 1 %, sodium deoxycholate 0.1 %; pH 8.0), 2x in RIPA-500 buffer (containing Tris-HCl 50 mM, NaCl 500 mM, EDTA 1 mM, SDS 0.1 %, Triton X-100 1 %, sodium deoxycholate 0.1 %; pH 8.0), 2x in RIPA LiCl buffer (containing Tris-HCl 50 mM, EDTA 1 mM, NP-40 1 %, sodium deoxycholate 0.7 %, $LiCl_2$ 500 mM; pH 8.0), and 2x in TE buffer (containing Tris-HCl 10 mM, EDTA 1 mM; pH 8.0). Samples and Inputs were diluted in Elution buffer (containing SDS 1 %, $NaHCO_3$ 0.1 M, NaCl 0.2 M) and incubated with 2 µl of RNase A 10 mg/ml (Fermentas) overnight at 65 ºC in agitation to reverse crosslink. Samples were then placed on a magnetic rack, allowing beads to clump. Supernatants were transferred to new tubes and incubated with 1 µl of Proteinase K 20 mg/ml (Thermo Scientific) for 4 h at 55 ºC, in agitation. Finally, DNA was precipitated using phenol-chloroform method and analysed by RT-qPCR (described in the following section). The primers used are listed in **Table 5**.

Target	Forward	Reverse
gRNA P1 binding site	TTGGTCACGTAACTGGCTCA	GCTGGGGAACTTGTTGCTTT
gRNA P4 binding site	ATGCAATGCCCTGGAACGG	CTGCCTTGACGTGAGCTGT
Region 1 gRNA P1	GCCTACACCTTTTCGCTCAG	GCGGCTTGAGTTGAATGAA

Region 2 gRNA P1	GGTGTGACCTGAGCAGTGG	CAGCTTTCTCAACGCCTGTC
Region 3 gRNA P1	CTGTAGTCGCCAAGGTGGAT	AAGTTCGGCTTTGCTCAGTG
Region 4 gRNA P4	ACCAAACAAAAACGGTCCAA	AGGCAGCAACAACACATCAA
Region 5 gRNA P4	AAATGGAGCTTCTCGCTGAA	AGTCTTTGGTGGCCGATATG

Table 5. Primer sequences used in ChIP-qPCR experiments.

3.13 RNA extraction, retrotranscription and RT-qPCR

All steps were performed in RNase-free conditions and at 4 °C unless indicated otherwise. RNA extraction from sorted CA1 and DG nuclei, N2a cells and primary hippocampal neurons was performed using TRI-reagent (Merck) as previously described (Scandaglia et al., 2017). Obtained RNA was treated with RNase-free DNase I (Qiagen) for 30 min at 25 °C to eliminate genomic DNA and RNA was precipitated using the phenol-chloroform method. Resulting RNA concentration was measured using NanoDropOne (Themo Scientific).

Total RNA was retrotranscribed to cDNA combining 0.5-1 µg RNA and H_2O-DEPC (Thermo Scientific) up to 11.5 µl, 2 µl of 10 mM dNTPS (Thermo Scientific) and 1 µl of 100 µM Random Hexamer Primers (Thermo Scientific). Mixture was warmed at 65 °C for 3 min and chilled on ice. 4 µl buffer RT (Thermo Scientific), 1 µl of 200 U/µl RevertAid Reverse Transcriptase (Thermo Scientific) and 0.5 µl of 40 U/µl RiboLock RNase Inhibitor (Thermo Scientific) were added. Samples were left at room temperature for 5 min, warmed at 42 °C for 1 h and heated at 70 °C for 5 min. Resulting cDNA was diluted in 80 µl of H_2O-DEPC and kept at -20 °C.

cDNA obtained was analysed using QuantStudio 3 Real-Time PCR System (Thermo Scientific). For each primer, a master mix was generated adding 4 µl of PyroTaq Eva green (Cultek), 1 µl of 5 µM primer mix and 13 µl H_2O miliQ. 18 µl of master mix plus 2 µl of cDNA were added to each well of MicroAmp Fast 96-well Reaction Plate 0.1 ml (Thermo Scientific). The program used contain three stages: i) Stage 1 – Denaturation: 95 °C for 15 min; ii) Stage 2 – Amplification: 95

ºC for 15 sec followed by 60 ºC for 29 sec and 72 ºC for 29 sec (45 cycles); and iii) Stage 3 – Melting curve: 95 ºC for 15 sec, 60 ºC for 1 min and 95 ºC for 1 sec.

The gene *Gapdh* was used as housekeeping gene in all the RT-qPCR analysis. All the primers used are listed in **Table 6**.

Target	Forward	Reverse
dCas9	GACTTGCCCTTTTCCACTTTG	TGCCCCAAGTGAATATCGTG
GFP	GGGCACAAGCTGGAGTACAACT	ATGTTGTGGCGGATCTTGAAGT
gRNA Ctrl	CACCGGAGACGGACGTCTCT	CTCGGTGCCACTTTTTCAAG
gRNA P1	CACCGAGAATACCAGAAAAGCGCAG	CTCGGTGCCACTTTTTCAAG
gRNA P4	CACCGCACTAGAGTGTCTATTTCG	CTCGGTGCCACTTTTTCAAG
Bdnf I	AAGTCACACCAAGTGGTGGGC	GGATGGTCATCACTCTTCTCACCT
Bdnf IV	GTAAGAGTCTAGAACCTTGGGGACC	GGATGGTCATCACTCTTCTCACCT
Gapdh	CATGGACTGTGGTCATGAGCC	CTTCACCACCATGGAGAAGGC

Table 6. Primer sequences used in RT-qPCR experiments.

3.14 ATAC-seq

ATAC-seq was conducted following the protocol described in (Buenrostro et al., 2013, 2015). Briefly, 75,000 Sun1-GFP$^+$ sorted neuronal nuclei were subjected to centrifugation, resuspended in the transposase reaction mixture (TD buffer and Tn5 transposase, Illumina) and incubated at 37 ºC for 30 min. DNA extraction was immediately performed (Qiagen Minelute PCR Purification Kit) and samples were saved at -20 ºC. Once all samples had been collected, DNA libraries were generated using Custom Nextera PCR primers. The saturation level of the resulting libraries was monitored using RT-qPCR and afterwards DNA was purified by double-sided bead purification AMPure XP beads (Beckman Coulter) method, designed to eliminate primer dimers and fragments exceeding 1,000 bp. First, 0.5X volume of AMPure XP beads were mixed with the sample, incubated for 10 min and placed on a magnetic rack for 5 min. Subsequently, 1.3X original volume of AMPure XP beads were added to the supernatant, mixed thoroughly, incubated for 10 min and placed on a magnetic rack for 5 min. The supernatant was discarded, and the beads were washed with 80 % ethanol before being resuspended in 20 µl of miliQ H$_2$O. Purified libraries were stored at -20 ºC.

3.15 nuRNA-seq and ATAC-seq sequencing and data processing

For nuRNA-seq analysis, rRNA depletion libraries were prepared, and single-end 50 bp sequencing was conducted in a HiSeq 2500 apparatus (Illumina). *Fastq* files quality was analysed by FastQC (v0.11.9) (Andrews, 2010) and adapters were trimmed using TrimGalore (v0.39) (Krueger & Andrews, 2012). The reads obtained were aligned to the GRCm38.100 mouse genome (mm10) using STAR (v2.7.9a) (Dobin et al., 2013). Mitochondrial reads and reads with mapq < 30 were eliminated using Samtools (v1.13) (Li et al., 2009). Data analysis was conducted with custom R scripts (v4.1.0, 2021), Rsubreads (v2.6.4) (Liao et al., 2014) and Mus_musculus.GRCm38.100.gtf annotation data. For differential expression analysis and samples normalization, DESeq2 (v1.32.0) (Love et al., 2014) was used. To generate BigWigs, Deeptools (v3.5.1) (Ramírez et al., 2016) was used.

Gene ontology analyses were conducted with the WEB-based GEne SeT AnaLysis Toolkit (WebGestalt; (Liao et al., 2019; Wang et al., 2013, 2017; Zhang et al., 2005)) and over-representation analysis (ORA) method for enrichment was selected. For gene set enrichment analysis (GSEA), the complete list of nuRNA-seq genes were ranked according to $-\log_{10}(padj) * sign(\log_{10}(\log_2 FC))$ and analysed based on their differential expression rank. Obtained enriched pathways (NES (normalized enrichment score) < 0.05) were clustered by Cytoscape application, which displays pathways as a network where overlapping terms were clustered together to identify major biological terms (Reimand et al., 2019).

For the evaluation of GFP expression in KA-treated mice, all the nuRNAseq dataset from (Fernandez-Albert et al., 2019) were used to obtain the sfGFP sequence using velvet (v1.2.10) (Zerbino & Birney, 2008) and it was introduced as an additional chromosome into the mouse reference genome mm10. nuRNA-seq reads in vehicle and after 1 hour of KA injection were aligned to this new reference genome using STAR (v2.6.1a). Reads were then filtered for mapq > 30 using Samtools (v1.9), then counts were calculated with Rsubread (v2.4.3) for the reference Mus Musculus.GRCm38.99.gtf where the sfGFP was included. The differential expression analysis was performed using DESeq2 (v1.30.1).

For ATAC-seq analysis, paired-end, 50 bp length sequencing was conducted in a HiSeq 2500 sequencer (Illumina). *Fastq* files quality was analysed by FastQC (v0.11.9) and TrimGalore (v0.39) was used to trim the adapters. Reads obtained were aligned to the GRCm38.100 mouse genome (mm10) using Bowtie2 (v 2.4.2) (Langmead & Salzberg, 2012) and filtered to eliminate PCR duplicates using Picard (v2.26.2). Mitochondrial reads and reads with mapq < 30 were eliminated using Samtools (v1.13). Peakcalling was conducted using MACS2 (v2.2.7.1) (Zhang et al., 2008), and Diffbind (v3.0.15) (Stark & Brown, 2022) was used for principal component analysis (PCA). Differential accessibility analysis was done using DESeq2 (v1.32.0). To generate BigWigs, Deeptools (v3.5.1) was used to normalize reads by reads per genomic content. With GenomicFeatures (v 1.50.4; (Lawrence et al., 2013)) a TxDb object was created from the gtf file "Mus_musculus.GRCm38.100.gtf" and genes were annotated using ChipPeakAnno (v 3.32.0) (Zhu et al., 2010).

For TF prediction binding, accessible regions were classified into promoters-like or enhancers-like regions using bedtools (v2.30.0). Specifically, accessible regions that mapped to annotated mouse promoters (GRCm38) were considered promoter-like, and the rest were considered enhancers-like and tested for different epigenetic marks (H3K27ac, ATAC-seq reads – the resulting merge from 3 SC replicates –, H3K4me1, H3K4me3, CBP and RNAPolII). These defined promoters and enhancers regions were used for transcription factor footprints analysis, performed using Transcription factor Occupancy prediction By Investigation of ATAC-seq Signal (TOBIAS, v0.12.9) (Bentsen et al., 2020). Biological replicates for each condition (EE, SC and EI) were merged by SamTools (v1.13) and the resulting BAM files were corrected for insertion bias of the Tn5 transposase using the command ATACorrect. BigWig files were obtained using the command ScoreBigwig and footprinting scores were assigned using the jaspar vertebrate motif database (JASPAR2020_CORE_vertebrates_non-redundant_pfms_jaspar.txt). Differential TF footprinting for each comparison (EEvsSC and EIvsSC) was calculated with BINDetect command. Bubble plots represented increased and decreased predicted occupancy in red and blue, respectively, based on differential binding score (< -0.2 or > 0.2) and *P* value (< 0.05). Datasets generated in this study are detailed in **Table 7**.

Experiment	Mouse strain	Instrument	Single or paired end	Read length	Hippocampal layer	Condition	# Replicates	Library name	Index i7	Sequencing depth (bp)
nuRNA-seq	pCamKIIα-Sun1-GFP	Illumina HiSeq 2500	Single end	50 bp	CA1	EE	3	EE1_C1	TAGCTT	39899902
								EE2_C1	GGCTAC	39389922
								EE3_C1	CTTGTA	39251392
						EI	3	EI1_C1	CGTACG	40559930
								EI2_C1	GAGTGG	40292610
								EI3_C1	ACTGAT	40061037
						SC	3	NC1_C1	CCGTCC	39474986
								NC2_C1	GTCCGC	39370863
								NC3_C1	GTGAAA	39421546
					DG	EE	3	EE1_DG	ATCACG	38882438
								EE2_DG	CGATGT	39951507
								EE3_DG	TTAGGC	38276464
						EI	3	EI1_DG	CAGATC	39714656
								EI2_DG	ACTTGA	39609815
								EI3_DG	GATCAG	39554040
						SC	3	NC1_DG	TGACCA	40638579
								NC2_DG	ACAGTG	39594114
								NC3_DG	GCCAAT	39563504

									E1_C1A_lib	TAAGGC	88067958
ATAC-seq	pCamKIIα-Sun1-GFP	Illumina HiSeq 2500	Paired end	50 bp	CA1	EE	3		E2_C1A_lib	CGTACT	96423784
									E3_C1A_lib	AGGCAG	110611686
						EI	3		I1_C1A_lib	TAAGGC	84918979
									I2_C1A_lib	CGTACT	98897204
									I3_C1A_lib	AGGCAG	113708042
						SC	3		N1_C1A_lib	TAAGGC	88293064
									N2_C1A_lib	CGTACT	112240192
									N3_C1A_lib	AGGCAG	97776287
					DG	EE	3		E1_DGA_lib	TAAGGC	92943289
									E2_DGA_lib	CGTACT	97373126
									E3_DGA_lib	AGGCAG	105857406
						EI	3		I1_DGA_lib	TAAGGC	92526606
									I2_DGA_lib	CGTACT	92944581
									I3_DGA_lib	AGGCAG	108711342
						SC	3		N1_DGA_lib	TAAGGC	84863943
									N2_DGA_lib	CGTACT	113637310
									N3_DGA_lib	AGGCAG	95611935

Table 7. Datasets generated in this study.

3.16 Cloning

DBD modules. For obtaining the plasmid that expresses the chimeric protein dCas9-vhhGFP4 under the ubiquitous promoter EF1α, the dCAS9-VP64_GFP plasmid (Addgene #61422) was digested with BamHI and EcoRI restriction enzymes to eliminate VP64-GFP fragment. vhhGFP4 was amplified by PCR from pcDNA3_NSImB-vhhGFP4 (Addgene #35579) – using a forward primer that includes BamHI restriction site and a reverse primer with EcoRI restriction site – and cloned in this modified vector with BamHI and EcoRI sites. For the generation of the plasmid that expressed dCas9-vhhGFP4 under the neuronal promoter synapsin, vhhGFP4 was also amplified by PCR from pcDNA3_NSImB-vhhGFP4 – using a forward primer that includes XhoI restriction site and a reverse primer with EcoRI restriction site – and cloned into lenti SYN-FLAG-dCas9-VPR (Addgene #114196) with XhoI and EcoRI sites.

GFP-CMD modules. The transactivator domain VPR – formed by VP64, rTA and p65 – and the repressor domain KRAB-MeCP2, were amplified by PCR from lenti SYN-FLAG-dCas9-VPR (Addgene #114196) and lenti SYN-dCas9-KRAB-MeCP2 (Addgene #155365), respectively, using a forward primer that includes XhoI restriction site and a reverse primer with NotI restriction site. After purification by phenol-chloroform method, amplicons and vector (LV_pSyn-GFP-XhoI-NotI, previously generated in Dr. Barco's laboratory) were digested with XhoI and NotI sites and ligated to obtain the pSyn_GFP-VPR and pSyn-GFP-KRAB-MeCP2 plasmids, respectively.

The GFP-CMD modules pSyn-VP16-GFP and pSyn-KAT-GFP were previously generated in Dr. Barco's laboratory.

gRNAs. Sequence-specific gRNAs for *Bdnf* promoter I and IV (obtained from (Savell et al., 2019)) were cloned in CRISPseq-mCherry-backbone (Addgene #85708) with BsmBI. Each of these plasmids expressed a different gRNA to guide the system to the promoter I or IV of Bdnf, respectively. CRISPseq-mCherry-backbone was used as control gRNA.

GFP-CMD and gRNAs combined plasmids. gRNAs were amplified by PCR – using primers that introduce SanDI restriction sites at 5' and 3' ends – from

previous cloned gRNAs plasmids. Amplicons and vector (LV_pSyn-GFP-VPR, previously generated) were digested with SanDI sites and ligated to obtain the plasmids that express simultaneously a specific gRNA and the CMD module GFP-VPR.

All the primers used for plasmid cloning are listed in **Table 8**. All the lentiviral plasmids obtained and used in the study are listed in **Table 9**.

Target	Forward	Reverse
vhhGFP4	GACAGTCGGATCCCACCTCGAG ATGGATCAA (includes BamHI and XhoI restriction sites)	GACAGTCGAATTCTCTAGATTA GCTGGAGACG (includes EcoRI restriction site)
VPR	GACAGTCCTCGAGCCGACGCAT TGGACGATTTT (includes XhoI restriction site)	GACAGTCGCGGCCGCTTGAAT TCTCAAAACAGAG (includes NotI restriction site)
KRAB	GACAGTCCTCGAGCGAAAAGGC CGGCGGCCACG (includes XhoI restriction site)	GACAGTCGCGGCCGCCCTATG AGACTCTCTCAGTCACGGG (includes NotI restriction site)
gRNAs	ACCCCGAGGGGACCCAGA (includes SanDI restriction site)	GACAGTCGGGTCCCTCAAGAT CTAGTTACGCCAAGC (includes SanDI restriction site)

Table 8. Primers sequences used in PCR amplification for plasmid cloning.

Epi-editing tool		Plasmid name	Production
S p li t d C a s 9 - C M D	DBD modules	pEF1a-dCas9-vhhGFP4	Generated for this study
		pSyn-dCas9-vhhGFP4	Generated for this study
	CMD modules	pSyn-VP16-GFP	Previously generated in Dr. Barco's laboratory
		pSyn-GFP-VPR	Generated for this study
		pSyn-GFP-KRAB-MeCP2	Generated for this study
		pSyn-KAT-GFP	Previously generated in Dr. Barco's laboratory
	gRNAs	pU6-gRNACtrl-pEF1a-mCherry	Generated for this study
		pU6-gRNAP1-pEF1a-mCherry	Generated for this study
		pU6-gRNAP4-pEF1a-mCherry	Generated for this study
	GFP-CMD + gRNAs (combined)	pU6-gRNACtrl-pSyn-GFP-VPR	Generated for this study
		pU6-gRNAP1-pSyn-GFP-VPR	Generated for this study
		pU6-gRNAP4-pSyn-GFP-VPR	Generated for this study
Traditional CRISPR system		pSyn-dCas9-VPR	Addgene #114196

Table 9. Lentiviral plasmids used in this study.

3.17 Statistical methods

For all statistical analysis, GraphPad Prism (v9.5.1; GraphPad Software, La Jolla CA) program was used. The specific statistical test conducted for each experiment can be found in the figure legend of each figure. For two groups comparison analysis, Shapiro-Wilk test was used for the normality test, followed by a t-test or a Mann-Whitney test if samples did or did not have a normal distribution, respectively. For several groups comparison, Shapiro-Wilk test was also used for the normality test, followed by a one-way ANOVA or ANOVA corrected with Brown-Forsythe and Welch ANOVA test if samples did or did not have a normal distribution, respectively. The MWM and fear extinction experiments were analysed using Two-way repeated measures ANOVA. Freezing levels evolution in the fear extinction experiment was analysed using repeated measures ANOVA. The effect of KCl and infection with gRNAs in primary cultures co-infected with dCas9-vhhGFP4, GFP-KRAB-MeCP2 and a gRNA were analysed using two-way ANOVA.

For all pairwise multiple comparison, Dunnett's test was used when data was analysed using one-way ANOVA and ANOVA corrected with Brown-Forsythe and Welch ANOVA tests. Turkey's test was used when data was analysed by two-way ANOVA. Šídák's and Turkey's test was used when data was analysed using repeated measures ANOVA and Two-way repeated measures ANOVA.

Bar plots represent means ± s.e.m; raw data is also shown in dots. In all analysis, p values were considered significant when α was lower than 0.05, and they are represented as follows: * $p < 0.05$, ** $p < 0.01$, *** $p < 0.001$, **** $p < 0.0001$.

3.18 Data access

In this study, we have used several previously published datasets (**Table 10**).

Dataset	GEO accession number	Reference
nuRNAseq from adult KA-treated and Sal-treated mice. PolII ChIPseq from Sal-treated mice.	GSE125068	(Fernandez-Albert et al., 2019)
CBP and H3K27ac ChIPseq from adult mouse hippocampus	GSE133018	(Lipinski et al., 2020)
H3K4me1, H3K4me3 and ChIA-PET from adult mouse hippocampus	GSE236182	(del Blanco et al., 2024)
ATACseq from primary cortical cultures	GSE147056	(Wenderski et al., 2020)
CBP ChIPseq from primary cortical cultures without reelin	GSE66710	(Telese et al., 2015)
H3K27ac ChIPseq from primary cortical cultures untreated	GSE131025	(Beagan et al., 2020)

Table 10. Published datasets used in this study.

4. RESULTS

Section 1

Transcriptional and epigenetic bases of modulation of cognitive abilities by rearing conditions

The following study is highly multidisciplinary and has been conducted in collaboration with several members of the laboratory of Prof. Ángel Barco, at the Instituto de Neurociencias (UMH-CSIC).

Alejandro Medrano Fernández performed the initial behavioural characterization of C57BL/6J mice raised in different environmental conditions. Miguel Fuentes Ramos conducted most of the bioinformatical analyses of sequencing data with the assistance of Sergio Niñerola Rives. Furthermore, Miguel contributed to the design of the engram experiments. Román Olivares Escalona managed the mouse colonies and Carina Racovac Farinha assisted with mice perfusion. Federico Miozzo collected FOS immunostaining images at basal levels.

I conducted additional behavioural experiments, including the strong fear conditioning paradigm, context discrimination and fear extinction experiments with C57BL/6J mice, as well as the strong fear conditioning paradigm and engram evaluation with TRAP2-Sun1-GFP mice. Additionally, I performed all the CA1 and DG dissections, FANS and molecular experiments for nuRNA-seq and ATAC-seq with CamKIIα-Sun1-GFP mice. I also performed several bioinformatical analysis. The results obtained in this study have been interpreted under the supervision of Prof. Ángel Barco, with significant inputs from all the coauthors mentioned above.

4.1 Modulation of cognitive abilities by environmental conditions

To assess the persistence of changes induced by early environmental conditions on cognitive performance in adulthood, 3-week-old C57BL/6J female mice were randomly allocated to one of three contrasting environmental conditions: (i) The Environmental Enrichment (EE) condition comprised a large cage (61 x 141 x 26 cm), filled with nesting materials, toys, wheels, and tunnels, where groups of 10 to 15 mice were housed together. This set up promotes voluntary exercise, exploration, and social interaction among the mice. To maintain novelty, the toys were rotated every two weeks (**Figure 9A, left**). (ii) Conversely, the Environmental Impoverishment (EI) condition confined a single mouse in a small cage (13 x 24 x 13 cm), which in turn was placed within a Styrofoam box to minimize exposure to social and acoustic stimuli, effectively isolating the mouse from environmental interactions (**Figure 9A, right**). We chose this paradigm because in our hand, EI worked much better than unpredictable stressors to observe a negatively impact in cognitive performance in C57BL/6J mice. (iii) Both the EE and EI groups were compared with littermates housed in Standard Cages (SC; 21 x 37 x 14 cm cages, 4-5 mice per cage with nesting materials, **Figure 9A, middle**).

In total, we had four groups of mice: one EE group, one EI group, and two independent groups of SC animals made of littermates from the EE and EI cohorts. After 1 month, the EE and EI mice returned to SC housing for one additional month before cognitive performance was assessed (**Figure 9B**).
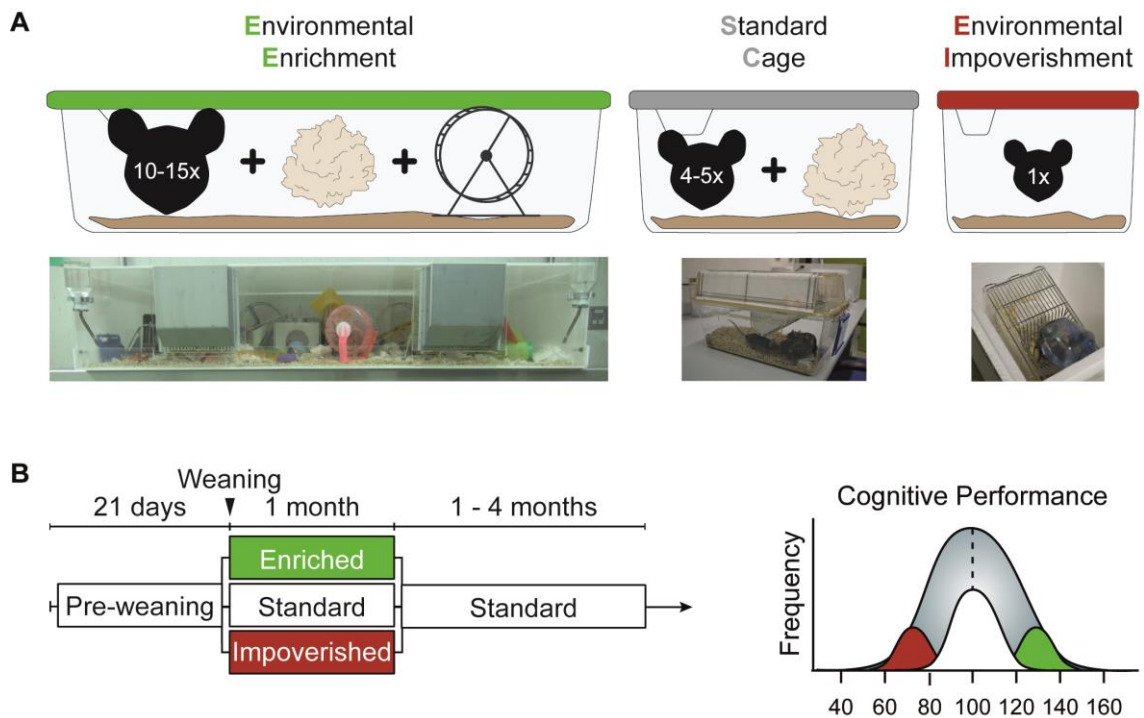
Figure 9. Models of environmental paradigms and experimental design. A. Top: scheme of Environmental Enrichment (EE, green), Standard Cage (SC, grey or white) and Environmental Impoverishment (EI, red) conditions. Each scheme includes the number of mice per cage and the presence or absence of nesting materials and toys. Bottom: representative pictures of EE, SC and EI conditions. **B**. Experimental design. Upon weaning (P21), littermate female mice were randomly distributed in EE, SC or EI condition for one month and then returned to SC condition for an additional month before the behavioural analysis to evaluate cognitive performance began.

First, we examined the influence of environmental conditions on basal exploratory behaviour in an open field test. Both EE and EI mice moved a greater total distance (**Figure 10A**) than their SC groups. EE mice roam more in the centre and middle of the arena compared with SC mice (**Figure 10B, top**) and have a higher average speed (**Figure 10C, top**), whereas EI mice showed no difference when compared to SC mice (**Figure 10B-C, bottom**). These results show a higher exploration activity of animals housed in EE at an early stage of their development, while the EI condition has no effect on the exploration activity of the mice.
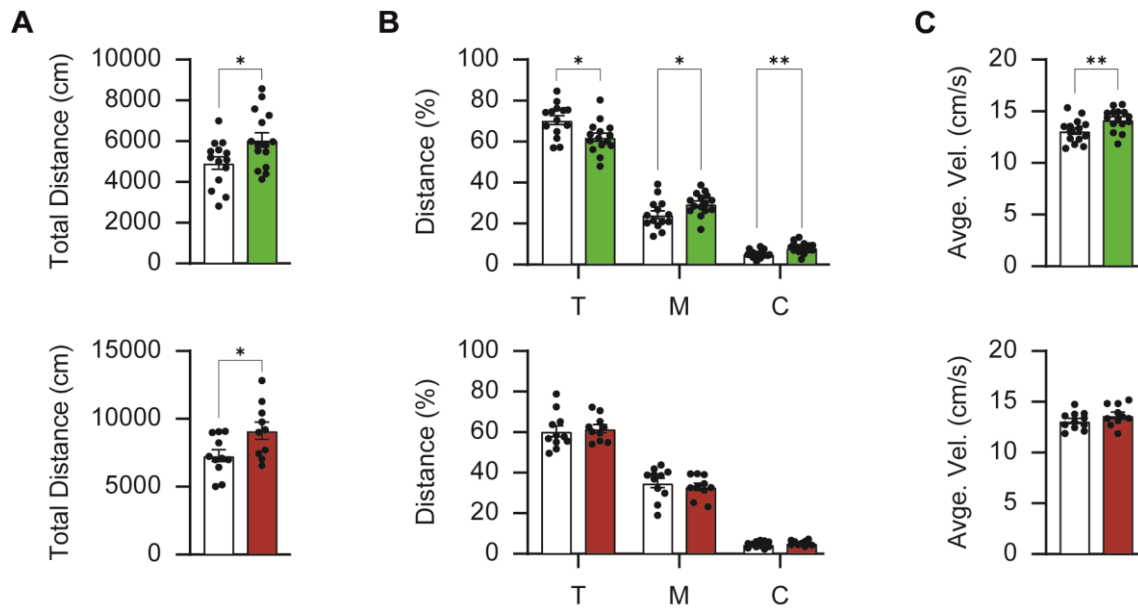
Figure 10. Exploratory behaviour in EE, SC and EI mice. A-C. Open field test results. **A**. Travel distance measured in cm. **B**. Percentage of distance travelled in each area of the arena. T: thigmotaxis; M: middle; C: centre. **C**. Average velocity measured in cm/s. Data is analysed using Mann-Whitney test. * $p < 0.05$; ** $p < 0.01$.

To investigate the long-lasting effects of housing conditions during the juvenile period on cognitive abilities in adulthood, we employed a battery of memory-related tests. Initially, we used a Y-maze task to evaluate working memory. Remarkably, EE mice improved performance and reduced the number of errors, whereas EI mice had the opposite effect and greatly increased the number of errors (**Figure 11A**). During spatial navigation in the Morris water maze, EE mice showed better learning performance (**Figure 11B, top**) than their control littermates. However, during transfer trials, all mice made more entries into the target quadrant, without differences in performance between conditions (**Figure 11C, top**). In contrast, EI mice took a similar amount of time to reach the platform compared to SC mice (**Figure 11B, bottom**) and, although all mice made more target quadrant entries during transfer trials, there were deficits in EI mice during the reversal phase, compared to SC mice (**Figure 11C, bottom**). To investigate whether novel object recognition memory was improved after EE, we used a difficult version of the task in which the mice were allowed to explore the object for only 3 minutes during the training session. We observed that the EE group remembered the familiar object after this brief exposure, whereas their control littermates could not (**Figure 11D, left**). To examine the performance of the EI

mice, we used our standard protocol consisting of 15 minutes of training. We observed that the EI mice exhibited impaired memory retention, whereas their control littermates housed in SC significantly discriminated between the familiar and novel objects (**Figure 11D, right**). Finally, mice's memory was evaluated in a standard contextual fear conditioning task, in which animals received a single 0.4 mA, 2 sec footshock and recall was assessed 24 hours later. We found that EE mice froze slightly more during recall, whereas EI mice behaved similarly to SC mice (**Figure 11E**). These findings suggest that the housing conditions experienced during the juvenile period had a positive or negative impact on hippocampal-dependent memory processes in the EE or EI groups, respectively, highlighting the critical role of early-life environmental conditions in shaping hippocampal function and memory abilities.
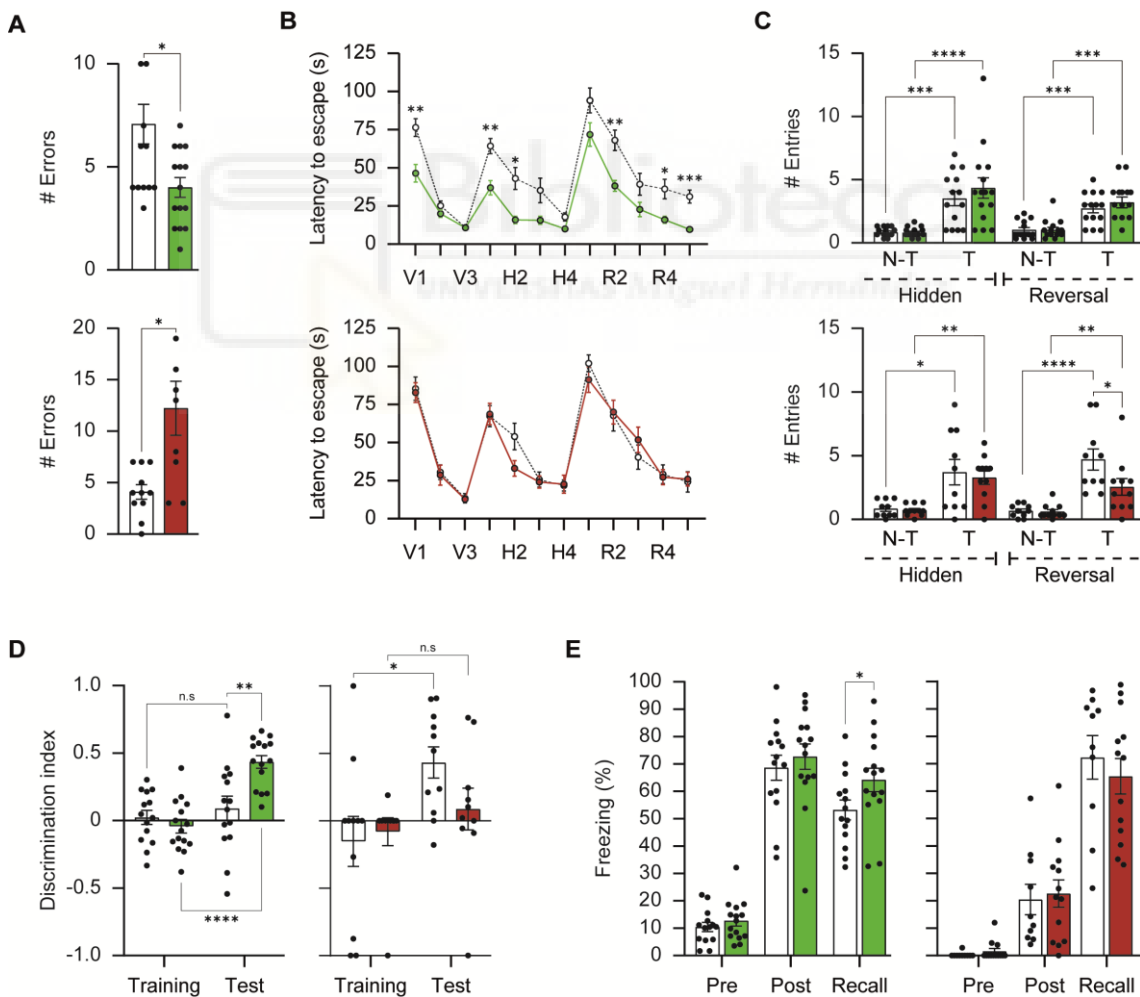

Figure 11. Modulation of cognitive abilities by environmental conditions. A. Working memory measured as the number of errors in a Y-maze. Data is analysed using Mann-Whitney test. **B**. Spatial memory measured as the latency to escape in the Morris Water Maze in seconds.

V: visible phase; H: hidden phase; R: reversal phase. Data is analysed using Two-way repeated measures ANOVA and corrected for multiple comparisons using Šídák's test. Top (EEvsSC): Time: ****, Rearing Conditions: ****. Bottom (EIvsSC): Time: ****, Rearing Conditions: n.s. **C**. Cognitive flexibility measured as the number of entries during probe trials. N-T: non-target quadrants; T: target quadrant. Data is analysed using Mann-Whitney test. **D**. Recognition memory measured by discrimination index in the novel object recognition test. Data is analysed using Mann-Whitney test. **E**. Percentage of freezing before the footshock (Pre), after the footshock (Post) and 24h after training (Recall) in the contextual fear conditioning test. Data is analysed using Mann-Whitney test. $* p < 0.05$; $** p < 0.01$; $*** p < 0.001$; $**** p < 0.0001$.

4.2 Effects of environmental conditions on memory engram formation

We next investigated the impact of environmental conditions on memory engram formation. Towards this end, we used the Targeted Recombination in Active Populations (TRAP2) reporter strain (Allen et al., 2017; DeNardo et al., 2019) that uses an activity-dependent gene promoter (pFos) to drive the expression of tamoxifen-inducible CreER^{T2}, along with a transgenic Cre-dependent nuclear reporter (Sun1-GFP) (**Figure 12A**). The resulting mouse strain is abbreviated as TRAP2-Sun1-GFP mice. In this system, the activation of *Fos* promoter in response to a stimulus leads to the expression of the CreER^{T2} protein, which remains in the cytoplasm. Upon administration of hydroxy-tamoxifen (4-OHT), the activity-induced CreER^{T2} translocates to the nucleus, cleaves out the STOP codon, and facilitates the permanent expression of a reporter that consist in a fusion protein between the nuclear envelope protein Sun1 and GFP (Sun1-GFP) (**Figure 12B**). 3-week-old TRAP2-Sun1-GFP female mice were distributed in EE or EI conditions for 1.5 months and then returned to SC condition for additional 2 weeks – TRAP2-Sun1-GFP mice housed in SC during this period were used as the control group (**Figure 12C**).

To label the engram corresponding to an aversive context, we subjected the mice to a stronger fear conditioning training paradigm than the one described in the previous section (the procedure included five 0.5 mA footshocks rather than a single 0.4 mA footshock). With this modification, based on preliminary assays, we aimed to guarantee that a sufficient number of cells will be tagged as result of the

experience for a more reliable quantification. More in detail, TRAP2 mice were trained for 30 min in a 40 x 40 cm arena with objects and received footshocks (0.5 mA, 2 sec) every 5 min. Immediately after, 4-OHT (50 mg/kg, intraperitoneal) was injected to induce the permanent expression of Sun1-GFP in neurons that were activated during training (experience cells). After 6 days, mice were re-exposed to the same context, and activated neurons were detected by FOS immunostaining. This allowed for the differentiation between Fos$^+$ cells and engram cells (Sun1-GFP$^+$/Fos$^+$ neurons) (**Figure 12D**). Importantly, all mice displayed a prominent freezing response during the recall (R) phase in comparison with the training (T) phase, with no significant difference in freezing behaviour between the three conditions (**Figure 12E**).
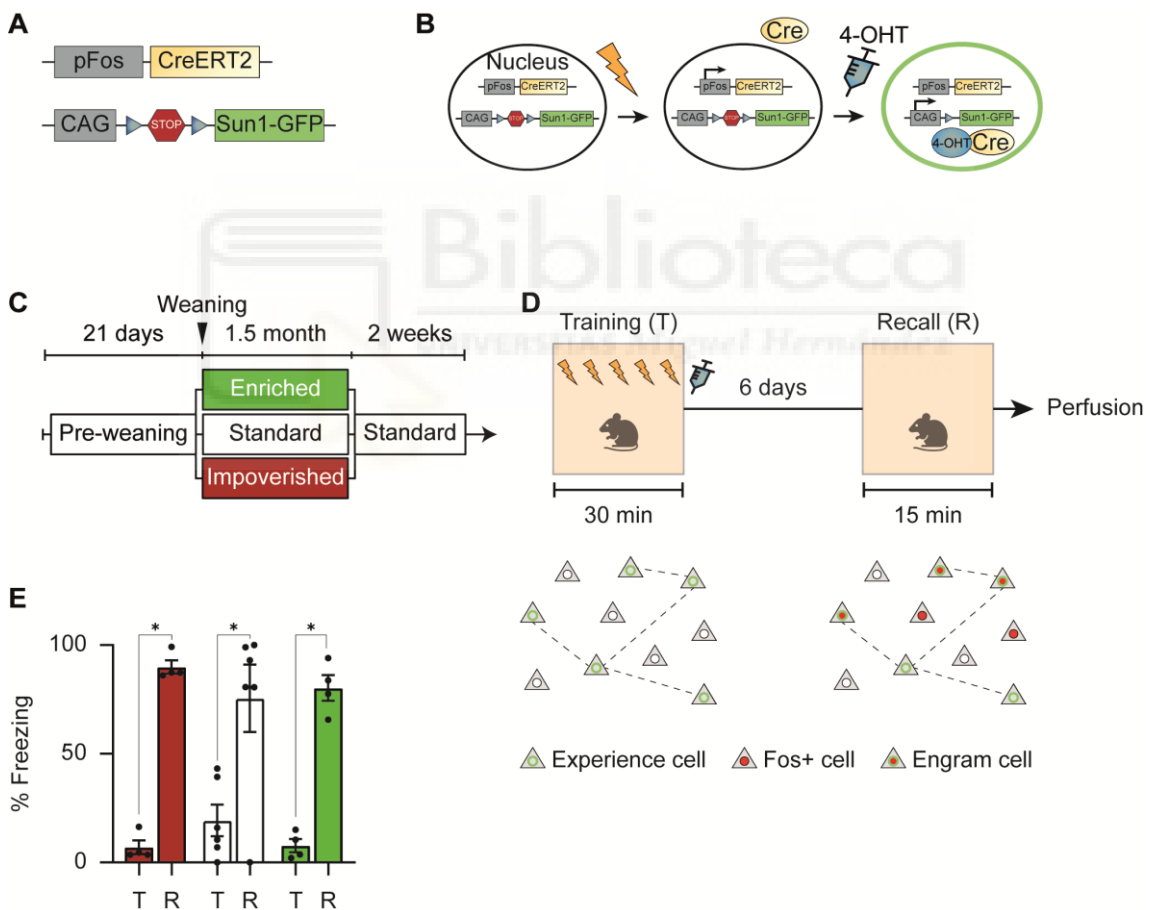
Figure 12. TRAP2-Sun1-GFP mice are used for analysing engram formation following fear conditioning. A. pFos-CreER^{T2} (TRAP2) mice were crossed with CAG-[STOP]-Sun1-GFP mice. **B**. After stimulation, *Fos* promoter drives the expression of CreER^{T2} protein, which remains in the cytoplasm. Upon 4-OHT administration, CreER^{T2} translocates to the nucleus and cleaves the STOP codon, allowing the permanent nuclear tagging by Sun1-GFP reporter. **C**. Upon weaning (P21), TRAP2-Sun1-GFP littermates were randomly distributed in EE (green), SC (white) or EI

(red) environment for 1.5 months and returned to SC for 2 additional weeks. **D**. TRAP2-Sun1-GFP mice were subjected to the stronger fear conditioning training paradigm – 30 min in a 40 x 40 cm arena with objects and received footshocks (0.5 mA, 2 sec) every 5 min – and immediately after were administered 4-OHT (50 mg/kg, i.p.) to induce permanent expression of Sun1-GFP in activated neurons (experience cells: Sun1-GFP$^+$ neurons). Mice were re-exposed to the same context after 6 days and sacrificed 75 minutes after recall. Activated neurons were detected by FOS immunostaining. Engram cells: Sun1-GFP$^+$/Fos$^+$ neurons. **E**. Percentage of freezing during the first minute of recording. T: training session; R: recall session. Data is analysed using Mann-Whitney test. * p < 0.05.

To evaluate engram formation, we focused on the dentate gyrus (DG) and *cornu ammonis 1* (CA1) layers of the hippocampus, since they have a major role in learning and memory (Anand & Dhikav, 2012). We first evaluate engram formation in granule neurons by quantifying the number of Sun1-GFP$^+$, Fos$^+$ and Sun1-GFP$^+$/Fos$^+$ cells in the upper and lower blades of DG by confocal microscopy (**Figure 13A**). We did not observe significant differences in the number of neurons activated by the fear conditioning training experience (Sun1-GFP$^+$, experience cells), nor in the number of neurons activated during recall (Fos$^+$ cells) among the different environmental conditions (**Figure 13B, top**). However, the percentage of reactivated cells (Sun1-GFP$^+$/Fos$^+$, engram cells) over chance was slightly higher in EE in comparison to SC and EI conditions (pAdj (EEvsEI) = 0.2598; pAdj (EEvsSC) = 0.1776) (**Figure 13B, bottom**). We also evaluate engram formation in CA1 pyramidal neurons (**Figure 13C**), but we did not find significant differences in the number of Sun1-GFP$^+$ cells, nor in the number of Fos$^+$ cells or reactivated cells over chance (**Figure 13D**).
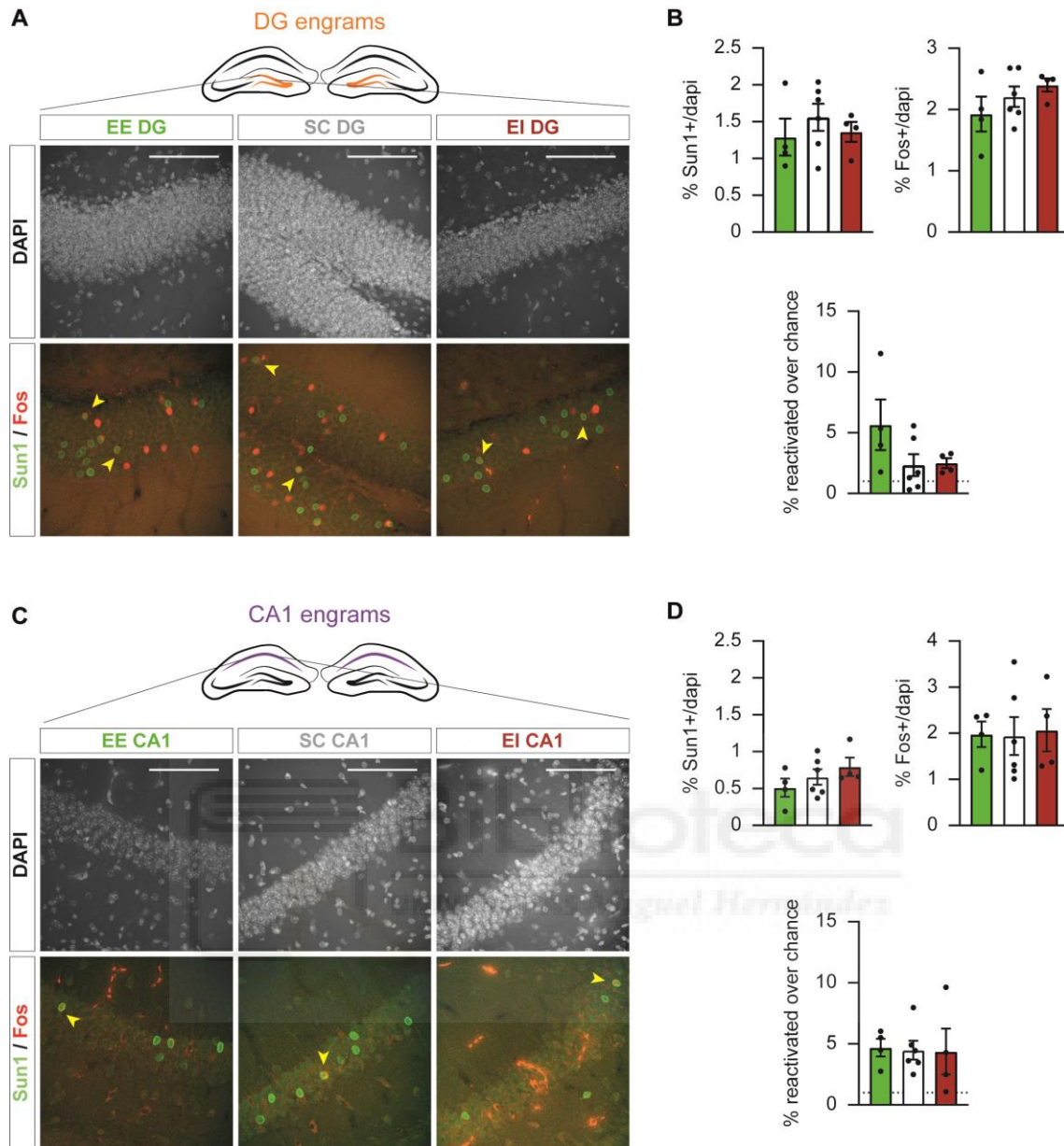
Figure 13. Memory engram evaluation in granule cells and pyramidal neurons. A. Engram evaluation in DG granule cells. Sun1-GFP$^+$ cells are labelled in green and Fos$^+$ cells in red. Yellow arrows indicate reactivated cells (Sun1-GFP$^+$/Fos$^+$). Scale bar: 100 μm. **B**. Top left: percentage of Sun1-GFP$^+$ cells relative to DAPI. Top right: percentage of Fos$^+$ cells relative to DAPI. Bottom: percentage of reactivated (engram) cells over chance. **C**. Engram evaluation in CA1 pyramidal cells. Sun1-GFP$^+$ cells are labelled in green and Fos$^+$ cells in red. Yellow arrows indicate reactivated cells (Sun1-GFP$^+$/Fos$^+$). Scale bar: 100 μm. **D**. Top left: percentage of Sun1-GFP$^+$ cells relative to DAPI. Top right: percentage of Fos$^+$ cells relative to DAPI. Bottom: percentage of reactivated (engram) cells over chance. Data is analysed using one-way ANOVA.

To further investigate the features of this "extended" fear conditioning paradigm, we conducted additional experiments in a separate cohort of C57BL/6J WT mice reared in EE or EI for 1.5 months and returned to SC condition for an additional

two weeks. This time, 6 days after training, mice were first re-exposed to the training arena, termed Context A, to evaluate long-term memory and after to a completely different arena, termed Context B, to assess context discrimination ability (**Figure 14A, left**). Measuring freezing behaviour during the first minute in each context indicated that all groups of mice exhibited increased freezing upon re-exposure to Context A (A), while freezing levels in Context B (B) were significantly reduced, demonstrating successful context discrimination (**Figure 14B**), without significant differences between environmental conditions. These results indicate that the housing conditions experienced during the juvenile period did not have a noticeable impact on the ability of the mice to undergo context discrimination when the extended and stronger contextual fear conditioning paradigm was used, which is consistent with the results obtained in the engram tagging experiment.

We also evaluated extinction learning by exposing the mice to Context A in the absence of footshock every day for 1 week (**Figure 14A, right**). We measured the percentage of freezing exhibited by the mice during the first 3 minutes of each session (**Figure 14C**) and throughout the duration of the session (15 min, **Figure 14D**). In both graphs, we observed a gradual decrease in freezing levels across all conditions, with significant differences between the EE condition and SC and EI conditions in the early days of extinction. Additionally, we compared freezing levels between each day in the EE and EI conditions, during the first 3 minutes of recording (**Figure 14E**) and throughout the duration of the session (**Figure 14F**). Notably, the EE condition exhibited greater differences between freezing levels in the initial and final days, while these differences were smaller in the EI condition. These results indicate a better extinction learning capacity in EE mice, suggesting enhanced adaptability.
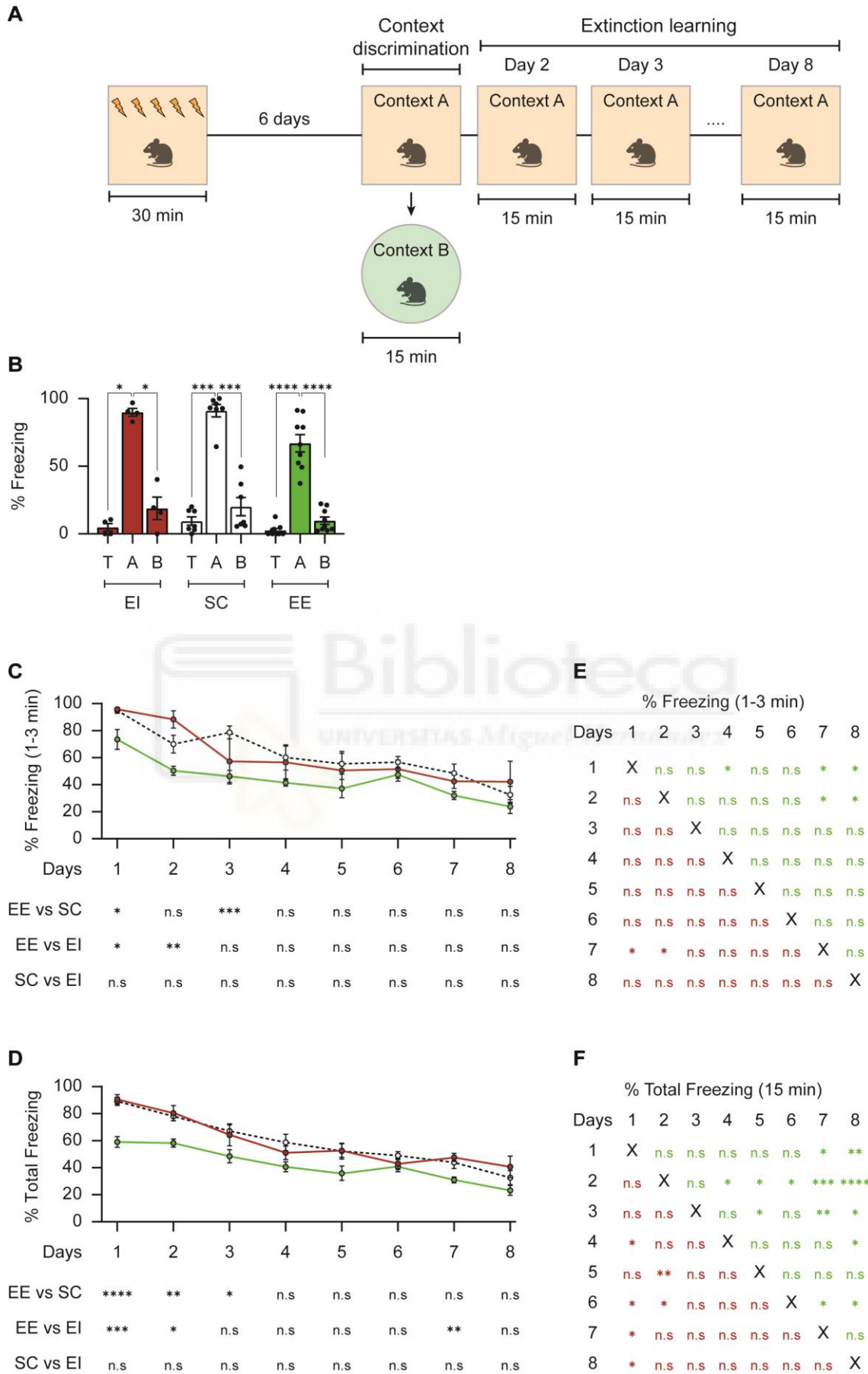
A

Context
discrimination   Extinction learning

                                    Day 2   Day 3   Day 8

[lightning symbols]   6 days   Context A   Context A   Context A .... Context A

30 min   ↓

                                    Context B

                        15 min   15 min   15 min

                        15 min

B

% Freezing

	T	A	B		T	A	B		T	A	B

* * (EI)   *** *** (SC)   **** **** (EE)

EI   SC   EE

C

% Freezing (1-3 min)

Days: 1 2 3 4 5 6 7 8

	1	2	3	4	5	6	7	8
EE vs SC	*	n.s	***	n.s	n.s	n.s	n.s	n.s
EE vs EI	*	**	n.s	n.s	n.s	n.s	n.s	n.s
SC vs EI	n.s	n.s	n.s	n.s	n.s	n.s	n.s	n.s

E

% Freezing (1-3 min)

Days	1	2	3	4	5	6	7	8
1	X	n.s	n.s	*	n.s	n.s	*	*
2	n.s	X	n.s	n.s	n.s	n.s	*	*
3	n.s	n.s	X	n.s	n.s	n.s	n.s	n.s
4	n.s	n.s	n.s	X	n.s	n.s	n.s	n.s
5	n.s	n.s	n.s	n.s	X	n.s	n.s	n.s
6	n.s	n.s	n.s	n.s	n.s	X	n.s	n.s
7	*	*	n.s	n.s	n.s	n.s	X	n.s
8	n.s	n.s	n.s	n.s	n.s	n.s	n.s	X

D

% Total Freezing

Days: 1 2 3 4 5 6 7 8

	1	2	3	4	5	6	7	8
EE vs SC	****	**	*	n.s	n.s	n.s	n.s	n.s
EE vs EI	***	*	n.s	n.s	n.s	n.s	**	n.s
SC vs EI	n.s	n.s	n.s	n.s	n.s	n.s	n.s	n.s

F

% Total Freezing (15 min)

Days	1	2	3	4	5	6	7	8
1	X	n.s	n.s	n.s	n.s	n.s	*	**
2	n.s	X	n.s	*	*	*	***	****
3	n.s	n.s	X	n.s	*	n.s	**	*
4	*	n.s	n.s	X	n.s	n.s	n.s	*
5	n.s	**	n.s	n.s	X	n.s	n.s	n.s
6	*	*	n.s	n.s	n.s	X	*	*
7	*	n.s	n.s	n.s	n.s	n.s	X	n.s
8	*	n.s	n.s	n.s	n.s	n.s	n.s	X

107

Figure 14. Context discrimination and fear extinction in EE, SC and EI mice. A. Left: mice were trained for 30 min in a 40 x 40 cm arena – termed Context A – and received footshocks (0.5 mA, 2 sec) every 5 min. After 6 days, animals were re-exposed to Context A to evaluate long-term memory, and to a completely different context, termed Context B, to assess context discrimination ability. Right: mice were consecutively exposed to Context A for 1 week to evaluate extinction learning. **B**. Percentage of freezing during the first minute of recording in the training session (T), Context A reexposition (A) or Context B exposure (B). Data is analysed using Mann-Whitney test. **C, D**. Percentage of freezing during the first 3 minutes of recording (**C**) or percentage of total freezing (15 minutes, **D**) during exposure to Context A over 1 week. (1-8: consecutive days, where day 1 corresponds to Context A re-exposition during the context discrimination test). Daily freezing level comparisons between environmental conditions are presented below each graph. Data is analysed using Two-way repeated measures ANOVA and corrected for multiple comparisons using Turkey's test (Graph C: Time: ****, Rearing Conditions: **; Graph D: Time: ****, Rearing Conditions: ***). **E, F**. Comparison of freezing level across the days of fear extinction under EE (green) and EI (red) conditions, during the first 3 minutes of recording (**E**) or throughout the total session (15 minutes, **F**). Data is analysed using repeated measures ANOVA and corrected for multiple comparisons using Turkey's test. * $p < 0.05$; ** $p < 0.01$; *** $p < 0.001$; **** $p < 0.0001$.

4.3 Sun1-GFP nuclear tagging for isolating neuronal nuclei and analysing hippocampal-layer differences among rearing conditions

To investigate whether the behavioural changes induced by EE or EI correlated with modifications in the transcriptome and epigenome of hippocampal principal neurons, CamKIIα-CreER^{T2} mice were crossed with the transgenic Cre-dependent reporter mouse strain CAG-[STOP]-Sun1-GFP (**Figure 15A**) (abbreviated as CaMKIIα-Sun1-GFP). The CaMKIIα promoter selectively drives the expression of CreER^{T2} protein in forebrain principal neurons, where it remained in the cytoplasm. Upon administration of tamoxifen (TMX), the CreER^{T2} protein translocates to the nucleus, removing the STOP codon, and enabling the permanent expression of the Sun1-GFP fusion protein (**Figure 15A**). 3-week-old CaMKIIα-Sun1-GFP female mice were housed in either EE, SC or EI for 3 months and TMX was administered at half of the total housing duration to switch on the expression of Sun1-GFP (**Figure 15B**).
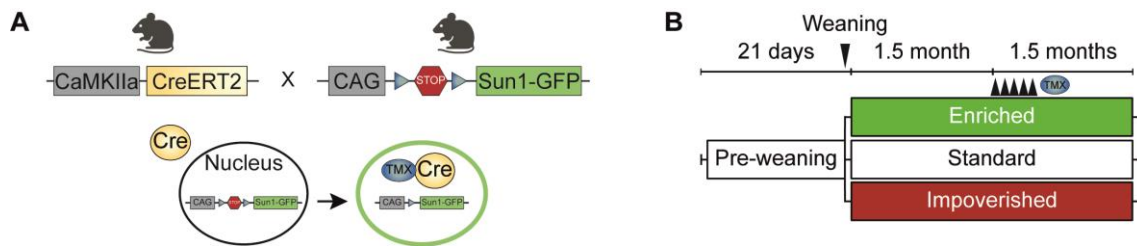
Figure 15. Sun1-GFP nuclear tagging as a system to isolate neuronal nuclei. A. CamKIIα-CreER^{T2} mice were crossed with CAG-[STOP]-Sun1-GFP mice. Upon TMX administration, CreER^{T2} removes the STOP codon, enabling the permanent expression of Sun1-GFP protein. **B**. Upon weaning (P21), CaMKIIα-Sun1-GFP littermates were randomly distributed in EE (green), SC (white) or EI (red) paradigm for three months. TMX was administered at half of the total housing duration (1.5 months).

First, Sun1-GFP⁺ neuronal nuclei from total hippocampus were isolated by fluorescence activated nuclear sorting (FANS) (**Figure 16A**), a technique that enables the efficient isolation of nuclei for subsequent nuclear RNA (nuRNA) quantification and epigenomic analyses (Fernandez-Albert et al., 2019). Interestingly, flow cytometry already revealed some intriguing differences between groups. Specifically, Sun1-GFP⁺ nuclei from EE mice displayed a bimodal distribution of fluorescein isothiocyanate-A (FITC-A) channel signal, whereas Sun1-GFP⁺ nuclei from SC and EI samples showed a unimodal distribution (**Figure 16B**). Since the expression of Sun1-GFP is controlled by the artificial CAG promoter, which contains sequences of the CMV enhancer (Hitoshi et al., 1991; Jun-ichi et al., 1989) known to be bound by activity-regulated transcription factors such as the cAMP response element binding protein (CREB) and the activator protein 1 (AP1) (Bäck, et al., 2019a), we speculated that the bimodal distribution may reflect the existence of a population of hippocampal cells with higher tonic levels of activity in EE animals. To assess this hypothesis, we investigated whether Sun1-GFP levels were indeed regulated by activity. The CaMKIIα-Sun1-GFP mice were injected with 25 mg/kg of kainic acid (KA), which causes strong and synchronized hippocampal activation, or saline solution. We observed an increase of GFP transcripts in KA-treated animals confirming that the expression of this reporter is activity-dependent (**Figure 16C**).
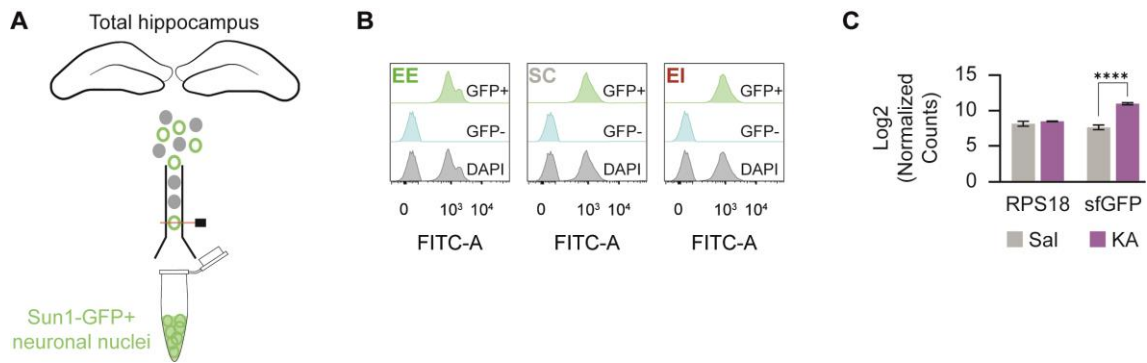
Figure 16. Sun1-GFP fluorescence signal from total hippocampus. A. Sun1-GFP$^+$ nuclei were isolated from total hippocampus by FANS. **B**. Flow cytometer histograms (number of events versus FITC-A channel signal) showing Sun1-GFP$^+$ singlet nuclei, Sun1-GFP$^-$ singlet nuclei and DAPI signal from EE, SC and EI conditions. **C**. Normalized counts for mice treated with saline or kainic acid (KA) and sacrificed 1-hour post-treatment. Mice treated with KA present increased expression of sfGFP (pAdj = 7,14E-17). *Rps18* is used as housekeeping gene. nuRNAseq data was obtained from (Fernandez-Albert et al., 2019) and analysed using DESeq2.

Next, given the distinct cellular composition and functional differences among hippocampal layers, we investigated whether the FITC-A signal exhibited changes in specific neuronal populations in response to EE. Specifically, we manually dissected CA1 and DG layers of the hippocampus and isolated the Sun1-GFP$^+$ nuclei from CA1 pyramidal neurons and DG granule neurons by FANS (**Figure 17A**). The accuracy of the dissections was validated measuring the expression of specific hippocampal-layer markers. In the DG region, we assessed the expression of *Dsp* and *Tdo2* genes by RT-qPCR and observed a specific enrichment of these genes in DG granule cells compared to CA1 samples (**Figure 17B**). We also examined the expression of the gene *Nov*, a CA1 layer-specific marker, and, as expected, we found a higher expression in CA1 samples than in DG samples (**Figure 17C**).

After isolating Sun1-GFP$^+$ nuclei from DG granule cells of EE, SC and EI mice, we found a relatively uniform distribution of FITC-A signal across all three conditions (**Figure 17D**). However, in the case of CA1 nuclei, FITC-A signal displayed a wider distribution, indicating that there is a larger range of activation levels in CA1 pyramidal neurons (**Figure 17E**). To quantify the percentage of GFP$^+$ CA1 nuclei exhibiting the highest FITC-A values across the diverse environmental conditions, we established a gate with a specific length, based on the bimodal distribution of FITC-A signal observed in CA1 EE replicates (**Figure**

17F, left). This constant gate was aligned with the highest FITC-A value in each biological replicate. Interestingly, we observed that the wider distribution in pyramidal neurons was enhanced in EE mice, which presented a larger percentage of GFP$^+$ nuclei at the highest values of FITC-A signal in comparison to SC and EI nuclei (**Figure 17F, right**). These results suggest that CA1 pyramidal neurons of EE animals show an increase in tonic activity-dependent transcription than those of EI and SC animals.
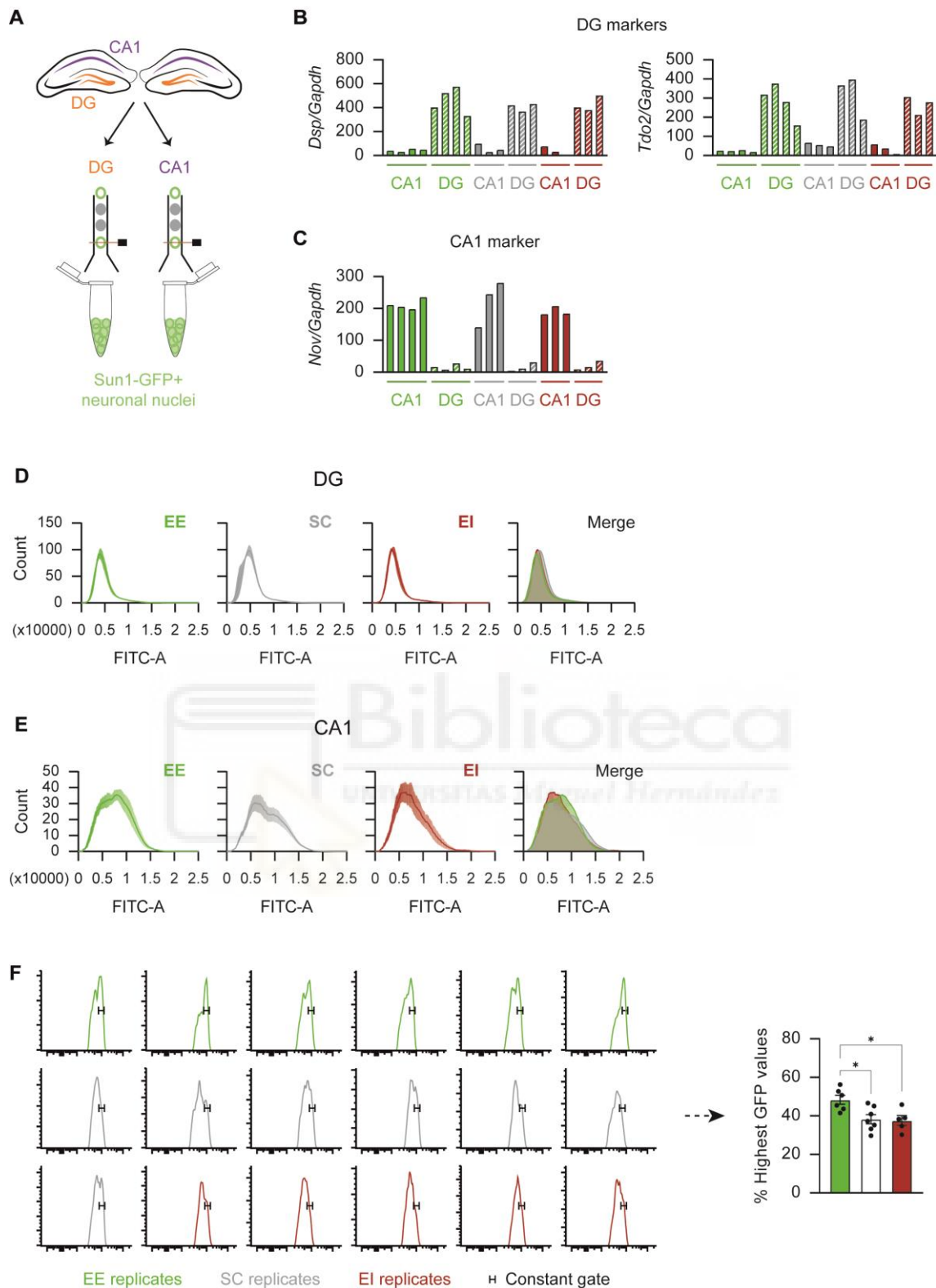
Figure 17. DG and CA1 Sun1-GFP fluorescence signal differences among environmental conditions. A. Sun1-GFP[+] nuclei were isolated from manually dissected DG and CA1 by FANS. **B**. RT-qPCR analysis of *Dsp* (left) and *Tdo2* (right) indicate specific dissection of DG layer. **C**. RT-qPCR analysis of *Nov* indicates specific dissection of CA1 layer. **D**. Flow cytometer histograms (number of events versus FITC-A channel signal) showing Sun1-GFP[+] DG singlet nuclei. Left:

FITC-A signal (mean ± SEM) of EE, SC and EI conditions. Right: merge of mean FITC-A signal from the 3 environmental conditions (numbers in the x axis are multiplied by 10,000). **E**. Flow cytometer histograms (number of events versus FITC-A channel signal) showing Sun1-GFP⁺ CA1 singlet nuclei. Left: FITC-A signal (mean ± SEM) of EE, SC and EI conditions. Right: merge of mean FITC-A signal from the 3 environmental conditions (numbers in the x axis are multiplied by 10,000). **F**. Left: diagram illustrating the alignment of a constant gate – established based on the bimodal distribution of FITC-A signal observed in CA1 EE replicates – set to the highest FITC-A value observed in each biological replicate, to assess the percentage of nuclei exhibiting the highest FITC-A values under each condition. Right: percentage of nuclei falling within the established constant gate across different environmental conditions. Data is analysed using Mann-Whitney test. * p < 0.05.

The differences observed in the flow cytometry analyses between DG and CA1 layers highlight the efficacy of manual dissection followed by FANS in obtaining high-quality samples of granule and pyramidal cells, respectively. This method enables precise exploration and comparison of the transcriptional and epigenetic alterations occurring in both hippocampal layers following early exposure to various environmental conditions (**Figure 18**).
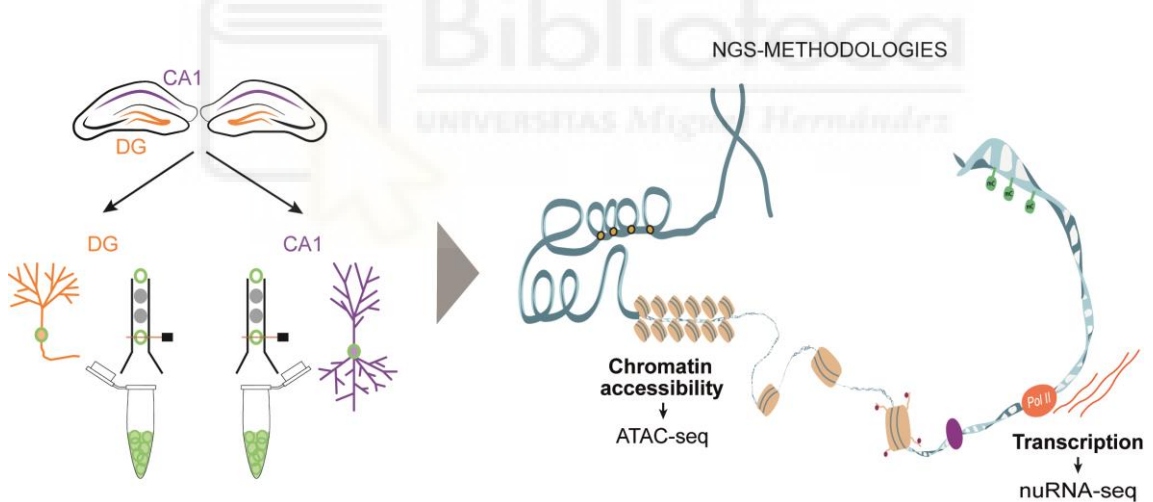

Figure 18. Transcriptomic and epigenetic analysis of DG granule cells and CA1 pyramidal neurons. Left. Granule and pyramidal neurons were manually dissected and sorted by FANS. Right. ATAC-seq and nuRNA-seq were used for chromatin accessibility and transcriptome analysis, respectively.

4.4 Transcriptional differences and increased AP1 binding in the DG of EE mice

In the analysis of nuclei from granule neurons in DG samples, a principal component analysis (PCA) of nuRNA-seq data showed a slight segregation of the EE samples, while EI and SC samples were intermingled (**Figure 19A**). Among the 74 differentially expressed genes (DEGs) identified, two distinct clusters were observed. One cluster was formed by 14 genes with reduced expression in the EE condition, while the other cluster consisted of the remaining 60 genes that exhibited higher expression in EE (**Figure 19B**). In contrast, SC and EI samples showed similar expression levels for the 74 DEGs. Gene ontology analysis did not reveal any common pathway among these DEG clusters, suggesting that the differences observed among environmental paradigms did not result in specific changes in a particular pathway or process. Similarly, ATAC-seq-based screen for differentially accessible regions (DARs) retrieved 225 regions with increased accessibility in EE samples compared to SC and EI samples (**Figure 19C**).
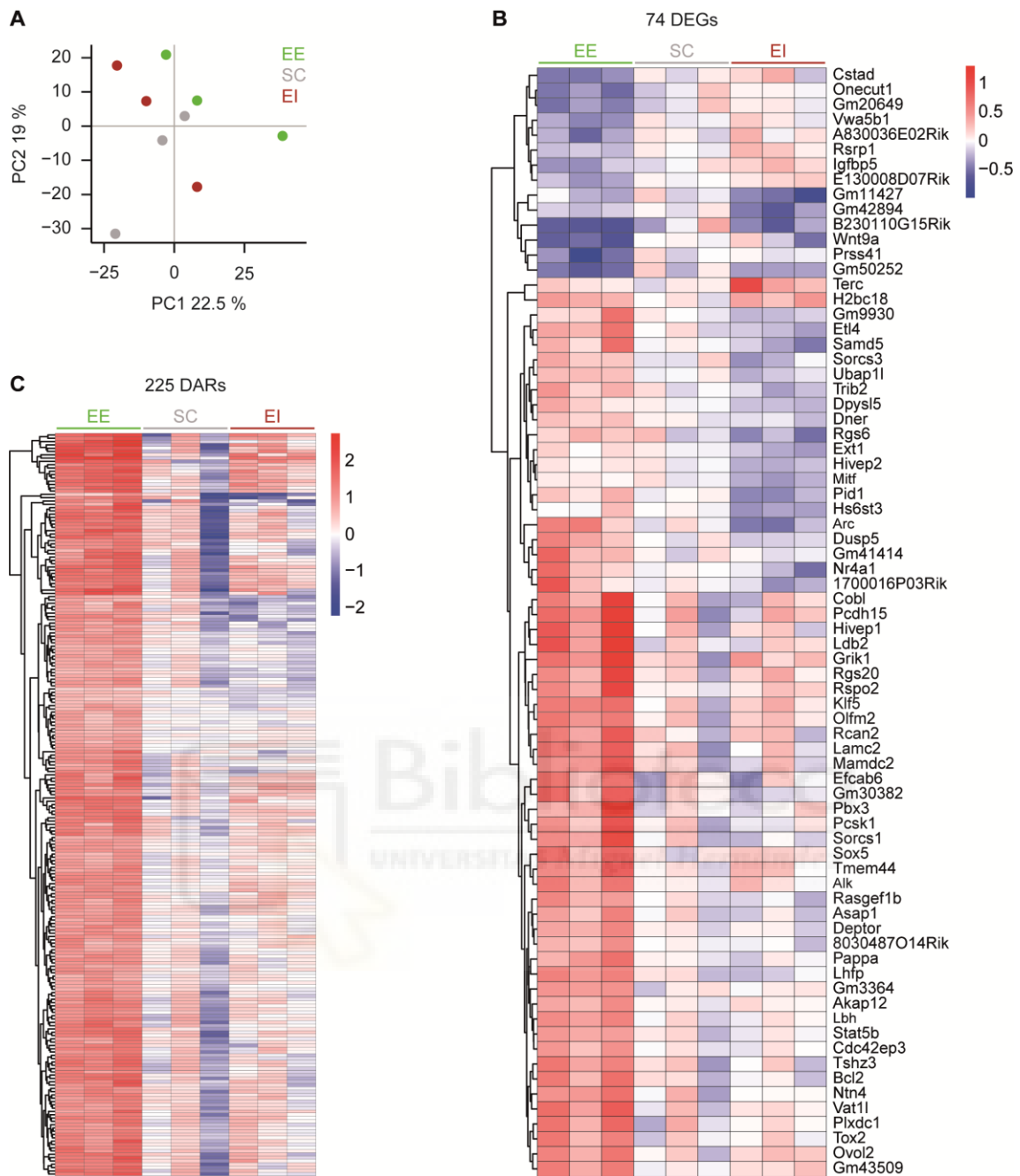
Figure 19. Transcriptional and accessibility differences among environmental conditions in the DG granule neurons. A. PCA of nuRNA-seq profiles for EE, SC and EI DG samples. **B**. Heatmap of DEGs retrieved in the nuRNA-seq screen (pAdj < 0.1). **C**. Heatmap of DARs retrieved in the ATAC-seq screen (pAdj < 0.1).

When annotating the obtained DARs to the nearest gene, 3 DEGs (*Etl4*, *Ext1* and *Asap1*) were identified. *Etl4* gene has been associated with epilepsy and is involved in embryonic skeletal system development; *Ext1* gene is implicated in the biosynthesis of heparan sulphate, which has been related with brain development and autism-like communicative deficits and stereotypies when it is

conditionally inactivated in postnatal neurons (Irie et al., 2012); and *Asap1* is a GTPase-activating protein which directly binds actin filaments and regulates the dynamics and the formation of higher-order actin structures (Chen et al., 2020). Interestingly, all 3 DEGs were differentially upregulated in EE and exhibited higher accessibility regions after EE exposure. However, for *Etl4* and *Ext1*, the increase in transcription did not seem to correlate directly with the gain in accessibility, since these DAR peaks were not located neither at the promoters nor the enhancers of these DEGs, and there was no clear relationship between them and chromatin interaction analysis by paired-end tag sequencing (ChIA-PET) (**Figure 20A, B**). Regarding *Asap1*, while the DAR peak is proximal to the non-coding exon I (distance: 2756 bp), no concurrent transcriptional changes were observed in the *Asap1* transcript variants that contain this exon – *Asap1* comprises 19 transcript variants, and the findings revealed unequal transcriptional expression among them under varying environmental conditions (**Figure 20C**). This lack of clear correlation between changes in transcription and accessibility could be attributed to the fact that most DARs were located into intergenic regions and introns (**Figure 20D**).
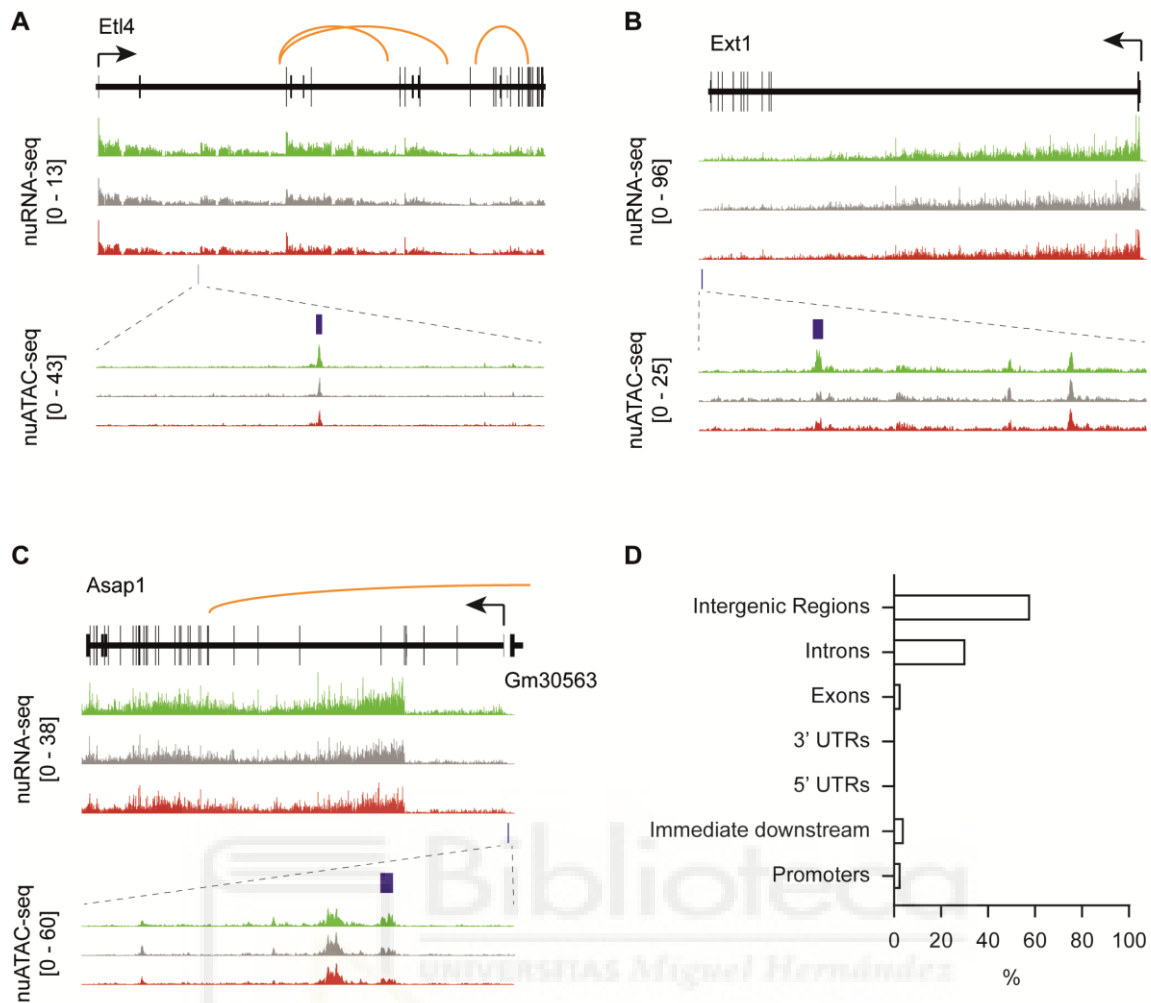
Figure 20. Transcriptional differences do not correlate with changes in accessibility in DG granule neurons. A-C. Genomic snapshots of nuRNA-seq and ATAC-seq tracks for *Etl4* (**A**), *Ext1* (**B**) and *Asap1* (**C**) genes. Values represent counts in RPM (reads per million). ChIA-PET data was obtained from (del Blanco et al., 2024) and loops are depicted in orange. The arrows indicate transcript directionality. **D**. DARs genomic distribution.

Next, to conduct a more comprehensive study on the chromatin occupancy by transcription factors (TFs), the 122,738 accessible regions identified by ATAC-seq were classified into promoters (19,039 regions) or enhancers (103,699 regions) based on the presence or absence of the epigenetic mark histone 3 lysine 4 trimethylation (H3K4me3), respectively (**Figure 21A**). Interestingly, when TF binding prediction was performed in EE and EI conditions (compared with SC), we observed a specific enrichment of AP1 TF in the EE condition, both in enhancer regions and promoters (**Figure 21B**). AP1 is a well-known activity-dependent TF family, composed of members from the Jun and Fos protein families that associate to form dimeric TFs, which has been involved in neuronal

117

plasticity processes, such as learning and memory (Benito & Barco, 2015). Analysis of the footprint for AP1-Fos shown a stronger binding in EE than in SC, particularly at enhancer regions (**Figure 21C**). This result may indicate that rearing the animals in EE led to changes in the occupancy of regulatory regions in granule cells that particularly affects AP1 binding sites, suggesting that DG granule cells in the hippocampus of EE-reared animals are more prone to respond to new stimuli.
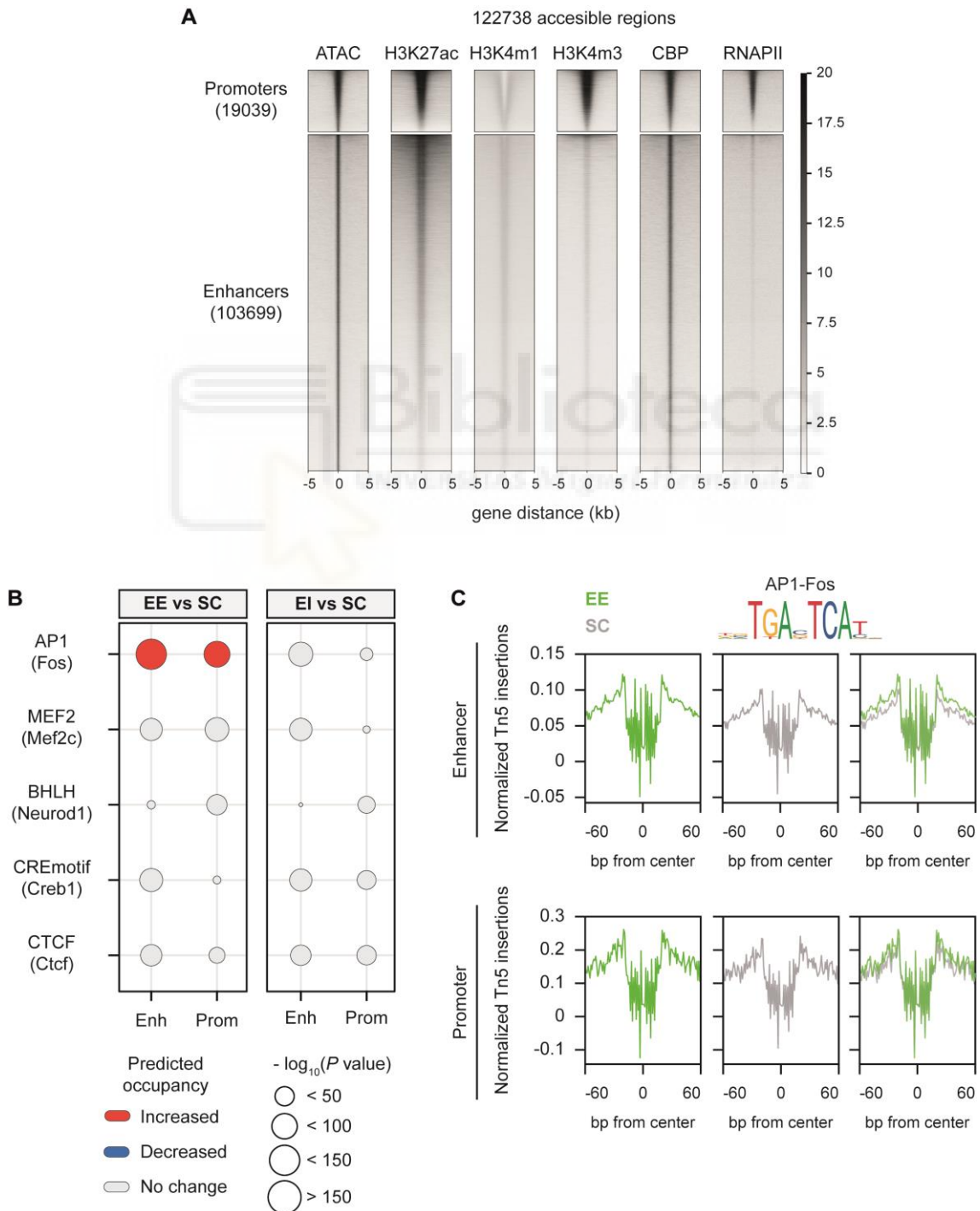
Figure 21. EE alters AP1 transcription factor binding prediction in enhancers and promoters of DG granule neurons. A. K-mean clustering was applied to identify accessible regions (± 5 kb window), using profiles from ATAC-seq (specific reads from DG chromatin) and H3K27ac, H3K4me1, H3K4me3, CBP and RNAPII binding in hippocampal chromatin of naive mice. ATAC-seq, H3K27ac and CBP-ChIP signals denote a regulatory role, while H3K4me3 primarily labels promoter regions. **B**. TF binding prediction in enhancers and promoters between the different environmental conditions. Circle size indicates motif enrichment *P* value and colours refer to the prediction of occupancy by the TFs. **C**. Digital footprint for AP1 (Fos motif) in EE and SC accessible peaks (top: enhancers; bottom: promoters). Values correspond to normalized Tn5 insertions.

4.5 Transcriptional differences and decreased AP1 binding in the CA1 of EI mice

In the analysis of CA1 samples, the PCA did not reveal a distinct distribution that categorizes the various environmental conditions (**Figure 22A**). However, gene set enrichment analysis (GSEA) of the genes obtained in the nuRNAseq data showed statistically significant pathways upregulated in the EE condition when it was compared with EI (**Figure 22B**). Among the pathways obtained, we found *signalling by NTRKs* (NES (normalized enrichment score) = 1.88), *RNA transport* (NES = 1.74), *regulation of miRNA metabolic process* (NES = 1.71) or *regulation of dendritic spine morphogenesis* (NES = 1.69). These pathways were clustered together by Cytoscape tool, and the major biological themes identified were MAPK nuclear signalling, RNA transport and miRNA regulation (**Figure 22B**). When EE, SC and EI conditions were compared, 58 DEGs were identified, including a cluster of activity-dependent genes that were enriched in the EE condition (**Figure 22C**), consistent with GSEA enrichment in MAPK nuclear signalling pathways. Additionally, a cluster predominantly formed by non-coding RNAs (ncRNAs) exhibits reduced expression in both the EE and EI conditions (**Figure 22C**), which could also be related to the enrichment found in miRNA regulation pathways and RNA transport. Remarkably, 25/35 (71.4 %) of the identified ncRNAs were categorized within the snoRNAs subset (highlighted in blue), which are known for their involvement in posttranscriptional modifications of rRNAs, tRNAs and mRNAs (Huang et al., 2022). Moreover, 3 ribosome-related

genes (highlighted in orange), 1 miRNA (highlighted in purple) and 2 lncRNA (highlighted in green) were also found within this cluster.
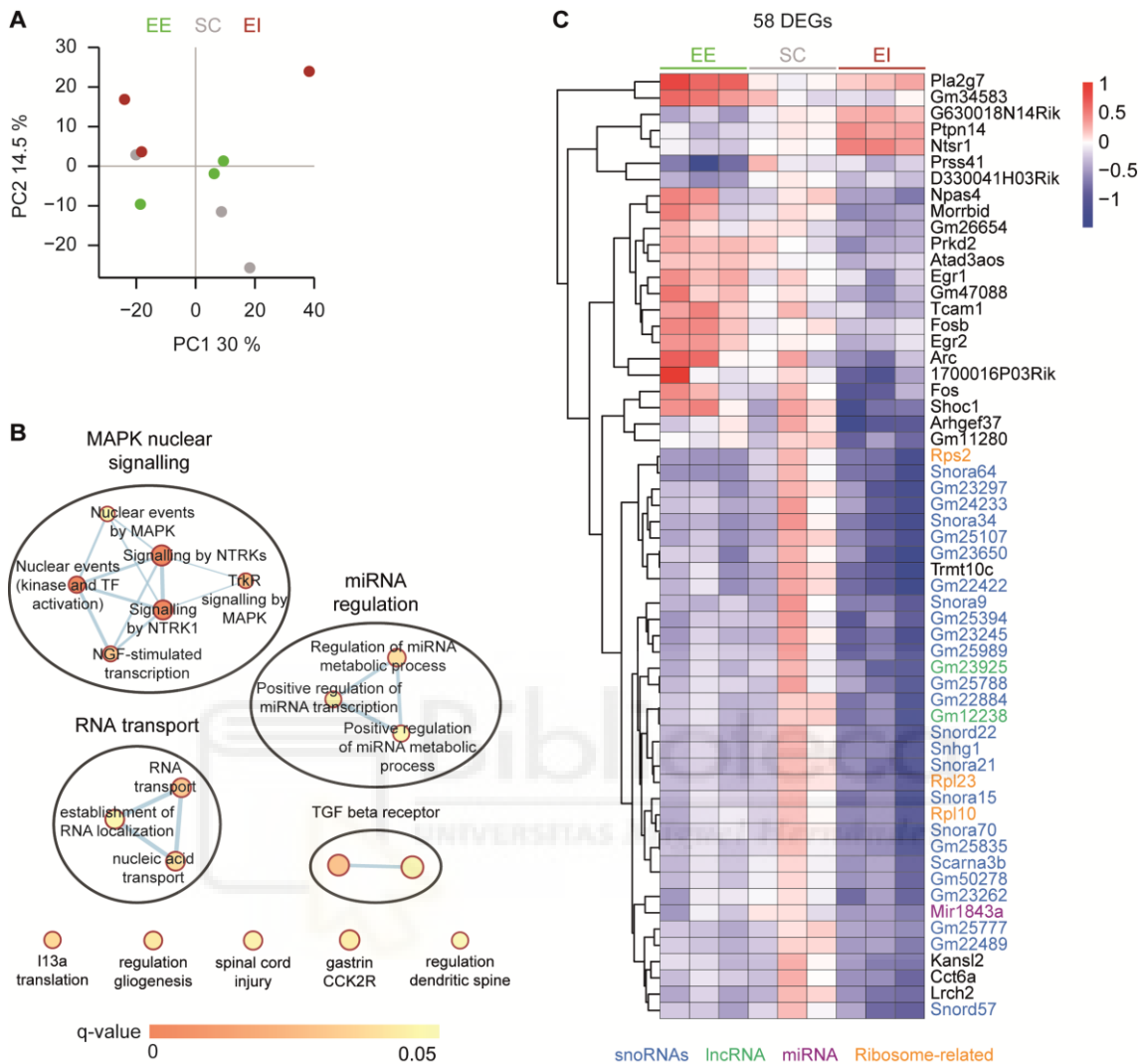

Figure 22. EE alters the expression of activity-dependent genes in CA1 pyramidal neurons. **A**. PCA of nuRNA-seq profiles for EE, SC and EI CA1 samples. **B**. Enrichment map of GSEA pathways was created with parameters q-value < 0.05, and Jaccard Overlap combined coefficient > 0.375 with combined constant = 0.5. Circle border colour indicates NES (red: enrichment in EE; blue: enrichment in EI) and circle filled colour reflects q-value. Blue lines indicate connections between related pathways. **C**. Heatmap of DEGs retrieved in the nuRNA-seq screen (pAdj < 0.1).

To evaluate changes in TF binding, the 158,797 total accessible regions were classified into promoters (20,606 regions) or enhancers (138,191 regions) based on the presence or absence of H3K4me3, respectively (**Figure 23A**). Notably, none of these regions showed a significant change in accessibility when comparing the different conditions. However, when these regions were used to predict differential occupancy by TFs, we observed a decrease AP1 binding at

enhancer regions of the EI condition (**Figure 23B (first row), C**), as well as a decrease in MEF2 binding specifically in EE enhancer regions (**Figure 23B, second row**). Myocyte-enhancing factor 2 (MEF2) proteins are a family of evolutionarily conserved transcription factors with a distinctive role in memory due to MEF2 constrains (rather than promotes) memory formation (Cole et al., 2012; Rashid et al., 2014). Furthermore, there was an increase in basic helix-loop-helix (BHLH) predicted binding on EI promoters (**Figure 23B, third row**), which is a broad family of transcription factors involved in neuronal fate determination (Dennis et al., 2019). These results suggest alterations in the occupancy of the TF AP1 in pyramidal cells, akin to what was observed in granule cells, thereby proposing AP1 as the primary mediator of the effects that environmental conditions exert on the epigenome. Furthermore, the observed changes in the occupancy of MEF2 and BHLH TFs may imply that epigenetic responses to environmental exposure are cell-specific, as evidenced by the discrepancies observed between changes in CA1 and DG.
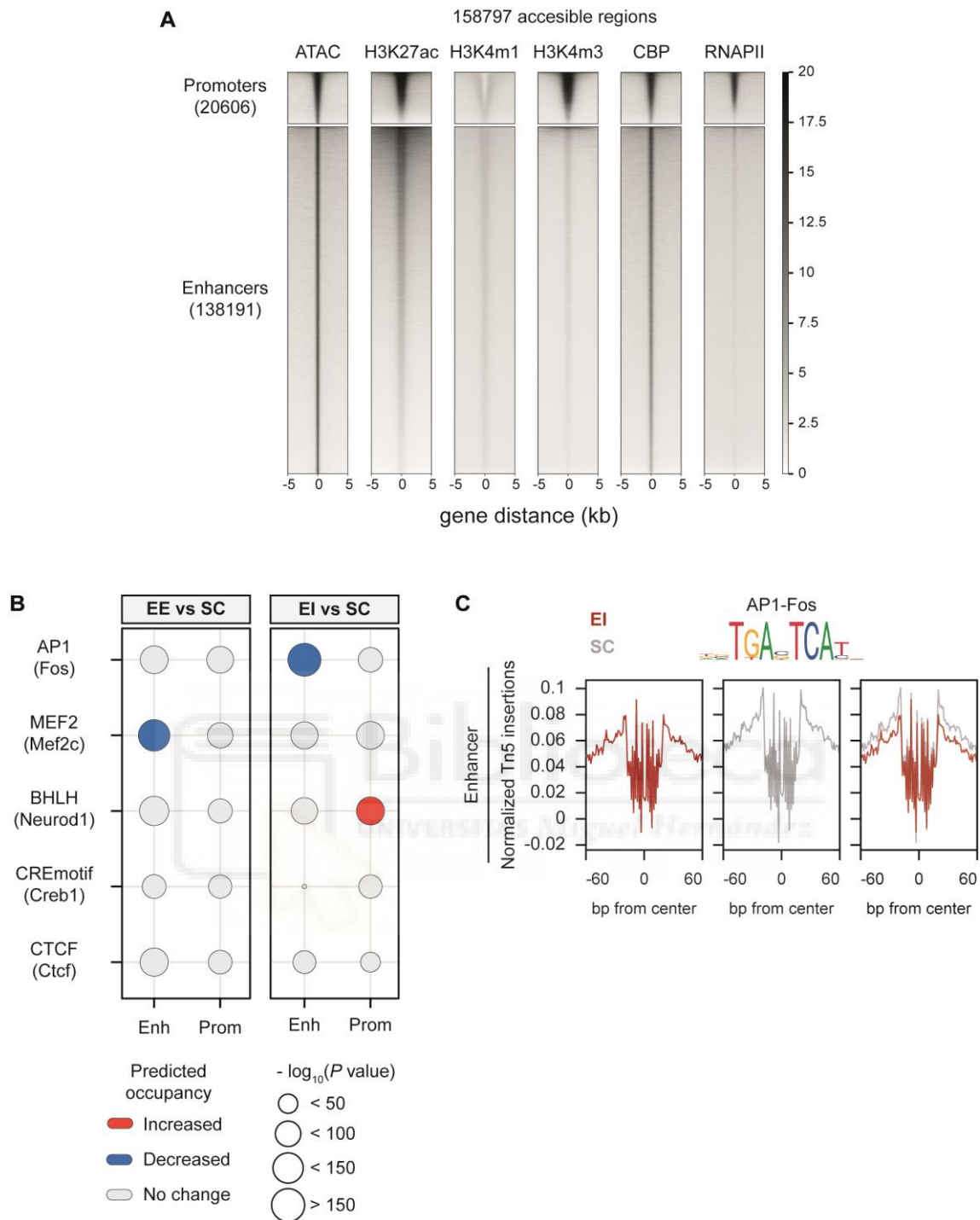
Figure 23. EI reduces AP1 transcription factor binding prediction in enhancers of CA1 layer. A. K-mean clustering was applied to identify accessible regions (± 5 kb window), using profiles from ATAC-seq (specific reads from CA1 chromatin) and H3K27ac, H3K4me1, H3K4me3, CBP and RNAPII binding in hippocampal chromatin of naive mice. ATAC-seq, H3K27ac and CBP-ChIP signals denote a regulatory role, while H3K4me3 primarily labels promoter regions. **B**. TF binding prediction in enhancers and promoters between the different environmental conditions. Circle size indicates motif enrichment *P* value and colours refer to the prediction of occupancy by the TFs. **C**. Digital footprint for AP1 (Fos motif) in EI and SC enhancer accessible. Values correspond to normalized tn5 insertions.

122

The collective findings of this initial results section suggest that early-life exposure to diverse environmental conditions modulates cognitive capacities during adulthood, although we could not correlate these outcomes with changes in engram formation using a strong training in a fear conditioning paradigm. Analysing the transcriptional and accessibility changes in hippocampal cells, we observed that CA1 pyramidal neurons in EE-exposed animals exhibit an increase in activity-dependent transcription, potentially correlating with predicted changes in AP1 occupancy. Within the DG, granule cells of EE-exposed mice display a generalized increase in transcription and accessibility, alongside variations in the predicted occupancy of AP1. Additional changes associated with ncRNAs and MEF2 and BHLH TFs have also been observed, suggesting that different epigenetic mechanisms may be involved in the adaptation of animals to environmental factors.

To delve deeper into the significance and causality of these epigenetic mechanisms in environmental adaptation and their impact on cognitive performance, the development of epigenome editing tools becomes imperative. These tools would enable targeted manipulation of diverse epigenetic marks, allowing us to decipher their necessity and/or sufficiency. Addressing this main objective constitutes the focus of the second *Results* section of this thesis.

RESULTS

Section 2
Development of a toolbox for precise neuronal epigenome editing

The following study was conducted in collaboration with several members of the laboratory of Prof. Ángel Barco, at the Instituto de Neurociencias (UMH-CSIC).

Dr. Beatriz del Blanco designed the innovative split dCas9-CMD toolbox and contributed to the cloning of certain plasmids. Carina Racovac Farinha also participated in the cloning of some plasmids. I conducted all the evaluation of the split dCas9-CMD toolbox in cell lines and primary cultures and contributed to the cloning of certain plasmids. The results obtained in this study have been interpreted under the supervision of Dr. Beatriz del Blanco and Prof. Ángel Barco.

4.6 Generation of a split dCas9-CMD toolbox for neuronal epigenome editing based on nanobody technology

The conventional CRISPR epigenetic editing system comprises a guide RNA (gRNA), complementary to the region of interest, and a chimeric protein, formed by fusing the nuclease-deficient dCas9 protein with the catalytic domain of epigenetic enzymes (termed chromatin modifying domain, CMD, in this project) (Policarpi et al., 2021). However, resulting chimeric proteins are often large in size and beyond the packaging capacity of neurotropic vectors. To overcome this limitation, we have developed a novel and modular epi-editing system, termed the split dCas9-CMD toolbox, which divides the conventional chimeric proteins into two smaller elements. The first element involves fusing the dCas9 protein with a nanobody (Nb) derived from a llama, referred to as vhhGFP4 (Caussinus et al., 2011; Saerens et al., 2005). This Nb selectively recognizes the green fluorescent protein (GFP), thus forming a DNA binding domain (DBD) in conjunction with a gRNA. The second element forms the CMD module by fusing the catalytic domain of various epigenetic proteins with GFP (**Figure 24A**).

The resulting split dCas9-CMD neuronal epigenome editing toolbox operates in a *trans* manner. The gRNA, which is complementary to the target region, is recognized by the chimeric protein dCas9-vhhGFP4. Subsequently, the CMD module is recruited through the robust intermolecular interaction between vhhGFP4 and GFP. This innovative design grants the system greater versatility, and its reduced size enhances its packaging efficiency in viral vectors, including AAVs (**Figure 24B**).
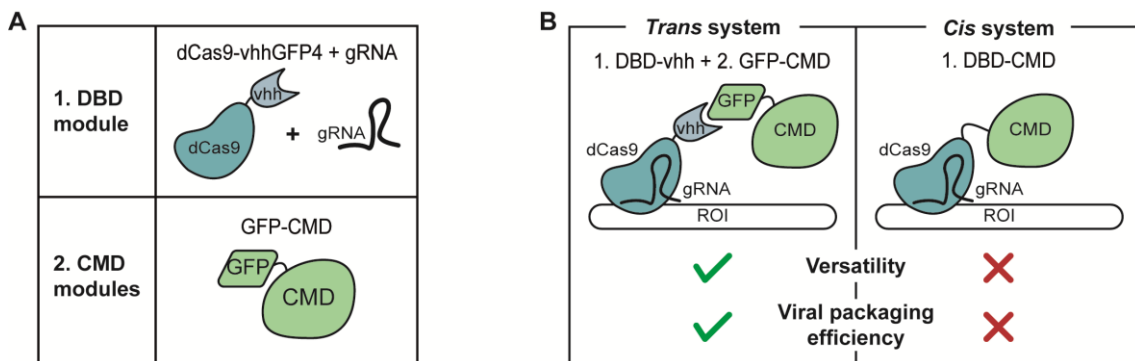

Figure 24. Split dCas9-CMD neuronal epigenome editing toolbox. A. Components of the split dCas9-CMD neuronal epigenome editing toolbox. Above, the DNA-binding domain (DBD)

module, consisting of the nanobody vhhGFP4 (vhh) – with specificity against GFP – fused to dCas9 in combination with a gRNA. Below, the chromatin-modifying domain (CMD) modules, consisting of GFP bound to the CMD of epigenetic regulators. **B**. Left: in the *trans* system, the DBD module (component 1) and the CMD module (component 2) are brought together by the strong intermolecular interaction of vhhGFP4 and GFP, which offers higher versatility and viral packaging efficiency. Right: in the *cis* system, the DBD is fused to the CMD creating a chimeric protein with less versatility and viral packaging restrictions due to its larger size.

4.7   Selection of cell subpopulations that simultaneously express all the constituents of the split dCas9-CMD system

The split dCas9-CMD epi-editing toolbox comprises 3 constituents: the dCas9-vhhGFP4 fusion protein, a gRNA, and the GFP-CMD fusion protein. Hence, to accurately assess the epigenetic modification capabilities of the split dCas9-CMD toolbox, it is necessary to ensure the concurrent expression of these three constituent elements within each target cell. Consequently, we first conducted an evaluation of the split dCas9-CMD toolbox employing a *Mus musculus* neuroblastoma cell line (N2a), since they are mitotic cells with neuronal and amoeboid stem cell morphology isolated from mouse brain tissue. N2a cells can be sorted and selected according to the simultaneous expression of all three components.

The plasmid that allows the expression of the DBD module dCas9-vhhGFP4 lacks fluorescence and antibiotic resistance cassettes. Hence, N2a cells were first infected with lentiviruses carrying the dCas9-vhhGFP4 construct and single cell sorted to obtain one cell clone per well (**Figure 25A**). We checked the expression of dCas9-vhhGFP4 in the obtained clones by RT-qPCR (**Figure 25B**) and observed that clone 8 was positive for dCas9-vhhGFP4 expression.

Infection with lentivirus resulted in the integration of the construct of interest into the genome, allowing its long-lasting expression. To verify that dCas9-vhhGFP4 was correctly integrated into clone 8, its expression was tested at different time points and found it to be stable over time (**Figure 25C**). This clone was named N2a^dCas9-vhhGFP4.
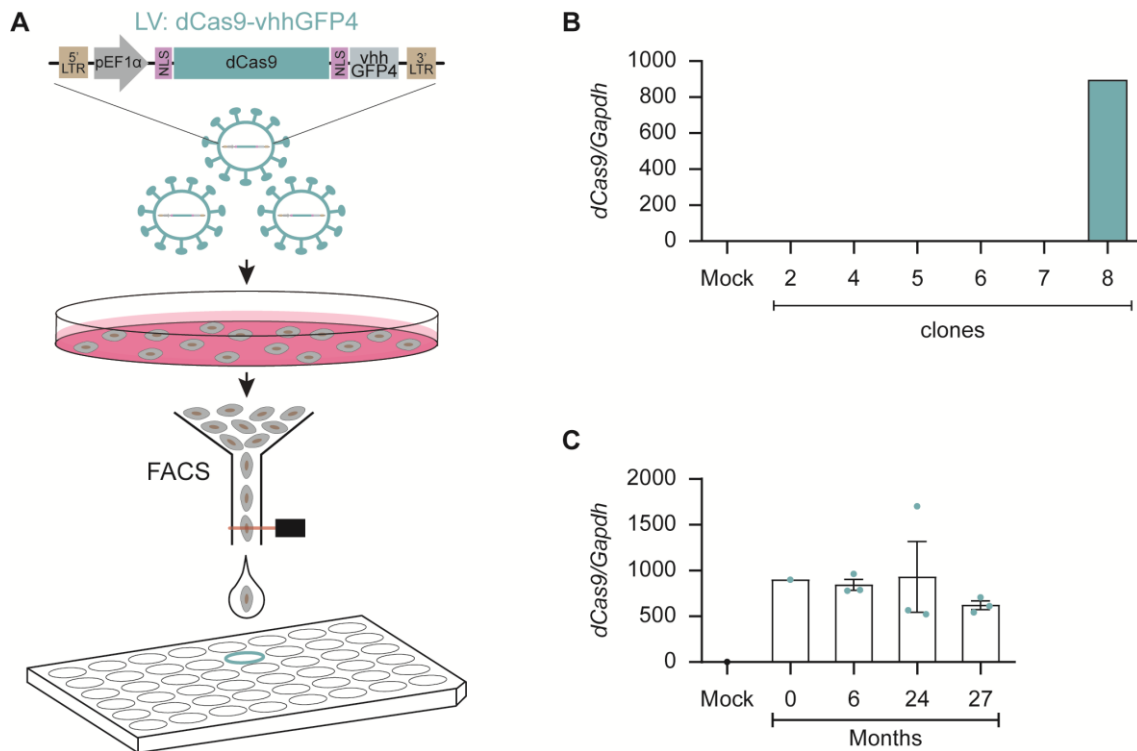
Figure 25. N2a^dCas9-vhhGFP4 clone generation. A. Top: scheme of dCas9-vhhGFP4 plasmid formed by the 5' and 3' LTR sequences that allow its integration into lentiviral vectors, the ubiquitous promoter of elongation factor 1 alpha (pEF1α), two nuclear localization sequences (NLS) for the correct translocation of the construct to the nucleus, and the chimeric dCas9-vhhGFP4 protein. Bottom: infection of N2a cells with lentivirus containing the dCas9-vhhGFP4 construct and single cell isolation to obtain individual cell clones. **B**. RT-qPCR analysis of *dCas9* indicates upregulation in clone 8. **C**. RT-qPCR analysis of *dCas9* indicates stability of *dCas9* expression in clone 8 over time. Time points correspond to: 0 months = August 2019; 6 months = February 2020; 24 months = August 2021; 27 months = November 2021. Uninfected cells (Mock) are used as control.

Next, cells from the generated N2a^dCas9-vhhGFP4 stable clone were co-infected with combinations of lentivirus expressing the CMD of interest and the selected gRNAs. The CMD modules contain the fluorescent protein GFP fused to different epigenetic effectors (**Figure 26A, left**), while the plasmids that allow the expression of the gRNAs contain a cassette with the fluorescent protein mCherry (**Figure 26A, right**). We can take advantage of the presence of both fluorescent proteins to select those cell subpopulations that express all elements of the split dCas9-CMD toolbox by flow cytometry. Specifically, the subpopulation of positive cells for FITC-A (detects GFP signal) and PE-Texas Red-A (detects mCherry signal) were selected and re-plated for growth (**Figure 26B**). We performed a second isolation to further enrich the percentage of GFP+/mCherry+

cells. This way we obtained cell subpopulations that have been selected for expressing, at the same time, the 3 modules of the split dCas9-CMD toolbox: dCas9-vhhGFP4 module, GFP-CMD module and gRNA.
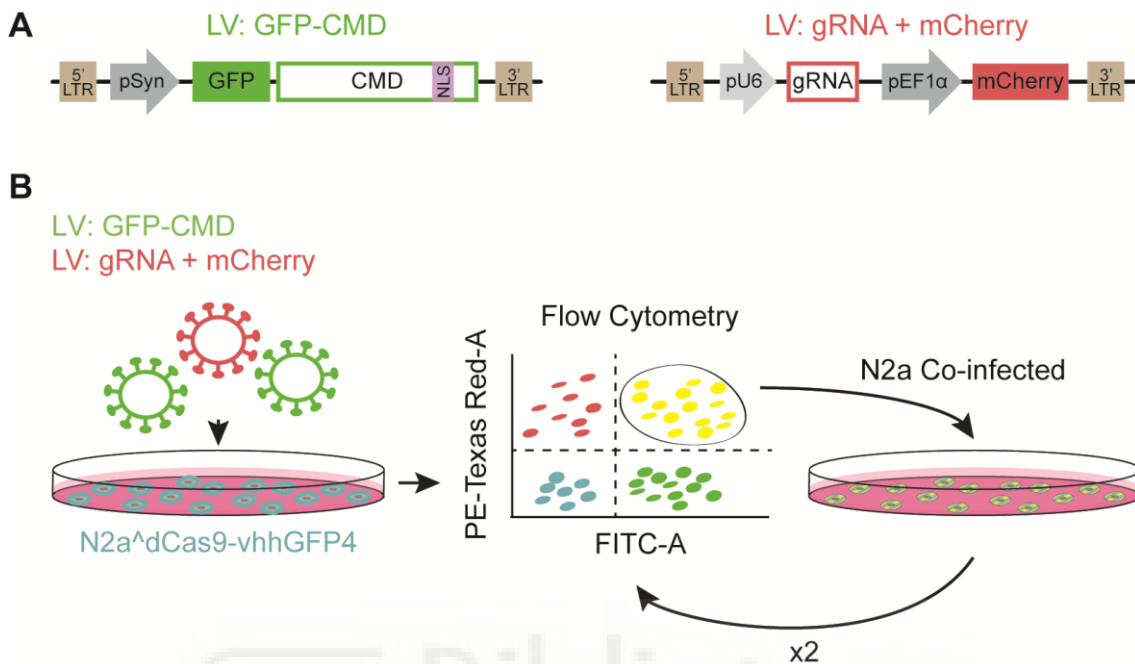

Figure 26. Obtaining N2a cell subpopulations that simultaneously express the 3 elements of the split dCas9-CMD toolbox. A. Left: scheme of GFP-CMD plasmid formed by the 5' and 3' LTR sequences that allow its integration into lentiviral vectors, the neuron-specific promoter synapsin (pSyn), a nuclear localization sequence (NLS) for the correct translocation of the construct to the nucleus, and the chimeric GFP-CMD protein. Right: scheme of gRNA plasmid formed by the 5' and 3' LTR sequences, the RNA polymerase III-dependent U6 promoter, which drives the expression of the gRNA - consisting of the target sequence and the gRNA scaffold - and the fluorescent protein mCherry, whose expression depends on the ubiquitous promoter EF1α. **B**. N2a^dCas9vhhGFP4 cells are infected with a combination of lentivirus expressing the GFP-CMD module and a gRNA of interest. Double positive cells (GFP+/mCherry+) are isolated twice by flow cytometry for further enrichment.

4.8 Assessment of transcriptional editing capacity using the VP16 transactivator domain

VP16 is a herpes simplex virus (HSV) type 1 transcription factor implicated in the activation of immediate early viral genes (Flint & Shenk, 1997). When an animal cell is infected by HSV, VP16 is released and binds to the host nuclear proteins HCF and Oct-1. As VP16 cannot interact directly with the DNA, Oct-1 recognizes

129

the target sequence at the promoters of immediate early genes, while HCF stabilizes the interaction between VP16 and Oct-1 (Wu et al., 1994; Wysocka & Herr, 2003). This allows VP16 to activate the expression of immediate early viral genes in infected cells through the interaction of its transcriptional activation domain and numerous transcription factors.

The transcriptional activation domain of VP16 has been fused, among others, with transcription factors to amplify their activity and study their gene regulation mechanism, or with epigenetic editing systems in which VP16 functions as a transactivator module that coordinates the recruitment of the transcriptional machinery and activates the expression of genes of interest (Hirai et al., 2010). In this project, VP16 is fused to GFP for the generation of a transactivator CMD module.

N2a^dCas9-vhhGFP4 cells were co-infected with a combination of lentiviruses expressing the VP16-GFP transactivator module and the control gRNA (Ctrl), the gRNA that recognizes the *Bdnf* promoter I (gRNA P1) or the one that recognizes *Bdnf* promoter IV (gRNA P4). After the first sorting, we obtained 64.1 %, 57.4 % and 61.8 % of cells co-infected (GFP$^+$/mCherry$^+$) with the VP16-GFP module and the gRNA Ctrl, gRNA P1 or gRNA P4, respectively (**Figure 27A, B**). After the second sorting, these percentages were enriched to 71.7 %, 87.0 % and 74.0 %, respectively (**Figure 27C, D**). In both cases, N2a cells uninfected with any of the modules (mock) were used as negative control.
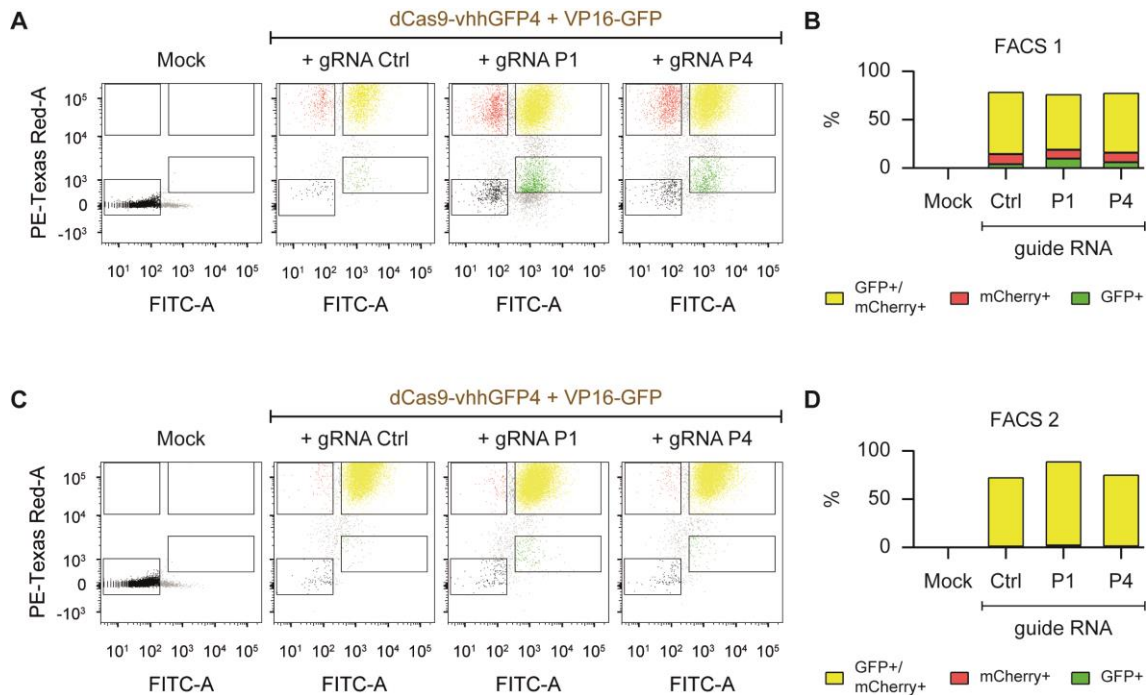
Figure 27. Isolation of N2a subpopulations expressing dCas9-vhhGFP4, VP16-GFP and gRNA (Ctrl, P1 or P4) modules. A. Flow cytometry dot plots (PE-Texas Red channel signal versus FITC-A channel signal) were used for gating and isolating GFP⁺/mCherry⁺ cell subpopulations during the initial sorting. **B**. Percentage of GFP⁺, mCherry⁺ and GFP⁺/mCherry⁺ cells obtained after the first sorting. **C**. Flow cytometry dot plots (PE-Texas Red channel signal versus FITC-A channel signal) were used for gating and isolating GFP⁺/mCherry⁺ cell subpopulations for further enrichment. **D**. Percentage of GFP⁺, mCherry⁺ and GFP⁺/mCherry⁺ cells obtained after the second sorting.

To confirm the correct integration of the different elements of the toolbox, the expression of dCas9 and GFP in the isolated subpopulations were compared with mock cells. We can appreciate the significant expression of both elements in infected cells (**Figure 28A**). Similarly, we only observed expression of gRNA P1 in the subpopulation infected with this element, and the same for gRNA P4 (**Figure 28B**). Immunostaining results further validate the specific expression of dCas9, GFP and mCherry at the protein level (**Figure 28C**).

The proper integration and concurrent expression of the 3 elements enables gRNA P1 or P4 to direct the dCas9-vhhGFP4 module to promoter I or IV of *Bdnf*, respectively. In turn, vhhGFP4 recruits the VP16-GFP module to interact with the transcriptional machinery and induce the expression of *Bdnf* transcript variants (**Figure 28D**). The results obtained demonstrate that this combination enables precise stimulation of the transcription of the variant produced by *Bdnf* promoter

IV, leading to an increase in its expression (**Figure 28E, left**). However, it does not stimulate the expression of the variant produced by promoter I (**Figure 28E, right**). This result indicates that the same molecular toolbox may display different transactivation efficacy depending on the genomic context of the promoter.
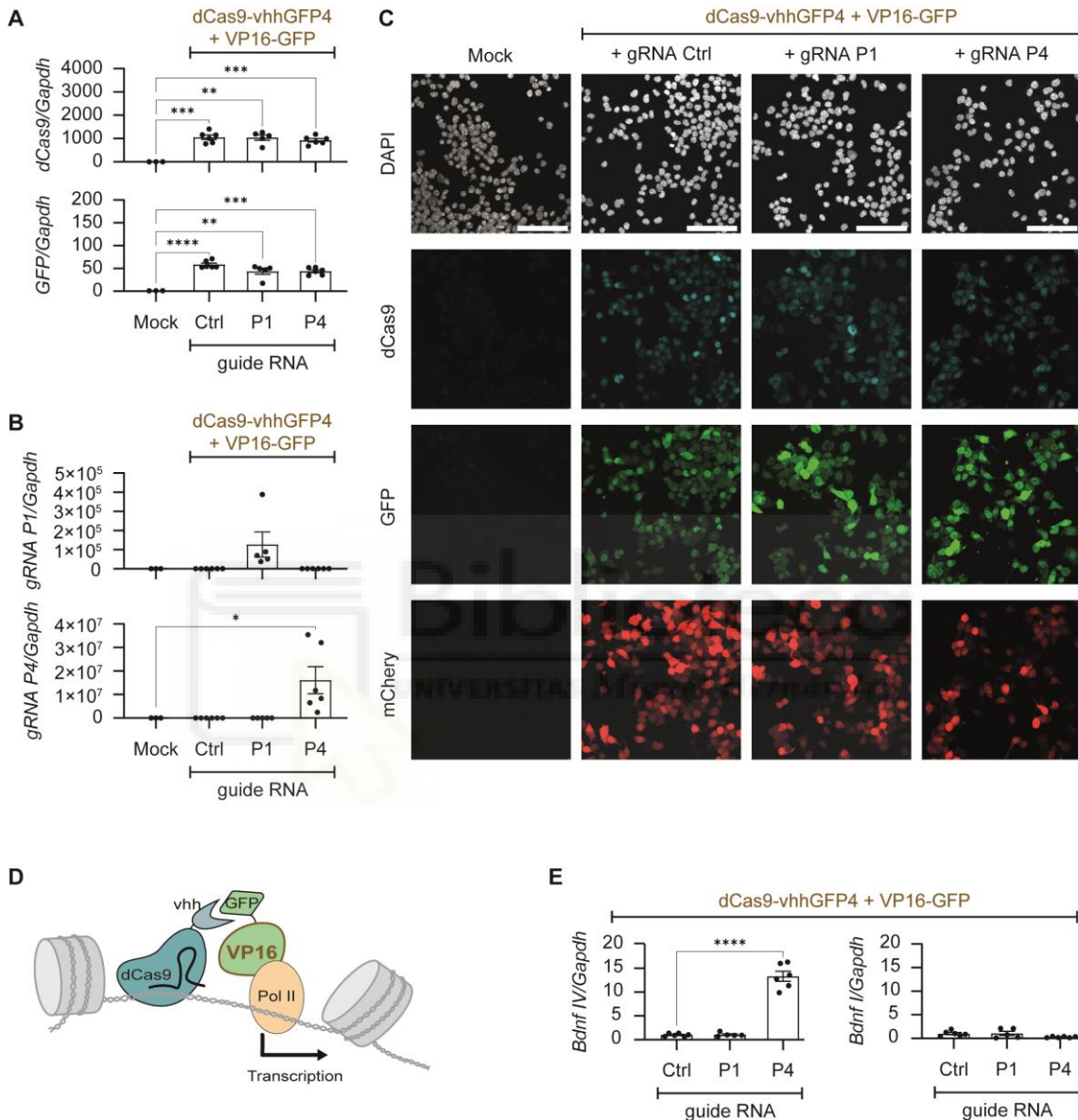

Figure 28. Evaluation of the split dCas9-CMD toolbox when the transactivator module VP16-GFP is used in N2a cells. A. RT-qPCR analysis of *dCas9* (top) and *GFP* (bottom) indicates upregulation of both elements in all conditions. **B**. RT-qPCR analysis of *gRNA P1* (top) and *gRNA P4* (bottom) indicates specific expression of both gRNAs. **C**. Immunostaining of dCas9 and GFP indicates the expression of dCas9-vhhGFP4 and VP16-GFP, respectively, in the selected subpopulations. The mCherry signal corresponds to the protein expressed by the plasmid that also allows the expression of gRNAs. DNA was counterstained with DAPI. Scale bar: 100 µm. **D**. Scheme depicting the recruitment of RNA polymerase II by the VP16-GFP effector module, which can lead to increased transcription. The VP16-GFP module is targeted to the region of interest by

the DBD module dCas9-vhhGFP4 in combination with a gRNA. **E**. RT-qPCR analysis of *Bdnf IV* (left) indicates a specific increase when cells are co-infected with gRNA P4. Induction of *Bdnf I* (right) is not observed when cells are co-infected with gRNA P1. All graphs are analysed by one-way ANOVA and corrected for multiple comparisons using Dunnett's test. *$p<0.05$; **$p<0.01$; ***$p<0.001$; ****$p<0.0001$.

4.9   Assessment of transcriptional editing capacity using the VPR transactivator domain

To achieve a stronger transactivation activity, the VPR transactivator domain combines VP64 (results from the combination of 4 VP16 domains), p65 (is a subunit of the transcription factor NFκB), and rta (is an activator of Epstein-Barr virus genes). The binding of these 6 activator domains has been described to facilitate interaction with multiple proteins involved in transcription initiation, resulting in potent transcriptional induction (Chavez et al., 2015). Therefore, we designed a CMD module that fuses GFP and VPR to test its transcriptional induction capacity.

Co-infection of the GFP-VPR transactivator module with gRNA Ctrl, P1 or P4 in N2a^dCas9-vhhGFP4 cells resulted in 7.1 %, 7.4 % and 6.1 % GFP$^+$/mCherry$^+$ cells, respectively, after the first sorting (**Figure 29A, B**). These subpopulations were selected and plated for growth, which increased the percentage of GFP$^+$/mCherry$^+$ cells to 27.5 %, 15.7 % and 15.6 % after the second sorting (**Figure 29C, D**).
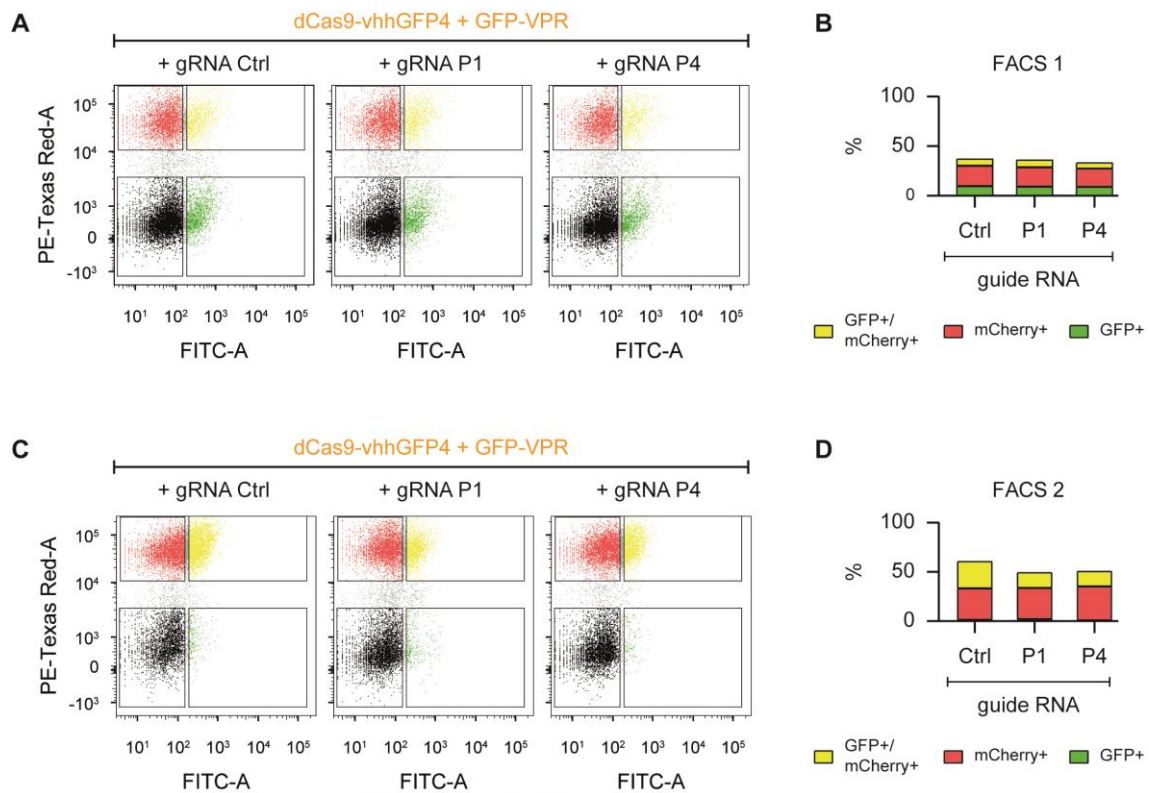
Figure 29. Isolation of N2a subpopulations expressing dCas9-vhhGFP4, GFP-VPR and gRNA (Ctrl, P1 or P4) modules. A. Flow cytometry dot plots (PE-Texas Red channel signal versus FITC-A channel signal) were used for gating and isolating GFP$^+$/mCherry$^+$ cell subpopulations during the initial sorting. **B**. Percentage of GFP$^+$, mCherry$^+$ and GFP$^+$/mCherry$^+$ cells obtained after the first sorting. **C**. Flow cytometry dot plots (PE-Texas Red channel signal versus FITC-A channel signal) were used for gating and isolating GFP$^+$/mCherry$^+$ cell subpopulations for further enrichment. **D**. Percentage of GFP$^+$, mCherry$^+$ and GFP$^+$/mCherry$^+$ cells obtained after the second sorting.

The reduced intensity of the GFP fluorescence signal observed in flow cytometry was consistent with the findings in the microscopy images (**Figure 30A**). The analysis of the images revealed that none of the conditions showed a proportion of GFP$^+$ cells exceeding 30 % (**Figure 30B**). Similarly, only slight GFP expression was observed in infected subpopulations (**Figure 30C**) compared to mock cells (uninfected N2a cells). In contrast, expression of the dCas9-vhhGFP4 construct was observed in all selected subpopulations, both at the protein (**Figure 30A**) and RNA (**Figure 30D**) levels. Finally, the correct integration and expression of the different gRNAs used resulted in the expression of the mCherry protein (**Figure 30A**), and the specific expression of gRNA P1 (**Figure 30E, top**) and gRNA P4 (**Figure 30E, bottom**) in each subpopulation.

Analysis of *Bdnf* transcriptional induction demonstrated that the VPR transactivator module specifically edits the expression of the *Bdnf* variant produced by promoter I (**Figure 30F, top**) and IV (**Figure 30F, bottom**). These results demonstrate that the achieved co-infection rates were adequate for the proper functionality of the split dCas9-CMD toolbox. This allows the gRNAs to effectively guide the dCas9-vhhGFP4 module to each *Bdnf* promoter and facilitate the recruitment of the GFP-VPR module. The GFP-VPR module interacts with various proteins involved in transcription initiation, leading to the induction of *Bdnf* variants I and IV (**Figure 30G**). The comparison of the results obtained using VP16 and VPR suggests that the genomic constrains that prevented the transactivation by VP16 in promoter I can be overcome if a stronger transactivation domain, like VPR, is used.
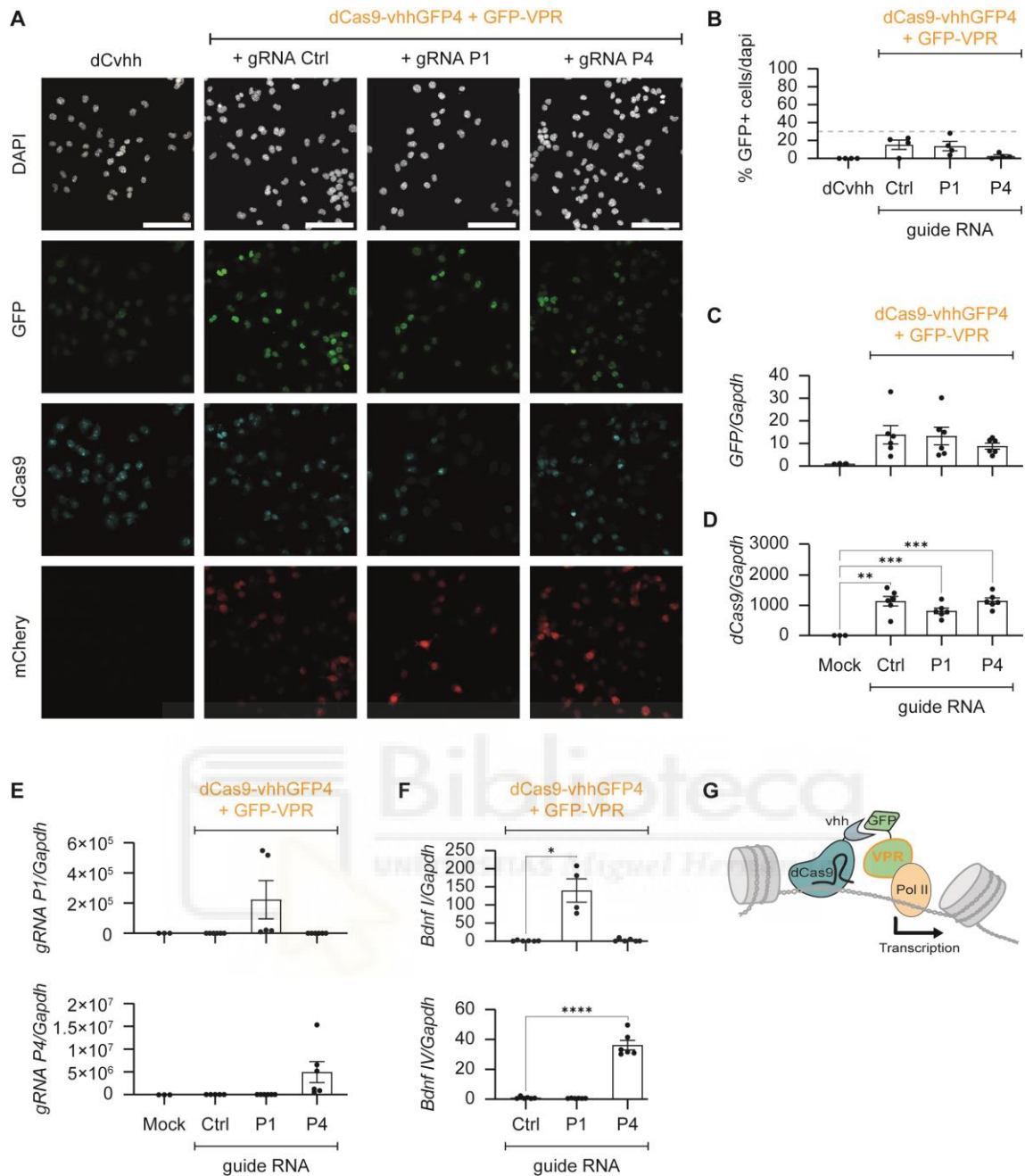
Figure 30. Evaluation of the split dCas9-CMD toolbox when the transactivator module GFP-VPR is used in N2a cells. A. Immunostaining of GFP and dCas9 indicates the expression of GFP-VPR and dCas9-vhhGFP4, respectively, in the selected subpopulations. The mCherry signal corresponds to the protein expressed by the plasmid that also allows expression of gRNAs. DNA was counterstained with DAPI. Scale bar: 100 µm. **B**. Percentage of GFP+ cells (relative to DAPI) in the selected subpopulations. **C**. RT-qPCR analysis of *GFP* indicates weak expression of GFP-VPR in infected cells. **D**. RT-qPCR analysis of *dCas9* indicates upregulation of dCas9-vhhGFP4 in infected cells. **E**. RT-qPCR analysis of *gRNA P1* (top) and *gRNA P4* (bottom) show the expression of both gRNAs. **F**. RT-qPCR analysis of *Bdnf I* (top) and *Bdnf IV* (bottom) indicates specific upregulation when cells are co-infected with gRNA P1 or P4, respectively. **G**. Scheme depicting recruitment of RNA polymerase II by the GFP-VPR CMD module, which can lead to

transcriptional upregulation. The GFP-VPR module is targeted to the region of interest by the DBD module dCas9-vhhGFP4 in combination with a gRNA. All graphs are analysed by one-way ANOVA and corrected for multiple comparisons using Dunnett's test. *p<0.05; **p<0.01; ***p<0.001; ****p<0.0001.

4.10 Assessment of epigenetic editing capacity using the KAT domain

The histone acetylation CMD module KAT-GFP fuses GFP with the lysine acetyltransferase (KAT) catalytic domain of the CBP protein, whose function is to introduce acetyl groups into the lysine residues of histone tails.

To assess the editing capacity of the KAT-GFP module when targeting precise regions of the genome, it was co-infected with a gRNA Ctrl, gRNA P1 or gRNA P4 in N2a^dCas9-vhhGFP4 cells. After the first sorting, the percentages of GFP$^+$/mCherry$^+$ cells were 7.1 %, 5.8 % and 4.6 %, respectively (**Figure 31A, B**). These values were enriched to 16.5 %, 18.3 % and 13.6 % after the second sorting (**Figure 31C, D**).
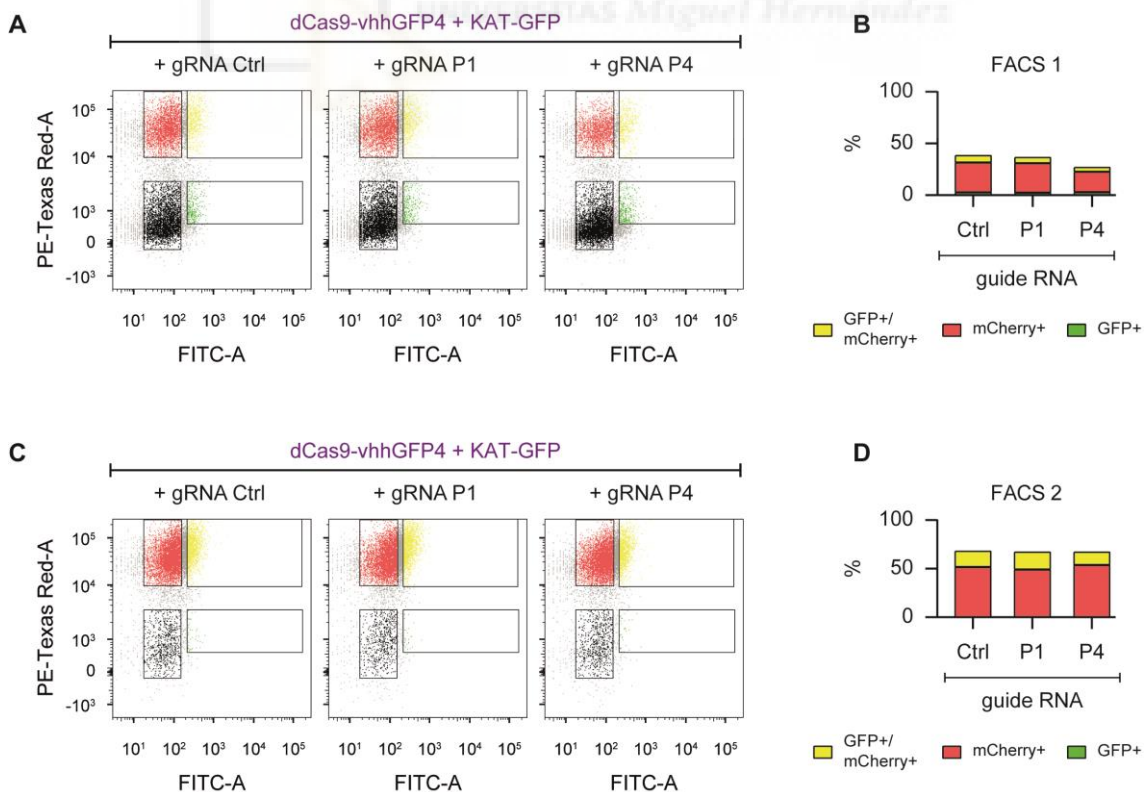

Figure 31. Isolation of N2a subpopulations expressing dCas9-vhhGFP4, KAT-GFP and gRNA (Ctrl, P1 or P4) modules. A. Flow cytometry dot plots (PE-Texas Red channel signal

versus FITC-A channel signal) were used for gating and isolating GFP⁺/mCherry⁺ cell subpopulations during the initial sorting. **B**. Percentage of GFP⁺, mCherry⁺ and GFP⁺/mCherry⁺ cells obtained after the first sorting. **C**. Flow cytometry dot plots (PE-Texas Red channel signal versus FITC-A channel signal) were used for gating and isolating GFP⁺/mCherry⁺ cell subpopulations for further enrichment. **D**. Percentage of GFP⁺, mCherry⁺ and GFP⁺/mCherry⁺ cells obtained after the second sorting.

Despite observing a lower-than-expected enrichment of GFP⁺/mCherry⁺ cells (as 50% of the cells were only mCherry⁺, **Figure 31D**), the RT-qPCR analysis revealed a significant increase in the expression of both dCas9-vhhGFP4 and KAT-GFP in the infected subpopulations compared to the mock cells (**Figure 32A**). Similarly, the expression of gRNA P1 and P4 was condition-specific (**Figure 32B**). This translated into a significant and specific increase in transcription of *Bdnf* variant I (**Figure 32C, top**) or IV (**Figure 32C, bottom**) when cells expressed gRNA P1 or P4, respectively.
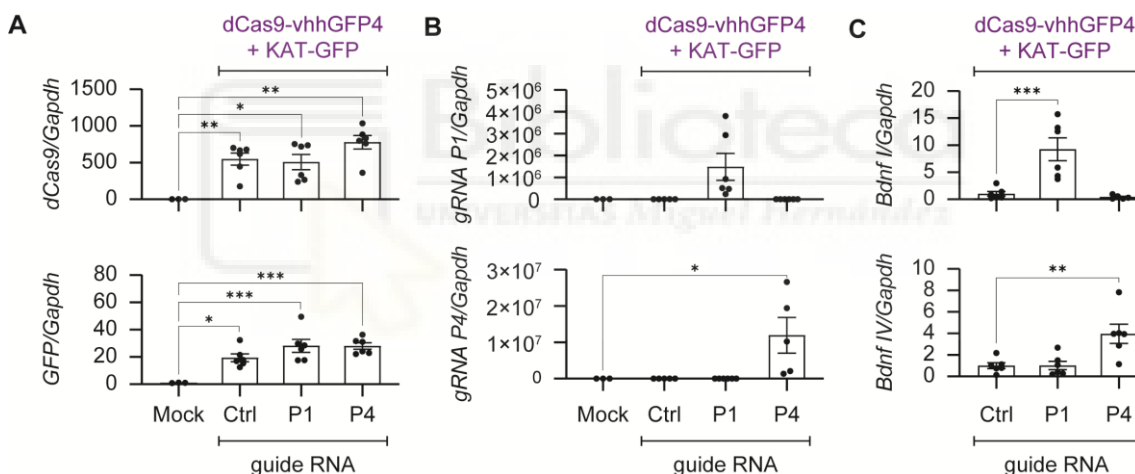

Figure 32. Evaluation of the split dCas9-CMD toolbox when the epigenetic module KAT-GFP is used in N2a cells. A. RT-qPCR analysis of *dCas9* (top) and *GFP* (bottom) indicates upregulation of dCas9-vhhGFP4 and KAT-GFP in infected cells. **B**. RT-qPCR analysis of *gRNA P1* (top) and *gRNA P4* (bottom) indicates specific expression of both gRNAs. **C**. RT-qPCR analysis of *Bdnf I* (top) and *Bdnf IV* (bottom) indicates specific upregulation when cells are coinfected with gRNA P1 or P4, respectively. Graphs are analysed by one-way ANOVA and corrected for multiple comparisons using Dunnett's test. $*p<0.05$; $**p<0.01$; $***p<0.001$.

Acetylation of the lysine residues of histone tails has been associated with a loss in the electrostatic attraction between histones and the DNA molecule, relaxing the chromatin structure and enhancing accessibility to the transcriptional machinery (Ip et al., 1988; Roth et al., 2001), which could explain the

transcriptional increase we observed when increasing acetylation levels in *Bdnf* promoters I and IV in a targeted manner. Analysing the chromatin environment of each promoter under basal condition, we observed that the region around *Bdnf* promoter I exhibits low accessibility, modest CBP binding and H3K27ac peaks. In contrast, the region neighbouring *Bdnf* promoter IV displays higher accessibility and similarly shows both CBP binding and levels of H3K27ac (**Figure 33A**). After editing, H3K27ac levels remained unchanged in the regions (Region 1-3) surrounding the gRNA binding site of promoter I (**Figure 33B**), while there was a specific increase in the regions (Region 4-5) surrounding the gRNA binding site of promoter IV (**Figure 33C**). These results demonstrated that our toolbox enables the rewriting of specific epigenetic marks at precise locations in the genome (**Figure 33D**).
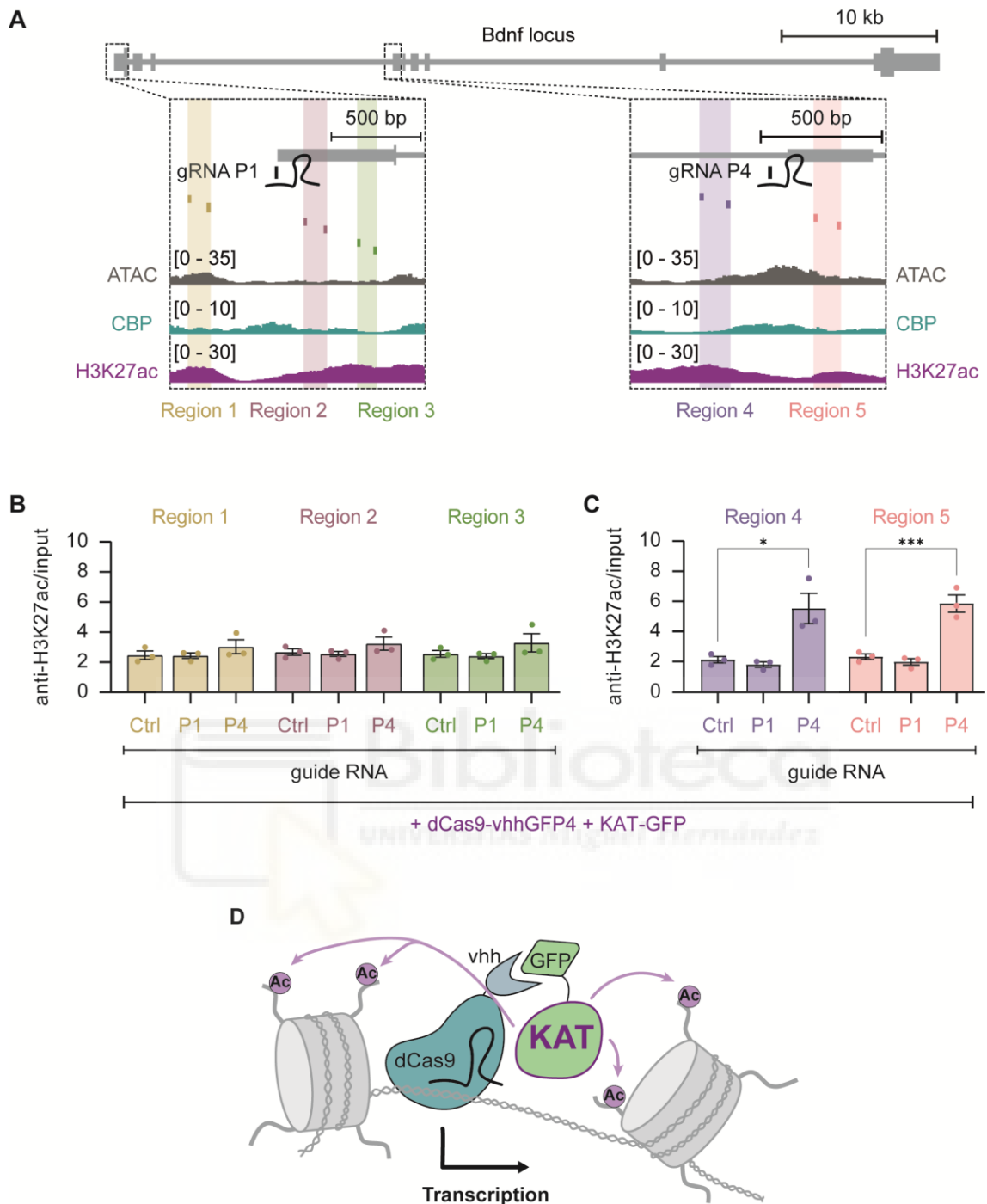
Figure 33. Assessment of histone acetylation editing using the split dCas9-CMD toolbox.
A. *Bdnf* locus with magnified view of promoters I and IV. Elements shown: gRNA binding sites, regions analysed by ChIP-qPCR and *in vitro* ATAC, CBP and H3K27ac profiles derived from primary cortical cultures obtained from public repositories (Beagan et al., 2020; Telese et al., 2015; Wenderski et al., 2020). **B**. ChIP-qPCR of H3K27ac around the gRNA P1 binding site. Three specific pairs of primers were designed to analyse regions surrounding gRNA P1 binding site (regions 1-3). **C**. ChIP-qPCR of H3K27ac around the gRNA P4 binding site. Two specific pairs of primers were designed to analyse regions surrounding gRNA P4 binding site (regions 4-5). **D**. Scheme depicting acetylation of histone tails by the effector module KAT-GFP, which can lead to

increased transcription. The KAT-GFP module is targeted to the region of interest by the DBD module dCas9-vhhGFP4 in combination with a gRNA. All graphs are analysed by one-way ANOVA and corrected for multiple comparisons using Dunnett's test. *p<0.05; ***p<0.001.

4.11 The vhhGFP4 nanobody specifically recruits the GFP-CMD modules to the target region

To ensure optimal functioning of the *trans* system, it is crucial that the nanobody vhhGFP4 of the DBD module specifically recognizes and recruits the GFP of the CMD module. This interaction is essential for the proper localization and targeting of the GFP-CMD module to the region of interest, enabling efficient and effective epigenome editing without off-target effects. We performed a ChIP-qPCR against GFP and observed that the combination of dCas9-vhhGFP4 with the gRNA P1 (**Figure 34A**) accurately recruits the GFP-VPR (**Figure 34B**), GFP-KRAB-MeCP2 (**Figure 34C**) and KAT-GFP (**Figure 34D**) modules to *Bdnf* promoter I. Similarly, when using gRNA P4 (**Figure 34E**), the recruitment of the different effector modules was specific to *Bdnf* promoter IV (**Figure 34F-H**). These results demonstrate the versatility of our toolbox, as it efficiently recruits different CMD modules to different target regions with high precision.
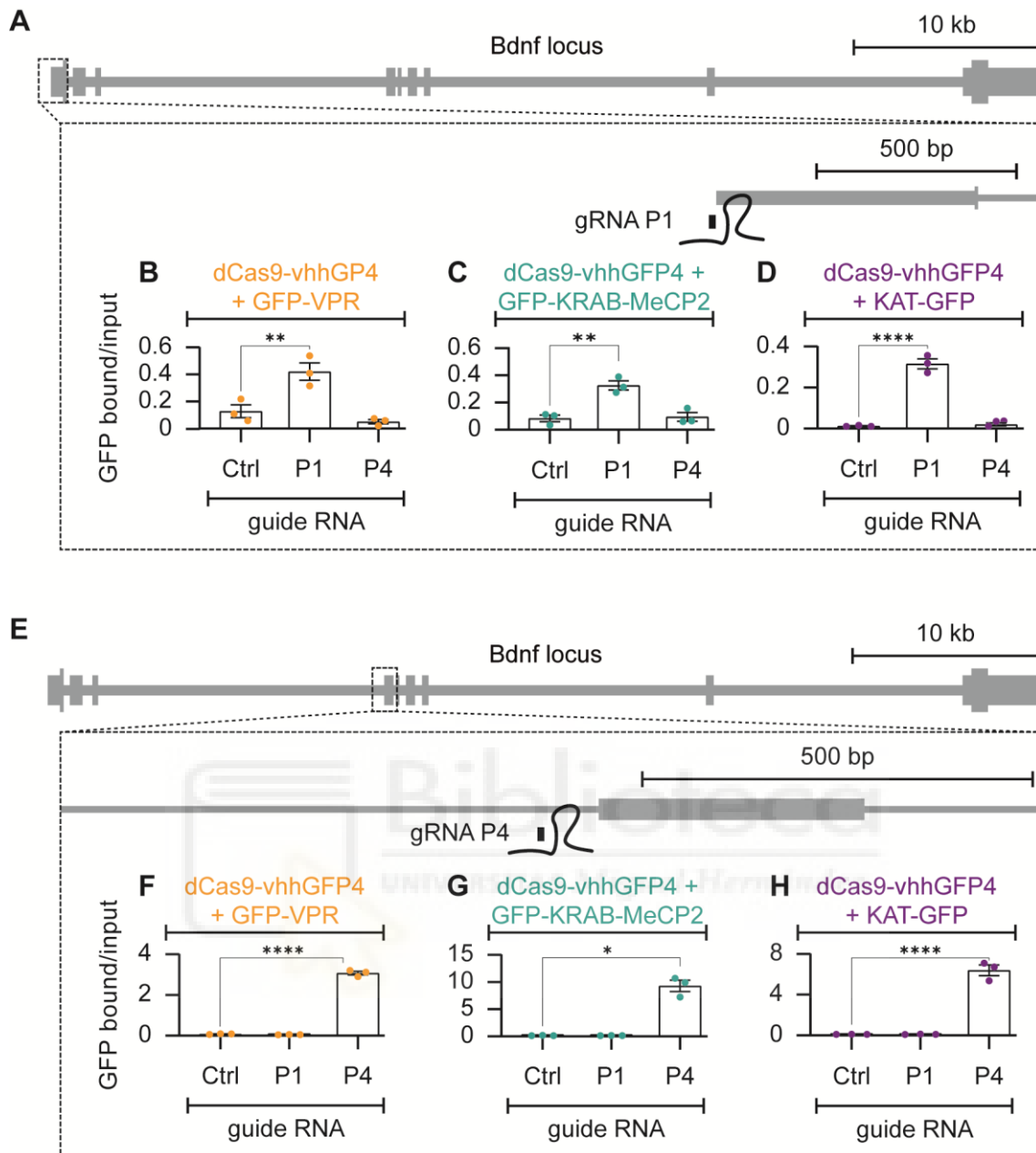
Figure 34. vhhGFP4 recruits CMD modules to target regions. A. *Bdnf* locus with magnified view of promoter I, highlighting gRNA P1 binding site. **B-D**. Recruitment of GFP-CMD to gRNA P1 binding site is assessed by anti-GFP ChIP-qPCR. Combinations of dCas9-vhhGFP4 and gRNA P1 with GFP-VPR (**B**), GFP-KRAB-MeCP2 (**C**) or KAT-GFP (**D**) CMD domains demonstrate precise recruitment to gRNA P1 binding site. **E**. *Bdnf* locus with magnified view of promoter IV, highlighting gRNA P4 binding site. **F-H**. Recruitment of GFP-CMD to gRNA P4 binding site is assessed by anti-GFP ChIP-qPCR. Combinations of dCas9-vhhGFP4 and gRNA P4 with GFP-VPR (**F**), GFP-KRAB-MeCP2 (**G**) or KAT-GFP (**H**) CMD domains demonstrate precise recruitment to gRNA P4 binding site. All graphs are analysed by one-way ANOVA and corrected for multiple comparisons using Dunnett's test. *p<0.05; **p<0.01; ****p<0.0001.

4.12 Expression of the split dCas9-CMD toolbox constituents in primary mouse neuronal cultures

One of the main advantages of the split dCas9-CMD toolbox is that it can be used in both mitotic and postmitotic cells, which allows us to evaluate its efficacy in primary neuronal cultures through gain and loss of function experiments. Mouse embryonic hippocampi were dissected at 17 days of gestation (E17). At DIV0-1, cultured neurons were co-infected with a lentivirus cocktail expressing dCas9-vhhGFP4, a GFP-CMD module and a gRNA Ctrl or complementary to *Bdnf* promoter I or IV (**Figure 35**). Neurons were allowed to grow for 9-10 days before sample collection to assess the efficacy of the editing toolbox.
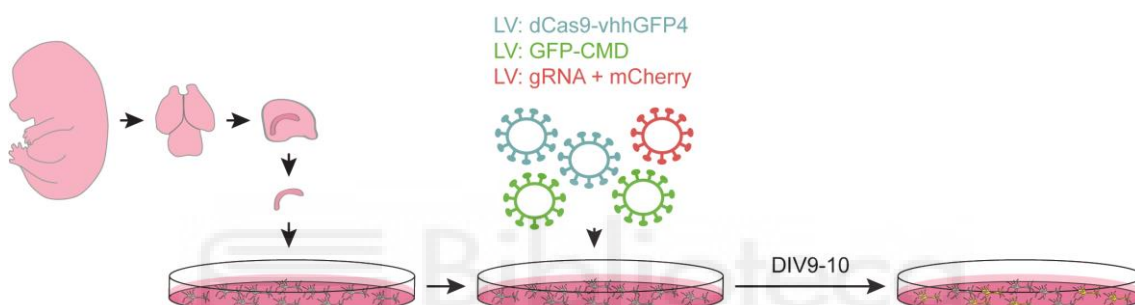

Figure 35. E17 mouse embryos were dissected for hippocampal primary culture. At DIV0-1, cells were infected with lentivirus expressing dCas9-vhhGFP4, specific CMD modules and gRNAs. Co-infected primary hippocampal cells were analysed at DIV9-10.

4.13 Evaluation of the split dCas9-CMD toolbox in primary neuronal cultures. VPR module and differential efficacy of the promoters driving its expression

In contrast to cell lines, the isolation of primary culture subpopulations that express all 3 modules simultaneously is not feasible. Therefore, the efficient expression of the different elements is crucial for accurate evaluation. The ubiquitous EF1α promoter used in N2a experiments to drive dCas9-vhhGFP4 expression has been reported to be less efficient in primary cultures compared to neuron-specific promoters, like the synapsin promoter (Savell et al., 2019). Therefore, we first evaluated its effectiveness in primary neuronal cultures.

The combination of the dCas9-vhhGFP4 module – whose expression is controlled by the ubiquitous EF1α promoter – with the GFP-VPR module and the gRNA Ctrl, P1 or P4 (**Figure 36A**) in primary cultures failed to increase the expression of *Bdnf* variants I and IV (**Figure 36B**), despite the positive result obtained in N2a cells (**Figure 30**). In contrast, the combination of the dCas9-VPR construct – whose expression is controlled by the neuron-specific promoter synapsin – with the gRNA Ctrl, P1 or P4 (**Figure 36C**) in primary cultures did result in increased expression of both *Bdnf* transcript variants (**Figure 36D**).

The differences in the results of these two experiments might stem from variations in co-infection rates – since the split dCas9-CMD toolbox comprises 3 elements (**Figure 36A**) and the classical CRISPR system just 2 elements (**Figure 36C**). Alternatively, the unsuccessful attempt of using the split dCas9-CMD toolbox combined with VPR in primary neuronal cultures may be originated by the low efficiency of the EF1α promoter in primary neurons. To test this hypothesis, we generated a new plasmid in which the expression of the chimeric dCas9-vhhGFP4 protein is driven by the neuronal synapsin promoter (**Figure 36E**). In addition, this plasmid contains 3 FLAG-tag sequences that facilitate its evaluation by immunostaining.
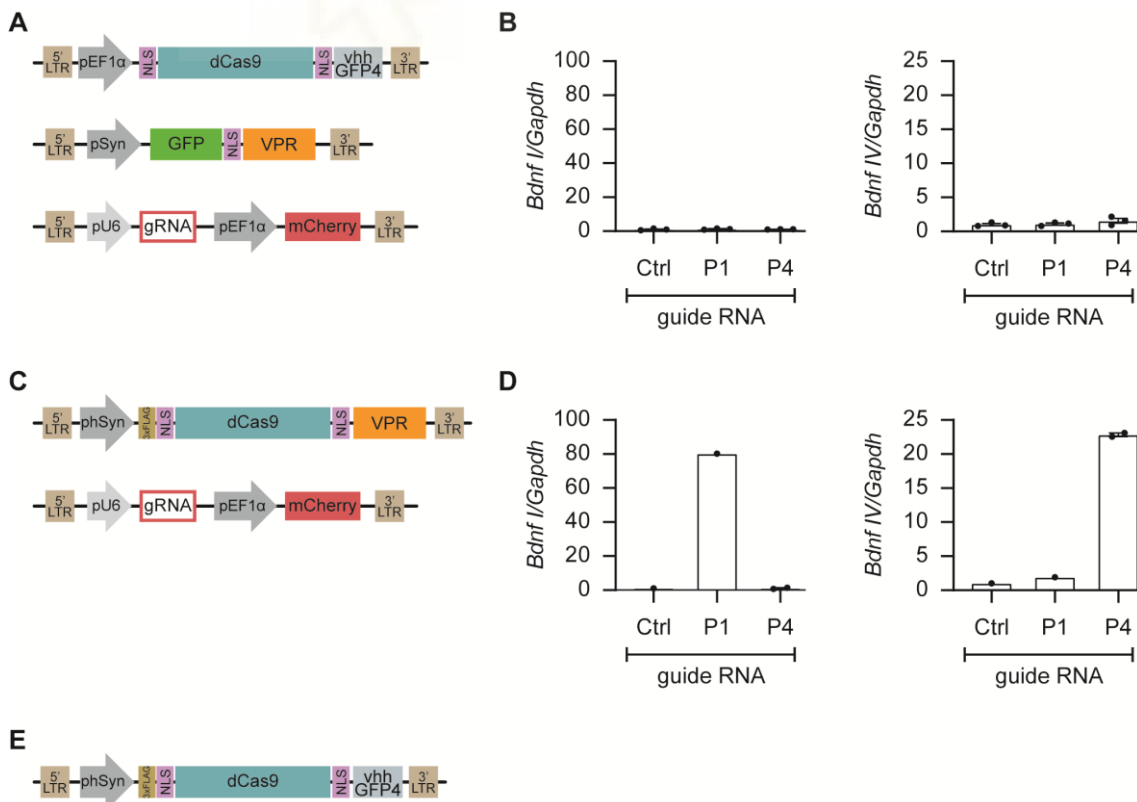
Figure 36. Comparison of EF1α and Syn promoter efficiency. A. Scheme of pEF1α-dCas9-vhhGFP4 (top), GFP-VPR (middle) and gRNA (bottom) plasmids. **B**. RT-qPCR analysis of *Bdnf I* (left) and *Bdnf IV* (right) in primary cultures of neurons infected with the plasmids depicted in A. Data is analysed using one-way ANOVA. **C**. Scheme of the dCas9-VPR plasmid, whose expression depends on the neuronal promoter Syn (top), and the gRNA plasmid (bottom). **D**. RT-qPCR analysis of *Bdnf I* (left) and *Bdnf IV* (right) in primary cultures of neurons infected with the plasmids shown in C. **E**. Scheme of the plasmid dCas9-vhhGFP4 whose expression is driven by the neuronal promoter Syn.

To repeat the same gain-of-function experiment in primary cultures using the new dCas9-vhhGFP4 plasmid whose expression is driven by the synapsin promoter, we combined it with the GFP-VPR transactivator module and the gRNA Ctrl, P1 or P4. As in the N2a cells, we detected a slight expression of GFP compared to the flag signal, which reflects the expression of the dCas9-vhhGFP4 protein, and the mCherry signal, which indicates the expression of the gRNA plasmid (**Figure 37A**). The percentage of simultaneous expression of all 3 elements was 38 %, 40.9 % and 20.5 % when primary cultures were co-infected with dCas9-vhhGFP4, GFP-VPR and the gRNA Ctrl, P1 or P4, respectively (**Figure 37B**). We also detected the specific expression of gRNA P1 and P4 in cultures infected with each of these gRNAs (**Figure 37C**).

The editing capacity of the split dCas9-CMD toolbox was evaluated in primary neuronal cultures by assessing the capacity of GFP-VPR module to interact with the transcriptional machinery in the targeted regions and initiate transcription (**Figure 37D**). Remarkably, despite the reduced GFP signal, the GFP-VPR module effectively triggered the transcriptional expression of *Bdnf* variant I (**Figure 37E, left**) and slightly induced *Bdnf* variant IV in a precise and targeted manner (**Figure 37E, right**), recapitulating the findings observed in N2a cells (**Figure 30**). These results show that the co-infection rates obtained were adequate and sufficient for targeted editing of *Bdnf* transcript expression using our epi-editing toolbox and highlight the comparative efficiency of the synapsin promoter versus the EF1α promoter. As a result, this new plasmid was employed in all subsequent experiments within primary neuronal cultures.
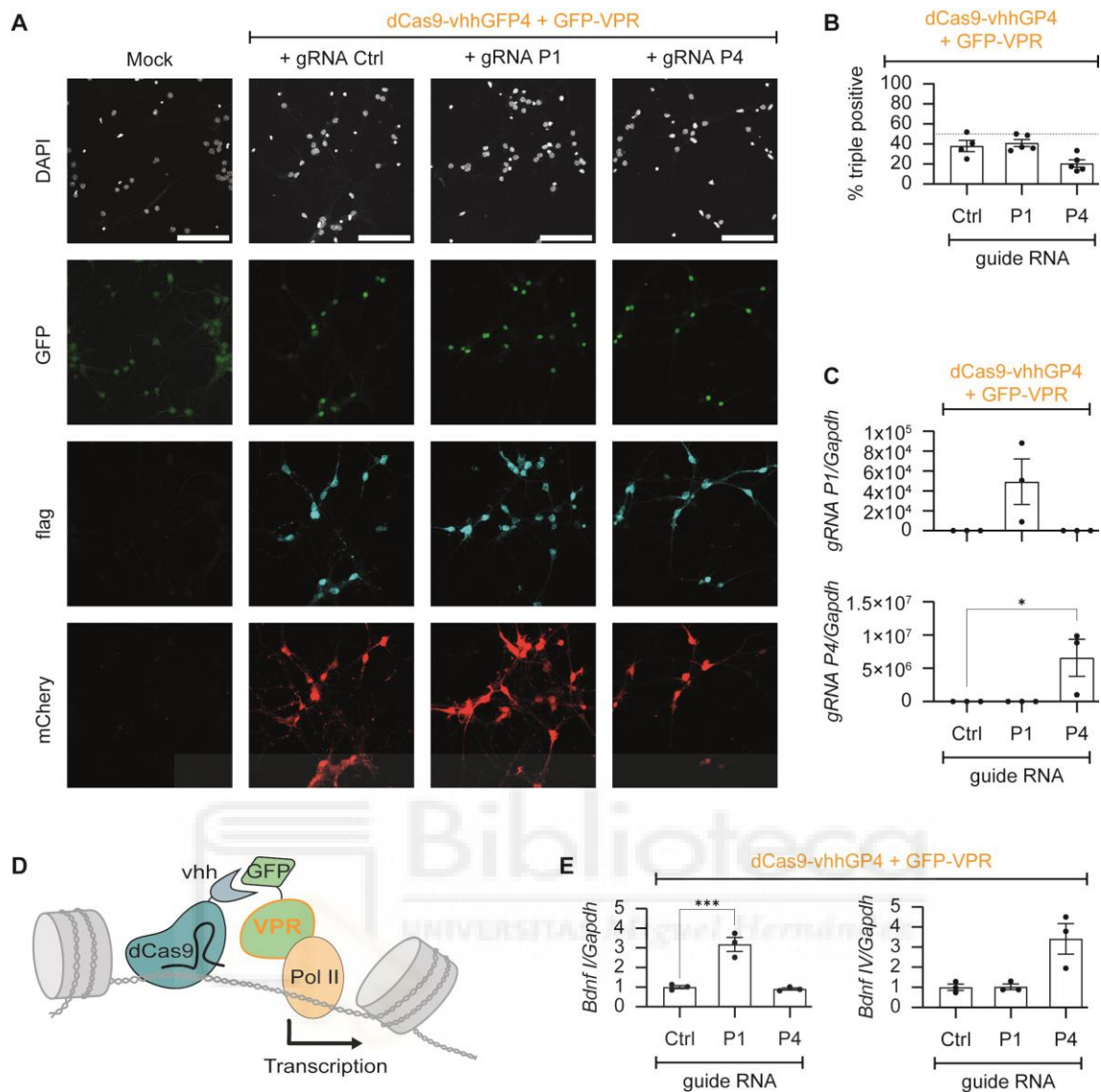
Figure 37. Evaluation of the split dCas9-CMD toolbox when the VPR transactivator module is used in primary cultures. A. GFP immunostaining is slightly detectable in conditions infected with the GFP-VPR module. Flag immunostaining indicates expression of dCas9-vhhGFP4 in cultures infected with this element. The mCherry signal corresponds to the protein expressed by the plasmid that also allows expression of the gRNAs. DNA was counterstained with DAPI. Scale bar: 100 μm. **B**. Percentage of simultaneous co-infection of the 3 elements of the system (GFP+/Flag+/mCherry+). **C**. RT-qPCR analysis of *gRNA P1* (top) and *gRNA P4* (bottom) indicates specific expression of both gRNAs. **D**. Scheme depicting recruitment of RNA polymerase II by the GFP-VPR effector module, which can lead to increased transcription. The GFP-VPR module is targeted to the region of interest by the DBD module dCas9-vhhGFP4 in combination with a gRNA. **E**. RT-qPCR analysis of *Bdnf* transcript variants indicates robust increase in *Bdnf I* (left) and slight tendency in *Bdnf IV* (right) when cultures are co-infected with gRNA P1 or P4, respectively. All graphs are analysed by one-way ANOVA and corrected for multiple comparisons using Dunnett's test. *p<0.05; ***p<0.001.

4.14 Evaluation of the split dCas9-CMD toolbox in primary neuronal cultures. KAT module

To assess the ability of the split dCas9-CMD toolbox to edit specific epigenetic marks in primary cultures, we combined the KAT-GFP module with dCas9-vhhGFP4 and gRNA Ctrl or gRNA P4. Microscopy images show GFP, flag and mCherry signal (**Figure 38A**), with a simultaneous expression rate of all 3 elements of 39.6 % and 37.8 % when cultures were co-infected with gRNA Ctrl or P4, respectively (**Figure 38B**). RT-qPCR analyses show the specific expression of the gRNAs in each case (**Figure 38C**).

Since primary cultures did not allow for the selection of subpopulations expressing simultaneously the different elements of our toolbox, we evaluated the editing capacity of the KAT-GFP module when specifically targeted to the region of interest (**Figure 38D**) in the entire set of cells in each condition. Remarkably, the achieved co-infection rates were adequate for effective epigenome editing, since the targeted acetylation of *Bdnf* promoter IV leads to a significant increase in transcription exclusively of the variant produced by this promoter, while leaving the transcription of variant I unaffected (**Figure 38E**). Interestingly, these results in primary neuronal cultures were consistent with our initial observations in N2a cells, which may indicate that *Bdnf* promoter IV is more suitable than promoter I for regulation using dCas9-based tools.
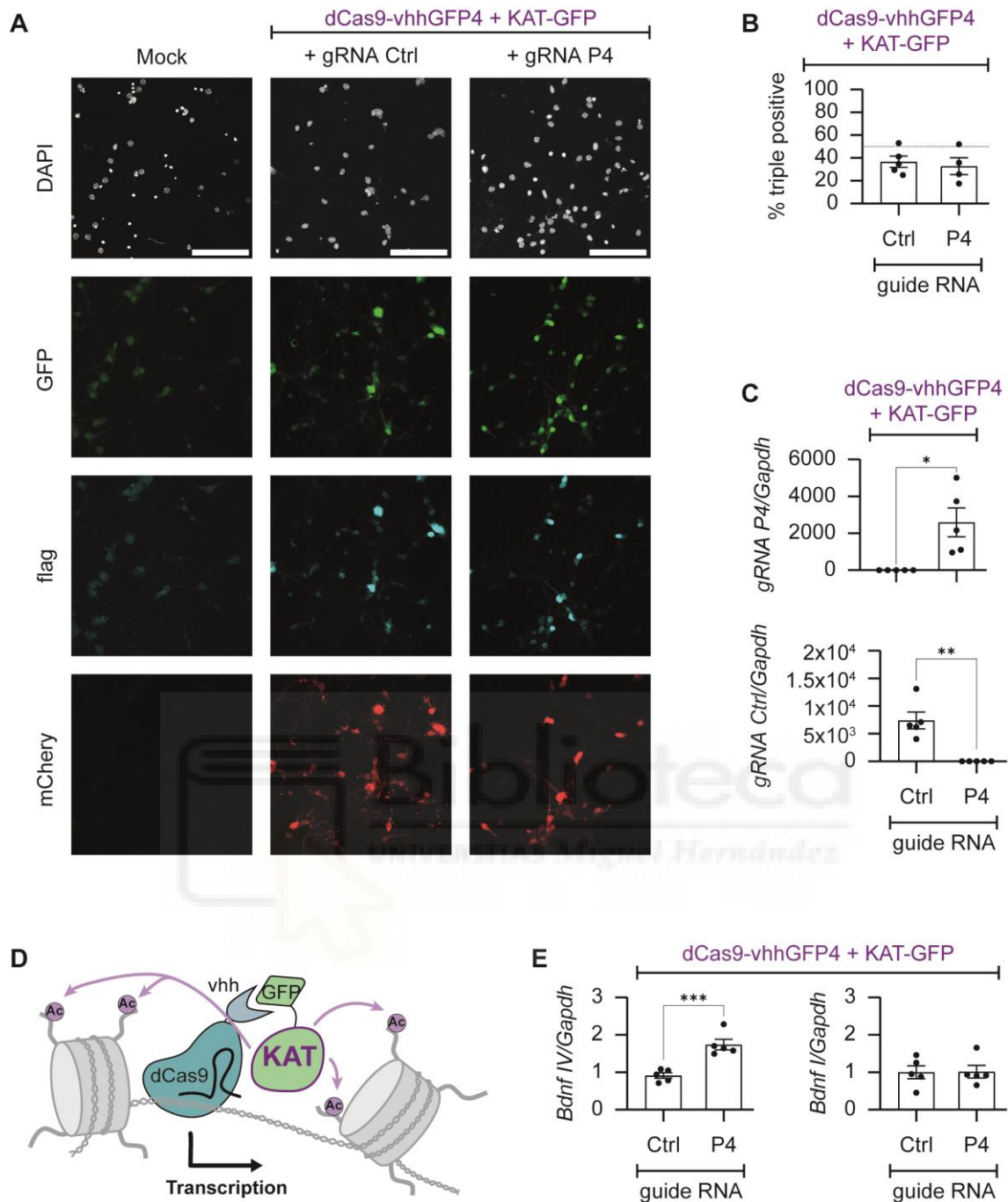
Figure 38. Evaluation of the split dCas9-CMD toolbox when the epigenetic KAT-GFP module is used in primary cultures. A. GFP and flag immunostaining indicates the expression of KAT-GFP and dCas9-vhhGFP4 in infected cultures, respectively. The mCherry signal corresponds to the protein expressed by the plasmid that also allows expression of the gRNAs. DNA was counterstained with DAPI. Scale bar: 100 μm. **B**. Percentage of simultaneous co-infection of the 3 elements of the system. **C**. RT-qPCR analysis of *gRNA P4* (top) and *gRNA Ctrl* (bottom) indicates specific expression of both gRNAs. **D**. Scheme depicting acetylation of histone tails by the effector module KAT-GFP, which can lead to increased transcription. The KAT-GFP module is targeted to the region of interest by the dCas9-vhhGFP4 DBD module in combination

148

with a gRNA. **E**. RT-qPCR analysis of *Bdnf IV* (left) indicates specific upregulation, without affecting *Bdnf I* (right). All graphs are analysed by unpaired t-test. *p<0.05; **p<0.01; ***p<0.001.

4.15 Evaluation of the split dCas9-CMD toolbox in primary neuronal cultures. KRAB-MeCP2 module

KRAB (Krüppel-associated box) is a domain present in numerous mammalian repressors whose function is to attract various epigenetic and chromatin modifiers to induce heterochromatin formation and block transcription. MeCP2 (methyl-CpG binding protein 2) recognizes the repressive transcriptional state and helps to maintain it (Duke et al., 2020). The combination of these two inhibitory domains has been described to produce robust and selective repression (Yeo et al., 2018), allowing us to assess the performance of the split dCas9-CMD toolbox in loss-of-function experiments.

In primary cultures of mouse hippocampal neurons, the inhibitory GFP-KRAB-MeCP2 module was combined with the dCas9-vhhGFP4 module and a gRNA Ctrl or P1 in a first experiment (**Figure 39A, C, E, H, I**), and a gRNA Ctrl or P4 in a second experiment (**Figure 39B, D, F, J, K**). In both experiments, all conditions were infected with dCas9-vhhGFP4 and GFP-KRAB-MeCP2 modules, which explains the absence of differences in the expression levels of dCas9 (**Figure 39A, B**) and GFP (**Figure 39C, D**) among the various experimental conditions. The expression of gRNAs was specific in each experiment (**Figure 39E, F**).

Bdnf is an activity-dependent gene that can be induced by adding KCl to the medium. *Bdnf* expression levels were evaluated at different time points, revealing peak expression of *Bdnf* variants I and IV at 3 hours after KCl addition (**Figure 39G**). Based on this finding, a 3-hour KCl treatment was applied, resulting in the induction of *Bdnf* I and IV in all infected conditions compared to infected conditions without KCl (comparison between conditions with KCl and without it – basal state – are represented by #) (**Figure 39H-K**). However, when dCas9-vhhGFP4 and GFP-KRAB-MeCP2 modules were targeted to *Bdnf* promoter I, we observed a specific repression of transcription of the variant produced by this promoter despite KCl-promoted transcriptional induction (**Figure 39H**), while transcription of variant IV was not affected (**Figure 39I**). Contrary, targeting of

split dCas9-CMD toolbox to *Bdnf* promoter IV did not affect the expression of transcript variant I (**Figure 39J**), while the variant produced by promoter IV was repressed despite the presence of KCl (**Figure 39K**). These results show the ability of the split dCas9-CMD toolbox to regulate *Bdnf* transcription when the GFP-KRAB-MeCP2 repressor module is targeted to the region of interest through interaction with dCas9-vhhGFP4 and the specific gRNA (**Figure 39L**) in the presence of KCl treatment.
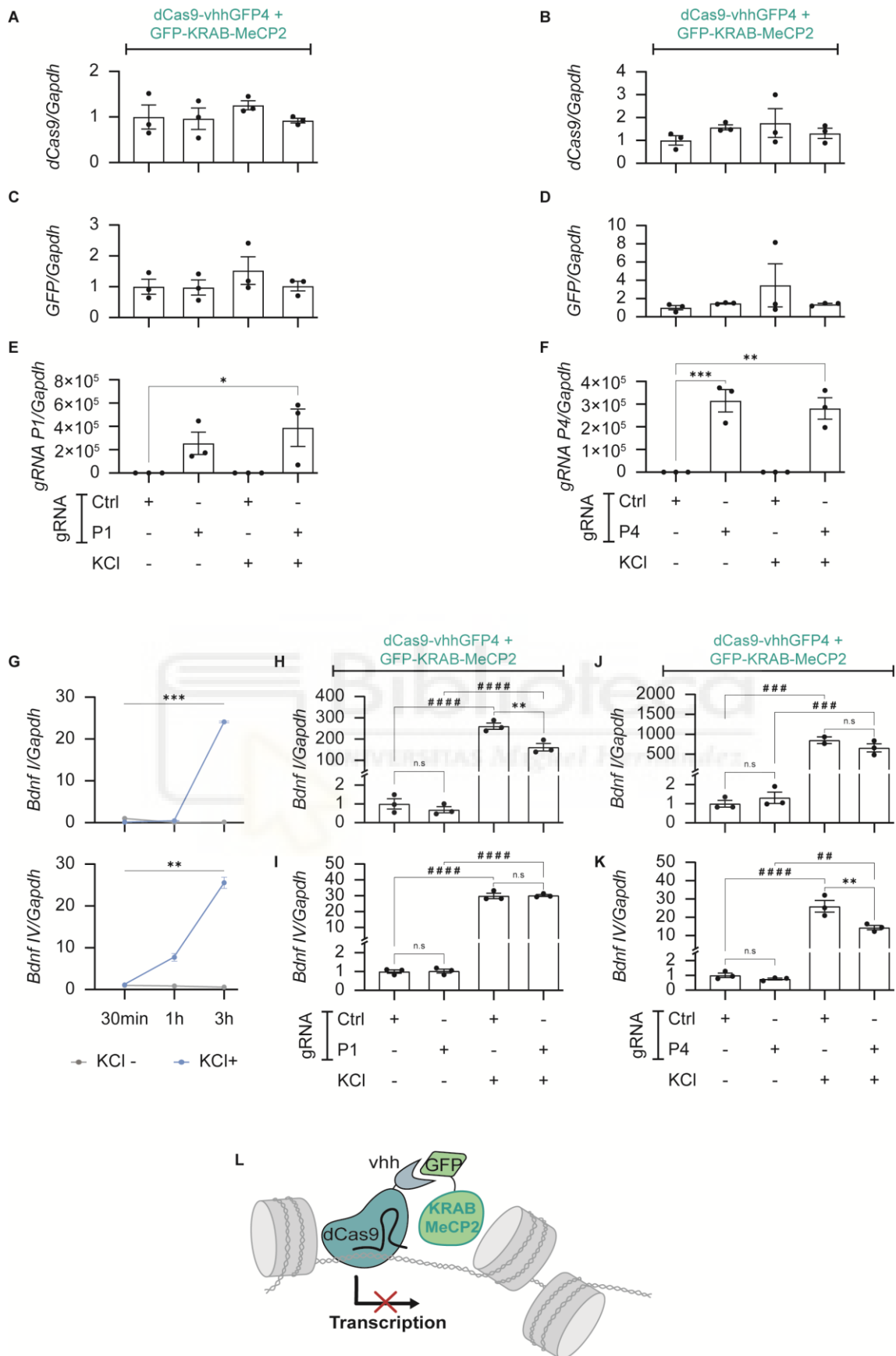
Figure 39. Evaluation of the split dCas9-CMD toolbox when the repressor GFP-KRAB-MeCP2 module is used in primary cultures. **A, B**. RT-qPCR analysis of *dCas9* indicates similar

expression of dCas9-vhhGFP4 in all conditions. **C, D**. RT-qPCR analysis of *GFP* indicates similar expression of GFP-KRAB-MeCP2 in all conditions. **E, F**. RT-qPCR of *gRNA P1* (**E**) and *gRNA P4* (**F**) is specific to conditions infected with each gRNA. **G**. RT-qPCR analysis of *Bdnf I* (top) and *Bdnf IV* (bottom) induction at 30 min, 1h and 3 h after KCl administration to the medium. **H-K**. RT-qPCR analysis of *Bdnf I* (**H, J**) and *Bdnf IV* (**I, K**) indicates specific repression depending on the gRNA used when KCl is added to the medium. **L**. Scheme depicting the induction of chromatin compaction by the CMD module GFP-KRAB-MeCP2, which can lead to a decrease in transcription. The GFP-KRAB-MeCP2 module is targeted to the region of interest by the dCas9-vhhGFP4 module in combination with a gRNA. Graphs A-F are analysed by one-way ANOVA. Graph G is analysed using repeated measures ANOVA (*Bdnf I*: Time: ***, KCl: ***; *Bdnf IV*: Time: **, KCl: *). Graphs H-K are analysed by two-way ANOVA and corrected for multiple comparisons using Turkey's test (**H**: gRNA: **, KCl: ****; **I**: gRNA: n.s, KCl: ****; **J**: gRNA: n.s, KCl: ****; **K**: gRNA: **, KCl: ****). *p<0.05; **p<0.01; ***p<0.001; ****p<0.0001.

4.16 Combination of the GFP-CMD module and gRNA in the same expression element to adapt the split dCas9-CMD toolbox for *in vivo* epigenome editing

The presented results show the expression of each individual module of the split dCas9-CMD toolbox separately. Consequently, the co-infection of 3 distinct viral particles is required for its proper functionality. However, this characteristic poses a potential limitation for *in vivo* applications due to the challenges associated with integrating and expressing three separate viral particles within the same cell, which could compromise the effectiveness of our editing toolbox, especially *in vivo*.

The size reduction achieved with the use of the vhhGFP4 nanobody provides the flexibility to express the gRNA and the GFP-CMD module in the same plasmid (**Figure 40A**) without exceeding the packaging capacity of lentiviral vectors (~ 8.5 kb). Therefore, by co-infecting a cell with only two viral particles – one carrying the dCas9-vhhGFP4 construct and the other containing the gRNA plus the GFP-CMD module – it becomes possible to express all 3 elements of the toolbox, allowing targeted editing of the neuronal epigenome.

To assess the viability of this strategy, N2a^dCas9-vhhGFP4 cells were infected with lentiviruses expressing, simultaneously, the transactivator module GFP-VPR and the gRNA Ctrl, P1 or P4. This construct lacks the mCherry cassette, hence

subpopulations of infected cells were selected based on the FITC-A signal (**Figure 40B**), whereas the absence of mCherry$^+$ and GFP$^+$/mCherry$^+$ cells were expected. After the first sorting, the percentage of GFP$^+$ cells were 53.2 %, 24.8 % and 45.2 %, respectively (**Figure 40C**), values that were enriched to 57.9 %, 38.9 % and 55.9 % after the second sorting (**Figure 40D, E**). The RT-qPCR results illustrate the specific expression of each gRNA (**Figure 40F**) compared to cells that only express dCas9-vhhGFP4 (termed vhh). Furthermore, the analysis unveiled the targeted editing of the *Bdnf* variants produced by promoters I or IV in the subpopulations specifically expressing gRNA P1 or P4, as evidenced by a specific increase in *Bdnf I* and *Bdnf IV*, respectively (**Figure 40G**). These results highlight the versatility of the split dCas9-CMD toolbox, as it offers the flexibility to combine various elements in either the same or separate plasmids, without compromising its ability to perform precise editing of the neuronal epigenome.
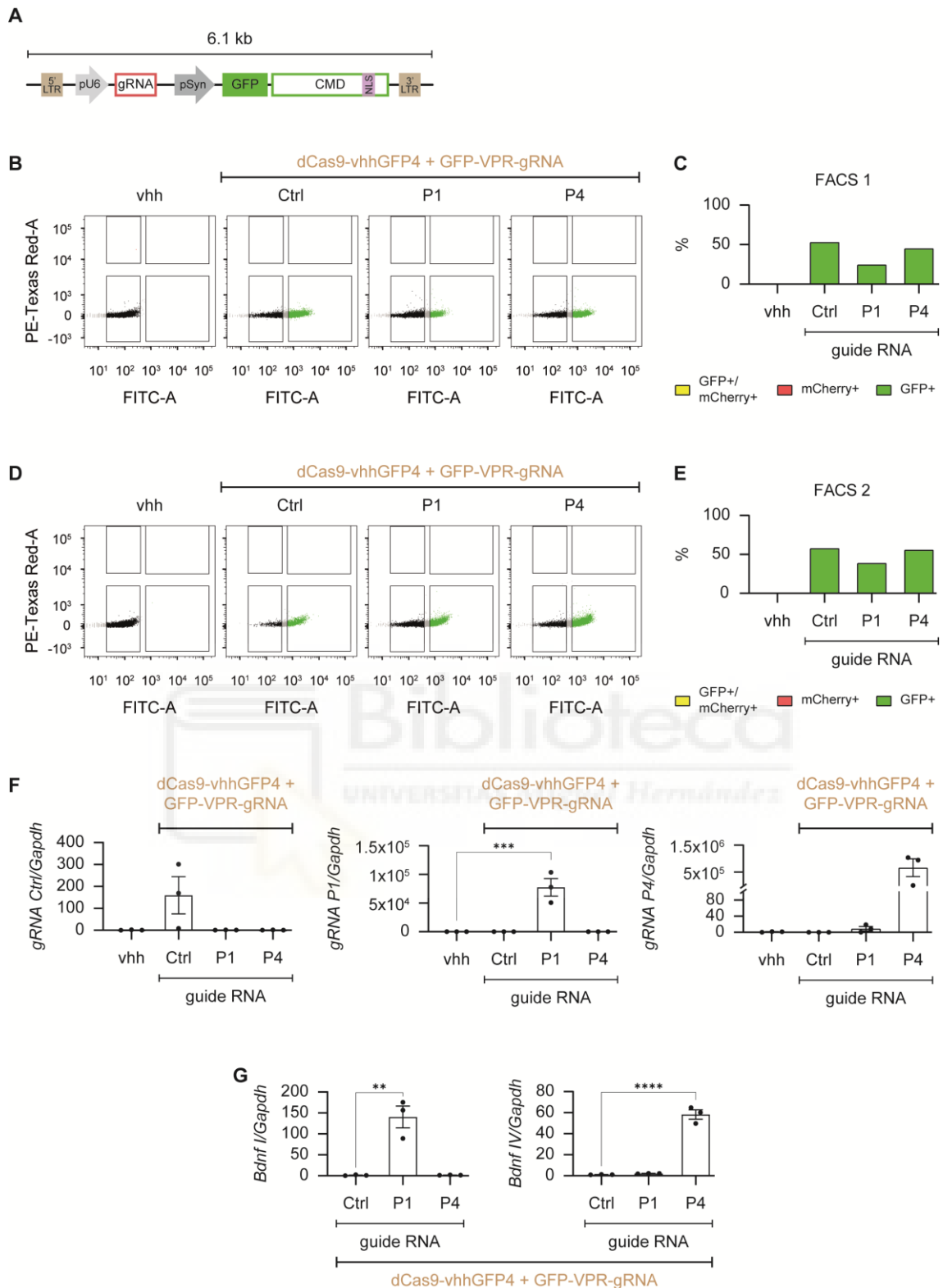
Figure 40. Evaluation of the combination of GFP-CMD and gRNA modules in the same expression plasmid. A. Scheme of the plasmid expressing simultaneously the gRNA, driven by the U6 promoter, and the GFP-CMD module, driven by the synpasin promoter. **B**. Flow cytometry dot plots (PE-Texas Red channel signal versus FITC-A channel signal) were used for gating and isolating GFP$^+$ cell subpopulations during the initial sorting. **C**. Percentage of GFP$^+$, mCherry$^+$ and

GFP$^+$/mCherry$^+$ cells obtained after the first sorting. **D**. Flow cytometry dot plots (PE-Texas Red channel signal versus FITC-A channel signal) were used for gating and isolating GFP$^+$ cell subpopulations for further enrichment. **E**. Percentage of GFP$^+$, mCherry$^+$ and GFP$^+$/mCherry$^+$ cells obtained after the second sorting. **F**. RT-qPCR of *gRNA Ctrl* (left), *gRNA P1* (middle) and *gRNA P4* (right) is specific of those conditions infected with each gRNA. **G.** RT-qPCR analysis of *Bdnf I* (left) and *Bdnf IV* (right) indicates specific induction depending on the gRNA used. All graphs are analysed using one-way ANOVA and corrected for multiple comparisons using Dunnett's test. $^{**}p<0.01$; $^{***}p<0.001$; $^{****}p<0.0001$.

The collective findings indicate that our split dCas9-CMD toolbox, which combines nanobodies technology with the CRISPR system, possesses three main advantages: i) modularity, as it comprises three different elements combinable in various ways; ii) adaptability, demonstrated by its utility in both mitotic cell lines and postmitotic neurons; and iii) versatility, enabling the use of different effectors for gene transcription editing. These promising outcomes, coupled with the reduced size achieved with the split dCas9-CMD toolbox, have allowed the transfer of all the constructs used *in vitro* into adeno-associated viral (AAV) vectors. AAV vectors offer higher infection efficiency *in vivo* compared to lentiviral vectors, and they do not integrate into the genome, reducing the risk of introducing point mutations (Edry et al., 2011). This approach ensures safer and more efficient delivery of the split dCas9-CMD constituents to target neurons in animal models, allowing the *in vivo* evaluation of the split dCas9-CMD toolbox in future experiments.

5. DISCUSSION

Section 1

Transcriptional and epigenetic bases of modulation of cognitive abilities by rearing conditions

5.1 Environmental factors and their influence on the modulation of cognitive capacities and engram formation

In our study, isogenic mice were exposed to different environmental paradigms during early development (from P21 to P51). Subsequently, they were returned to a standard cage (SC) for 1-4 additional months (**Figure 9**). This approach allowed us to assess the persistence of behavioural changes long after the animals left the EE or EI conditions, in contrast to the majority of gene-environment interaction studies, which primarily focus on analysing the impact of environmental factors on cognitive abilities while animals remain within the paradigms (Kempermann, 2019; van Praag et al., 2000). Our experimental design may pose limitations by not reflecting the genetic and environmental variability inherent in human populations, thereby oversimplifying gene-environment interactions. Nevertheless, observations indicate that isogenic mice housed in enriched environments for three months exhibit individualized behaviours, highlighting that even under conditions controlling genetic background and housing in a shared environment among different mice, early-life experiences lead to lasting and personalized changes in behaviour, brain plasticity, and epigenetics (Zocher et al., 2020).

The results obtained supported previous research suggesting an enhancement in cognitive abilities associated with enriched environments and a deterioration in cognitive capacities linked to impoverished environments. Specifically, we observed that mice exposed to environmental enrichment (EE) exhibited increased exploratory behaviour and outperformed their SC counterparts in various hippocampus-related tasks involving learning and memory. Conversely, mice exposed to environmental impoverishment (EI) displayed reduced performance in these same tasks compared to SC mice (**Figures 10, 11**).

However, not every behavioural protocol was affected. For instance, strong training in a fear conditioning paradigm did not reveal significant differences in freezing response among EE, EI and SC mice (**Figure 12E**). The intensified training protocol was specifically chosen for labelling engram cells due to preliminary assays indicating that a stronger training paradigm resulted in a higher number of tagged cells, necessary for reliable quantification. Consistent with behavioural results, engram characterization in CA1 and DG regions revealed a percentage of reactivated cells that exceeded what would be expected by chance in all environmental conditions, suggesting proper engram formation in each of them. However, there were no significant differences in the number of reactivated cells among the conditions (**Figure 13**). These results suggest that the more intense training led to equally robust memory formation in mice from all three environmental conditions, hindering our ability to discern whether behavioural differences translate into variations in engram formation.

Although the commonly employed protocol for engram cell labelling is based on fear conditioning, alternative protocols have also been developed, such as the novel object location task designed to label cells activated when the location of a familiar object is altered (Karaca et al., 2020, 2021). Therefore, to investigate potential correlations between variations in memory performance and discrepancies in engram formation, it would be necessary to perform additional engram tagging experiments adapting one of the tasks wherein distinct performance was observed among the three experimental groups (**Figure 11**) for efficient engram cell labelling and quantification.

5.2 The role of transcriptional and epigenetic mechanisms in gene-environment interactions

5.2.1 Transcriptional and accessibility changes in DG and CA1 regions

The persistence of the observed behavioural changes on hippocampus-related tasks after the mice return to SC implies the existence of mechanisms that enable these alterations to endure even after the stimuli have disappeared. This

suggests the potential involvement of epigenetic mechanisms in the adaptation of hippocampal cells to external stimuli.

The hippocampus, a subcortical structure located in the temporal lobe of the brain, comprises the *cornu ammonis* (CA), the dentate gyrus (DG), and the hilus, intricately interconnected through a neuronal circuit known as the "trisynaptic loop", where the information is transmitted through sequential synapses from the entorhinal cortex to the DG, then to CA3, which in turn relay information to CA1, ultimately closing the circuit by sending information back to the entorhinal cortex (Knierim, 2015). Owing to the distinct cellular composition and functional variances between pyramidal CA neurons and granule neurons at the DG, alongside the observed shifts in the distribution pattern of the FITC-A signal in cytometry experiments (**Figure 17**), we focused on the epigenetic and transcriptomic alterations within both hippocampal layers.

In the pyramidal cells of CA1, we did not observe significant differences in accessibility when comparing the various conditions. However, we did detect changes in gene expression related to enhanced expression of activity-dependent genes at the basal state in the EE condition (**Figure 22**), which may be linked to the bimodal distribution observed in the FITC-A signal of Sun1-GFP$^+$ nuclei in CA1 neurons in the EE condition (**Figure 17E, F**). This association arises from the activity-dependent nature of Sun1-GFP expression (**Figure 16C**) – driven by the CAG promoter –, signifying an increased tonic activation of activity-regulated genes within the CA1 pyramidal cells of EE mice. Based on these findings, it would be reasonable to anticipate a higher proportion of Sun1-GFP$^+$ cells in TRAP2 mice housed under the EE condition compared to those in SC and EI conditions, since the expression of Sun1-GFP is regulated by the activity-dependent gene promoter pFos (**Figure 12A, B**). However, the results obtained did not demonstrate variations among the different environmental conditions (**Figure 13D**). This apparent discrepancy might be attributed to differences in sensitivity between confocal microscopy (used in **Figure 13**) and flow cytometry (utilized in **Figure 17**). While confocal microscopy features enable high-resolution fluorescent imaging, it may limit the detection of weak fluorescent signals and the evaluation of rare cell subpopulations within heterogeneous samples. In contrast, flow cytometry prioritizes speed of acquisition and sensitivity, allowing for the

detection of rare cell populations with statistical significance (Basiji et al., 2007). To explore further, conducting flow cytometry experiments with TRAP2 mice exposed to varying environmental conditions would be necessary to ascertain the presence of a bimodal distribution in the FITC-A signal when Sun1-GFP expression is governed by the *Fos* promoter.

We also detected changes in ncRNA levels in CA1 pyramidal cells, decreased both in the EE and EI conditions (**Figure 22**). The decreased expression of this set of genes in both EE and EI poses an intriguing paradox, as these are two opposing environmental paradigms. These ncRNAs are implicated in various regulatory mechanisms, such as protein translation and rRNA modifications. Therefore, their modulation by environmental conditions could suggest that they play a role in fine-tuning the transcription programs activated in EE and EI. The analyses conducted within this thesis have not allowed for the identification of a common link among these ncRNAs, as many of them are not documented in the literature nor classified in ontology databases. Nevertheless, these findings open new avenues for investigating the role of ncRNAs, particularly snoRNAs, in gene-environment interactions (71.4 % of the identified ncRNAs were categorized within the snoRNAs subset, **Figure 22C**). Additional gain- and loss-of-function experiments would be of interest to validate their role in regulating gene expression following exposure to different environments, as well as to study the half-life of these ncRNAs and their potential involvement in sustaining the observed behavioural changes once environmental stimuli have ceased.

In the granule cells of the DG, despite the modulation of the neurogenesis process by the environment (Garthe et al., 2016; van Praag et al., 2000; Zocher et al., 2020), our focus has been on understanding the changes in mature excitatory neurons, overlooking the exploration of epigenetic changes linked to neuronal progenitors. In both the EI and SC conditions, similar patterns were observed, whereas the EE condition stood out for showing a generalized increase in transcription and accessibility levels (60/74 DEGs and 225/225 DARs were exclusively increased in EE, **Figure 19B, C**). However, these changes do not correlate or belong to a common pathway or process. One possible explanation for this result is that 58.2 % of the DARs were in intergenic regions (**Figure 20D**). While it is generally assumed that intergenic regions regulate the expression of

the nearest gene *in cis*, this rule is not always applicable (Javierre et al., 2016; Mifsud et al., 2015). Several studies have emphasized that regions distantly located in the linear genome, yet in close contact due to the 3D chromatin configuration, may play a crucial role in the regulation of activity-induced genes (Beagan et al., 2020; Joo et al., 2016; Winick-Ng et al., 2021). 3D chromatin interactions can be established prior to the transcription process, creating a primed state and facilitating a future rapid and targeted neuronal response (D'Ippolito et al., 2018; Oti et al., 2016; Paliou et al., 2019). Hence, it would be of interest to investigate this hypothesis by performing 3D long-range interactions experiments in mice reared in different environmental conditions and exploring the 3D connections established between the DARs and DEGs identified in this thesis project.

5.2.2 Genomic priming by AP1

In both hippocampal layers (CA1 and DG), the apparent disconnect between alterations in chromatin accessibility at regulatory sites and the limited impact on transcription may indicate that changes in accessibility represent a manifestation of epigenetic priming. Epigenetic priming is characterized by a transcriptional state in which various TFs and histone modifications collaborate to enhance chromatin accessibility, preparing it to facilitate transcriptional activation, amplify gene production, or contribute to the establishment of new transcriptional programs (Arzate-Mejia & Mansuy, 2023; Bonifer & Cockerill, 2017; Burns & Gräff, 2021). Specifically, the results obtained using the TOBIAS program in the DG and CA1 accessible regions (**Figures 21, 23**) predicted the involvement of the TF AP1 in the changes that occur as a consequence of exposure to different environments. The differential occupancy of AP1 sites may influence the subsequent activity of loci, acting as a form of genomic priming that modulates the future response of neurons to similar or different stimuli.

Studies with immune system cells propose a model that describes how, following exposure to an external agent, the activation of AP1 leads to nucleosome remodelling (Bevington et al., 2016; Johnson et al., 2004) by recruiting remodelers like BGR1 and histone modifiers like CBP (Ito et al., 2001; Ndlovu et al., 2009). As a result, TF binding sites that were originally concealed become accessible due to the increased chromatin accessibility mediated by AP1 (**Figure**

41). Similarly, in the field of neuroscience, it has been described that during postnatal neuronal maturation, AP1 activation recruits the SWI/SNF BAF complex to new neuronal enhancers (Stroud et al., 2020). This recruitment process remodels nucleosomes and facilitates TF binding (Su et al., 2017; Vierbuchen et al., 2017), which, in turn, leads to increased expression of gene sets crucial for the neuronal maturation process.
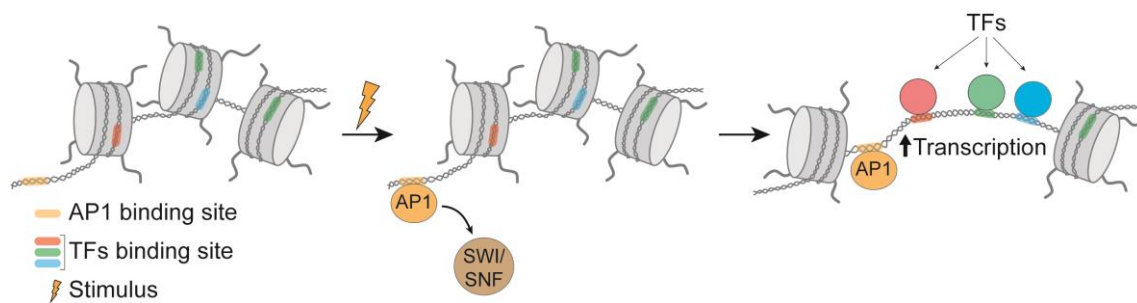

Figure 41. Graphical model depicting the influence of neuronal activity on chromatin dynamics and transcription factor binding. Upon stimulus arrival, AP1 binds to its specific site, facilitating the recruitment of nucleosome remodelers, such as the SWI/SNF complex, and triggers the opening of chromatin, rendering previously inaccessible TF binding sites accessible and leading to dynamic alterations in neuronal gene expression. Colour bars represent TFs binding sites.

Once the stimulus disappears and transcriptional levels return to their basal state, the increase in chromatin accessibility is observed to persist in some regions. This allows TFs and RNA polymerase to remain bound in a primed state, facilitating the initiation of transcription in response to a second stimulus (Liu et al., 2017; Vihervaara et al., 2021). A study conducted with epidermal stem cells postulates that the maintenance of accessibility in certain regions is mediated by members of the AP1 family whose expression is constitutive. Specifically, this study describes that, following local inflammation, there is an increase in the expression of the transcription factor *Stat3*, which promotes the expression and recruitment of AP1 family members to promoters and enhancers. Once the stimulus vanishes and the transient binding of FOS to chromatin ceases, other constitutive AP1 family TFs, such as JUN or ATF3, remain bound (Larsen et al., 2021). As a result, upon the establishment of increased accessibility resulting from the binding of activity-dependent TFs, these sites become susceptible to occupation by additional TFs that could recognize their DNA binding motif. Therefore, the presence of multiple AP1 domains in sequences gaining

162

accessibility can be a distinctive feature of primed chromatin regions. This characteristic could explain the persistence of changes in the cognitive capacity of adult mice induced by early exposure to different environmental conditions.

The levels of FOS protein and Sun1-GFP (whose expression is dependent on CreER^{T2}, which in turn depends on the *Fos* promoter) remained constant across different environmental conditions when analysed in the engram formation experiments (**Figure 13**). Thus, in line with the proposed hypothesis, when considering the combined results, we might infer that environmental exposure does not induce significant changes in the quantity of FOS, one of the primary constituents of AP1, but rather in the sites where this factor binds. To validate this hypothesis and the predictions generated by TOBIAS, experiments involving CUT&RUN of various AP1 family members could be conducted to assess their differential binding in different environmental conditions. Moreover, the AP1 binding sites could be blocked using the CRISPR system, which would allow the investigation of the necessity and/or sufficiency of the observed changes.

In addition to AP1, other epigenetic marks, such as H3K4me1 and DNA methylation, have been associated with the epigenetic predisposition of regulatory regions during development and neuronal maturation (Calo & Wysocka, 2013; Stroud et al., 2020). Hence, these marks could also contribute to the priming phenomenon following neuronal response to external stimuli.

5.2.3 Additional TFs involved in gene-environment interactions

While AP1 was discussed above as the primary candidate to explain the persistence of chromatin changes induced by rearing conditions, predictions generated by the TOBIAS program also indicate a decrease in the binding of MEF2 in the EE condition, and an increase in BHLH TFs in the EI condition (**Figure 23**).

Several studies have investigated the contribution of MEF2 to learning and memory in mouse models (Assali et al., 2019; Rashid et al., 2014). While mice with double deletion of *Mef2a* and *Mef2d* genes exhibit normal learning and memory in a conditioned fear paradigm (Akhtar et al., 2012), under subthreshold conditions, the reduction of MEF2A and MEF2D in the hippocampus facilitates spatial learning and memory (Cole et al., 2012). These findings align with the

observation that levels of *Mef2a* and *Mef2d* decrease in the adult hippocampus during contextual fear-related learning and memory paradigms (Cole et al., 2012). Interestingly, brain deletion of *Mef2c* during embryonic development results in significant deficits in fear-related learning and memory (Harrington et al., 2016), deficits that do not occur when *Mef2c* suppression is performed in postnatal forebrain excitatory neurons (Adachi et al., 2016). Furthermore, the expression of the constitutively active form of MEF2 (MEF2-VP16) in the anterior cingulate cortex of adult mice after a contextual fear conditioning paradigm inhibits memory consolidation (Vetere et al., 2011), while the expression of MEF2-VP16 in the nucleus accumbens of adult mice increases their preference for cocaine-conditioned places in a drug reward learning and memory test (Pulipparacharuvil et al., 2008). Additionally, exposure to an enriched environment has been associated with an increase in MEF2 in the prefrontal cortex, a result that correlates with greater cognitive resilience (Barker et al., 2021). These seemingly contradictory results suggest that MEF2 activity exerts selective influences in specific brain regions, as supported by previous research suggesting that increased MEF2 expression in the dentate gyrus inhibits spatial memory formation, while overexpression in the cortex can facilitate learning. The predicted reduction in MEF2 binding in CA1 pyramidal neurons by TOBIAS aligns with previous research indicating that reduced MEF2 in the hippocampus facilitates learning and memory.

Regarding BHLH TFs, prior investigations in our laboratory suggest that BHLH and AP1 TFs compete for the transcriptional coactivators CBP/p300 when neuronal activity is present, leading to a transient shutdown of BHLH-dependent genes during IEG bursting transcription (Fernandez-Albert et al., 2019, Niñerola et al., in preparation). This appears to be in line with the results obtained through TOBIAS in CA1, where we observed an increase in BHLH binding in the regulatory regions associated with EI, which simultaneously exhibited a decrease in AP1 binding.

Taken together, these findings suggest that while AP1 is identified as the main mediator in DG and CA1 to maintain changes induced by early exposure to diverse environments into adulthood, other TFs – such as MEF2 and BHLH – also appear to play a significant role in this process in CA1 pyramidal cells.

164

5.3 Differences between CA1 and DG AP1 binding

The differences observed in AP1 binding to regulatory sites in response to environmental conditions between granule and pyramidal cells may relate to the different roles of these two types of neurons processing information and to their distinct firing patterns.

Notably, the DG has been associated with a process known as pattern separation, wherein distinct output patterns are generated in response to similar input patterns, enabling cognitive discrimination between similar representations in the brain (Leutgeb et al., 2007; Neunuebel & Knierim, 2014; Treves & Rolls, 1994). Conversely, the CA1 region acts as a pivotal output node of the hippocampus, detecting novelty, comparing inputs, and enhancing output information, potentially by redistributing information from CA3 through a greater number of output neurons (Soltesz & Losonczy, 2018).

Consistently with these two differential roles, DG granule cells exhibit remarkably sparse activity, with a scattered firing pattern and fewer than 5% of them active during spatial exploration (Hainmueller & Bartos, 2020), whereas CA1 pyramidal cells present a more regular firing pattern, both spatially and temporally, giving rise to hippocampal frequency and temporal codes (Ahmed & Mehta, 2009). These distinct properties are reflected in the basal expression of FOS, which is ubiquitous but faint in CA1 pyramidal neurons, while only a few granule neurons in the DG layer show FOS expression (**Figure 42**). Furthermore, the flow cytometry data presented in this thesis demonstrate that CA1 cells exhibit varying levels of activation, reflected in a broader FITC-A signal (**Figure 17E**), in contrast to DG cells, which display a more uniform FITC-A signal (**Figure 17D**). These observations suggest that granule cells tend to remain relatively inactive under basal conditions, which could facilitate the detection of changes leading to an increase in TF binding. In contrast, pyramidal cells show higher basal activity, making it easier to detect a decrease in TF binding. Therefore, the increase in AP1 binding in the EE condition in DG and its decrease in the EI condition in CA1 could suggest that, although the mechanism mediating the maintenance of changes induced by external stimuli is similar in both hippocampal layers, this

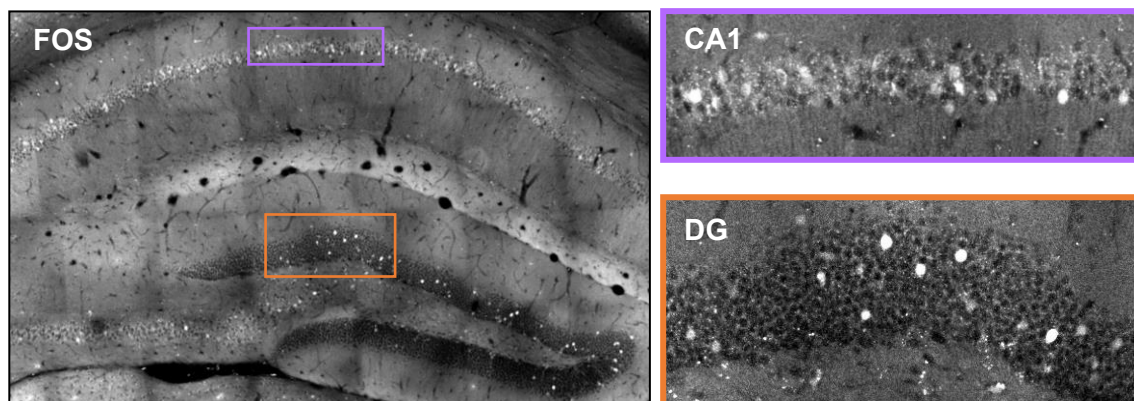mechanism adapts according to the specific activity patterns, properties, and functions of each cell type.

Figure 42. Basal expression of FOS in CA1 and DG hippocampal layers. Left: immunostaining of FOS in the hippocampus. Right: 20x magnification of CA1 (purple) and DG (orange) layers.

5.4 The significance of studying gene-environment interactions

The debate nature vs. nurture is fundamental in fields such as psychology, genetics, sociology, and biology, seeking to understand how human characteristics develop and to what extent they are influenced by genetics (nature) or the environment (nurture) (Ridley, 2004). While genes lay the groundwork for our biology, their expression and function can significantly vary due to environmental influences. Investigating gene-environment interactions aids in understanding how these two components intertwine to shape our physical, mental, and emotional traits.

Understanding the relative influence of nature and nurture is also crucial in fields like mental health, as certain disorders may have genetic and environmental components. This might be the case with stress, categorized by the World Health Organization as the predominant epidemic of the 21st century due to increasing episodes at ever-earlier ages. Studying epigenetic modifications in mice exposed to stressful environments holds the potential to unravel the role of epigenetic mechanisms in the detrimental effects associated with adverse childhood experiences and chronic stress. This approach enhances our comprehension of the underlying mechanisms of these mental health challenges and could

ultimately facilitate the development of more precise and personalized therapeutic strategies aimed at mitigating their negative impact on the population.

By better comprehending how environmental factors affect gene expression and health, we can also design more effective public health strategies. For instance, studying epigenetic modifications resulting from exposure to stimulating environments has the potential to identify the molecular basis of occupational therapy, widely used to improve the quality of life in patients experiencing long-term cognitive decline, such as those with intellectual disabilities or Alzheimer's disease. Similarly, studying these mechanisms also facilitates the development of programs to reduce the negative impact of the environment on health, along with policies promoting healthier environments for everyone. Therefore, the nature vs. nurture debate and the study of how genes and the environment interact are essential for advancing science, medicine, and public health, potentially improving people's quality of life, and addressing significant global health challenges.

Additionally, to discern between mere presence and functionality of epigenetic mechanisms induced by exposure to different environmental factors, we have developed a molecular tool enabling targeted epigenome editing. The outcomes of this tool are discussed in the following *Discussion* section.

Section 2

Development of a toolbox for precise neuronal epigenome editing

5.5 Regulation of *Bdnf* promoters by different effector modules

The split dCas9-CMD toolbox developed in this thesis is based on the intermolecular interaction mediated by the nanobody vhhGFP4 (fused with dCas9), which recognizes the GFP (fused to the CMD) with high affinity and specificity, enabling its recruitment to the target region for epigenetic editing. The results obtained using this toolbox demonstrate variable effects on the transcription from *Bdnf* promoters I and IV, depending on the CMD module used.

In N2a cells, the transactivator module VP16 leads to increased transcription of *Bdnf* variant IV but does not affect *Bdnf* variant I (**Figure 28E**). However, the VPR module enhances the transcription of both transcripts (**Figure 30F**). These findings not only highlight the greater potency of the VPR transactivator (Chavez et al., 2016), but also suggest that promoter I is in a more silent state than promoter IV under basal conditions. Hence, using a more potent transactivation domain is necessary to overcome the restrictions imposed by the specific genomic configuration of the promoter.

These differences in the epigenetic configuration of both promoters are also reflected in the results of N2a cells edited with the epigenetic module KAT. Despite observing an increase in the transcription of the *Bdnf I* transcript when the KAT-GFP domain is recruited to this region by gRNA P1 and dCas9-vhhGFP4 (**Figure 32C**), we do not detect an increase in H3K27ac levels in the analysed regions. Conversely, combining the KAT-GFP module with dCas9-vhhGFP4 and gRNA P4 leads to higher transcription and increased H3K27ac levels in the *Bdnf IV* transcript (**Figure 32C, 33**). This result again suggests that promoter I is more silent than promoter IV under basal conditions, which would explain the challenge of the KAT-GFP module in altering the levels of H3K27ac. Furthermore,

169

performing additional ChIP experiments to assess whether the KAT domain, corresponding to the catalytic domain of CBP, is acetylating other lysine residues that are also targeted by this protein, such as H3K18 or H2B (Weinert et al., 2018), holds promise in understanding the mechanisms underlying the increased transcription of *Bdnf I* transcript when the KAT-GFP module is targeted to its promoter by gRNA P1.

Additionally, it would be highly insightful to further explored the extent of heterochromatin formation catalysed by the repressive module KRAB-MeCP2 in primary neuronal cultures. For instance, investigating how levels of the repressive mark H3K9me3 or accessibility levels are affected when this module is targeted to *Bdnf* promoters will improve our understanding of the chromatin landscape of both *Bdnf* promoters, as well as to facilitate the interpretation of the partial reduction in the expression of both *Bdnf* transcripts when the module KRAB-MeCP2 is targeted to promoters I and IV in the presence of KCl (**Figure 39H-K**).

Taken together, our results showed that *Bdnf* promoters I and IV have distinct epigenetic configurations, causing them to respond differently to editing mediated by the split-dCas9 CMD toolbox. The findings also revealed a great level of specificity, since manipulation of *Bdnf* promoters I and IV exclusively influences the transcription of the respective transcripts, indicating precise and specific effects in all cases (**Figures 28E, 30F, 32C, 33, 37E, 38E, 39H-K, 40G**). However, in order to rule out potential off-target effects resulting from our split dCas9-CMD editing toolbox when combined with different effector domains, deep sequencing would be necessary.

5.6 Precision of the split dCas9-CMD toolbox in editing the *Bdnf* gene

The precision of the split dCas9-CMD toolbox in targeting different promoters of *Bdnf* open the possibility of investigating in greater detail the role and specific transcriptional and epigenetic regulation of each variant. It has been reported that individual transcripts of *Bdnf* contribute differentially and specifically to total *Bdnf* levels in various brain regions. For instance, male mutant mice in which *Bdnf*

production from promoters I and II has been disrupted exhibit increased aggression and changes in the expression of specific genes related to serotonin signalling (Maynard et al., 2016), while female mutant mice experience alterations in their sexual and maternal behaviour (Maynard et al., 2018). In contrast, male mutant mice in which *Bdnf* production from promoters IV and VI has been disrupted do not display aggression but do show alterations in the expression of GABAergic genes (Maynard et al., 2016). Understanding the regulation of transcription of different *Bdnf* variants is essential not only for unravelling fundamental epigenetic questions, but also for deciphering the roles these variants play in diseases. For example, the dysregulation of specific *BDNF* transcripts in humans has been associated with various brain disorders such as Huntington's disease, schizophrenia, or Alzheimer's disease (Garzon et al., 2002; Wong et al., 2010; Zuccato et al., 2001). Additionally, the selective removal of exons I-III of *BDNF* – without affecting the rest of the gene – is sufficient to induce obesity in humans (Han et al., 2008). The precision of the split dCas9-CMD toolbox in targeting specific promoters within the same gene and editing their transcription allows us to address these questions. Moreover, it enables us to rescue defects associated with the transcription of a specific variant, either by increasing its transcription or by enhancing the expression of another variant to compensate for total *Bdnf* levels.

Furthermore, by designing gRNAs that direct the split dCas9-CMD toolbox to other genomic regions, we can explore the epigenetic regulation of any locus, opening numerous avenues for study. It may be also possible to direct our toolbox to enhancer regions, such as the *Bdnf* enhancer that boosts the transcription of promoter I (Tuvikene et al., 2021), or any other transcription-regulating enhancer. These approaches would allow us to investigate the necessity and/or sufficiency of these regulatory regions in controlling and enhancing transcription, as well as to explore the role played by different epigenetic marks in this function.

5.7 Advantages, limitations, and future perspectives of the split dCas9-CMD toolbox

The experiments conducted with the split dCas9-CMD toolbox demonstrate its capacity to achieve precise and targeted epigenome editing. This stands in contrast to drugs that block the action of epigenetic enzymes, which act indiscriminately across the entire genome, resulting in reduced efficacy and the occurrence of side effects. Moreover, the modularity of the toolbox allows for the combination of its elements in different ways, enabling the editing of diverse epigenetic marks. Additionally, the developed toolbox is viable and functional in both mitotic and post-mitotic cells, making it suitable for use in various tissues and cell types, expanding its applicability beyond the field of neuroscience.

Despite all these advantages, our toolbox also has limitations. Firstly, one might think that the composition of the toolbox, consisting in three different elements that need to be co-infected in the same cell for proper functioning, could pose a barrier for its use *in vivo*. However, *in vitro* results indicate that the observed co-infection ratio is sufficient for specific and efficient epigenome editing (**Figures 37B, 38B**). Secondly, the continuous expression of the split dCas9-CMD toolbox's components might lead to immune complications, as the dCas9 protein originates from bacteria that infect humans (Charlesworth et al., 2019). Likewise, it is important to assess the capacity of the effector domains to target proteins beyond the chromatin, as observed in the p300 or CREB proteins, which interact with different oncoproteins (Goodman & Smolik, 2000), potentially leading to tumour development.

These limitations emphasize the ongoing need for research and collaborative efforts to develop epigenome editing tools that are more effective and safer, with the goal of translating them into clinical applications for the treatment of human diseases. By rewriting epigenetic marks to control gene expression without inducing alterations in the DNA sequence, the split dCas9-CMD toolbox exhibits promising therapeutic potential for addressing various genetic diseases. In addition, its compact size resolves the challenges of packaging the CRISPR system into AAV vectors, allowing for the *in vivo* administration of the toolbox components in future experiments. To date, editing tools have been combined

with AAV vectors to reduce brain levels of the TAU protein in mice, which is implicated in Alzheimer's disease (Wegmann et al., 2021), and to reduce levels of the HTT protein responsible for Huntington's disease (Zeitler et al., 2019). Other groups have used AAV vectors to administer CRISPRa systems, increasing the expression of haploinsufficient genes, where one copy of the gene is non-functional, leading to abnormally low expression. This strategy has rescued a hereditary obesity phenotype (Matharu et al., 2019) and a form of Dravet syndrome, a severe epileptic encephalopathy (Colasante et al., 2020). Similarly, other groups have employed AAV vectors to administer the CRISPRi system, reducing serum cholesterol levels in adult mice for 24 weeks after a single AAV administration (Thakore et al., 2018) or to deactivate the sodium channel Nav1.7, involved in pain perception, for months (Moreno et al., 2018), potentially serving as an alternative to opioid treatment.

These examples highlight the promising prospect of addressing the root causes of diseases through epigenome editing tools. However, they present a significant limitation, since all these studies utilized synthetic effector domains of reduced dimensions, such as VP64 and KRAB. To advance in the development of therapies for epigenome-associated diseases based on targeted epigenome editing, it is necessary to engineer epigenome editing systems that do not encounter packaging issues in viral vectors, such as our split dCas9-CMD toolbox. This would enable the precise targeting of the catalytic domain of any epigenetic enzyme to specific chromatin regions, regardless of their size.

Furthermore, it is essential to progress in the development of viral vector systems that enable the effective administration of these tools *in vivo* (Davidson et al., 2000). In the case of AAV vectors, an understanding of the biology of natural serotypes has led to the development of modified capsids that enhance tissue selectivity and prevent neutralization by host antibodies (Colella et al., 2017; Mingozzi & High, 2011). AAVs employ specific amino acids from their capsid proteins to interact with host cell membrane receptors, conferring different tropisms to different serotypes. Variations in these amino acids affect the receptors to which the capsid proteins bind, providing a wide range of tropisms to meet various experimental and therapeutic needs. This has enabled the design of variants capable of crossing the blood-brain barrier, which may allow the *in*

vivo administration of epigenome editing tools through less invasive routes, such as intravenous administration or retro-orbital injection. For example, two AAV9 serotype variants, known as PHP.B and PHP.eB, can transduce the brains of C57BL/6J mice through systemic injection (Chan et al., 2017; Deverman et al., 2016). However, these properties do not extend to other laboratory mouse strains or non-human primates (Hordeaux et al., 2018; Liguore et al., 2019; Matsuzaki et al., 2018). Other studies based on RNA libraries – which do not depend on transgenic mouse lines for AAVs modifications generation – have identified new variants capable of crossing the blood-brain barrier in different species (Nonnenmacher et al., 2021), significantly expanding the possibilities of transducing brain cells through systemic routes. These advances will not only allow the integration of the elements of our split dCas9-CMD toolbox into systemically administered AAVs; the successful translation of these developments from the laboratory to real-world scenarios holds great promise for advancing our understanding of neurobiology and improving the prospects for targeted therapies in the realm of epigenome-associated diseases.
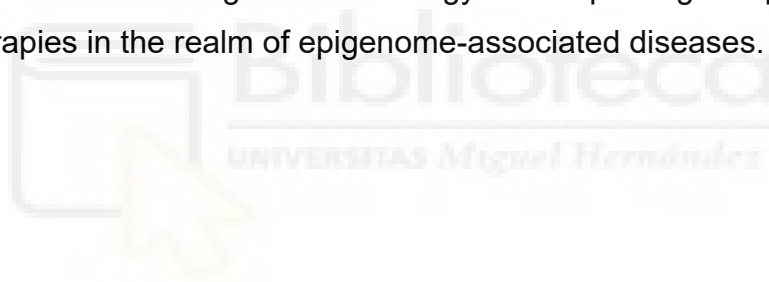
6. CONCLUSIONS

1. Environmental enrichment experienced during early development enhances cognitive abilities in adulthood, specifically in working memory, spatial memory, object recognition, and conditioned fear tasks.

2. Environmental impoverishment experienced during early development worsens cognitive abilities in adulthood, particularly in working memory, cognitive flexibility, and object recognition tasks.

3. Mice housed in different environmental conditions respond similarly to intense training in the conditioned fear paradigm and show no differences in engram formation or *Fos* induction.

4. Pyramidal cells show a wide distribution of Sun1-GFP signal in the EE condition, while the signal is uniform in granule cells, suggesting a wider range of activation levels in CA1 cells in the EE condition.

5. Granule cells display changes in transcription and chromatin accessibility specifically associated with the EE condition, without a clear correlation between both types of changes.

6. Pyramidal cells in the EE condition show an increase in the expression of activity-dependent genes, while both EE and EI pyramidal cells show a reduction in the expression of ncRNAs.

7. Granule cells in the EE condition display an increased predicted binding of AP1, both in promoter and enhancer regions, whereas pyramidal cells in the EI condition show a decrease in the predicted binding of the same transcription factor.

8. The fusion between dCas9 and the nanobody vhhGFP4 specifically recruits GFP-CMD modules to the region-of-interest complementary to the gRNA.

9. The experiments targeting promoters I and IV of *Bdnf* show that the same transactivator module (VP16 or VPR) may display different transactivation efficacy depending on the epigenetic context of the targeted promoter.

10. The KAT module locally increases H3K27ac levels in the region surrounding the binding site of gRNA P4 and induces the expression of Bdnf variants I and IV.

11. The KRAB-MeCP2 repressor module reduces the expression of *Bdnf* variants I and IV when neurons are activated by KCl administration.

12. GFP-CMD modules can be efficiently combined with a specific gRNA in a single lentiviral plasmid, reducing the number of viral particles needed to co-express all 3 elements of the split dCas9-CMD system into the same cell.

CONCLUSIONES

1. El enriquecimiento ambiental experimentado durante la etapa temprana del desarrollo mejora las capacidades cognitivas en la etapa adulta, en concreto, la memoria de trabajo, la memoria espacial, el reconocimiento de objetos y la respuesta al miedo condicionado.

2. El empobrecimiento ambiental experimentado durante la etapa temprana del desarrollo empeora las capacidades cognitivas en la etapa adulta, en concreto, la memoria de trabajo, la flexibilidad cognitiva y el reconocimiento de objetos.

3. Los ratones estabulados en las distintas condiciones ambientales responden de forma similar al entrenamiento intenso en el paradigma de miedo condicionado y no muestran diferencias ni en la formación del engrama ni en la inducción de *Fos*.

4. Las células piramidales de la condición EE presentan una distribución de la señal de Sun1-GFP amplia, mientras que la señal es homogénea en las células granulares, lo que sugiere un rango más amplio de niveles de activación de las células de CA1 en la condición EE.

5. Las células granulares muestran cambios en la transcripción y la accesibilidad asociados específicamente con la condición EE, sin que exista una correlación entre ambos tipos de cambios.

6. En la condición de EE, las células piramidales muestran un aumento en la expresión de genes dependientes de actividad, mientras que tanto las células piramidales de EE como de EI muestran una reducción en la expresión de ncRNAs.

7. Las células granulares de la condición EE muestran un aumento en la unión predicha de AP1, tanto en las regiones promotoras como en las potenciadoras, mientras que las células piramidales de la condición EI muestran una disminución en la unión predicha del mismo factor de transcripción.

8. La fusión entre dCas9 y el nanocuerpo vhhGFP4 recluta de forma específica a los módulos GFP-CMD a la región de interés complementaria al gRNA.

177

9. Los experimentos dirigidos a los promotores I y IV de *Bdnf* demuestran que el mismo módulo transactivador (VP16 o VPR) puede mostrar diferentes eficacias dependiendo del contexto epigenético del promotor diana.

10. El módulo KAT aumenta localmente los niveles de H3K27ac en la región que rodea al sitio de unión del gRNA P4, e induce la expresión de las variantes I y IV de *Bdnf*.

11. El módulo represor KRAB-MeCP2 reduce la expresión de las variantes I y IV de *Bdnf* cuando las neuronas son activadas por la administración de KCl.

12. Los módulos GFP-CMD se pueden combinar con un gRNA específico en un mismo plásmido lentiviral de forma eficiente, reduciendo el número de partículas virales necesarias para co-expresar los 3 elementos de la herramienta dCas9-CMD dividida en la misma célula.

REFERENCES

Adachi, M., Lin, P. Y., Pranav, H., & Monteggia, L. M. (2016). Postnatal loss of Mef2c results in dissociation of effects on synapse number and learning and memory. *Biol Psychiatry*, *80*(2), 140–8. https://doi.org/10.1016/J.BIOPSYCH.2015.09.018

Ago, Y., Takahashi, K., Nakamura, S., Hashimoto, H., Baba, A., & Matsuda, T. (2007). Anxiety-like and exploratory behaviors of isolation-reared mice in the staircase test. *J Pharmacol Sci*, *104*(2), 153–8. https://doi.org/10.1254/JPHS.FP0070325

Ahmed, O. J., & Mehta, M. R. (2009). The hippocampal rate code: anatomy, physiology and theory. *Trends Neurosci*, *32*(6), 329–38. https://doi.org/10.1016/j.tins.2009.01.009

Aid, T., Kazantseva, A., Piirsoo, M., Palm, K., & Timmusk, T. (2007). Mouse and rat BDNF gene structure and expression revisited. *J Neurosci Res*, *85*(3), 525–35. https://doi.org/10.1002/JNR.21139

Akhtar, M. W., Kim, M. S., Adachi, M., Morris, M. J., Qi, X., Richardson, J. A., et al. (2012). In vivo analysis of MEF2 transcription factors in synapse regulation and neuronal survival. *PLoS ONE*, *7*(4), 34863. https://doi.org/10.1371/JOURNAL.PONE.0034863

Allen, W. E., DeNardo, L. A., Chen, M. Z., Liu, C. D., Loh, K. M., Fenno, L. E., et al. (2017). Thirst-associated preoptic neurons encode an aversive motivational drive. *Science*, *357*(6356), 1149–55. https://doi.org/10.1126/science.aan6747

Amiri, S., Haj-Mirzaian, A., Rahimi-balaei, M., Razmi, A., Kordjazy, N., Shirzadian, A., et al. (2015). Co-occurrence of anxiety and depressive-like behaviors following adolescent social isolation in male mice; possible role of nitrergic system. *Physiol Behav*, *145*, 38–44. https://doi.org/10.1016/J.PHYSBEH.2015.03.032

An, J. J., Gharami, K., Liao, G. Y., Woo, N. H., Lau, A. G., Vanevski, F., et al. (2008). Distinct role of long 3' UTR BDNF mRNA in spine morphology and synaptic plasticity in hippocampal neurons. *Cell*, *134*(1), 175–87. https://doi.org/10.1016/J.CELL.2008.05.045

Anand, K., & Dhikav, V. (2012). Hippocampus in health and disease: An overview. *Ann Indian Acad Neurol*, *15*(4), 239. https://doi.org/10.4103/0972-2327.104323

Andersen, S. L., Lyss, P. J., Dumont, N. L., & Teicher, M. H. (1999). Enduring neurochemical effects of early maternal separation on limbic structures. *Ann N Y Acad Sci*, *877*, 756–9. https://doi.org/10.1111/J.1749-6632.1999.TB09317.X

Andrews, S. (2010). *FastQC: a quality control tool for high throughput sequence data*. Babraham Bioinformatics. https://www.bioinformatics.babraham.ac.uk/projects/fastqc/

Aravin, A. A., Lagos-Quintana, M., Yalcin, A., Zavolan, M., Marks, D., Snyder, B., et al. (2003). The small RNA profile during Drosophila melanogaster development. *Dev Cell*, *5*(2), 337–50. https://doi.org/10.1016/S1534-5807(03)00228-4

Arroyo-Olarte, R. D., Bravo Rodríguez, R., & Morales-Ríos, E. (2021). Genome editing in bacteria: CRISPR-Cas and beyond. *Microorganisms, 9*(4), 844. https://doi.org/10.3390/MICROORGANISMS9040844

Arzate-Mejia, R. G., & Mansuy, I. M. (2023). Remembering through the genome: the role of chromatin states in brain functions and diseases. *Transl Psychiatry*, *13*(1), 1–11. https://doi.org/10.1038/s41398-023-02415-4

Assali, A., Harrington, A. J., & Cowan, C. W. (2019). Emerging roles for MEF2 in brain development and mental disorders. *Curr Opin Neurobiol*, *59*, 49-58. https://doi.org/10.1016/J.CONB.2019.04.008

Bäck, S., Dossat, A., Parkkinen, I., Koivula, P., Airavaara, M., Richie, C. T., et al. (2019a). Neuronal activation stimulates cytomegalovirus promoter-driven transgene expression. *Mol Ther Methods Clin Dev*, *3*(14), 180–8. https://doi.org/10.1016/j.omtm.2019.06.006

Bäck, S., Necarsulmer, J., Whitaker, L. R., Coke, L. M., Koivula, P., Heathward, E. J., et al. (2019b). Neuron-specific genome modification in the adult rat brain using CRISPR-Cas9 transgenic rats. *Neuron*, *102*(1), 105-19. https://doi.org/10.1016/J.NEURON.2019.01.035

Bai, M., Zhu, X., Zhang, Y., Zhang, S., Zhang, L., Xue, L., et al. (2012). Abnormal hippocampal BDNF and miR-16 expression is associated with depression-like behaviors induced by stress during early life. *PloS One*, *7*(10). https://doi.org/10.1371/JOURNAL.PONE.0046921

Bao, G., Tang, M., Zhao, J., & Zhu, X. (2021). Nanobody: a promising toolkit for molecular imaging and disease therapy. *EJNMMI Res*, *11*(1), 6. https://doi.org/10.1186/S13550-021-00750-5

Barker, S. J., Raju, R. M., Milman, N. E. P., Wang, J., Davila-Velderrain, J., Gunter-Rahman, F., et al. (2021). MEF2s are key regulators of cognitive function and confer resilience to neurodegeneration. *Sci Transl Med*, *13*(618). https://doi.org/10.1126/SCITRANSLMED.ABD7695

Barrangou, R., Fremaux, C., Deveau, H., Richards, M., Boyaval, P., Moineau, S., et al. (2007). CRISPR provides acquired resistance against viruses in prokaryotes. *Science, 315*(5819), 1709–12. https://doi.org/10.1126/SCIENCE.1138140

Bartels, M., Rietveld, M. J. H., Van Baal, G. C. M., & Boomsma, D. I. (2002). Genetic and environmental influences on the development of intelligence. *Behav Genet*, *32*(4), 237–49. https://doi.org/10.1023/A:1019772628912

Bartosovic, M., & Castelo-Branco, G. (2022). Multimodal chromatin profiling using nanobody-based single-cell CUT&Tag. *Nat Biotechnol, 41*(6), 794–805. https://doi.org/10.1038/s41587-022-01535-4

Bashtrykov, P., & Jeltsch, A. (2017). Epigenome editing in the brain. *Adv Exp*

Med Biol, *978*, 409–24. https://doi.org/10.1007/978-3-319-53889-1_21/FIGURES/3

Basiji, D. A., Ortyn, W. E., Liang, L., Venkatachalam, V., & Morrissey, P. (2007). Cellular Image Analysis and Imaging by Flow Cytometry. *Clin Lab Med*, *27*(3), 653. https://doi.org/10.1016/J.CLL.2007.05.008

Beagan, J. A., Pastuzyn, E. D., Fernandez, L. R., Guo, M. H., Feng, K., Titus, K. R., et al. (2020). Three-dimensional genome restructuring across timescales of activity-induced neuronal gene expression. *Nat Neurosci*, *23*(6), 707–17. https://doi.org/10.1038/S41593-020-0634-6

Beck, D., Ben Maamar, M., & Skinner, M. K. (2022). Genome-wide CpG density and DNA methylation analysis method (MeDIP, RRBS, and WGBS) comparisons. *Epigenetics*, *17*(5), 518–30. https://doi.org/10.1080/15592294.2021.1924970

Becker, P. B., & Workman, J. L. (2013). Nucleosome remodeling and epigenetics. *Cold Spring Harb Perspect Biol*, *5*(9). https://doi.org/10.1101/CSHPERSPECT.A017905

Beerli, R. R., & Barbas, C. F. (2002). Engineering polydactyl zinc-finger transcription factors. *Nat Biotechnol*, *20*(2), 135–41. https://doi.org/10.1038/nbt0202-135

Belton, J. M., McCord, R. P., Gibcus, J. H., Naumova, N., Zhan, Y., & Dekker, J. (2012). Hi-C: a comprehensive technique to capture the conformation of genomes. *Methods*, *58*(3), 268–76. https://doi.org/10.1016/J.YMETH.2012.05.001

Benito, E., & Barco, A. (2015). The neuronal activity-driven transcriptome. *Mol Neurobiol*, *51*(3), 1071–88. https://doi.org/10.1007/S12035-014-8772-Z

Benito, E., Valor, L. M., Jimenez-Minchan, M., Huber, W., & Barco, A. (2011). cAMP response element-binding protein is a primary hub of activity-driven neuronal gene expression. *J Neurosci*, *31*(50), 18237–50. https://doi.org/10.1523/JNEUROSCI.4554-11.2011

Bentsen, M., Goymann, P., Schultheis, H., Klee, K., Petrova, A., Wiegandt, R., et al. (2020). ATAC-seq footprinting unravels kinetics of transcription factor binding during zygotic genome activation. *Nat Commun*, *11*(1), 4267. https://doi.org/10.1038/s41467-020-18035-1

Bergmann, O., Liebl, J., Bernard, S., Alkass, K., Yeung, M. S. Y., Steier, P., et al. (2012). The age of olfactory bulb neurons in humans. *Neuron*, *74*(4), 634–9. https://doi.org/10.1016/J.NEURON.2012.03.030

Beveridge, N. J., Santarelli, D. M., Wang, X., Tooney, P. A., Webster, M. J., Weickert, C. S., et al. (2014). Maturation of the human dorsolateral prefrontal cortex coincides with a dynamic shift in microRNA expression. *Schizophr Bull*, *40*(2), 399–409. https://doi.org/10.1093/SCHBUL/SBS198

Bevington, S. L., Cauchy, P., Piper, J., Bertrand, E., Lalli, N., Jarvis, R. C., et al. (2016). Inducible chromatin priming is associated with the establishment of immunological memory in T cells. *EMBO J*, *35*(5), 515-35.

https://doi.org/10.15252/EMBJ.201592534

Black, I. (1999). Trophic regulation of synaptic plasticity. *J Neurobiol*, *41*(1), 108–18. https://pubmed.ncbi.nlm.nih.gov/10504198/

Blankvoort, S., Descamps, L. A. L., & Kentros, C. (2020). Enhancer-Driven Gene Expression (EDGE) enables the generation of cell type specific tools for the analysis of neural circuits. *Neurosci Res*, *152*, 78–86. https://doi.org/10.1016/J.NEURES.2020.01.009

Boccaletto, P., MacHnicka, M. A., Purta, E., Pitkowski, P., Baginski, B., Wirecki, T. K., et al. (2018). MODOMICS: a database of RNA modification pathways. 2017 update. *Nucleic Acids Res*, *46*(D1), D303–7. https://doi.org/10.1093/NAR/GKX1030

Boch, J., Scholze, H., Schornack, S., Landgraf, A., Hahn, S., Kay, S., et al. (2009). Breaking the code of DNA binding specificity of TAL-type III effectors. *Science*, *326*(5959), 1509–12. https://doi.org/10.1126/SCIENCE.1178811

Boersma, S., Khuperkar, D., Verhagen, B. M. P., Sonneveld, S., Grimm, J. B., Lavis, L. D., et al. (2019). Multi-color single-molecule imaging uncovers extensive heterogeneity in mrna decoding. *Cell*, *178*(2), 458-72. https://doi.org/10.1016/J.CELL.2019.05.001

Böldicke, T. (2017). Single domain antibodies for the knockdown of cytosolic and nuclear proteins. *Protein Sci*, *26*(5), 925–45. https://doi.org/10.1002/PRO.3154

Boldrini, M., Fulmore, C. A., Tartt, A. N., Simeon, L. R., Pavlova, I., Poposka, V., et al. (2018). Human hippocampal neurogenesis persists throughout aging. *Cell Stem Cell*, *22*(4), 589-99. https://doi.org/10.1016/J.STEM.2018.03.015

Bonifer, C., & Cockerill, P. N. (2017). Chromatin priming of genes in development: Concepts, mechanisms and consequences. *Exp Hematol*, *49*: 1–8. https://doi.org/10.1016/J.EXPHEM.2017.01.003

Bramham, C. R., Worley, P. F., Moore, M. J., & Guzowski, J. F. (2008). The immediate early gene arc/arg3.1: regulation, mechanisms, and function. *J Neurosci*, *28*(46), 11760–7. https://doi.org/10.1523/JNEUROSCI.3864-08.2008

Branchi, I., Francia, N., & Alleva, E. (2004). Epigenetic control of neurobehavioural plasticity: the role of neurotrophins. *Behav Pharmacol*, *15*(5–6), 353–62. https://doi.org/10.1097/00008877-200409000-00006

Bredy, T. W., Wu, H., Crego, C., Zellhoefer, J., Sun, Y. E., & Barad, M. (2007). Histone modifications around individual BDNF gene promoters in prefrontal cortex are associated with extinction of conditioned fear. *Learn Mem*, *14*(4), *268–76*. https://doi.org/10.1101/LM.500907

Brennecke, J., Aravin, A. A., Stark, A., Dus, M., Kellis, M., Sachidanandam, R., et al. (2007). Discrete small RNA-generating loci as master regulators of transposon activity in Drosophila. *Cell*, *128*(6), 1089–103. https://doi.org/10.1016/J.CELL.2007.01.043

Briley, D. A., & Tucker-Drob, E. M. (2013). Explaining the increasing heritability

of cognitive ability across development: a meta-analysis of longitudinal twin and adoption studies. *Psychol Sci*, *24*(9), 1704-13. https://doi.org/10.1177/0956797613478618

Brouns, S. J. J., Jore, M. M., Lundgren, M., Westra, E. R., Slijkhuis, R. J. H., Snijders, A. P. L., et al. (2008). Small CRISPR RNAs guide antiviral defense in prokaryotes. *Science,* *321*(5891), 960-4. https://doi.org/10.1126/SCIENCE.1159689

Buenrostro, J. D., Giresi, P. G., Zaba, L. C., Chang, H. Y., & Greenleaf, W. J. (2013). Transposition of native chromatin for fast and sensitive epigenomic profiling of open chromatin, DNA-binding proteins and nucleosome position. *Nat Methods*, *10*(12), 1213–8. https://doi.org/10.1038/NMETH.2688

Buenrostro, J. D., Wu, B., Chang, H. Y., & Greenleaf, W. J. (2015). ATAC-seq: A Method for Assaying Chromatin Accessibility Genome-Wide. *Curr Protoc Mol Biol*, *109*, 21.29.1-21.29.9. https://doi.org/10.1002/0471142727.MB2129S109

Burgess, A., Lorca, T., & Castro, A. (2012). Quantitative live imaging of endogenous dna replication in mammalian cells. *PLoS ONE*, 7(9), e45726. https://doi.org/10.1371/JOURNAL.PONE.0045726

Burns, A. M., & Gräff, J. (2021). Cognitive epigenetic priming: leveraging histone acetylation for memory amelioration. *Curr Opin Neurobiol*, *67,* 75–84. https://doi.org/10.1016/J.CONB.2020.08.011

Calo, E., & Wysocka, J. (2013). Modification of enhancer chromatin: what, how, and why? *Mol Cell*, *49*(5), 825–37. https://doi.org/10.1016/J.MOLCEL.2013.01.038

Cao, L., Liu, X., Lin, E. J. D., Wang, C., Choi, E. Y., Riban, V., et al. (2010). Environmental and genetic activation of a brain-adipocyte BDNF/leptin axis causes cancer remission and inhibition. *Cell*, *142*(1), 52–64. https://doi.org/10.1016/J.CELL.2010.05.029

Carlezon, W. A. Jr., Nestler, E. J., & Neve, R. L. (2000). Herpes simplex virus-mediated gene transfer as a tool for neuropsychiatric research. *Crit Rev Neurobiol*, *14*(1), 47–67. https://doi.org/10.1080/08913810008443546

Caroni, P., Donato, F., & Muller, D. (2012). Structural plasticity upon learning: regulation and functions. *Nat Rev Neurosci*, *13*(7), 478–90. https://doi.org/10.1038/NRN3258

Carthew, R. W., & Sontheimer, E. J. (2009). Origins and mechanisms of miRNAs and siRNAs. *Cell*, *136*(4), 642–55. https://doi.org/10.1016/J.CELL.2009.01.035

Carullo, N. V. N., Hinds, J. E., Revanna, J. S., Tuscher, J. J., Bauman, A. J., & Day, J. J. (2021). A cre-dependent CRISPR/dCas9 system for gene expression regulation in neurons. e*Neuro*, *8*(4). https://doi.org/10.1523/ENEURO.0188-21.2021

Casey, B. J., Giedd, J. N., & Thomas, K. M. (2000). Structural and functional brain development and its relation to cognitive development. *Biol Psychol*, *54*(1–

3), 241–57. https://doi.org/10.1016/S0301-0511(00)00058-2

Castren, E., Berninger, B., Leingartner, A., & Lindholm, D. (1998). Regulation of brain-derived neurotrophic factor mRNA levels in hippocampus by neuronal activity. *Prog Brain Res*, *117,* 57–64. https://doi.org/10.1016/S0079-6123(08)64007-8

Caussinus, E., Kanca, O., & Affolter, M. (2011). Fluorescent fusion protein knockout mediated by anti-GFP nanobody. *Nat Struct Mol Biol*, *19*(1), 117–21. https://doi.org/10.1038/nsmb.2180

Chan, K. Y., Jang, M. J., Yoo, B. B., Greenbaum, A., Ravi, N., Wu, W. L., et al. (2017). Engineered AAVs for efficient noninvasive gene delivery to the central and peripheral nervous systems. *Nat Neurosci*, *20*(8), 1172–9. https://doi.org/10.1038/NN.4593

Chang, H. Y., & Qi, L. S. (2023). Reversing the Central Dogma: RNA-guided control of DNA in epigenetics and genome editing. *Mol Cell*, *83*(3), 442–51. https://doi.org/10.1016/J.MOLCEL.2023.01.010

Charles A Janeway, J., Travers, P., Walport, M., & Shlomchik, M. J. (2001). Immunobiology: The Immune System in Health and Disease. The structure of a typical antibody molecule. *Garland Science, 5th edition.* https://www.ncbi.nlm.nih.gov/books/NBK27144

Charlesworth, C. T., Deshpande, P. S., Dever, D. P., Camarena, J., Lemgart, V. T., Cromer, M. K., et al. (2019). Identification of preexisting adaptive immunity to Cas9 proteins in humans. *Nat Med*, *25*(2), 249–54. https://doi.org/10.1038/S41591-018-0326-X

Chavez, A., Scheiman, J., Vora, S., Pruitt, B. W., Tuttle, M., P R Iyer, E., et al. (2015). Highly efficient Cas9-mediated transcriptional programming. *Nat Methods*, *12*(4), 326–8. https://doi.org/10.1038/NMETH.3312

Chavez, A., Tuttle, M., Pruitt, B. W., Ewen-Campen, B., Chari, R., Ter-Ovanesyan, D., et al. (2016). Comparison of Cas9 activators in multiple species. *Nat Methods*, *13*(7), 563–7. https://doi.org/10.1038/NMETH.3871

Chen, P. W., Billington, N., Maron, B. Y., Sload, J. A., Chinthalapudi, K., & Heissler, S. M. (2020). The BAR domain of the Arf GTPase-activating protein ASAP1 directly binds actin filaments. *J Biol Chem*, *295*(32), 11303-15. https://doi.org/10.1074/JBC.RA119.009903

Chew, W. L., Tabebordbar, M., Cheng, J. K. W., Mali, P., Wu, E. Y., Ng, A. H. M., et al. (2016). A multi-functional AAV-CRISPR-Cas9 and its host response. *Nat Methods*, *13*(10), 868-74. https://doi.org/10.1038/NMETH.3993

Choi, J.-E., Kim, J., & Kim, J. (2020). Capturing activated neurons and synapses. *Neurosci Res*, *152*, 25–34. https://doi.org/10.1016/j.neures.2019.12.020

Choi, J.-H., Sim, S.-E., Kim, J., Choi, D. Il, Oh, J., Ye, S., et al. (2018). Interregional synaptic maps among engram cells underlie memory formation. *Science*, *360*(6387), 430–5. https://doi.org/10.1126/science.aas9204

Cohen-Cory, S., Kidane, A. H., Shirkey, N. J., & Marshak, S. (2010). Brain-derived neurotrophic factor and the development of structural neuronal

connectivity. *Dev Neurobiol*, *70*(5), 271–88. https://doi.org/10.1002/DNEU.20774

Colasante, G., Lignani, G., Brusco, S., Di Berardino, C., Carpenter, J., Giannelli, S., et al. (2020). dCas9-based Scn1a gene activation restores inhibitory interneuron excitability and attenuates seizures in Dravet syndrome mice. *Mol Ther*, *28*(1), 235-53. https://doi.org/10.1016/J.YMTHE.2019.08.018

Cole, C. J., Mercaldo, V., Restivo, L., Yiu, A. P., Sekeres, M. J., Han, J. H., et al. (2012). MEF2 negatively regulates learning-induced structural plasticity and memory formation. *Nat Neurosci*, *15*(9), 1255–64. https://doi.org/10.1038/NN.3189

Colella, P., Ronzitti, G., & Mingozzi, F. (2017). Emerging issues in AAV-mediated in vivo gene therapy. *Mol Ther Methods Clin Dev*, *8*, 87–104. https://doi.org/10.1016/J.OMTM.2017.11.007

Cunha, C., Brambilla, R., & Thomas, K. L. (2010). A simple role for BDNF in learning and memory? *Front Mol Neurosci*, *3,* 1. https://doi.org/10.3389/NEURO.02.001.2010

D'Ippolito, A. M., McDowell, I. C., Barrera, A., Hong, L. K., Leichter, S. M., Bartelt, L. C., et al. (2018). Pre-established chromatin interactions mediate the genomic response to glucocorticoids. *Cell Syst*, *7*(2), 146-60. https://doi.org/10.1016/J.CELS.2018.06.007

Davidson, B. L., Stein, C. S., Heth, J. A., Martins, I., Kotin, R. M., Derksen, T. A., et al. (2000). Recombinant adeno-associated virus type 2, 4, and 5 vectors: transduction of variant cell types and regions in the mammalian central nervous system. *Proc Natl Acad Sci U S A*, *97*(7), 3428–32. https://doi.org/10.1073/PNAS.97.7.3428

Davis-Dusenbery, B. N., & Hata, A. (2010). Mechanisms of control of microRNA biogenesis. *J Biochem*, *148*(4), 381-92. https://doi.org/10.1093/JB/MVQ096

Day, J. J. (2019). Genetic and epigenetic editing in nervous system. *Dialogues Clin Neurosci*, *21*(4), 359–68. https://doi.org/10.31887/DCNS.2019.21.4/jday

De Genst, E., Silence, K., Decanniere, K., Conrath, K., Loris, R., Kinne, J., et al. (2006). Molecular basis for the preferential cleft recognition by dromedary heavy-chain antibodies. *Proc Natl Acad Sci U S A*, *103*(12), 4586–91. https://doi.org/10.1073/PNAS.0505379103

Deaton, A. M., & Bird, A. (2011). CpG islands and the regulation of transcription. *Genes Dev*, *25*(10), 1010–22. https://doi.org/10.1101/GAD.2037511

Decanniere, K., Muyldermans, S., & Wyns, L. (2000). Canonical antigen-binding loop structures in immunoglobulins: more structures, more canonical classes? *J Mol Biol*, *300*(1), 83–91. https://doi.org/10.1006/JMBI.2000.3839

Dekaban, A. S., & Sadowsky, D. (1978). Changes in brain weights during the span of human life: relation of brain weights to body heights and body weights. *Ann Neurol*, *4*(4), 345–56. https://doi.org/10.1002/ANA.410040410

del Blanco, B., & Barco, A. (2018). Impact of environmental conditions and

chemicals on the neuronal epigenome. *Curr Opin Chem Biol, 45,* 157-65. https://doi.org/10.1016/j.cbpa.2018.06.003

del Blanco, B., Niñerola, S., Martín-González, A. M., Paraíso-Luna, J., Kim, M., Muñoz-Viana, R., et al. (2024). Kdm1a safeguards the topological boundaries of PRC2-repressed genes and prevents aging-related euchromatinization in neurons. *Nat Commun*, *15*(1), 1–20. https://doi.org/10.1038/s41467-024-45773-3

Deltcheva, E., Chylinski, K., Sharma, C. M., Gonzales, K., Chao, Y., Pirzada, Z. A., et al. (2011). CRISPR RNA maturation by trans-encoded small RNA and host factor RNase III. *Nature*, *471*(7340), 602–7. https://doi.org/10.1038/nature09886

DeNardo, L. A., Liu, C. D., Allen, W. E., Adams, E. L., Friedmann, D., Fu, L., et al. (2019). Temporal evolution of cortical ensembles promoting remote memory retrieval. *Nat Neurosci*, *22*(3), 460–9. https://doi.org/10.1038/s41593-018-0318-7

DeNardo, L., & Luo, L. (2017). Genetic strategies to access activated neurons. *Curr Opin Neurobiol*, *45*, 121–9. https://doi.org/10.1016/j.conb.2017.05.014

Dennis, D. J., Han, S., & Schuurmans, C. (2019). bHLH transcription factors in neural development, disease, and reprogramming. *Brain Res*, *1705*, 48–65. https://doi.org/10.1016/J.BRAINRES.2018.03.013

Deverman, B. E., Pravdo, P. L., Simpson, B. P., Kumar, S. R., Chan, K. Y., Banerjee, A., et al. (2016). Cre-dependent selection yields AAV variants for widespread gene transfer to the adult brain. *Nat Biotechnol*, *34*(2), 204–9. https://doi.org/10.1038/NBT.3440

Dhaliwal, N. K., & Mitchell, J. A. (2016). Nuclear RNA Isolation and Sequencing. *Methods Mol Biol*, *1402*, 63–71. https://doi.org/10.1007/978-1-4939-3378-5_7

Diamond, M. C., Johnson, R. E., Protti, A. M., Ott, C., & Kajisa, L. (1985). Plasticity in the 904-day-old male rat cerebral cortex. *Exp Neurol*, *87*(2), 309–17. https://doi.org/10.1016/0014-4886(85)90221-3

Diamond, M. C., Krech, D., & Rosenzweig, M. R. (1964). The effects of an enriched environment on the histology of the rat cerebral cortex. *J Comp Neurol*, *123*(1), 111–19. https://doi.org/10.1002/CNE.901230110

Diamond, M. C., Rosenzweig, M. R., Bennett, E. L., Lindner, B., & Lyon, L. (1972). Effects of environmental enrichment and impoverishment on rat cerebral cortex. *J Neurobiol*, *3*(1), 47–64. https://doi.org/10.1002/neu.480030105

Dixon, J. R., Selvaraj, S., Yue, F., Kim, A., Li, Y., Shen, Y., et al. (2012). Topological domains in mammalian genomes identified by analysis of chromatin interactions. *Nature*, *485*(7398), 376–80. https://doi.org/10.1038/nature11082

Dobin, A., Davis, C. A., Schlesinger, F., Drenkow, J., Zaleski, C., Jha, S., et al. (2013). STAR: ultrafast universal RNA-seq aligner. *Bioinformatics*, *29*(1),

15–21. https://doi.org/10.1093/BIOINFORMATICS/BTS635

Dostie, J., Richmond, T. A., Arnaout, R. A., Selzer, R. R., Lee, W. L., Honan, T. A., et al. (2006). Chromosome Conformation Capture Carbon Copy (5C): A massively parallel solution for mapping interactions between genomic elements. *Genome Res*, *16*(10), 1299-309. https://doi.org/10.1101/GR.5571506

Dudai, Y. (2012). The restless engram: consolidations never end. *Annu Rev Neurosci*, *35*, 227–47. https://doi.org/10.1146/ANNUREV-NEURO-062111-150500

Duke, C. G., Bach, S. V., Revanna, J. S., Sultan, F. A., Southern, N. T., Davis, M. N., et al. (2020). An improved CRISPR/dCas9 interference tool for neuronal gene suppression. *Front Genome Ed*, *2,* 9. https://doi.org/10.3389/FGEED.2020.00009

Edry, E., Lamprecht, R., Wagner, S., & Rosenblum, K. (2011). Virally mediated gene manipulation in the adult CNS. *Front Mol Neurosci, 4,* 57. https://doi.org/10.3389/fnmol.2011.00057

Erdmann, G., Schütz, G., & Berger, S. (2007). Inducible gene inactivation in neurons of the adult mouse forebrain. *BMC Neurosci*, *8,* 63. https://doi.org/10.1186/1471-2202-8-63

Erwin, S. R., Sun, W., Copeland, M., Lindo, S., Spruston, N., & Cembrowski, M. S. (2020). A sparse, spatially biased subtype of mature granule cell dominates recruitment in hippocampal-associated behaviors. *Cell Rep*, *31*(4), 107551. https://doi.org/10.1016/j.celrep.2020.107551

Espeso-Gil, S., Holik, A. Z., Bonnin, S., Jhanwar, S., Chandrasekaran, S., Pique-Regi, R., et al. (2021). Environmental enrichment induces epigenomic and genome organization changes relevant for cognition. *Front Mol Neurosci*, *14*, 664912. https://doi.org/10.3389/FNMOL.2021.664912/BIBTEX

Esvald, E.-E., Tuvikene, J., Kiir, C. S., Avarlaid, A., Tamberg, L., Sirp, A., et al. (2023). Revisiting the expression of BDNF and its receptors in mammalian development. *Front Mol Neurosci*, *16,* 1182499. https://doi.org/10.3389/FNMOL.2023.1182499

Fan, G., & Hutnick, L. (2005). Methyl-CpG binding proteins in the nervous system. *Cell Res, 15*(4), 255–61. https://doi.org/10.1038/sj.cr.7290294

Feingold, E. A., Good, P. J., Guyer, M. S., Kamholz, S., Liefer, L., Wetterstrand, K., et al. (2004). The ENCODE (ENCyclopedia Of DNA Elements) Project. *Science*, *306*(5696), 636–40. https://doi.org/10.1126/SCIENCE.1105136

Fernandez-Albert, J., Lipinski, M., Lopez-Cascales, M. T., Rowley, M. J., Martin-Gonzalez, A. M., del Blanco, B., et al. (2019). Immediate and deferred epigenomic signatures of in vivo neuronal activation in mouse hippocampus. *Nat Neurosci*, *22*(10), 1718–30. https://doi.org/10.1038/s41593-019-0476-2

Fischer, A., Sananbenesi, F., Wang, X., Dobbin, M., & Tsai, L. H. (2007). Recovery of learning and memory is associated with chromatin remodelling. *Nature*, *447*(7141), 178–82. https://doi.org/10.1038/nature05772

Flajnik, M. F., Deschacht, N., & Muyldermans, S. (2011). A case of convergence: why did a simple alternative to canonical antibodies arise in sharks and camels? *PLOS Biol*, *9*(8), e1001120. https://doi.org/10.1371/JOURNAL.PBIO.1001120

Flajnik, M. F., & Kasahara, M. (2009). Origin and evolution of the adaptive immune system: genetic events and selective pressures. *Nat Rev Genet*, *11*(1), 47–59. https://doi.org/10.1038/nrg2703

Flint, J., & Shenk, T. (1997). Viral transactivating proteins. *Annu Rev Genet*, *31*, 177–212. https://doi.org/10.1146/ANNUREV.GENET.31.1.177

Francia, S. (2015). Non-coding RNA: sequence-specific guide for chromatin modification and DNA damage signaling. *Front Genet*, *6, 320*. https://doi.org/10.3389/FGENE.2015.00320

Fu, H., Feng, J., Liu, Q., Sun, F., Tie, Y., Zhu, J., et al. (2009). Stress induces tRNA cleavage by angiogenin in mammalian cells. *FEBS Lett*, *583*(2), 437–42. https://doi.org/10.1016/J.FEBSLET.2008.12.043

Fu, Y., Dominissini, D., Rechavi, G., & He, C. (2014). Gene expression regulation mediated through reversible m^{6}A RNA methylation. *Nat Rev Genet*, *15*(5), 293–306. https://doi.org/10.1038/NRG3724

Fuentes-Ramos, M., Alaiz-Noya, M., & Barco, A. (2021). Transcriptome and epigenome analysis of engram cells: Next-generation sequencing technologies in memory research. *Neurosci Biobehav Rev*, *127*, 865–75. https://doi.org/10.1016/j.neubiorev.2021.06.010

Fujita, Y., Pather, S. R., Ming, G. li, & Song, H. (2022). 3D spatial genome organization in the nervous system: From development and plasticity to disease. *Neuron*, *110*(18), 2902–15. https://doi.org/10.1016/J.NEURON.2022.06.004

Fukuchi, M., & Tsuda, M. (2010). Involvement of the 3'-untranslated region of the brain-derived neurotrophic factor gene in activity-dependent mRNA stabilization. *J Neurochem*, *115*(5), 1222–33. https://doi.org/10.1111/J.1471-4159.2010.07016.X

Garneau, J. E., Dupuis, M. È., Villion, M., Romero, D. A., Barrangou, R., Boyaval, P., et al. (2010). The CRISPR/cas bacterial immune system cleaves bacteriophage and plasmid DNA. *Nature, 468*(7320), 67-71. https://doi.org/10.1038/nature09523

Garthe, A., Roeder, I., & Kempermann, G. (2016). Mice in an enriched environment learn more flexibly because of adult hippocampal neurogenesis. *Hippocampus*, *26*(2), 261–71. https://doi.org/10.1002/HIPO.22520

Garzon, D., Yu, G., & Fahnestock, M. (2002). A new brain-derived neurotrophic factor transcript and decrease in brain-derived neurotrophic factor transcripts 1, 2 and 3 in Alzheimer's disease parietal cortex. *J Neurochem*, *82*(5), 1058–64. https://doi.org/10.1046/J.1471-4159.2002.01030.X

Gascón, S., Paez-Gomez, J. A., Díaz-Guerra, M., Scheiffele, P., & Scholl, F. G.

(2008). Dual-promoter lentiviral vectors for constitutive and regulated gene expression in neurons. *J Neurosci Methods*, *168*(1), 104–12. https://doi.org/10.1016/J.JNEUMETH.2007.09.023

Gemberling, M. P., Siklenka, K., Rodriguez, E., Tonn-Eisinger, K. R., Barrera, A., Liu, F., et al. (2021). Transgenic mice for in vivo epigenome editing with CRISPR-based systems. *Nat Methods*, *18*(8), 965–74. https://doi.org/10.1038/s41592-021-01207-2

Gesell, A. (1925). The mental growth of the pre-school child: A psychological outline of normal development from birth to the sixth year, including a system of developmental diagnosis. *MacMillan Co.* https://doi.org/10.1037/11012-000

Gibson, E. M., Purger, D., Mount, C. W., Goldstein, A. K., Lin, G. L., Wood, L. S., et al. (2014). Neuronal activity promotes oligodendrogenesis and adaptive myelination in the mammalian brain. *Science*, *344*(6183), 1252304. https://doi.org/10.1126/SCIENCE.1252304

Gilbert, L. A., Larson, M. H., Morsut, L., Liu, Z., Brar, G. A., Torres, S. E., et al. (2013). CRISPR-mediated modular RNA-guided regulation of transcription in eukaryotes. *Cell*, *154*(2), 442-51. https://doi.org/10.1016/j.cell.2013.06.044

Gilmore, J. H., Knickmeyer, R. C., & Gao, W. (2018). Imaging structural and functional brain development in early childhood. *Nat Rev Neurosci*, *19*(3), 123–37. https://doi.org/10.1038/NRN.2018.1

Goodman, R. H., & Smolik, S. (2000). CBP/p300 in cell growth, transformation, and development. *Genes Dev*, *14*(13), 1553–77. https://doi.org/10.1101/GAD.14.13.1553

Gottfredson, L. S. (1997). Why g matters: The complexity of everyday life. *Intelligence*, *24*(1), 79–132. https://doi.org/10.1016/S0160-2896(97)90014-3

Greer, E. L., & Shi, Y. (2012). Histone methylation: A dynamic mark in health, disease and inheritance. *Nat Rev Genet,* *13*(5), 343-57. https://doi.org/10.1038/nrg3173

Gregory, M. L., & Szumlinski, K. K. (2008). Impoverished rearing impairs working memory and metabotropic glutamate receptor 5 expression. *Neuroreport,* *19*(2), 239-43. https://doi.org/10.1097/WNR.0b013e3282f4aa15

Grewal, S. I. S. (2010). RNAi-dependent formation of heterochromatin and its diverse functions. *Curr Opin Genet Dev*, *20*(2), 134–41. https://doi.org/10.1016/J.GDE.2010.02.003

Guenthner, C. J., Miyamichi, K., Yang, H. H., Heller, H. C., & Luo, L. (2013). Permanent genetic access to transiently active neurons via TRAP: targeted recombination in active populations. *Neuron*, *78*(5), 773–84. https://doi.org/10.1016/j.neuron.2013.03.025

Gunawardane, L. S., Saito, K., Nishida, K. M., Miyoshi, K., Kawamura, Y., Nagami, T., et al. (2007). A slicer-mediated mechanism for repeat-associated siRNA 5' end formation in Drosophila. *Science*, *315*(5818), 1587–

90. https://doi.org/10.1126/SCIENCE.1140494

Hagihara, H., Toyama, K., Yamasaki, N., & Miyakawa, T. (2009). Dissection of Hippocampal Dentate Gyrus from Adult Mouse. *J Vis Exp*, *33*, 1543. https://doi.org/10.3791/1543

Hainmueller, T., & Bartos, M. (2020). Dentate gyrus circuits for encoding, retrieval and discrimination of episodic memories. *Nat Rev Neurosci*, *21*(3), 153-68. https://doi.org/10.1038/S41583-019-0260-Z

Hamers-Casterman, C., Atarhouch, T., Muyldermans, S., Robinson, G., Hammers, C., Songa, E. B., et al. (1993). Naturally occurring antibodies devoid of light chains. *Nature, 363*(6428), 446-8. https://doi.org/10.1038/363446a0

Hamilton, P. J., Lim, C. J., Nestler, E. J., & Heller, E. A. (2018). Neuroepigenetic editing. *Methods Mol Biol, 1767,* 113-36. https://doi.org/10.1007/978-1-4939-7774-1_5

Han, J.-H., Kushner, S. A., Yiu, A. P., Hsiang, H.-L., Buch, T., Waisman, A., et al. (2009). Selective erasure of a fear memory. *Science*, *323*(5920), 1492-6. https://doi.org/10.1126/science.1164139

Han, J. C., Liu, Q.-R., Jones, M., Levinn, R. L., Menzie, C. M., Jefferson-George, K. S., et al. (2008). Brain-derived neurotrophic factor and obesity in the WAGR syndrome. *N Engl J Med*, *359*(9), 918–27. https://doi.org/10.1056/NEJMOA0801119

Harrington, A. J., Raissi, A., Rajkovich, K., Berto, S., Kumar, J., Molinaro, G., et al. (2016). MEF2C regulates cortical inhibitory and excitatory synapses and behaviors relevant to neurodevelopmental disorders. *Elife*, *5,* e20059. https://doi.org/10.7554/ELIFE.20059

Haworth, C. M. A., Wright, M. J., Luciano, M., Martin, N. G., De Geus, E. J. C., Van Beijsterveldt, C. E. M., et al. (2010). The heritability of general cognitive ability increases linearly from childhood to young adulthood. *Mol Psychiatry*, *15*(11), 1112–20. https://doi.org/10.1038/MP.2009.55

He, Y., & Ecker, J. R. (2015). Non-CG methylation in the human genome. *Annu Rev Genomics Hum Genet*, *16*, 55–77. https://doi.org/10.1146/ANNUREV-GENOM-090413-025437

Hebb, D. O. (1947). The effects of early experience on problem solving at maturity. *Am Psychol*, *2*(8), 306–7. https://www.scirp.org/reference/referencespapers?referenceid=2417868

Hebb, D. O. (1949). The organization of behavior. *Wiley, New York*. https://doi.org/10.1002/sce.37303405110

Heintzman, N. D., Stuart, R. K., Hon, G., Fu, Y., Ching, C. W., Hawkins, R. D., et al. (2007). Distinct and predictive chromatin signatures of transcriptional promoters and enhancers in the human genome. *Nat Genet*, *39*(3), 311–8. https://doi.org/10.1038/NG1966

Henras, A. K., Plisson-Chastang, C., O'Donohue, M. F., Chakraborty, A., & Gleizes, P. E. (2015). An overview of pre-ribosomal RNA processing in

eukaryotes. *Wiley Interdiscip Rev RNA*, *6*(2), 225–42. https://doi.org/10.1002/WRNA.1269

Hirai, H., Tani, T., & Kikyo, N. (2010). Structure and functions of powerful transactivators: VP16, MyoD and FoxA. *Int J Dev Biol*, *54*(11–12), 1589-96. https://doi.org/10.1387/IJDB.103194HH

Hitoshi, N., Ken-ichi, Y., & Jun-ichi, M. (1991). Efficient selection for high-expression transfectants with a novel eukaryotic vector. *Gene*, *108*(2), 193–9. https://doi.org/10.1016/0378-1119(91)90434-D

Holoch, D., & Moazed, D. (2015). RNA-mediated epigenetic regulation of gene expression. *Nat Rev Genet*, *16*(2), 71–84. https://doi.org/10.1038/nrg3863

Hordeaux, J., Wang, Q., Katz, N., Buza, E. L., Bell, P., & Wilson, J. M. (2018). The neurotropic properties of AAV-PHP.B are limited to C57BL/6J mice. *Mol Ther*, *26*(3), 664–8. https://doi.org/10.1016/J.YMTHE.2018.01.018

Huang, E. J., & Reichardt, L. F. (2001). Neurotrophins: roles in neuronal development and function. *Annu Rev Neurosci*, *24*, 677–736. https://doi.org/10.1146/ANNUREV.NEURO.24.1.677

Huang, H., Sabari, B. R., Garcia, B. A., David Allis, C., & Zhao, Y. (2014). SnapShot: histone modifications. *Cell*, *159*(2), 458-458.e1. https://doi.org/10.1016/J.CELL.2014.09.037

Huang, L., Gainkam, L. O. T., Caveliers, V., Vanhove, C., Keyaerts, M., Baetselier, P., et al. (2008). SPECT imaging with 99mTc-labeled EGFR-specific nanobody for in vivo monitoring of EGFR expression. *Mol Imaging Biol*, *10*(3), 167–75. https://doi.org/10.1007/S11307-008-0133-8/FIGURES/6

Huang, Z. H., Du, Y. P., Wen, J. T., Lu, B. F., & Zhao, Y. (2022). snoRNAs: functions and mechanisms in biological processes, and roles in tumor pathophysiology. *Cell Death Discov*, *8*(1), 1–10. https://doi.org/10.1038/s41420-022-01056-8

Huttenlocher, P. R. (1979). Synaptic density in human frontal cortex - Developmental changes and effects of aging. *Brain Res*, *163*(2), 195–205. https://doi.org/10.1016/0006-8993(79)90349-4

Huttenlocher, P. R., & Dabholkar, A. S. (1997). Regional differences in synaptogenesis in human cerebral cortex. *J Comp Neurol*, *387*(2), 167–78. https://doi.org/10.1002/(SICI)1096-9861(19971020)387:2

Ibi, D., Takuma, K., Koike, H., Mizoguchi, H., Tsuritani, K., Kuwahara, Y., et al. (2008). Social isolation rearing-induced impairment of the hippocampal neurogenesis is associated with deficits in spatial memory and emotion-related behaviors in juvenile mice. *J Neurochem*, *105*(3), 921–32. https://doi.org/10.1111/J.1471-4159.2007.05207.X

Ickes, B. R., Pham, T. M., Sanders, L. A., Albeck, D. S., Mohammed, A. H., & Granholm, A. C. (2000). Long-term environmental enrichment leads to regional increases in neurotrophin levels in rat brain. *Exp Neurol*, *164*(1), 45–52. https://doi.org/10.1006/EXNR.2000.7415

Ingolia, N. T., Ghaemmaghami, S., Newman, J. R. S., & Weissman, J. S. (2009). Genome-wide analysis in vivo of translation with nucleotide resolution using ribosome profiling. *Science*, *324*(5924), 218–23. https://doi.org/10.1126/SCIENCE.1168978

Ip, Y. T., Jackson, V., Meier, J., & Chalkley, R. (1988). The separation of transcriptionally engaged genes. *J Biol Chem*, *263*(28), 14044–52. https://doi.org/10.1016/S0021-9258(18)68182-7

Irie, F., Badie-Mahdavi, H., & Yamaguchi, Y. (2012). Autism-like socio-communicative deficits and stereotypies in mice lacking heparan sulfate. *Proc Natl Acad Sci U S A*, *109*(13), 5052–6. https://doi.org/10.1073/PNAS.1117881109/SUPPL_FILE/SM10.MOV

Ishino, Y., Shinagawa, H., Makino, K., Amemura, M., & Nakatura, A. (1987). Nucleotide sequence of the iap gene, responsible for alkaline phosphatase isozyme conversion in Escherichia coli, and identification of the gene product. *J Bacteriol,* *169*(12), 5429-33. https://doi.org/10.1128/JB.169.12.5429-5433.1987

Ito, T., Yamauchi, M., Nishina, M., Yamamichi, N., Mizutani, T., Ui, M., et al. (2001). Identification of SWI.SNF complex subunit BAF60a as a determinant of the transactivation potential of Fos/Jun dimers. *J Biol Chem*, *276*(4), 2852–7. https://doi.org/10.1074/JBC.M009633200

Jankele, R., & Svoboda, P. (2014). TAL effectors: tools for DNA Targeting. *Brief Funct Genomics*, *13*(5), 409–19. https://doi.org/10.1093/BFGP/ELU013

Javierre, B. M., Sewitz, S., Cairns, J., Wingett, S. W., Várnai, C., Thiecke, M. J., et al. (2016). Lineage-specific genome architecture links enhancers and non-coding disease variants to target gene promoters. *Cell*, *167*(5), 1369-84. https://doi.org/10.1016/J.CELL.2016.09.037

Jayanthi, B., Bachhav, B., Wan, Z., Martinez Legaspi, S., & Segatori, L. (2021). A platform for post-translational spatiotemporal control of cellular proteins. *Synthetic Biol (Oxf)*, *6*(1). https://doi.org/10.1093/SYNBIO/YSAB002

Jin, B. K., Odongo, S., Radwanska, M., & Magez, S. (2023). Nanobodies: A review of generation, diagnostics and therapeutics. *Int J Mol Sci*, *24*(6), 5994. https://doi.org/10.3390/IJMS24065994

Jinek, M., Chylinski, K., Fonfara, I., Hauer, M., Doudna, J. A., & Charpentier, E. (2012). A programmable dual-RNA-guided DNA endonuclease in adaptive bacterial immunity. *Science*, *337*(6096), 816–21. https://doi.org/10.1126/science.1225829

Jinek, M., East, A., Cheng, A., Lin, S., Ma, E., & Doudna, J. (2013). RNA-programmed genome editing in human cells. *Elife*, *2*, e00471. https://doi.org/10.7554/ELIFE.00471

Johnson, B. V., Bert, A. G., Ryan, G. R., Condina, A., & Cockerill, P. N. (2004). Granulocyte-macrophage colony-stimulating factor enhancer activation requires cooperation between NFAT and AP-1 elements and is associated with extensive nucleosome reorganization. *Mol Cell Biol*, *24*(18), 7914-30. https://doi.org/10.1128/MCB.24.18.7914-7930.2004

Joo, J. Y., Schaukowitch, K., Farbiak, L., Kilaru, G., & Kim, T. K. (2016). Stimulus-specific combinatorial functionality of neuronal c-fos enhancers. *Nat Neurosci*, *19*(1), 75–83. https://doi.org/10.1038/NN.4170

Josselyn, S. A., & Frankland, P. W. (2018). Memory allocation: mechanisms and function. *Annu Rev Neurosci*, *41*(1), 389–413. https://doi.org/10.1146/annurev-neuro-080317-061956

Josselyn, S. A., & Tonegawa, S. (2020). Memory engrams: Recalling the past and imagining the future. *Science*, *367*(6473), eaaw4325. https://doi.org/10.1126/science.aaw4325

Jun-ichi, M., Satoshi, T., Kimi, A., Fumi, T., Akira, T., Kiyoshi, T., et al. (1989). Expression vector system based on the chicken beta-actin promoter directs efficient production of interleukin-5. *Gene*, *79*(2), 269–77. https://doi.org/10.1016/0378-1119(89)90209-6

Karaca, K. G., Brito, D. V. C., Kupke, J., Zeuch, B., & Oliveira, A. M. M. (2021). Engram reactivation during memory retrieval predicts long-term memory performance in aged mice. *Neurobiol Aging*, *101*, 256–61. https://doi.org/10.1016/J.NEUROBIOLAGING.2021.01.019

Karaca, K. ., Kupke, J., Brito, D. V. C., Zeuch, B., Thome, C., Weichenhan, D., et al. (2020). Neuronal ensemble-specific DNA methylation strengthens engram stability. *Nat Commun*, *11*(1), 639. https://doi.org/10.1038/S41467-020-14498-4

Kaya-Okur, H. S., Wu, S. J., Codomo, C. A., Pledger, E. S., Bryson, T. D., Henikoff, J. G., et al. (2019). CUT&Tag for efficient epigenomic profiling of small samples and single cells. *Nat Commun*, *10*(1), 1930. https://doi.org/10.1038/s41467-019-09982-5

Kempermann, G. (2019). Environmental enrichment, new neurons and the neurobiology of individuality. *Nat Rev Neurosci,* *20*(4), 235-45. https://doi.org/10.1038/s41583-019-0120-x

Kempermann, G., Gast, D., & Gage, F. H. (2002). Neuroplasticity in old age: sustained fivefold induction of hippocampal neurogenesis by long-term environmental enrichment. *Ann Neurol*, *52*(2), 135–43. https://doi.org/10.1002/ANA.10262

Kempermann, G., Song, H., & Gage, F. H. (2015). Neurogenesis in the adult hippocampus. *Cold Spring Harb Perspect Biol*, *7*(9), a018812. https://doi.org/10.1101/CSHPERSPECT.A018812

Kempfer, R., & Pombo, A. (2019). Methods for mapping 3D chromosome architecture. *Nat Rev Genet*, *21*(4), 207–26. https://doi.org/10.1038/s41576-019-0195-2

Keyaerts, M., Xavier, C., Heemskerk, J., Devoogdt, N., Everaert, H., Ackaert, C., et al. (2016). Phase I study of 68Ga-HER2-Nanobody for PET/CT assessment of HER2 expression in breast carcinoma. *J Nucl Med*, *57*(1), 27–33. https://doi.org/10.2967/JNUMED.115.162024

Khare, T., Pai, S., Koncevicius, K., Pal, M., Kriukiene, E., Liutkeviciute, Z., et al.

(2012). 5-hmC in the brain is abundant in synaptic genes and shows differences at the exon-intron boundary. *Nat Struct Mol Biol*, *19*(10), 1037–43. https://doi.org/10.1038/NSMB.2372

Kim, Y. K., Kim, B., & Kim, V. N. (2016). Re-evaluation of the roles of DROSHA, Export in 5, and DICER in microRNA biogenesis. *Proc Natl Acad Sci U S A*, *113*(13), E1881–9. https://doi.org/10.1073/PNAS.1602532113

Kiss, T. (2002). Small nucleolar RNAs: an abundant group of noncoding RNAs with diverse cellular functions. *Cell*, *109*(2), 145–8. https://doi.org/10.1016/s0092-8674(02)00718-3

Kitamura, T., Ogawa, S. K., Roy, D. S., Okuyama, T., Morrissey, M. D., Smith, L. M., et al. (2017). Engrams and circuits crucial for systems consolidation of a memory. *Science*, *356*(6333), 73–8. https://doi.org/10.1126/science.aam6808

Kleinjan, D. A., & Van Heyningen, V. (2005). Long-range control of gene expression: emerging mechanisms and disruption in disease. *Am J Hum Genet*, *76*(1), 8–32. https://doi.org/10.1086/426833

Knickmeyer, R. C., Gouttard, S., Kang, C., Evans, D., Wilber, K., Smith, J. K., et al. (2008). A structural MRI study of human brain development from birth to 2 years. *J Neurosci*, *28*(47), 12176–82. https://doi.org/10.1523/JNEUROSCI.3479-08.2008

Knierim, J. J. (2015). The hippocampus. *Curr Biol*, *25*(23), R1116–21. https://doi.org/10.1016/J.CUB.2015.10.049

Koike, H., Ibi, D., Mizoguchi, H., Nagai, T., Nitta, A., Takuma, K., et al. (2009). Behavioral abnormality and pharmacologic response in social isolation-reared mice. *Behav Brain Res*, *202*(1), 114–21. https://doi.org/10.1016/J.BBR.2009.03.028

Könning, D., Zielonka, S., Grzeschik, J., Empting, M., Valldorf, B., Krah, S., et al. (2017). Camelid and shark single domain antibodies: structural features and therapeutic potential. *Curr Opin Struct Biol*, *45*, 10–16. https://doi.org/10.1016/J.SBI.2016.10.019

Konorski, J. (1948). Conditioned reflexes and neuron organization. *Cambridge University Press*. https://doi.org/10.1176/appi.psychotherapy.1950.4.1.155

Krech, D., Rosenzweig, M. R., & Bennett, E. L. (1960). Effects of environmental complexity and training on brain chemistry. *J Comp Physiol Psychol, 53,* 509-19. https://doi.org/10.1037/h0045402

Krech, D., Rosenzweig, M. R., & Bennett, E. L. (1962). Relations between brain chemistry and problem-solving among rats raised in enriched and impoverished environments. *J Comp Physiol Psychol, 55,* 801-7. https://doi.org/10.1037/h0044220

Kriaucionis, S., & Heintz, N. (2009). The nuclear DNA base 5-hydroxymethylcytosine is present in Purkinje neurons and the brain. *Science, 324*(5929), 929–30. https://doi.org/10.1126/SCIENCE.1169786

Krueger, F., & Andrews, S. (2012). Quality Control, trimming and alignment of

Bisulfite-Seq data (Prot 57). *Department of Medicine, Hematology and Oncology, Domagkstr, 3*(48149), 1-13. https://api.semanticscholar.org/CorpusID:12843502

Kügler, S., Kilic, E., & Bähr, M. (2003). Human synapsin 1 gene promoter confers highly neuron-specific long-term transgene expression from an adenoviral vector in the adult rat brain depending on the transduced area. *Gene Ther, 10*(4), 337-47. https://doi.org/10.1038/sj.gt.3301905

Kundakovic, M., & Champagne, F. A. (2015). Early-life experience, Epigenetics, and the developing brain. *Neuropsychopharmacology, 40*(1), 141–53. https://doi.org/10.1038/npp.2014.140

Kuzumaki, N., Ikegami, D., Tamura, R., Hareyama, N., Imai, S., Narita, M., et al. (2011). Hippocampal epigenetic modification at the brain-derived neurotrophic factor gene induced by an enriched environment. *Hippocampus, 21*(2), 127–32. https://doi.org/10.1002/HIPO.20775

Lam, L. L., Emberly, E., Fraser, H. B., Neumann, S. M., Chen, E., Miller, G. E., et al. (2012). Factors underlying variable DNA methylation in a human community cohort. *Proc Natl Acad Sci U S A, 109 Suppl 2*(Suppl 2), 17253–60. https://doi.org/10.1073/PNAS.1121249109

Langmead, B., & Salzberg, S. L. (2012). Fast gapped-read alignment with Bowtie 2. *Nat Methods, 9*(4), 357–9. https://doi.org/10.1038/NMETH.1923

Larsen, S. B., Cowley, C. J., Sajjath, S. M., Barrows, D., Yang, Y., Carroll, T. S., et al. (2021). Establishment, maintenance, and recall of inflammatory memory. *Cell Stem Cell, 28*(10), 1758-1774.e8. https://doi.org/10.1016/J.STEM.2021.07.001

Lau, C. H., & Suh, Y. (2018). In vivo epigenome editing and transcriptional modulation using CRISPR technology. *Transgenic Res, 27*(6), 489-509. https://doi.org/10.1007/S11248-018-0096-8

Lawrence, M., Huber, W., Pagès, H., Aboyoun, P., Carlson, M., Gentleman, R., et al. (2013). Software for computing and annotating genomic ranges. *PLoS Comput Biol, 9*(8), e1003118. https://doi.org/10.1371/JOURNAL.PCBI.1003118

Lea, A. J., Vockley, C. M., Johnston, R. A., Del Carpio, C. A., Barreiro, L. B., Reddy, T. E., et al. (2018). Genome-wide quantification of the effects of DNA methylation on human gene regulation. *Elife, 7,* e37513. https://doi.org/10.7554/ELIFE.37513

Lee, Y. S., Shibata, Y., Malhotra, A., & Dutta, A. (2009). A novel class of small RNAs: tRNA-derived RNA fragments (tRFs). *Genes Dev, 23*(22), 2639–49. https://doi.org/10.1101/GAD.1837609

Legnini, I., Emmenegger, L., Zappulo, A., Rybak-Wolf, A., Wurmus, R., Martinez, A. O., et al. (2023). Spatiotemporal, optogenetic control of gene expression in organoids. *Nat Methods, 20*(10), 1544-52. https://doi.org/10.1038/s41592-023-01986-w

Lehmann, J., Pryce, C. R., Bettschen, D., & Feldon, J. (1999). The maternal

separation paradigm and adult emotionality and cognition in male and female Wistar rats. *Pharmacol Biochem and Behav, 64*(4), 705–15. https://doi.org/10.1016/S0091-3057(99)00150-1

Leutgeb, J. K., Leutgeb, S., Moser, M. B., & Moser, E. I. (2007). Pattern separation in the dentate gyrus and CA3 of the hippocampus. *Science, 315*(5814), 961–6. https://doi.org/10.1126/SCIENCE.1135801

Li, G., Cai, L., Chang, H., Hong, P., Zhou, Q., Kulakova, E. V., et al. (2014). Chromatin Interaction Analysis with Paired-End Tag (ChIA-PET) sequencing technology and application. *BMC Genomics, 15 Suppl 12*(Suppl 12), S11. https://doi.org/10.1186/1471-2164-15-S12-S11

Li, H., Handsaker, B., Wysoker, A., Fennell, T., Ruan, J., Homer, N., et al. (2009). The Sequence Alignment/Map format and SAMtools. *Bioinformatics, 25*(16), 2078-9. https://doi.org/10.1093/BIOINFORMATICS/BTP352

Li, L., Zhuang, Y., Zhao, X., & Li, X. (2019). Long non-coding RNA in neuronal development and neurological disorders. *Front Genet, 9*, 744. https://doi.org/10.3389/FGENE.2018.00744/BIBTEX

Li, R., Xia, X., Wang, X., Sun, X., Dai, Z., Huo, D., et al. (2020). Generation and validation of versatile inducible CRISPRi embryonic stem cell and mouse model. *PLoS Biol, 18*(11), e3000749. https://doi.org/10.1371/JOURNAL.PBIO.3000749

Li, W., Jones, K., Burke, T. J., Hossain, M. A., & Lariscy, L. (2022). Epigenetic regulation of nucleotide excision repair. *Front Cell Dev Biol, 10*, 847051. https://doi.org/10.3389/FCELL.2022.847051/BIBTEX

Liao, Y., Smyth, G. K., & Shi, W. (2014). featureCounts: an efficient general purpose program for assigning sequence reads to genomic features. *Bioinformatics, 30*(7), 923–30. https://doi.org/10.1093/BIOINFORMATICS/BTT656

Liao, Y., Wang, J., Jaehnig, E. J., Shi, Z., & Zhang, B. (2019). WebGestalt 2019: gene set analysis toolkit with revamped UIs and APIs. *Nucleic Acids Res, 47*(W1), W199–W205. https://doi.org/10.1093/NAR/GKZ401

Lichter, P., Cremer, T., Borden, J., Manuelidis, L., & Ward, D. C. (1988). Delineation of individual human chromosomes in metaphase and interphase cells by in situ suppression hybridization using recombinant DNA libraries. *Hum Genet, 80*(3), 224–34. https://doi.org/10.1007/BF01790090

Lieberman-Aiden, E., Van Berkum, N. L., Williams, L., Imakaev, M., Ragoczy, T., Telling, A., et al. (2009). Comprehensive mapping of long-range interactions reveals folding principles of the human genome. *Science, 326*(5950), 289–93. https://doi.org/10.1126/SCIENCE.1181369

Liguore, W. A., Domire, J. S., Button, D., Wang, Y., Dufour, B. D., Srinivasan, S., et al. (2019). AAV-PHP.B administration results in a differential pattern of CNS biodistribution in non-human primates compared with mice. *Mol Ther, 27*(11), 2018–37. https://doi.org/10.1016/J.YMTHE.2019.07.017

Link, W., Konietzko, U., Kauselmann, G., Krug, M., Schwanke, B., Frey, U., et al.

(1995). Somatodendritic expression of an immediate early gene is regulated by synaptic activity. *Proc Natl Acad Sci U S A*, *92*(12), 5734-8. https://doi.org/10.1073/PNAS.92.12.5734

Lipinski, M., Muñoz-Viana, R., del Blanco, B., Marquez-Galera, A., Medrano-Relinque, J., Caramés, J. M., et al. (2020). KAT3-dependent acetylation of cell type-specific genes maintains neuronal identity in the adult mouse brain. *Nat Commun*, *11*(1), 2588. https://doi.org/10.1038/s41467-020-16246-0

Lister, R., Pelizzola, M., Dowen, R. H., Hawkins, R. D., Hon, G., Tonti-Filippini, J., et al. (2009). Human DNA methylomes at base resolution show widespread epigenomic differences. *Nature*, *462*(7271), 315–22. https://doi.org/10.1038/NATURE08514

Liu, J., Wu, X., Zhang, H., Pfeifer, G. P., & Lu, Q. (2017). Dynamics of RNA polymerase II pausing and bivalent histone H3 methylation during neuronal differentiation in brain development. *Cell Rep*, *20*(6), 1307–18. https://doi.org/10.1016/J.CELREP.2017.07.046

Liu, Q. R., Lu, L., Zhu, X. G., Gong, J. P., Shaham, Y., & Uhl, G. R. (2006). Rodent BDNF genes, novel promoters, novel splice variants, and regulation by cocaine. *Brain Res,* *1067*(1), 1–12. https://doi.org/10.1016/J.BRAINRES.2005.10.004

Liu, X., Ramirez, S., Pang, P. T., Puryear, C. B., Govindarajan, A., Deisseroth, K., et al. (2012). Optogenetic stimulation of a hippocampal engram activates fear memory recall. *Nature*, *484*(7394), 381–5. https://doi.org/10.1038/nature11028

Lopez-Atalaya, J. P., Ciccarelli, A., Viosca, J., Valor, L. M., Jimenez-Minchan, M., Canals, S., et al. (2011). CBP is required for environmental enrichment-induced neurogenesis and cognitive enhancement. *EMBO J*, *30*(20), 4287–98. https://doi.org/10.1038/emboj.2011.299

Love, M. I., Huber, W., & Anders, S. (2014). Moderated estimation of fold change and dispersion for RNA-seq data with DESeq2. *Genome Biol*, *15*(12), 550. https://doi.org/10.1186/S13059-014-0550-8

Lu, Y., Christian, K., & Lu, B. (2008). BDNF: a key regulator for protein synthesis-dependent LTP and long-term memory? *Neurobiol Learn Mem*, *89*(3), 312–23. https://doi.org/10.1016/J.NLM.2007.08.018

Lubin, F. D., Roth, T. L., & Sweatt, J. D. (2008). Epigenetic regulation of BDNF gene transcription in the consolidation of fear memory. *J Neurosci*, *28*(42), 10576–86. https://doi.org/10.1523/JNEUROSCI.1786-08.2008

Lyford, G. L., Yamagata, K., Kaufmann, W. E., Barnes, C. A., Sanders, L. K., Copeland, N. G., et al. (1995). Arc, a growth factor and activity-regulated gene, encodes a novel cytoskeleton-associated protein that is enriched in neuronal dendrites. *Neuron*, *14*(2), 433–45. https://doi.org/10.1016/0896-6273(95)90299-6

Lykken, D. T., Bouchard, T. J., McGue, M., & Tellegen, A. (1993). Heritability of interests: a twin study. *J Appl Psychol*, *78*(4), 649–61. https://doi.org/10.1037/0021-9010.78.4.649

Manolio, T. A., Collins, F. S., Cox, N. J., Goldstein, D. B., Hindorff, L. A., Hunter, D. J., et al. (2009). Finding the missing heritability of complex diseases. *Nature*, *461*(7265), 747–53. https://doi.org/10.1038/NATURE08494

Matharu, N., Rattanasopha, S., Tamura, S., Maliskova, L., Wang, Y., Bernard, A., et al. (2019). CRISPR-mediated activation of a promoter or enhancer rescues obesity caused by haploinsufficiency. *Science*, *363*(6424), eaau0629. https://doi.org/10.1126/science.aau0629

Matsuzaki, Y., Konno, A., Mochizuki, R., Shinohara, Y., Nitta, K., Okada, Y., et al. (2018). Intravenous administration of the adeno-associated virus-PHP.B capsid fails to upregulate transduction efficiency in the marmoset brain. *Neurosci Lett*, *665*, 182–8. https://doi.org/10.1016/J.NEULET.2017.11.049

Maxwell, E. S., & Fournier, M. J. (1995). The small nucleolar RNAs. *Annu Rev Biochem*, *64*, 897–934. https://doi.org/10.1146/ANNUREV.BI.64.070195.004341

Mayford, M., Bach, M. E., Huang, Y. Y., Wang, L., Hawkins, R. D., & Kandel, E. R. (1996). Control of memory formation through regulated expression of a CaMKII transgene. *Science*, *274*(5293), 1678–83. https://doi.org/10.1126/SCIENCE.274.5293.1678

Maynard, K. R., Hill, J. L., Calcaterra, N. E., Palko, M. E., Kardian, A., Paredes, D., et al. (2016). Functional role of BDNF production from unique promoters in aggression and serotonin signaling. *Neuropsychopharmacology*, *41*(8), 1943–55. https://doi.org/10.1038/NPP.2015.349

Maynard, K. R., Hobbs, J. W., Phan, B. N., Gupta, A., Rajpurohit, S., Williams, C., et al. (2018). BDNF-TrkB signaling in oxytocin neurons contributes to maternal behavior. *Elife*, *7,* e33676. https://doi.org/10.7554/ELIFE.33676

McGowan, P. O., Sasaki, A., D'Alessio, A. C., Dymov, S., Labonte, B., Szyf, M., et al. (2009). Epigenetic regulation of the glucocorticoid receptor in human brain associates with childhood abuse. *Nat Neurosci*, *12*(3), 342–8. https://doi.org/10.1038/nn.2270

McGue, M., Bacon, S., & Lykken, D. T. (1993). Personality stability and change in early adulthood: a behavioral genetic analysis. *Dev Psychol*, *29*(1), 96–109. https://doi.org/10.1037/0012-1649.29.1.96

McKenzie, A. T., Wang, M., Hauberg, M. E., Fullard, J. F., Kozlenkov, A., Keenan, A., et al. (2018). Brain cell type specific gene expression and co-expression network architectures. *Sci Rep*, *8*(1), 8868. https://doi.org/10.1038/S41598-018-27293-5

McKinnon, K. M. (2018). Flow cytometry: an overview. *Curr Protoc Immunol*, *120*, 5.1.1-5.1.11. https://doi.org/10.1002/CPIM.40

Meissner, A., Gnirke, A., Bell, G. W., Ramsahoye, B., Lander, E. S., & Jaenisch, R. (2005). Reduced representation bisulfite sequencing for comparative high-resolution DNA methylation analysis. *Nucleic Acids Res*, *33*(18), 5868–77. https://doi.org/10.1093/NAR/GKI901

Melendez, R. I., Gregory, M. L., Bardo, M. T., & Kalivas, P. W. (2004).

Impoverished rearing environment alters metabotropic glutamate receptor expression and function in the prefrontal cortex. *Neuropsychopharmacology, 29*(11), 1980-7. https://doi.org/10.1038/sj.npp.1300507

Mellén, M., Ayata, P., Dewell, S., Kriaucionis, S., & Heintz, N. (2012). MeCP2 binds to 5hmC enriched within active genes and accessible chromatin in the nervous system. *Cell, 151*(7), 1417–30. https://doi.org/10.1016/J.CELL.2012.11.022

Mifsud, B., Tavares-Cadete, F., Young, A. N., Sugar, R., Schoenfelder, S., Ferreira, L., et al. (2015). Mapping long-range promoter contacts in human cells with high-resolution capture Hi-C. *Nat Genet, 47*(6), 598–606. https://doi.org/10.1038/ng.3286

Mingozzi, F., & High, K. A. (2011). Therapeutic in vivo gene transfer for genetic disease using AAV: progress and challenges. *Nat Rev Genet, 12*(5), 341–55. https://doi.org/10.1038/NRG2988

Mitchell, L. S., & Colwell, L. J. (2018). Analysis of nanobody paratopes reveals greater diversity than classical antibodies. *Protein Eng Des Sel, 31*(7–8), 267–75. https://doi.org/10.1093/PROTEIN/GZY017

Mo, A., Mukamel, E. A., Davis, F. P., Luo, C., Henry, G. L., Picard, S., et al. (2015). Epigenomic signatures of neuronal diversity in the mammalian brain. *Neuron, 86*(6), 1369–84. https://doi.org/10.1016/J.NEURON.2015.05.018

Mojica, F. J. M., Díez-Villaseñor, C., García-Martínez, J., & Almendros, C. (2009). Short motif sequences determine the targets of the prokaryotic CRISPR defence system. *Microbiology (Reading), 155*(Pt 3), 733–40. https://doi.org/10.1099/MIC.0.023960-0

Mojica, F. J. M., Díez-Villaseñor, C., García-Martínez, J., & Soria, E. (2005). Intervening sequences of regularly spaced prokaryotic repeats derive from foreign genetic elements. *J Mol Evol, 60*(2), 174–82. https://doi.org/10.1007/s00239-004-0046-3

Moreno, A. M., Fu, X., Zhu, J., Katrekar, D., Shih, Y. R. V., Marlett, J., et al. (2018). In situ gene therapy via AAV-CRISPR-Cas9-mediated targeted gene regulation. *Mol Ther, 26*(7), 1818–27. https://doi.org/10.1016/J.YMTHE.2018.04.017

Movahedi, K., Schoonooghe, S., Laoui, D., Houbracken, I., Waelput, W., Breckpot, K., et al. (2012). Nanobody-based targeting of the macrophage mannose receptor for effective in vivo imaging of tumor-associated macrophages. *Cancer Res, 72*(16), 4165–77. https://doi.org/10.1158/0008-5472.CAN-11-2994

Muyldermans, S. (2013). Nanobodies: natural single-domain antibodies. *Annu Rev Biochem, 82*, 775-97. https://doi.org/10.1146/ANNUREV-BIOCHEM-063011-092449

Muyldermans, S. (2021). Applications of nanobodies. *Annu Rev Anim Biosci, 9*, 401–21. https://doi.org/10.1146/ANNUREV-ANIMAL-021419-083831

Muyldermans, S., Atarhouch, T., Saldanha, J., Barbosa, J. A. R. G., & Hamers,

R. (1994). Sequence and structure of VH domain from naturally occurring camel heavy chain immunoglobulins lacking light chains. *Protein Eng*, 7(9), 1129–35. https://doi.org/10.1093/PROTEIN/7.9.1129

Muyldermans, S., Baral, T. N., Retamozzo, V. C., De Baetselier, P., De Genst, E., Kinne, J., et al. (2009). Camelid immunoglobulins and nanobody technology. *Vet Immunol Immunopathol*, 128(1–3), 178–83. https://doi.org/10.1016/J.VETIMM.2008.10.299

Nair, A., Vadodaria, K. C., Banerjee, S. B., Benekareddy, M., Dias, B. G., Duman, R. S., et al. (2007). Stressor-specific regulation of distinct brain-derived neurotrophic factor transcripts and cyclic AMP response element-binding protein expression in the postnatal and adult rat hippocampus. *Neuropsychopharmacology*, 32(7), 1504–19. https://doi.org/10.1038/SJ.NPP.1301276

Nakamura, M., Gao, Y., Dominguez, A. A., & Qi, L. S. (2021). CRISPR technologies for precise epigenome editing. *Nat Cell Biol*, 23(1), 11–22. https://doi.org/10.1038/s41556-020-00620-7

Ndlovu, 'Matladi N., Lint, C. Van, Wesemael, K. Van, Callebert, P., Chalbos, D., Haegeman, G., et al. (2009). Hyperactivated NF-κB and AP-1 transcription factors promote highly accessible chromatin and constitutive transcription across the interleukin-6 gene promoter in metastatic breast cancer cells. *Mol Cell Biol*, 29(20), 5488-504. https://doi.org/10.1128/MCB.01657-08

Nelson, C. E., & Gersbach, C. A. (2016). Engineering delivery vehicles for genome editing. *Annu Rev Chem Biomol Eng*, 7, 637–62. https://doi.org/10.1146/ANNUREV-CHEMBIOENG-080615-034711

Neunuebel, J. P., & Knierim, J. J. (2014). CA3 retrieves coherent representations from degraded input: direct evidence for CA3 pattern completion and dentate gyrus pattern separation. *Neuron*, 81(2), 416–27. https://doi.org/10.1016/J.NEURON.2013.11.017

Nguyen, G. T., Dhingra, Y., & Sashital, D. G. (2022). Miniature CRISPR-Cas12 endonucleases – Programmed DNA targeting in a smaller package. *Curr Opin Struct Biol*, 77, 102466. https://doi.org/10.1016/J.SBI.2022.102466

Nguyen, V. K., Hamers, R., Wyns, L., & Muyldermans, S. (2000). Camel heavy-chain antibodies: diverse germline VHH and specific mechanisms enlarge the antigen-binding repertoire. *EMBO J*, 19(5), 921–30. https://doi.org/10.1093/EMBOJ/19.5.921

Nihongaki, Y., Furuhata, Y., Otabe, T., Hasegawa, S., Yoshimoto, K., & Sato, M. (2017). CRISPR–Cas9-based photoactivatable transcription systems to induce neuronal differentiation. *Nat Methods*, 14(10), 963–6. https://doi.org/10.1038/nmeth.4430

Nithianantharajah, J., & Hannan, A. J. (2006). Enriched environments, experience-dependent plasticity and disorders of the nervous system. *Nat Rev Neurosci*, 7(9), 697–709. https://doi.org/10.1038/NRN1970

Nonaka, A., Toyoda, T., Miura, Y., Hitora-Imamura, N., Naka, M., Eguchi, M., et al. (2014). Synaptic plasticity associated with a memory engram in the

basolateral amygdala. *J Neurosci*, *34*(28), 9305–9. https://doi.org/10.1523/JNEUROSCI.4233-13.2014

Nonnenmacher, M., Wang, W., Child, M. A., Ren, X. Q., Huang, C., Ren, A. Z., et al. (2021). Rapid evolution of blood-brain-barrier-penetrating AAV capsids by RNA-driven biopanning. *Mol Ther Methods Clin Dev*, *20*, 366–78. https://doi.org/10.1016/j.omtm.2020.12.006

Nora, E. P., Lajoie, B. R., Schulz, E. G., Giorgetti, L., Okamoto, I., Servant, N., et al. (2012). Spatial partitioning of the regulatory landscape of the X-inactivation centre. *Nature*, *485*(7398), 381–5. https://doi.org/10.1038/NATURE11049

North, J. A., Javaid, S., Ferdinand, M. B., Chatterjee, N., Picking, J. W., Shoffner, M., et al. (2011). Phosphorylation of histone H3(T118) alters nucleosome dynamics and remodeling. *Nucleic Acids Res*, *39*(15), 6465–74. https://doi.org/10.1093/NAR/GKR304

Odonoghue, P., Ling, J., & Söll, D. (2018). Transfer RNA function and evolution. *RNA Biol*, *15*(4–5), 423-6. https://doi.org/10.1080/15476286.2018.1478942

Ohline, S. M., & Abraham, W. C. (2019). Environmental enrichment effects on synaptic and cellular physiology of hippocampal neurons. *Neuropharmacology*, *145* (Pt A), 3–12. https://doi.org/10.1016/j.neuropharm.2018.04.007

Okada, R., Fujiwara, H., Mizuki, D., Araki, R., Yabe, T., & Matsumoto, K. (2015). Involvement of dopaminergic and cholinergic systems in social isolation-induced deficits in social affiliation and conditional fear memory in mice. *Neuroscience*, *299*, 134–45. https://doi.org/10.1016/J.NEUROSCIENCE.2015.04.064

Osborne, C. S., Chakalova, L., Brown, K. E., Carter, D., Horton, A., Debrand, E., et al. (2004). Active genes dynamically colocalize to shared sites of ongoing transcription. *Nat Genet*, *36*(10), 1065–71. https://doi.org/10.1038/NG1423

Oti, M., Falck, J., Huynen, M. A., & Zhou, H. (2016). CTCF-mediated chromatin loops enclose inducible gene regulatory domains. *BMC Genomics*, *17*, 252. https://doi.org/10.1186/S12864-016-2516-6/FIGURES/4

Paliou, C., Guckelberger, P., Schöpflin, R., Heinrich, V., Esposito, A., Chiariello, A. M., et al. (2019). Preformed chromatin topology assists transcriptional robustness of Shh during limb development. *Proc Natl Acad Sci U S A*, *116*(25), 12390–9. https://doi.org/10.1073/PNAS.1900672116/-/DCSUPPLEMENTAL

Panizzon, M. S., Vuoksimaa, E., Spoon, K. M., Jacobson, K. C., Lyons, M. J., Franz, C. E., et al. (2014). Genetic and Environmental influences of general cognitive ability: is g a valid latent construct? *Intelligence*, *43*, 65-76. https://doi.org/10.1016/J.INTELL.2014.01.008

Panja, D., & Bramham, C. R. (2014). BDNF mechanisms in late LTP formation: A synthesis and breakdown. *Neuropharmacology*, *76 Pt C*, 664–76. https://doi.org/10.1016/J.NEUROPHARM.2013.06.024

Park, H., & Poo, M. M. (2013). Neurotrophin regulation of neural circuit development and function. *Nat Rev Neurosci*, *14*(1), 7–23. https://doi.org/10.1038/NRN3379

Park, P. J. (2009). ChIP–seq: advantages and challenges of a maturing technology. *Nat Rev Genet*, *10*(10), 669–80. https://doi.org/10.1038/nrg2641

Paterson, S. J., Heim, S., Thomas Friedman, J., Choudhury, N., & Benasich, A. A. (2006). Development of structure and function in the infant brain: implications for cognition, language and social behaviour. *Neurosci Biobehav Rev*, *30*(8), 1087–105. https://doi.org/10.1016/J.NEUBIOREV.2006.05.001

Pedersen, N. L., Plomin, R., Nesselroade, J. R., & Mcclearn, G. E. (1992). A quantitative genetic analysis of cognitive abilities during the second half of the life span. *Psychol Sci*, *3*(6), 346–53. https://doi.org/10.1111/J.1467-9280.1992.TB00045.X

Pinkel, D., Landegent, J., Collins, C., Fuscoe, J., Segraves, R., Lucas, J., et al. (1988). Fluorescence in situ hybridization with human chromosome-specific libraries: detection of trisomy 21 and translocations of chromosome 4. *Proc Natl Acad Sci U S A*, *85*(23), 9138-42. https://doi.org/10.1073/PNAS.85.23.9138

Plomin, R., & Deary, I. J. (2015). Genetics and intelligence differences: five special findings. *Mol Psychiatry*, *20*(1), 98–108. https://doi.org/10.1038/MP.2014.105

Policarpi, C., Dabin, J., & Hackett, J. A. (2021). Epigenetic editing: Dissecting chromatin function in context. *BioEssays*, *43*(5), e2000316. https://doi.org/10.1002/BIES.202000316

Prole, D. L., & Taylor, C. W. (2019). A genetically encoded toolkit of functionalized nanobodies against fluorescent proteins for visualizing and manipulating intracellular signalling. *BMC Biol*, *17*(1), 41. https://doi.org/10.1186/S12915-019-0662-4/FIGURES/2

Provençal, N., Suderman, M. J., Guillemin, C., Massart, R., Ruggiero, A., Wang, D., et al. (2012). The signature of maternal rearing in the methylome in rhesus macaque prefrontal cortex and T cells. *J Neurosci*, *32*(44), 15626–42. https://doi.org/10.1523/JNEUROSCI.1470-12.2012

Pulipparacharuvil, S., Renthal, W., Hale, C. F., Taniguchi, M., Xiao, G., Kumar, A., et al. (2008). Cocaine regulates MEF2 to control synaptic and behavioral plasticity. *Neuron*, *59*(4), 621–33. https://doi.org/10.1016/J.NEURON.2008.06.020

Qi, L. S., Larson, M. H., Gilbert, L. A., Doudna, J. A., Weissman, J. S., Arkin, A. P., et al. (2013). Repurposing CRISPR as an RNA-guided platform for sequence-specific control of gene expression. *Cell*, *152*(5), 1173–83. https://doi.org/10.1016/j.cell.2013.02.022

Ramírez, F., Ryan, D. P., Grüning, B., Bhardwaj, V., Kilpert, F., Richter, A. S., et al. (2016). deepTools2: a next generation web server for deep-sequencing data analysis. *Nucleic Acids Res*, *44*(W1), W160–5.

https://doi.org/10.1093/NAR/GKW257

Ramirez, S., Liu, X., Lin, P.-A., Suh, J., Pignatelli, M., Redondo, R. L., et al. (2013). Creating a false memory in the hippocampus. *Science*, *341*(6144), 387–91. https://doi.org/10.1126/science.1239073

Ramsahoye, B. H., Biniszkiewicz, D., Lyko, F., Clark, V., Bird, A. P., & Jaenisch, R. (2000). Non-CpG methylation is prevalent in embryonic stem cells and may be mediated by DNA methyltransferase 3a. *Proc Natl Acad Sci U S A*, *97*(10), 5237–42. https://doi.org/10.1073/PNAS.97.10.5237

Rashid, A. J., Cole, C. J., & Josselyn, S. A. (2014). Emerging roles for MEF2 transcription factors in memory. *Genes Brain Behav*, *13*(1), 118–25. https://doi.org/10.1111/GBB.12058

Redondo, R. L., Kim, J., Arons, A. L., Ramirez, S., Liu, X., & Tonegawa, S. (2014). Bidirectional switch of the valence associated with a hippocampal contextual memory engram. *Nature*, *513*(7518), 426–30. https://doi.org/10.1038/nature13725

Redondo, R. L., & Morris, R. G. M. (2011). Making memories last: the synaptic tagging and capture hypothesis. *Nat Rev Neurosci*, *12*(1), 17–30. https://doi.org/10.1038/NRN2963

Reijmers, L. G., Perkins, B. L., Matsuo, N., & Mayford, M. (2007). Localization of a Stable Neural Correlate of Associative Memory. *Science*, *317*(5842), 1230–3. https://doi.org/10.1126/science.1143839

Reimand, J., Isserlin, R., Voisin, V., Kucera, M., Tannus-Lopes, C., Rostamianfar, A., et al. (2019). Pathway enrichment analysis and visualization of omics data using g:Profiler, GSEA, Cytoscape and EnrichmentMap. *Nat Protoc*, *14*(2), 482–517. https://doi.org/10.1038/s41596-018-0103-9

Reinke, H., & Hörz, W. (2003). Histones are first hyperacetylated and then lose contact with the activated PHO5 promoter. *Mol Cell*, *11*(6), 1599–607. https://doi.org/10.1016/S1097-2765(03)00186-2

Revets, H., De Baetselier, P., & Muyldermans, S. (2005). Nanobodies as novel agents for cancer therapy. *Expert Opin Biol Ther*, *5*(1), 111–24. https://doi.org/10.1517/14712598.5.1.111

Ridley, M. (2004). The agile gene: how nature turns on nurture. *Harper Perennial*. https://cir.nii.ac.jp/crid/1130282269566175488

Ries, J., Kaplan, C., Platonova, E., Eghlidi, H., & Ewers, H. (2012). A simple, versatile method for GFP-based super-resolution microscopy via nanobodies. *Nat Methods*, *9*(6), 582–4. https://doi.org/10.1038/nmeth.1991

Robertson, H. A. (1992). Immediate-early genes, neuronal plasticity, and memory. *Biochem Cell Biol*, *70*(9), 729–37. https://doi.org/10.1139/O92-112

Roessmann, U., & Gambetti, P. (1986). Astrocytes in the developing human brain. An immunohistochemical study. *Acta Neuropathol*, *70*(3–4), 308–13. https://doi.org/10.1007/BF00686089

Rosenzweig, M. R., & Bennett, E. L. (1996). Psychobiology of plasticity: Effects

of training and experience on brain and behavior. *Behav Brain Res*, *78*(1), 57–65. https://doi.org/10.1016/0166-4328(95)00216-2

Rosenzweig, M. R., Krech, D., Bennett, E. L., & Zolman, J. F. (1962). Variation in environmental complexity and brain measures. *J Comp Physiol Psychol, 55,* 1092-5. https://doi.org/10.1037/h0042758

Rossi, C., Angelucci, A., Costantin, L., Braschi, C., Mazzantini, M., Babbini, F., et al. (2006). Brain-derived neurotrophic factor (BDNF) is required for the enhancement of hippocampal neurogenesis following environmental enrichment. *Eur J Neurosci*, *24*(7), 1850–6. https://doi.org/10.1111/J.1460-9568.2006.05059.X

Roth, S. Y., Denu, J. M., & Allis, C. D. (2001). Histone acetyltransferases. *Annu Rev Biochem*, *70*, 81–120. https://doi.org/10.1146/ANNUREV.BIOCHEM.70.1.81

Roth, T. L., Lubin, F. D., Funk, A. J., & Sweatt, J. D. (2009). Lasting epigenetic influence of early-life adversity on the BDNF gene. *Biol Psychiatry*, *65*(9), 760–9. https://doi.org/10.1016/j.biopsych.2008.11.028

Roy, D. S., Arons, A., Mitchell, T. I., Pignatelli, M., Ryan, T. J., & Tonegawa, S. (2016). Memory retrieval by activating engram cells in mouse models of early Alzheimer's disease. *Nature*, *531*(7595), 508–12. https://doi.org/10.1038/nature17172

Roy, D. S., Park, Y. G., Kim, M. E., Zhang, Y., Ogawa, S. K., DiNapoli, N., et al. (2022). Brain-wide mapping reveals that engrams for a single memory are distributed across multiple brain regions. *Nat Commun, 13*(1), 1799. *https://doi.org/10.1038/S41467-022-29384-4*

Ryan, T. J., Roy, D. S., Pignatelli, M., Arons, A., & Tonegawa, S. (2015). Memory. Engram cells retain memory under retrograde amnesia. *Science*, *348*(6238), 1007–13. https://doi.org/10.1126/science.aaa5542

Saerens, D., Pellis, M., Loris, R., Pardon, E., Dumoulin, M., Matagne, A., et al. (2005). Identification of a universal VHH framework to graft non-canonical antigen-binding loops of camel single-domain antibodies. *J Mol Biol*, *352*(3), 597–607. https://doi.org/10.1016/J.JMB.2005.07.038

Sander, J. D., Dahlborg, E. J., Goodwin, M. J., Cade, L., Zhang, F., Cifuentes, D., et al. (2011). Selection-free zinc-finger-nuclease engineering by context-dependent assembly (CoDA). *Nat Methods*, *8*(1), 67–9. https://doi.org/10.1038/nmeth.1542

Santos-Rosa, H., Schneider, R., Bannister, A. J., Sherriff, J., Bernstein, B. E., Emre, N. C. T., et al. (2002). Active genes are tri-methylated at K4 of histone H3. *Nature*, *419*(6905), 407–11. https://doi.org/10.1038/nature01080

Sapranauskas, R., Gasiunas, G., Fremaux, C., Barrangou, R., Horvath, P., & Siksnys, V. (2011). The Streptococcus thermophilus CRISPR/Cas system provides immunity in Escherichia coli. *Nucleic Acids Res*, *39*(21), 9275–82. https://doi.org/10.1093/NAR/GKR606

Sathanoori, M., Dias, B. G., Nair, A. R., Banerjee, S. B., Tole, S., & Vaidya, V. A.

(2004). Differential regulation of multiple brain-derived neurotrophic factor transcripts in the postnatal and adult rat hippocampus during development, and in response to kainate administration. *Brain Res Mol Brain Res*, *130*(1–2), 170–7. https://doi.org/10.1016/J.MOLBRAINRES.2004.08.002

Sauce, B., & Matzel, L. D. (2018). The paradox of intelligence: Heritability and malleability coexist in hidden gene-environment interplay. *Psychol Bull*, *144*(1), 26–47. https://doi.org/10.1037/bul0000131

Savell, K. E., Bach, S. V., Zipperly, M. E., Revanna, J. S., Goska, N. A., Tuscher, J. J., et al. (2019). A neuron-optimized CRISPR/dCas9 activation system for robust and specific gene regulation. *eNeuro*, *6*(1), ENEURO.0495-18.2019. https://doi.org/10.1523/ENEURO.0495-18.2019

Scandaglia, M., Lopez-Atalaya, J. P., Medrano-Fernandez, A., Lopez-Cascales, M. T., del Blanco, B., Lipinski, M., et al. (2017). Loss of Kdm5c causes spurious transcription and prevents the fine-tuning of activity-regulated enhancers in neurons. *Cell Rep*, *21*(1), 47–59. https://doi.org/10.1016/J.CELREP.2017.09.014

Schilling, K., Luk, D., Morgan, J. I., & Curran, T. (1991). Regulation of a fos-lacZ fusion gene: a paradigm for quantitative analysis of stimulus-transcription coupling. *Proc Natl Acad Sci U S A,* *88*(13), 5665–9. https://doi.org/10.1073/PNAS.88.13.5665

Schoenfelder, S., Javierre, B. M., Furlan-Magaril, M., Wingett, S. W., & Fraser, P. (2018). Promoter Capture Hi-C: high-resolution, genome-wide profiling of promoter interactions. *J Vis Exp*, (136), 57320. https://doi.org/10.3791/57320

Schultz, M. D., He, Y., Whitaker, J. W., Hariharan, M., Mukamel, E. A., Leung, D., et al. (2015). Human body epigenome maps reveal noncanonical DNA methylation variation. *Nature*, *523*(7559), 212–6. https://doi.org/10.1038/NATURE14465

Shahid, Z., Simpson, B., Miao, K. H., & Singh, G. (2023). Genetics, histone code. *StatPearls*. https://www.ncbi.nlm.nih.gov/books/NBK538477

Shapiro, L. A., Perez, Z. D., Foresti, M. L., Arisi, G. M., & Ribak, C. E. (2009). Morphological and ultrastructural features of Iba1-immunolabeled microglial cells in the hippocampal dentate gyrus. *Brain Res*, *1266*, 29–36. https://doi.org/10.1016/J.BRAINRES.2009.02.031

Shen, L., Wu, H., Diep, D., Yamaguchi, S., D'Alessio, A. C., Fung, H. L., et al. (2013). Genome-wide analysis reveals TET- and TDG-dependent 5-methylcytosine oxidation dynamics. *Cell*, *153*(3), 692–706. https://doi.org/10.1016/J.CELL.2013.04.002

Siomi, H., & Siomi, M. C. (2009). On the road to reading the RNA-interference code. *Nature*, *457*(7228), 396–404. https://doi.org/10.1038/NATURE07754

Skene, P. J., & Henikoff, S. (2017). An efficient targeted nuclease strategy for high-resolution mapping of DNA binding sites. *Elife*, *6*, e21856. https://doi.org/10.7554/eLife.21856

Sofroniew, M. V., & Vinters, H. V. (2010). Astrocytes: Biology and pathology. *Acta*

Neuropathol, *119*(1), 7–35. https://doi.org/10.1007/S00401-009-0619-8/FIGURES/9

Soltesz, I., & Losonczy, A. (2018). CA1 pyramidal cell diversity enabling parallel information processing in the hippocampus. *Nat Neurosci*, *21*(4), 484–93. https://doi.org/10.1038/s41593-018-0118-0

Song, C. X., Szulwach, K. E., Fu, Y., Dai, Q., Yi, C., Li, X., et al. (2011). Selective chemical labeling reveals the genome-wide distribution of 5-hydroxymethylcytosine. *Nat Biotechnol*, *29*(1), 68–72. https://doi.org/10.1038/NBT.1732

Song, G., Wang, G., Luo, X., Cheng, Y., Song, Q., Wan, J., et al. (2021). An all-to-all approach to the identification of sequence-specific readers for epigenetic DNA modifications on cytosine. *Nat Commun*, *12*(1), 795. https://doi.org/10.1038/S41467-021-20950-W

Sos, B. C., Fung, H. L., Gao, D. R., Osothprarop, T. F., Kia, A., He, M. M., et al. (2016). Characterization of chromatin accessibility with a transposome hypersensitive sites sequencing (THS-seq) assay. *Genome Biol*, *17,* 20. https://doi.org/10.1186/S13059-016-0882-7

Squire, L. R. (2009). Memory and brain systems: 1969–2009. *J Neurosci*, *29*(41), 12711–6. https://doi.org/10.1523/JNEUROSCI.3575-09.2009

Stankiewicz, A. M., Swiergiel, A. H., & Lisowski, P. (2013). Epigenetics of stress adaptations in the brain. *Brain Res Bull*, *98*, 76–92. https://doi.org/10.1016/j.brainresbull.2013.07.003

Stanton, M. E., & Levine, S. (1988). Maternal modulation of infant glucocorticoid stress responses: Role of age and maternal deprivation. *Psychobiology*, *16*(3), 223–8. https://doi.org/10.3758/BF03327311/METRICS

Stark, R., & Brown, G. (2022). *DiffBind: Differential binding analysis of ChIPSeq peak data*. *R package version,* 3.0.15. https://www.cruk.cam.ac.uk/core-facilities/bioinformatics-core/software/diffbind

Streltsov, V. A., Carmichael, J. A., & Nuttall, S. D. (2005). Structure of a shark IgNAR antibody variable domain and modeling of an early-developmental isotype. *Protein Sci*, *14*(11), 2901–9. https://doi.org/10.1110/PS.051709505

Stroud, H., Su, S. C., Hrvatin, S., Greben, A. W., Renthal, W., Boxer, L. D., et al. (2017). Early-life gene expression in neurons modulates lasting epigenetic states. *Cell*, *171*(5), 1151-1164.e16. https://doi.org/10.1016/J.CELL.2017.09.047

Stroud, H., Yang, M. G., Tsitohay, Y. N., Davis, C. P., Sherman, M. A., Hrvatin, S., et al. (2020). An activity-mediated transition in transcription in early postnatal neurons. *Neuron,* *107*(5), 874-90. https://doi.org/10.1016/j.neuron.2020.06.008

Su, J. H., Zheng, P., Kinrot, S. S., Bintu, B., & Zhuang, X. (2020). Genome-scale imaging of the 3D organization and transcriptional activity of chromatin. *Cell*, *182*(6), 1641-1659.e26. https://doi.org/10.1016/J.CELL.2020.07.032

Su, Y., Shin, J., Zhong, C., Wang, S., Roychowdhury, P., Lim, J., et al. (2017).

Neuronal activity modifies the chromatin accessibility landscape in the adult brain. *Nat Neurosci, 20*(3), 476-83. https://doi.org/10.1038/nn.4494

Sun, S., Ding, Z., Yang, X., Zhao, X., Zhao, M., Gao, L., et al. (2021). Nanobody: a small antibody with big implications for tumor therapeutic strategy. *Int J Nanomedicine, 16*, 2337–56. https://doi.org/10.2147/IJN.S297631

Szabo, Q., Bantignies, F., & Cavalli, G. (2019). Principles of genome folding into topologically associating domains. *Sci Adv, 5*(4), eaaw1668. https://doi.org/10.1126/SCIADV.AAW1668/ASSET/1920B784-9140-4F28-B7E2-EFF7540ECA00/ASSETS/GRAPHIC/AAW1668-F3.JPEG

Telese, F., Ma, Q., Perez, P. M., Notani, D., Oh, S., Li, W., et al. (2015). LRP8-reelin-regulated neuronal enhancer signature underlying learning and memory formation. *Neuron, 86*(3), 696-710. https://doi.org/10.1016/J.NEURON.2015.03.033

Thakore, P. I., Kwon, J. B., Nelson, C. E., Rouse, D. C., Gemberling, M. P., Oliver, M. L., et al. (2018). RNA-guided transcriptional silencing in vivo with S. aureus CRISPR-Cas9 repressors. *Nat Commun, 9*(1), 1674. https://doi.org/10.1038/S41467-018-04048-4

Timmusk, T., Palm, K., Metsis, M., Reintam, T., Paalme, V., Saarma, M., et al. (1993). Multiple promoters direct tissue-specific expression of the rat BDNF gene. *Neuron, 10*(3), 475-89. https://doi.org/10.1016/0896-6273(93)90335-O

Tonegawa, S., Morrissey, M. D., & Kitamura, T. (2018). The role of engram cells in the systems consolidation of memory. *Nat Rev Neurosci, 19*(8), 485–98. https://doi.org/10.1038/s41583-018-0031-2

Traenkle, B., Emele, F., Anton, R., Poetz, O., Haeussler, R. S., Maier, J., et al. (2015). Monitoring interactions and dynamics of endogenous beta-catenin with intracellular nanobodies in living cells. *Mol Cell Proteomics, 14*(3), 707–23. https://doi.org/10.1074/mcp.M114.044016

Treves, A., & Rolls, E. T. (1994). Computational analysis of the role of the hippocampus in memory. *Hippocampus, 4*(3), 374–91. https://doi.org/10.1002/HIPO.450040319

Tuvikene, J., Esvald, E. E., Rähni, A., Uustalu, K., Zhuravskaya, A., Avarlaid, A., et al. (2021). Intronic enhancer region governs transcript-specific bdnf expression in rodent neurons. *Elife, 10*, e65161. https://doi.org/10.7554/eLife.65161

Uffelmann, E., Huang, Q. Q., Munung, N. S., de Vries, J., Okada, Y., Martin, A. R., et al. (2021). Genome-wide association studies. *Nat Rev Methods Prim, 1*(1), 59. https://doi.org/10.1038/s43586-021-00056-9

Valadkhan, S. (2005). snRNAs as the catalysts of pre-mRNA splicing. *Curr Opin Cheml Biol, 9*(6), 603–8. https://doi.org/10.1016/J.CBPA.2005.10.008

van Praag, H., Kempermann, G., & Gage, F. H. (2000). Neural consequences of environmental enrichment. *Nat Rev Neurosci, 1*(3), 191–8. https://doi.org/10.1038/35044558

Van Praag, H., Kempermann, G., & Gage, F. H. (1999). Running increases cell proliferation and neurogenesis in the adult mouse dentate gyrus. *Nat Neurosci*, *2*(3), 266–70. https://doi.org/10.1038/6368

Van, M. V., Fujimori, T., & Bintu, L. (2021). Nanobody-mediated control of gene expression and epigenetic memory. *Nat Commun*, *12*(1), 537. https://doi.org/10.1038/s41467-020-20757-1

Varendi, K., Kumar, A., Härma, M. A., & Andressoo, J. O. (2014). miR-1, miR-10b, miR-155, and miR-191 are novel regulators of BDNF. *Cell Mol Life Sci*, *71*(22), 4443-56. https://doi.org/10.1007/S00018-014-1628-X

Vetere, G., Restivo, L., Cole, C. J., Ross, P. J., Ammassari-Teule, M., Josselyn, S. A., et al. (2011). Spine growth in the anterior cingulate cortex is necessary for the consolidation of contextual fear memory. *Proc Natl Acad Sci U S A*, *108*(20), 8456–60. https://doi.org/10.1073/pnas.1016275108

Vierbuchen, T., Ling, E., Cowley, C. J., Couch, C. H., Wang, X., Harmin, D. A., et al. (2017). AP-1 Transcription factors and the BAF complex mediate signal-dependent enhancer selection. *Mol Cell*, *68*(6), 1067-1082.e12. https://doi.org/10.1016/J.MOLCEL.2017.11.026

Vihervaara, A., Mahat, D. B., Himanen, S. V., Blom, M. A. H., Lis, J. T., & Sistonen, L. (2021). Stress-induced transcriptional memory accelerates promoter-proximal pause release and decelerates termination over mitotic divisions. *Mol Cell*, *81*(8), 1715-1731.e6. https://doi.org/10.1016/J.MOLCEL.2021.03.007

Virant, D., Traenkle, B., Maier, J., Kaiser, P. D., Bodenhöfer, M., Schmees, C., et al. (2018). A peptide tag-specific nanobody enables high-quality labeling for dSTORM imaging. *Nat Commun*, *9*(1), 930. https://doi.org/10.1038/s41467-018-03191-2

Vu, K. B., Ghahroudi, M. A., Wyns, L., & Muyldermans, S. (1997). Comparison of llama VH sequences from conventional and heavy chain antibodies. *Mol Immunol*, *34*(16–17), 1121–31. https://doi.org/10.1016/S0161-5890(97)00146-6

Waddington, C. H. (2012). The epigenotype. 1942. *Int J Epidemiol*, *41*(1), 10–3. https://doi.org/10.1093/IJE/DYR184

Wagner, T. R., & Rothbauer, U. (2021). Nanobodies – Little helpers unravelling intracellular signaling. *Free Radic Biol Med*, *176*, 46–61. https://doi.org/10.1016/J.FREERADBIOMED.2021.09.005

Wang, J., Duncan, D., Shi, Z., & Zhang, B. (2013). WEB-based GEne SeT AnaLysis Toolkit (WebGestalt): update 2013. *Nucleic Acids Res*, *41*(W1), W77–83. https://doi.org/10.1093/NAR/GKT439

Wang, J., Vasaikar, S., Shi, Z., Greer, M., & Zhang, B. (2017). WebGestalt 2017: a more comprehensive, powerful, flexible and interactive gene set enrichment analysis toolkit. *Nucleic Acids Res*, *45*(W1), W130–7. https://doi.org/10.1093/NAR/GKX356

Wang, S., Su, J. H., Beliveau, B. J., Bintu, B., Moffitt, J. R., Wu, C. T., et al. (2016).

Spatial organization of chromatin domains and compartments in single chromosomes. *Science*, *353*(6299), 598–602. https://doi.org/10.1126/SCIENCE.AAF8084

Wang, Z., Gerstein, M., & Snyder, M. (2009). RNA-Seq: a revolutionary tool for transcriptomics. *Nat Rev Genet,* *10*(1), 57–63. https://doi.org/10.1038/NRG2484

Watson, J. B. (1928). Psychological care of infant and child. *WW Norton.* https://psycnet.apa.org/record/1928-02003-000

Weaver, I. C., Cervoni, N., Champagne, F. A., D'Alessio, A. C., Sharma, S., Seckl, J. R., et al. (2004). Epigenetic programming by maternal behavior. *Nat Neurosci*, *7*(8), 847–54. https://doi.org/10.1038/nn1276

Wegmann, S., DeVos, S. L., Zeitler, B., Marlen, K., Bennett, R. E., Perez-Rando, M., et al. (2021). Persistent repression of tau in the brain using engineered zinc finger protein transcription factors. *Sci Adv*, *7*(12), eabe1611. https://doi.org/10.1126/SCIADV.ABE1611

Weinert, B. T., Narita, T., Satpathy, S., Srinivasan, B., Hansen, B. K., Schölz, C., et al. (2018). Time-resolved analysis reveals rapid dynamics and broad scope of the CBP/p300 acetylome. *Cell*, *174*(1), 231-244.e12. https://doi.org/10.1016/J.CELL.2018.04.033

Wenderski, W., Wang, L., Krokhotin, A., Walsh, J. J., Li, H., Shoji, H., et al. (2020). Loss of the neural-specific BAF subunit ACTL6B relieves repression of early response genes and causes recessive autism. *Proc Natl Acad Sci U S A*, *117*(18), 10055–66. https://doi.org/10.1073/PNAS.1908238117/-/DCSUPPLEMENTAL

West, A. E., Pruunsild, P., & Timmusk, T. (2014). Neurotrophins: transcription and translation. *Handb Exp Pharmacol*, *220*, 67–100. https://doi.org/10.1007/978-3-642-45106-5_4

Wiedenheft, B., Sternberg, S. H., & Doudna, J. A. (2012). RNA-guided genetic silencing systems in bacteria and archaea. *Nature,* *482*(7385), 331–8. https://doi.org/10.1038/nature10886

Wilkes, L. A., & Gesell, A. (1930). Infancy and human growth. *Am J Nurs*, *30*(2), 235-6. https://doi.org/10.2307/3409995

Will, C. L., & Lührmann, R. (2011). Spliceosome structure and function. *Cold Spring Harb Perspect Biol*, *3*(7), a003707. https://doi.org/10.1101/CSHPERSPECT.A003707

Will, T. J., Tushev, G., Kochen, L., Nassim-Assir, B., Cajigas, I. J., Dieck, S. T., et al. (2013). Deep sequencing and high-resolution imaging reveal compartment-specific localization of Bdnf mRNA in hippocampal neurons. *Sci Signal*, *6*(306), rs16. https://doi.org/10.1126/SCISIGNAL.2004520

Winick-Ng, W., Kukalev, A., Harabula, I., Zea-Redondo, L., Szabó, D., Meijer, M., et al. (2021). Cell-type specialization is encoded by specific chromatin topologies. *Nature*, *599*(7886), 684–91. https://doi.org/10.1038/s41586-021-04081-2

Woldemichael, B. T., Bohacek, J., Gapp, K., & Mansuy, I. M. (2014). Epigenetics of memory and plasticity. *Prog Mol Biol Transl Sci*, *122*, 305–40. https://doi.org/10.1016/B978-0-12-420170-5.00011-8

Wolfson, W. (2006). Ablynx makes nanobodies from llama bodies. *Chem Biol*, *13*(12), 1243–4. https://doi.org/10.1016/J.CHEMBIOL.2006.12.003

Wong, J., Hyde, T. M., Cassano, H. L., Deep-Soboslay, A., Kleinman, J. E., & Weickert, C. S. (2010). Promoter specific alterations of BDNF mRNA in schizophrenia. *Neuroscience*, *169*(3), 1071-84. https://doi.org/10.1016/J.NEUROSCIENCE.2010.05.037

Wu, T. J., Monokian, G., Mark, D. F., & Wobbe, C. R. (1994). Transcriptional activation by herpes simplex virus type 1 VP16 in vitro and its inhibition by oligopeptides. *Mol Cell Biol*, *14*(5), 3484-93. https://doi.org/10.1128/MCB.14.5.3484

Wysocka, J., & Herr, W. (2003). The herpes simplex virus VP16-induced complex: The makings of a regulatory switch. *Trends Biochem Sci*, *28*(6), 294–304. https://doi.org/10.1016/S0968-0004(03)00088-4

Xu, S. J., & Heller, E. A. (2019). Recent advances in neuroepigenetic editing. *Curr Opin Neurobiol*, *59*, 26–33. https://doi.org/10.1016/J.CONB.2019.03.010

Xu, X., Chemparathy, A., Zeng, L., Kempton, H. R., Shang, S., Nakamura, M., et al. (2021). Engineered miniature CRISPR-Cas system for mammalian genome regulation and editing. *Mol Cell*, *81*(20), 4333-4345.e4. https://doi.org/10.1016/j.molcel.2021.08.008

Xu, X., & Qi, L. S. (2019). A CRISP–dCas toolbox for genetic engineering and synthetic biology. *J Mol Biol*, *431*(1), 34–47. https://doi.org/10.1016/j.jmb.2018.06.037

Yeo, N. C., Chavez, A., Lance-Byrne, A., Chan, Y., Menn, D., Milanova, D., et al. (2018). An enhanced CRISPR repressor for targeted mammalian gene regulation. *Nat Methods*, *15*(8), 611–6. https://doi.org/10.1038/S41592-018-0048-5

Yim, Y. Y., Teague, C. D., & Nestler, E. J. (2020). In vivo locus-specific editing of the neuroepigenome. *Nat Rev Neurosci*, *21*(9), 471–84. https://doi.org/10.1038/s41583-020-0334-y

Ying, Y., Yang, X., Zhao, K., Mao, J., Kuang, Y., Wang, Z., et al. (2015). The Krüppel-associated box repressor domain induces reversible and irreversible regulation of endogenous mouse genes by mediating different chromatin states. *Nucleic Acids Res*, *43*(3), 1549-61. https://doi.org/10.1093/NAR/GKV016

Yong Joon Kim, J., Sang, Z., Xiang, Y., Shen, Z., & Shi, Y. (2023). Nanobodies: Robust miniprotein binders in biomedicine. *Adv Drug Deliv Rev*, *195*, 114726. https://doi.org/10.1016/J.ADDR.2023.114726

Zaghi, M., Broccoli, V., & Sessa, A. (2020). H3K36 methylation in neural development and associated diseases. *Front Genet*, *10,* 1291.

https://doi.org/10.3389/FGENE.2019.01291/FULL

Zeitler, B., Froelich, S., Marlen, K., Shivak, D. A., Yu, Q., Li, D., et al. (2019). Allele-selective transcriptional repression of mutant HTT for the treatment of Huntington's disease. *Nat Med*, *25*(7), 1131–42. https://doi.org/10.1038/S41591-019-0478-3

Zentner, G. E., Kasinathan, S., Xin, B., Rohs, R., & Henikoff, S. (2015). ChEC-seq kinetics discriminates transcription factor binding sites by DNA sequence and shape in vivo. *Nat Commun*, *6*, 8733. https://doi.org/10.1038/ncomms9733

Zerbino, D. R., & Birney, E. (2008). Velvet: Algorithms for de novo short read assembly using de Bruijn graphs. *Genome Res*, *18*(5), 821-9. https://doi.org/10.1101/GR.074492.107

Zhang, B., Kirov, S., & Snoddy, J. (2005). WebGestalt: an integrated system for exploring gene sets in various biological contexts. *Nucleic Acids Res*, *33*(Web Server issue), W741-8. https://doi.org/10.1093/NAR/GKI475

Zhang, P., Wu, W., Chen, Q., & Chen, M. (2019). Non-coding RNAs and their integrated networks. *J Integr Bioinform*, *16*(3), 20190027. https://doi.org/10.1515/JIB-2019-0027

Zhang, T. Y., Keown, C. L., Wen, X., Li, J., Vousden, D. A., Anacker, C., et al. (2018). Environmental enrichment increases transcriptional and epigenetic differentiation between mouse dorsal and ventral dentate gyrus. *Nat Commun*, *9*(1), 298. https://doi.org/10.1038/s41467-017-02748-x

Zhang, T., Cooper, S., & Brockdorff, N. (2015). The interplay of histone modifications – writers that read. *EMBO Rep*, *16*(11), 1467-81. https://doi.org/10.15252/EMBR.201540945

Zhang, Y., Liu, T., Meyer, C. A., Eeckhoute, J., Johnson, D. S., Bernstein, B. E., et al. (2008). Model-based analysis of ChIP-Seq (MACS). *Genome Biol*, *9*(9), R137. https://doi.org/10.1186/GB-2008-9-9-R137/FIGURES/3

Zhao, J., Herrera-Diaz, J., & Gross, D. S. (2005). Domain-wide displacement of histones by activated heat shock factor occurs independently of Swi/Snf and is not correlated with RNA polymerase II density. *Mol Cell Biol*, *25*(20), 8985–99. https://doi.org/10.1128/MCB.25.20.8985-8999.2005

Zhou, H., Liu, J., Zhou, C., Gao, N., Rao, Z., Li, H., et al. (2018). In vivo simultaneous transcriptional activation of multiple genes in the brain using CRISPR–dCas9-activator transgenic mice. *Nat Neurosci*, *21*(3), 440–6. https://doi.org/10.1038/s41593-017-0060-6

Zhu, L. J., Gazin, C., Lawson, N. D., Pagès, H., Lin, S. M., Lapointe, D. S., et al. (2010). ChIPpeakAnno: a Bioconductor package to annotate ChIP-seq and ChIP-chip data. *BMC Bioinformatics*, *11*, 237. https://doi.org/10.1186/1471-2105-11-237

Ziller, M. J., Gu, H., Müller, F., Donaghey, J., Tsai, L. T. Y., Kohlbacher, O., et al. (2013). Charting a dynamic DNA methylation landscape of the human genome. *Nature*, *500*(7463), 477–81.

https://doi.org/10.1038/NATURE12433

Zlotnik, G., & Vansintjan, A. (2019). Memory: an extended definition. *Front Psychol*, *10*, 2523. https://doi.org/10.3389/FPSYG.2019.02523/BIBTEX

Zocher, S., Schilling, S., Grzyb, A. N., Adusumilli, V. S., Lopes, J. B., Günther, S., et al. (2020). Early-life environmental enrichment generates persistent individualized behavior in mice. *Sci Adv*, *6*(35), eabb1478. https://doi.org/10.1126/SCIADV.ABB1478

Zuccato, C., Ciammola, A., Rigamonti, D., Leavitt, B. R., Goffredo, D., Conti, L., et al. (2001). Loss of huntingtin-mediated BDNF gene transcription in Huntington's disease. *Science*, *293*(5529), 493–8. https://doi.org/10.1126/SCIENCE.1059581

Zuo, L., Tan, Y., Wang, Z., Wang, K. S., Zhang, X., Chen, X., et al. (2016). Long non-coding RNAs in psychiatric disorders. *Psychiatr Genet*, *26*(3), 109-16. https://doi.org/10.1097/YPG.0000000000000129